

IAEA-TECDOC-1627

Pressurized Thermal Shock in Nuclear Power Plants: Good Practices for Assessment

*Deterministic Evaluation for the Integrity
of Reactor Pressure Vessel*



IAEA

International Atomic Energy Agency

Pressurized Thermal Shock in
Nuclear Power Plants:
Good Practices for Assessment

Deterministic Evaluation for the Integrity
of Reactor Pressure Vessel

The following States are Members of the International Atomic Energy Agency:

AFGHANISTAN	GHANA	NORWAY
ALBANIA	GREECE	OMAN
ALGERIA	GUATEMALA	PAKISTAN
ANGOLA	HAITI	PALAU
ARGENTINA	HOLY SEE	PANAMA
ARMENIA	HONDURAS	PARAGUAY
AUSTRALIA	HUNGARY	PERU
AUSTRIA	ICELAND	PHILIPPINES
AZERBAIJAN	INDIA	POLAND
BAHRAIN	INDONESIA	PORTUGAL
BANGLADESH	IRAN, ISLAMIC REPUBLIC OF	QATAR
BELARUS	IRAQ	REPUBLIC OF MOLDOVA
BELGIUM	IRELAND	ROMANIA
BELIZE	ISRAEL	RUSSIAN FEDERATION
BENIN	ITALY	SAUDI ARABIA
BOLIVIA	JAMAICA	SENEGAL
BOSNIA AND HERZEGOVINA	JAPAN	SERBIA
BOTSWANA	JORDAN	SEYCHELLES
BRAZIL	KAZAKHSTAN	SIERRA LEONE
BULGARIA	KENYA	SINGAPORE
BURKINA FASO	KOREA, REPUBLIC OF	SLOVAKIA
BURUNDI	KUWAIT	SLOVENIA
CAMBODIA	KYRGYZSTAN	SOUTH AFRICA
CAMEROON	LATVIA	SPAIN
CANADA	LEBANON	SRI LANKA
CENTRAL AFRICAN REPUBLIC	LESOTHO	SUDAN
CHAD	LIBERIA	SWEDEN
CHILE	LIBYAN ARAB JAMAHIRIYA	SWITZERLAND
CHINA	LIECHTENSTEIN	SYRIAN ARAB REPUBLIC
COLOMBIA	LITHUANIA	TAJIKISTAN
CONGO	LUXEMBOURG	THAILAND
COSTA RICA	MADAGASCAR	THE FORMER YUGOSLAV REPUBLIC OF MACEDONIA
CÔTE D'IVOIRE	MALAWI	TUNISIA
CROATIA	MALAYSIA	TURKEY
CUBA	MALI	UGANDA
CYPRUS	MALTA	UKRAINE
CZECH REPUBLIC	MARSHALL ISLANDS	UNITED ARAB EMIRATES
DEMOCRATIC REPUBLIC OF THE CONGO	MAURITANIA	UNITED KINGDOM OF GREAT BRITAIN AND NORTHERN IRELAND
DENMARK	MAURITIUS	UNITED REPUBLIC OF TANZANIA
DOMINICAN REPUBLIC	MEXICO	UNITED STATES OF AMERICA
ECUADOR	MONACO	URUGUAY
EGYPT	MONGOLIA	UZBEKISTAN
EL SALVADOR	MONTENEGRO	VENEZUELA
ERITREA	MOROCCO	VIETNAM
ESTONIA	MOZAMBIQUE	YEMEN
ETHIOPIA	MYANMAR	ZAMBIA
FINLAND	NAMIBIA	ZIMBABWE
FRANCE	NEPAL	
GABON	NETHERLANDS	
GEORGIA	NEW ZEALAND	
GERMANY	NICARAGUA	
	NIGER	
	NIGERIA	

The Agency's Statute was approved on 23 October 1956 by the Conference on the Statute of the IAEA held at United Nations Headquarters, New York; it entered into force on 29 July 1957. The Headquarters of the Agency are situated in Vienna. Its principal objective is "to accelerate and enlarge the contribution of atomic energy to peace, health and prosperity throughout the world".

IAEA-TECDOC-1627

Pressurized Thermal Shock in Nuclear Power Plants: Good Practices for Assessment

**Deterministic Evaluation for the Integrity
of Reactor Pressure Vessel**

INTERNATIONAL ATOMIC ENERGY AGENCY
VIENNA, 2010

COPYRIGHT NOTICE

All IAEA scientific and technical publications are protected by the terms of the Universal Copyright Convention as adopted in 1952 (Berne) and as revised in 1972 (Paris). The copyright has since been extended by the World Intellectual Property Organization (Geneva) to include electronic and virtual intellectual property. Permission to use whole or parts of texts contained in IAEA publications in printed or electronic form must be obtained and is usually subject to royalty agreements. Proposals for non-commercial reproductions and translations are welcomed and considered on a case-by-case basis. Enquiries should be addressed to the IAEA Publishing Section at:

Sales and Promotion, Publishing Section
International Atomic Energy Agency
Vienna International Centre
PO Box 100
1400 Vienna, Austria
fax: +43 1 2600 29302
tel.: +43 1 2600 22417
email: sales.publications@iaea.org
<http://www.iaea.org/books>

For further information on this publication, please contact:

Nuclear Power Engineering Section
International Atomic Energy Agency
Vienna International Centre
P.O. Box 100
1400 Vienna, Austria

**PRESSURIZED THERMAL SHOCK IN NUCLEAR POWER PLANTS:
GOOD PRACTICES FOR ASSESSMENT**

IAEA, VIENNA, 2010

IAEA-TECDOC-1627

ISBN 978-92-0-111109-8

ISSN 1011-4289

© IAEA, 2010

Printed by the IAEA in Austria

February 2010

FOREWORD

Starting in the early 1970s, a series of coordinated research projects (CRPs) was sponsored by the IAEA focusing on the effects of neutron radiation on reactor pressure vessel (RPV) steels and RPV integrity. In conjunction with these CRPs, many consultants meetings, specialists meetings, and international conferences, dating back to the mid-1960s, were held. Individual studies on the basic phenomena of radiation hardening and embrittlement were also performed to better understand increases in tensile strength and shifts to higher temperatures for the integrity of the RPV.

The overall objective of this CRP was to perform benchmark deterministic calculations of a typical pressurized thermal shock (PTS) regime, with the aim of comparing the effects of individual parameters on the final RPV integrity assessment, and then to recommend the best practices for their implementation in PTS procedures.

At present, several different procedures and approaches are used for RPV integrity assessment for both WWER 440-230 reactors and pressurized water reactors (PWRs). These differences in procedures and approaches are based, in principle, on the different codes and rules used for design and manufacturing, and the different materials used for the various types of reactor, and the different levels of implementation of recent developments in fracture mechanics.

Benchmark calculations were performed to improve user qualification and to reduce the user effect on the results of the analysis. This addressed generic PWR and WWER types of RPV, as well as sensitivity analyses. The complementary sensitivity analyses showed that the following factors significantly influenced the assessment: flaw size, shape, location and orientation, thermal hydraulic assumptions and material toughness. Applying national codes and procedures to the benchmark cases produced significantly different results in terms of allowable material toughness. This was mainly related to the safety factors used and the approaches to postulated defects, postulated transients and representation of material toughness.

The IAEA wishes to thank the participants for their contributions, especially the CRP chairman, M. Brumovský of Nuclear Research Institute Řež plc, Czech Republic. The IAEA officers responsible for this publication were K.S. Kang and L. Kupca of the Division of Nuclear Power.

EDITORIAL NOTE

The use of particular designations of countries or territories does not imply any judgement by the publisher, the IAEA, as to the legal status of such countries or territories, of their authorities and institutions or of the delimitation of their boundaries.

The mention of names of specific companies or products (whether or not indicated as registered) does not imply any intention to infringe proprietary rights, nor should it be construed as an endorsement or recommendation on the part of the IAEA.

CONTENTS

1.	INTRODUCTION	1
1.1.	Background.....	1
1.2.	RPV integrity studies.....	2
1.3.	Coordinated research project - 9.....	4
1.4.	Structure.....	6
1.5.	Results of benchmark calculations including sensitivity study	7
1.6.	References	8
2.	SELECTION OF OVERCOOLING SEQUENCES	9
2.1.	General considerations.....	9
2.2.	Precursors	9
2.3.	Categorization of sequences of initiating events and corresponding criteria	11
2.4.	Initiating events groups.....	11
2.5.	References	13
3.	THERMAL HYDRAULIC ANALYSES	14
3.1.	Sequence analysis plan	14
3.2.	Calculation method requirements	14
3.3.	Boundary conditions.....	15
3.3.1.	Plant operating conditions	15
3.3.2.	Symmetric cooling.....	16
3.3.3.	Plume cooling.....	16
3.3.4.	Failures	17
3.4.	Operator actions.....	17
3.5.	References	17
4.	TEMPERATURE AND STRESS FIELD CALCULATIONS	18
4.1.	Physical properties.....	18
4.2.	Temperature and stress fields	20
4.2.1.	Heat transfer analysis	20
4.2.2.	Stress and strain analysis	20
4.3.	Weld residual stresses.....	22
4.4.	Cladding residual stresses.....	24
4.5.	References	24
5.	CRACK TIP LOADING	25
5.1.	Postulated flaws.....	25
5.1.1.	Underclad vs. surface cracks	25
5.1.2.	Effect of flaw depth	25
5.1.3.	Effect of defect shape	26
5.1.4.	Orientation and position (axial/circumferential)	27
5.1.5.	Characterization of NDE indications.....	27
5.2.	Crack tip stress intensity factor.....	28
5.2.1.	Engineering methods.....	28
5.2.2.	FE cracked-body models	30
5.3.	References	32
6.	INTEGRITY ASSESSMENT	33
6.1.	Definition of material toughness	33
6.1.1.	Design fracture toughness curves.....	33
6.1.2.	Indexing of fracture toughness curves.....	33
6.1.3.	Master Curve approach.....	34
6.1.4.	Russian standards for fracture toughness temperature dependence $K_{IC}(T)$	36

6.1.5.	Material (base and weld) non-homogeneity and property gradients	36
6.1.6.	Cladding toughness	37
6.1.7.	Thermal ageing	38
6.2.	Comparison of applied loading and material resistance	41
6.2.1.	Basic assessment principle	41
6.2.2.	Uncertainty of results	43
6.2.3.	Crack front length effect.....	43
6.2.4.	Constraint effects.....	45
6.2.5.	Warm prestressing	46
6.3.	Crack arrest.....	47
6.3.1.	Simplified approach.....	47
6.3.2.	Complex approach.....	49
6.4.	Fatigue crack growth assessment.....	49
6.5.	Mitigation of PTS risks.....	49
6.5.1.	Reduction of flux and annealing.....	49
6.5.2.	Reduction of PTS loads.....	49
6.5.3.	Improvement of ISI performance	50
6.6.	References	50
7.	ANALYSIS OF NOZZLES	52
7.1.	Governing transients.....	52
7.2.	Postulated defect location	52
7.3.	Temperature and stress field.....	52
7.4.	K_I estimation methods and integrity assessment	53
8.	OTHER ISSUES	54
8.1.	Management system and quality assurance	54
8.1.1.	Use of computer codes	55
8.1.2.	Code validation.....	56
8.2.	International research and development	57
8.2.1.	IAEA Coordinated Research Projects on RPV integrity	57
8.2.2.	NEA/CSNI Projects.....	58
8.2.3.	EURATOM Supported Projects	59
8.3.	References	59
9.	CONCLUSIONS AND RECOMMENDATIONS	61
APPENDIX A:	NATIONAL PRACTICES FOR PTS ASSESSMENT	63
APPENDIX B:	RESULTS OF THE ANALYSIS BENCHMARK.....	69
APPENDIX C:	THERMOHYDRAULIC ANALYSIS OF PLUME EFFECTS	148
APPENDIX D:	K ESTIMATION METHODS.....	163
APPENDIX E:	RUSSIAN STANDARD FOR DETERMINATION OF K_{IC}	186
APPENDIX F:	CALCULATION OF CYCLIC CRACK GROWTH.....	192
APPENDIX G:	EXAMPLES OF NOZZLE ANALYSIS.....	197
NOMENCLATURE, ABBREVIATIONS AND SYMBOLS		213
CONTRIBUTORS TO DRAFTING AND REVIEW.....		217

1. INTRODUCTION

1.1. Background

Nuclear power plants (NPPs) operating equipments, are subjected to a variety of ageing mechanisms. The effects of ageing can lead to a reduction in design margins and/or an increase in forced outages and repairs of components. Ageing effects in NPPs are considered in design and manufacturing specifications with some design limits in accordance with plant safety analysis. Ageing effect of the reactor pressure vessel (RPV) have the potential to be NPP life-limiting conditions for a NPP as the RPV is impossible or economically unviable to replace.

The pressurized thermal shock (PTS) issue is concerned with the possibility of failure of pressurized-water-reactor (PWR) pressure vessels under a very specific set of conditions.

These conditions include:

- Occurrence of reactor transients that subject the vessel to severe thermal shock as well as the normal pressure loading;
- Existence of sharp, crack-like defects (flaws) at the inner surface of the vessel wall; and
- High enough fast neutron fluence and concentrations of copper and nickel in the vessel wall to result in a extensive radiation-included reduction in the fracture toughness of the vessel material [1].

During the operation of a NPP, the wall of RPV is exposed to:

- Neutron radiation, resulting in localized embrittlement of the steel and welds in the area of the reactor core;
- Thermal ageing;
- Load cycle fatigue.

The dominant and expected type of damage in the RPV is embrittlement under neutron irradiation of the RPV, especially in the core (beltline) area. If an embrittled RPV were to have a flaw of critical size and certain severe system transients were to occur, the flaw could propagate very rapidly through the vessel, possibly resulting in a through-wall crack and challenging the integrity of the RPV.

The severe transients of concern are:

- PTS, which is characterized by a rapid cooling (i.e. thermal shock) of the down-comer and internal RPV surface, followed sometime by repressurization of the RPV. Thus, a PTS event poses a potentially significant challenge to the structural integrity of the RPV in a PWR and water cooled and water moderated energy reactor (WVER);
- Cold overpressure characterised by high pressure at a low temperature (i.e., hydro-test or end of shutdown situation). These transients are not covered in this guideline, nevertheless similar procedures can be used.

There are no major differences between PWR and WVER in terms of PTS studies; for both reactors all the potential PTS events have to be identified and safety margins against brittle fracture have to be justified in an appropriate manner. All these analyses have to be consistent with the corresponding plant safety analysis report, the design and fabrication of the RPV and the major results have to be periodically reviewed to assure consistency with maintenance activities (such as in-service inspection, surveillance programme and fluence monitoring).

RPVs are designed and manufactured to serve its purposes without rupture under normal (e.g. plant heat up and cool down), upset (e.g. reactor trip and loss of load), emergency (e.g. small loss of coolant, small steam line break or complete loss of flow) and faulted (e.g. large loss-of-coolant or large steam line break) conditions.

Consequently, the RPV is built from appropriate materials using reliable design codes, manufactured using well tried methods-to high standards, tested, inspected and operated in the way assumed in the design. The ageing management programme has to confirm the safety margins continuously using in-service inspection (ISI) results and corresponding flaw evaluation, surveillance programs and dosimetry. PTS studies remain a part of this RPV ageing management programme.

1.2. RPV integrity studies

PTS analysis, which is a part of RPV structural integrity assessment, is associated with large thermal down shocks and, in some cases, with low temperature repressurization of the RPV after a certain time. The material, the design rules, the transient loads are similar (not identical) in both PWR and WWER technologies.

For plants currently in operation, the assessment methodologies have been developed around different codes:

- Flaw evaluation procedures: ASME Code section XI, Appendix A [2], RSE-M Code [3], KTA Code [4] ;
- Specific PTS rules: Russian utility procedure MRKR-SKhr-2004 [5], VERLIFE Unified Procedure [6] or international guideliness (IAEA guidelines for WWER PTS analysis [7], US NRC PTS screening criteria [8]).

Detailed analysis needs are connected to the fact that for some PTS events, the final temperature can be lower than the irradiated materials' ductile to brittle transition temperature.

During the life of a RPV, the following analyses are made and periodically updated:

- Design analysis with a codified evaluation of a postulated hypothetical deep crack, for all type of design transients (for some countries not for emergency and faulted conditions);
- Pressure-temperature (P-T) curve evaluation to define the maximum allowable pressure for different rates of temperature variation with respect to the current coolant temperature;
- Flaw evaluation for any indications discovered during in-service inspection;
- PTS screening evaluation or generic detailed analysis; and
- Probabilistic evaluation can be used for direct decision in some countries like USA or to highlight some uncertainty effects on the global margins in some other countries like France, Sweden, Russia, and Japan.

This report is focused on the irradiated area of the core shell which are all manufactured using circumferential welding of forged rings. Vessels fabricated from rolled plate with longitudinal welds are not considered in this report.

The general way to approach the PTS evaluation for plants in operation is shown in Figure 1.1 step by step:

- Review all the possible design basis transients of a given plant, in accordance with the plant safety analysis report;
- Establish criteria for transient selection in term of PTS margins;
- Select the more significant transients, and corresponding criteria (e.g. level A, B, C or D)¹;
- Perform thermal hydraulic evaluation of the fluid temperature distribution in the RPV in the nozzles and down comer, the corresponding heat transfer coefficient with the RPV inner surface;
- Define the crack location, size and shape in accordance with fabrication, non destructive examination, previous ISI or conventional values;
- Evaluate the residual stress level in cladding, under the cladding and in the circumferential welds;
- Evaluate the stress intensity factor K (SIF) through elastic or elasto-plastic approaches, through finite elements or engineering methods, for all the major transients;

¹ A : normal conditions; B: upset conditions; C: Emergency conditions; D: Faulted conditions

- Evaluate the crack tip area temperature and fluence level, the toughness level and its increase through the wall;
- Evaluate K_{IC} (the material toughness value) taking into account radiation embrittlement;
- Compare K_I (stress intensity factor) with K_{IC} for crack initiation with corresponding safety factors; at this level different aspects can be considered, like warm prestress (WPS) effects, constraint effects or crack front length effects, crack arrest;
- Analyze the results and consider safety margins, if necessary.

In performing an evaluation, a number of different issues arise. These include:

- Thermal hydraulic simulation of transients and comparison with tests for validation;
- Non-linear temperature evaluation through the wall;
- Pressure and thermal stresses through the wall;
- Fracture toughness curve shape, the indexation temperature, the radiation shift of toughness;
- Comparison of toughness values with surveillance programme results;
- Different reference temperature: RT_{NDT} in USA, France, Germany (T_0 is partly accepted) and all countries working by reference to ASME Code, T_0 in Finland, Czech Republic or T_k in Russia and other WWER countries;
- Heterogeneity aspects for forged rings: source of underclad defects and source of local low toughness value;
- Elastic K_I evaluation by engineering methods by comparison with finite element method (FEM);
- Plasticity effects through J integral evaluation or corresponding plasticity correction factors;
- Fracture criteria of the cladding, and comparison with tests;
- Toughness transferability from laboratory tests to plant configuration;
- Constraint effects through tests and simulations, including the crack length correction factors.

The crack initiation criteria, all along the crack front in the ferritic material, with safety factor (SF), is based on:

$$K_I (+ \text{plasticity effects}) < K_{IC} (\text{or } K_{IC}) / SF \quad (1.1)$$

This simple criteria can be expanded to consider other aspects such as warm prestressing or crack arrest. For cracks totally or partially in the cladding, some specific criteria have to be consolidated.

In parallel with these evaluations, some checks are needed to confirm the validity of the data used:

- Fluence measurements using dosimeters and calculation;
- Toughness or Charpy specimens from surveillance programme;
- Non accessible locations for ISI have to be considered in the assessment;
- Qualification level of the ISI has to be consistent with the analysis.

Thus, benchmark calculations of the same typical PTS regime (e.g. for a WWER-440 and PWR) should be performed using different procedures and approaches using the same geometric, thermal-hydraulic, and material data to compare results and to assess the effects of the aforementioned individual input parameters on the final integrity evaluation. Appendix A summarises the main criteria used to define the principal steps in PTS analysis according to existing procedures.

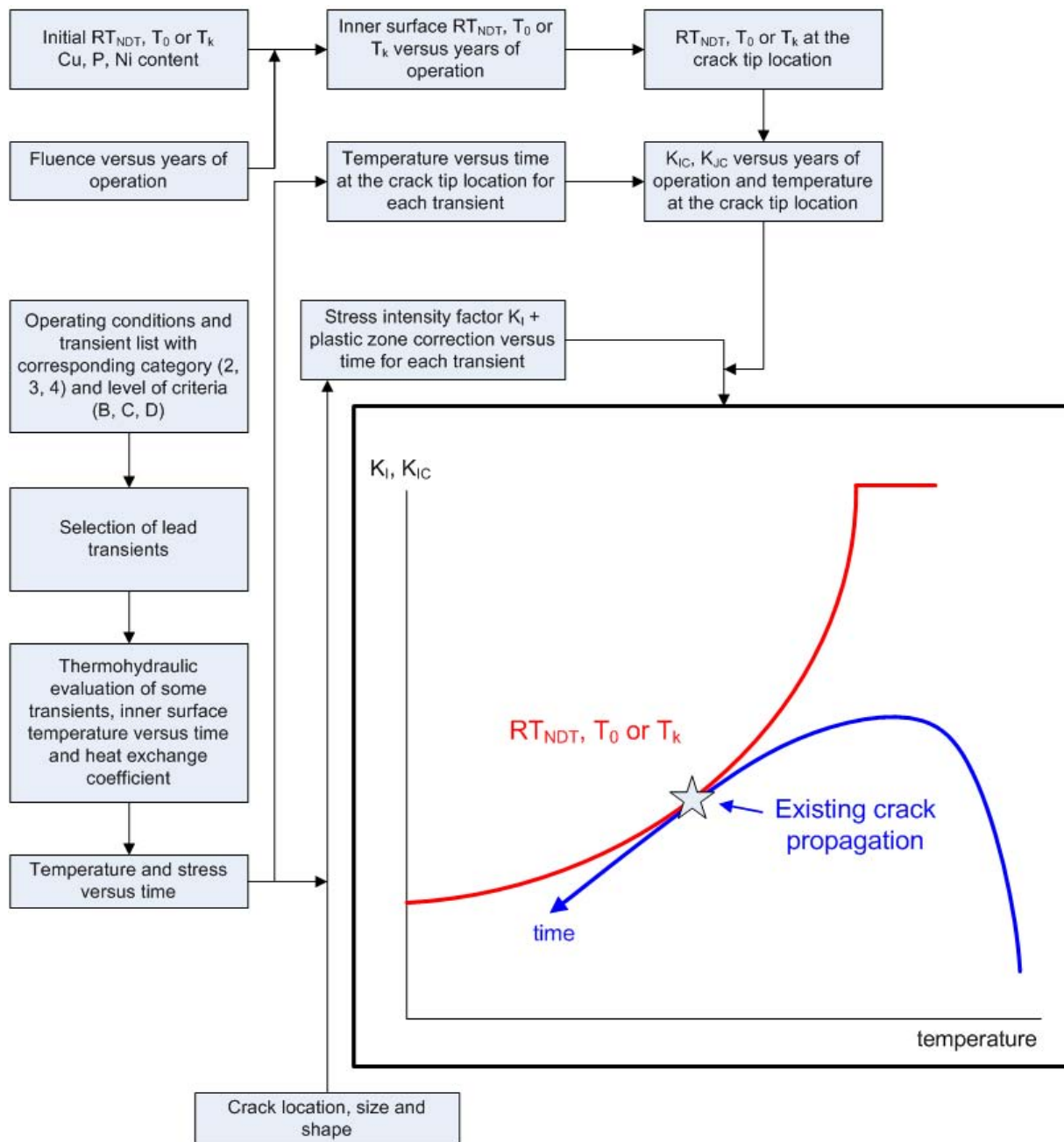


FIG. 1.1 – Schematic of a typical RPV integrity assessment process.

1.3. Coordinated research project – 9

At present several different procedures and approaches are used for RPV integrity assessment. This is the case not only between WWER and PWR reactor types, but also within each group. These differences are based, in principle, on different codes and rules used for design, manufacturing and materials used for the various types of reactors on one side, and on the different level of implementation of recent developments in fracture mechanics on the other side. It is also the main reason why results and final margin evaluation from calculations of PTS in different reactors cannot be directly compared. Moreover, with the enlargement of the European Union (EU), and also with the objective to assure sufficient safety of operating reactors in the whole of Europe as in the world, pressure has increased to demonstrate proper integrity and lifetime evaluation of PWR and WWER RPVs through round robin calculation and comparison to define the best practices.

The overall objective of this coordinated research project (CRP) was to perform benchmark deterministic calculations of a typical PTS regime with the aim of comparing effects of individual parameters on the final RPV integrity assessment, and then to recommend the best practice for their implementation in PTS procedures. This will allow better technical support to NPP operation safety and life management. It is noted that deterministic calculations also to provide a reference for probabilistic evaluations of RPV failure frequency and for optimising the fracture mechanics sub-routines used in such analyses.

The overall focus was concerned fracture mechanics issues, such as the representation of the material fracture toughness (RT_{NDT} , RT_{T0} or integral Master Curve type approaches), as well as looking in detail at issues such as:

- Postulated defect shape, size and location;
- Local thermo-mechanical loads (inner and outer surface in some cases) and through thickness stress distributions;
- Residual stresses in welds and in cladding;
- Cladding behaviour;
- Warm prestressing effect;
- Constraint effects due to shallow cracks, biaxial loading and crack length.

A major goal was to achieve a common view for PWR and WWER reactors concerning factors such as:

- Assessment scope (design, screening, flaw assessment, long term operation);
- Fracture mechanics requirements: engineering approaches and detailed finite element cracked body analyses;
- Background, criteria, definitions.

The technical activities were divided into three parts as follows:

Phase 1: “Benchmark analyses for generic PWR and WWER design”

- Definition of the benchmarks for generic WWER-440/213 and PWR-900 (3 Loop) designs, considering the participants own experience and the results previous international studies.
- Basic analysis of the benchmark problems and application of national code approaches i.e. including safety factors, as summarised in Table 1.1.
- Sensitivity studies to assess the impact of individual parameters.

The results are summarised in Appendix B.

Phase 2: “Good practice handbook for RPV deterministic integrity evaluation during PTS”.

The results of Phase 1 have been used to define the present best practices guidelines, taking into account also the knowledge of the project participants and existing data from other projects and the literature.

Phase 3: Overview on PTS assessment for the IAEA technical report series

A review of the state-of-the-art for PTS assessment technology has been performed and is published as an independent document.

Table 1.1 – Benchmark participants, national codes applied and benchmark cases studied

Participant	Reference Document	WWER			PWR		
		Basic case*	Nat. ref. doc A)**	Nat. codes B)***	Basic case*	Nat. codes A)**	Nat. codes B)***
SNERDI, China	ASME Section XI-Appendix A				+		+
NRI, Czech	VERLIFE	+	+	+	+	-	-
FNS, Finland	VERLIFE with national modification	+	+	+			
EdF, France	French RSEM code + complementary document				+		
CEA, France	French RSEM code	+			+		
AREVA NP, Germany	KTA	+			+	+	+
KFKI, Hungary	VERLIFE	+		+			
KINS, Korea	ASME Section XI Appendix A				+	+	+
OKB Hidropress, CRISM Prometey, Russia	MRKR SKhR-2004	+		+	+		
VUJE, Slovakia	VERLIFE	+	+	+			

Note:

* Basic case: benchmark analysis.

** National code A: national code approach are used, but postulated crack is the same as the basic case.

*** National code B: national code approach are used with national requirements on crack definition.

1.4. Structure

The PTS analysis is typically performed as series of sequential steps as shown in the flowchart in Figure 1.2. This Guideline follows the same basic structure. Chapter 2 discusses selection of the overcooling transients and accidents to be analysed. Chapter 3 concerns the thermal hydraulic analyses of the selected transients. Chapter 4 describes the temperature and stress field calculations, including definition of the relevant material physical and mechanical properties. Chapter 5 describes the determination of the stress intensity at real or postulated flaws, including definition of flaw geometry, location and orientation and the fracture mechanics approaches used. Chapter 6 gives details on structural analysis including the definition of the material toughness and the fracture mechanics integrity assessment. Chapter 7 provides some considerations for the assessment of flaws not located in the beltline region, such as those at nozzle corners. Chapter 8 addresses issues such as quality assurance of data and assessment tools, knowledge management and current research and development activities.

The main text is complemented by a series of Appendices, dealing with a summary of main PTS assessment criteria in different national approaches, the results of the benchmark calculations, stress intensity factor determination methods and fatigue crack growth assessment methods.

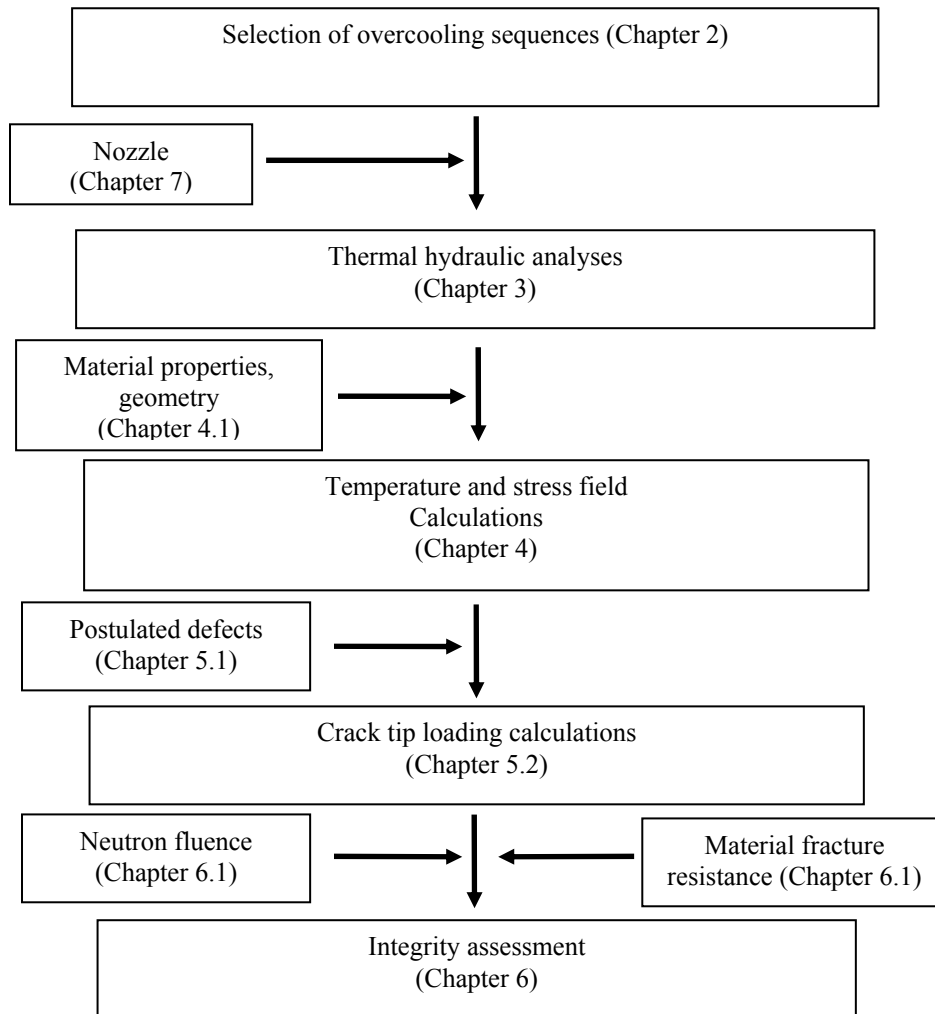


FIG. 1.2 – Basic evaluation scheme for PTS analysis.

1.5. Results of benchmark calculations including sensitivity study

This benchmark was established to validate the ability of the participants to perform correctly the assessment of reactor pressure vessel integrity for the accident of PTS type.

The benchmark was divided into three parts where first two parts were mandatory for all participants:

- First part was “Basic benchmark case” with two benchmark definitions (separately for PWR and WWER cases). The definitions of the problems were exactly prescribed and mandatory for the participants, to enable comparison of the results.;
- Second part was “National codes application”, where all participants should analyse the same transient as in the first part, but applying their own national codes;
- Third (non-mandatory) part was “Sensitivity studies”, where large set of possible sensitivity studies was divided among the participants. Altogether 15 institutes from 8 countries participated in the benchmark.

The benchmark discussed here concerns the assessment of component resistance against fast fracture for PTS events in the NPP. This assessment is based on the stress intensity factors K_I evaluation for a postulated crack and comparison with the material toughness K_{IC} .

For WWER, the PTS event “Pressurizer safety valve inadvertent opening with reclosure at 3600 s” was selected and analysed within the benchmark. Even if it is a realistic scenario for a reactor pressure vessel of the WWER 440/213 type, it is not specific for any individual NPP. The resulting maximum allowable critical temperature of brittleness T_k^a was within the range from 66°C to 71°C (results obtained by different participants). This result is only for considered hypothetical PTS events and postulated defects that are not realistic situation for any operating NPP as they were defined for the purpose of the benchmark definition.

As each participant used the different approaches, comparison of the benchmark results of national codes application is not realistic and difficult. As an example, the Code approaches are compared between ASME Code and RCCM/RSEM Code in reference [9].

Finally it can be stated, that participation in the IAEA PTS Benchmark was recognized as a very efficient way to improve the user qualification and to reduce user effect on results of analysis. The experience obtained within this benchmark provided a basis for the creation of this IAEA-TECDOC.

1.6. References

- [1] CHEVERTON, R. D., SELBY, D. L., A probabilistic approach to the evaluation of the pressurized thermal shock issue, US-USSR exchange meeting on reactor safety, 25–29 June, Moscow (1990).
- [2] AMERICAN SOCIETY FOR MECHANICAL ENGINEERS, ASME Boiler and Pressure Vessel Code, Section XI, “Rules for Inservice Inspection of Nuclear Power Plant Components”, New York (2004).
- [3] ASSOCIATION FRANÇAISE POUR LES REGLES DE CONCEPTION ET DE CONSTRUCTION DES MATERIELS DE CHAUDIERES ELECTRONUCLEAIRES, RSE-M, In-Service Inspection Rules for Mechanical Components of PWR Islands, Paris (1997).
- [4] KERNTECHNISCHER AUSSCHUSS, Components of the Reactor Coolant Pressure Boundary of Light Water Reactors, Design and Analysis, KTA 3201 Part 2, Cologne (1996).
- [5] CALCULATION PROCEDURE FOR EVALUATION OF BRITTLE STRENGTH OF VVER RPV DURING OPERATION, MRKR-SKhR-2004, RD EO 0606-2005, Moscow (2004).
- [6] UNIFIED PROCEDURE FOR LIFETIME ASSESSMENT OF COMPONENTS AND PIPING IN VVER NPPS “VERLIFE”, Řež (2008).
- [7] INTERNATIONAL ATOMIC ENERGY AGENCY, Guidelines on Pressurized Thermal Shock Analysis of WWER Nuclear Power Plants, IAEA-EBP-WWER-08, IAEA, Vienna (2005).
- [8] FAIDY, C., Comparison of French and USA practices for RPV Structural Integrity Rules, Pressure Vessel and Piping Conference – PVP 07, PVP-2007 26350, 22–26 July, San Antonio (2007).
- [9] U.S. NUCLEAR REGULATORY COMMISSION, Technical Basis for Revision of the Pressurized Thermal Shock Screening Limit in the PTS Rule (10 CFR 50.61): Summary Report, NUREG-1806, US NRC, Washington (2007).

2. SELECTION OF OVERCOOLING SEQUENCES

2.1. General considerations

The selection of PTS transients should be performed in a comprehensive way starting from the accident scenarios identified in the safety analysis report. The main goal is to select initiating events which by themselves are PTS events or along with other consequences can lead to a PTS event. The sequences to be considered in the PTS analysis are frequently unit specific and all relevant and meaningful plant features should be taken into account. The sequences may also need to be classified in terms of severity if this is foreseen in the code being applied. In this case, the selection should be consistent with probabilistic risk assessment (PRA), if used. Comprehensive probabilistic PTS studies are carried out in some countries to select the most important PTS sequences contributing to RPV failure risk. If the failure risk (sequence frequency \times conditional failure probability) is less than a described limit (e.g. 10^{-8}) the sequence is considered minor importance and it can be removed from the sequence list of PTS cases.

2.2. Precursors

Selection of the transients for deterministic analysis can be based on analysis and engineering judgment using the design basis accident analysis approach, combined with operational experience. It is important to consider several factors determining thermal and mechanical loading mechanisms in the downcomer during the overcooling events.

These factors are:

- Final temperature in the downcomer;
- Temperature decrease rate;
- Nonuniform cooling of the RPV, characterized by cold plumes and their interaction and by the nonuniformity of the coolant-to-wall heat transfer coefficient in the downcomer;
- Level of primary pressure;
- Width of cold plume;
- Initial temperature in downcomer;
- Stratification or stagnation of flow in cold leg.;

An alternative approach to the selection of transients is the probabilistic risk assessment. This can help in identifying those specific transient scenarios that contribute most significantly to the total PTS risk. In this case a broad risk assessment is performed to assess the PTS risk of several cooldown transients. It is noted that probabilistic PTS analysis is considered complementary to the deterministic analysis of the limiting scenarios.

As illustrated in the Figure 2.1, three main models (shown as solid blue squares), taken together, allow us to estimate the annual frequency of through-wall cracking in an RPV:

- Probabilistic risk assessment (PRA) event sequence analysis;
- Thermal-hydraulic (TH) analysis;
- Probabilistic fracture mechanics (PFM) analysis.

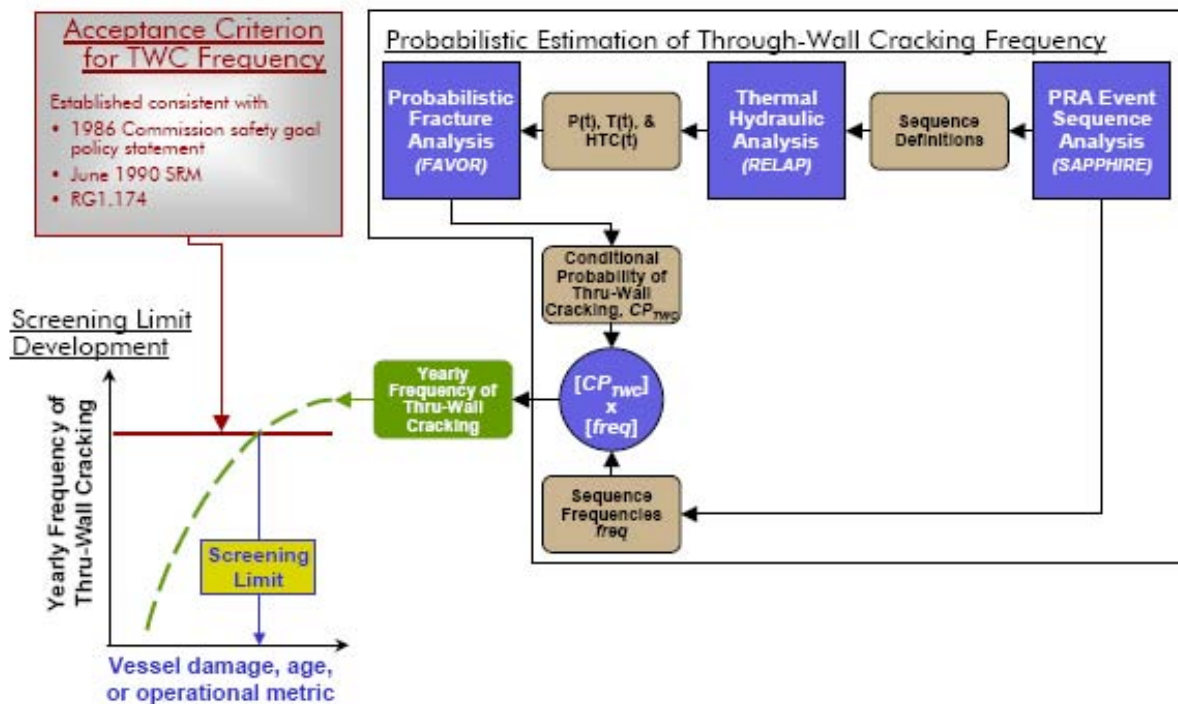


FIG. 2.1 – Schematic showing how a probabilistic estimate of through-wall cracking frequency (TWCF) is combined with a TWCF acceptance criterion to arrive at a proposed revision of the PTS screening limit A [3].

As such, while this section focuses on the PRA and HRA (hereafter referred to as PRA unless specifically dealing with HRA) aspects of the reanalysis, important interfaces with the other technical disciplines are noted and cannot be completely separated from what was done in the PRA portion of the PTS reanalysis project. A key final product of this reanalysis project is the estimation of TWCFs associated with severe overcooling scenarios.

The PRA portion of the reanalysis project had three primary purposes:

- (1) Define the overcooling scenarios (sequences) with the potential for being PTS challenges;
- (2) Direct the TH analysis as to the specific sequences to be modelled to obtain plant TH response information to be forwarded to the PFM analysts;
- (3) Estimate the frequencies, including uncertainties, for those overcooling sequences that are potentially important to the PTS results and provide that information to the PFM analysts.

A multi-step approach was followed to produce the probabilistic risk assessment products for the PTS reanalysis. Figure 2.2 depicts the steps followed to define the sequences of events that may lead to PTS (for input to the TH model), as well as the frequencies with which these sequences are expected to occur (for combination with the probabilistic fracture mechanics (PFM) results to estimate the annual frequency of through-wall cracking). Although the approach is illustrated in a serial fashion, its implementation involved multiple iterative passes through the various steps as the analyses and mathematical representations of each plant evolved.

The following sections describe seven steps that together comprise the PRA analysis:

- Step 1: Collect information;
- Step 2: Identify the scope and features of the PRA model;
- Step 3: Construct the PRA models;
- Step 4: Quantify and bin the PRA modelled sequences;
- Step 5: Revise PRA models and quantification;
- Step 6: Perform uncertainty analysis;
- Step 7: Incorporate uncertainty and finalize results.

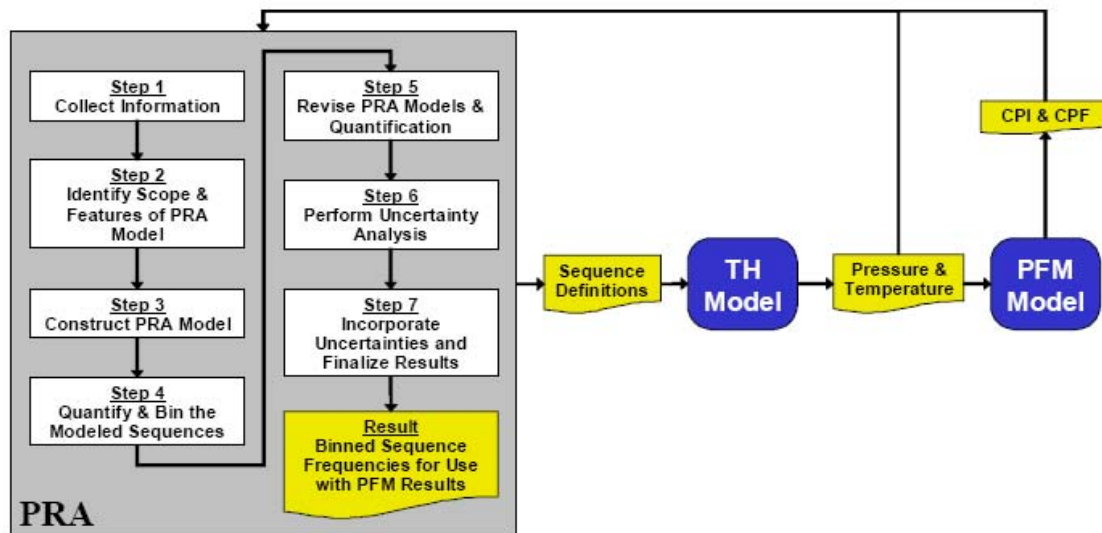


FIG. 2.2 – Diagrammatic representation of the PRA approach [3].

2.3. Categorization of sequences of initiating events and corresponding criteria

The complexity of many interacting systems and operator actions makes it very difficult to determine the limiting PTS sequences and what is their significance. Although most countries use a deterministic approach, it is also possible to perform integrated probabilistic PTS studies to reveal the probability of individual events. Potential risk from all credible overcooling events may be higher than from postulated limiting events, even though each event individually is less severe than the limiting one. Therefore for events with high probability of occurrence, more stringent requirements can be applied to assure RPV integrity. Based on the frequency of occurrence the initiating events may be categorized into the following groups:

Anticipated transients:

Defined as relatively frequent deviations (frequency of occurrence higher than 10^{-2} per reactor year) from normal operating conditions which are caused by malfunction of a component or operator error. These transients should not have safety related consequences to RPV integrity, which would prevent the continued plant operation.

Postulated accidents:

Defined as rare deviations from normal operation which are not expected to occur (less than 10^{-2} per reactor year globally) but are considered in the original design or in the design of plant upgrading or are based on plant safety reassessment. For these events, immediate resumption of operation may not be possible. For accident from this group the PTS analyses are usually performed.

Beyond design base accidents:

Defined as transients leading to core degradations or high radiological consequences, which are expected to occur with frequency of occurrence less than 10^{-5} per reactor year globally; PTS calculations are not performed for those events.

2.4. Initiating events groups

The aim of setting up a list of initiating events is to assure a complete analysis of the RPV response to postulated disturbances which may threaten its integrity. The analysis should determine the consequences and evaluate the capability built into the plant to withstand such loadings.

The sequences should be considered for various plant operating conditions: full power, hot zero power, heat-up, cooldown and cold shutdown.

The complexity of many interacting systems and operator actions makes it sometimes very difficult to choose the limiting transients. At least the following groups of initiating events should be taken into account.

Compilation of the list of initiating events corresponding to each of the following groups is usually based on engineering judgment while assisted with probabilistic consideration available in the Safety Analysis Report of the plant., taking into account the design features and implemented modification of the given nuclear plant.

Loss of coolant accidents

Different sizes of both cold and hot leg loss of coolant accidents (LOCA) which are characterized by rapid cooldown should be considered. Attention should be paid on the scenarios leading to flow stagnation which causes faster cooldown rate and cold plumes in the downcomer. Attention should be given to breaks sizes corresponding to existing pipes connected to primary system. Cold repressurization of the reactor vessel is usually prohibited in principle, but the possibility of isolating the leak and the subsequent repressurization have to be considered.

Stuck open pressurizer safety or relief valve

After an overcooling transient caused by a stuck open pressurizer safety or relief valve, possible reclosure can cause a severe repressurization. Even without the valve reclosing, the system pressure can remain high after having reached the final temperature. The low decay power may further lead to the main loop flow stagnation. In addition, the “feed and bleed” method of mitigation for loss of feedwater should be assessed.

Primary to secondary leakage accidents

Different sizes for both single and multiple steam generator tube ruptures up to the full steam generator collector cover opening should be considered. The risk of repressurization should be taken into account, if the relevant emergency operation procedure contains a requirement to isolate the affected steam generator by closing of main gate valves.

Large secondary leaks

Transients with secondary side de-pressurization caused either by the loss of integrity of the secondary circuit or by the inadvertent opening of a steam dump valve can cause significant cooldown of the primary side. Consequently, start of high pressure injection due to low primary pressure (and/or low pressurizer level or directly due to low secondary circuit parameters), which leads to repressurization, can be expected. The degree of secondary side de-pressurization is strongly dependent on the plant configurations (mainly presence of fast acting main steam isolation valves and the criteria for steam line isolation).

Possible sources of secondary side de-pressurization are as follows:

- Steam line break;
- Main steam header break;
- Spurious opening and sticking open of the turbine bypass valve, atmospheric dump valve and steam generator safety valve(s);
- Feedwater line break.

After the leaking steam generator(s) is (are) empty, the temperature increase in the primary circuit can lead to an increase in primary pressure (this pressurization is very fast, especially in the case when the primary circuit is completely filled by fluid due to previous ECCS injection). During this process, the opening of the pressurizer relief or safety valve can occur and the valve can stick open under fluid flow conditions. The resulting PTS effects should also be considered.

Inadvertent actuation of high pressure injection or make-up systems

This kind of accident can result in a rapid pressure increase in primary system. Cold, hot, and cooldown initial conditions should be considered.

Accidents resulting in cooling of the RPV from outside

In some NPPs, there are several possible sources capable to flood the whole reactor cavity (e.g. break of the biological shield tank, ECCS or containment spray system actuation, loss of coolant from primary or secondary circuit, intentional cavity flooding, unintentional inadvertent actuation of a cavity flooding system — system installed in some plants for severe accident mitigation). Moreover, if a leak is assumed close to the RPV nozzle, the subcooled water flowing out of the leak forms a water stripe on the outer RPV wall surface and slowly fills the reactor cavity. These events should be considered in this group of accidents.

2.5. References

- [1] INTERNATIONAL ATOMIC ENERGY AGENCY, Safety Assessment and Verification for Nuclear Power Plants, IAEA NS-G-1.2, IAEA, Vienna (2002).
- [2] INTERNATIONAL ATOMIC ENERGY AGENCY, Procedures for Analysis of Accidents in Shutdown Modes for WWER Nuclear Power Plants, IAEA-EBP-WWER-09, IAEA, Vienna (1997).
- [3] U.S. NUCLEAR REGULATORY COMMISSION, Technical Basis for Revision of the Pressurized Thermal Shock (PTS) Screening Limit in the PTS Rule (10 CFR 50.61), NUREG-1806, Vol. 1, US NRC, Washington (2007).

3. THERMAL HYDRAULIC ANALYSES

Thermal hydraulic (TH) analyses have two main objectives:

- To support the transient selection process²; and
- To provide the following input data for the structural analyses of the RPV:
 - Fluid temperature in the downcomer (and primary nozzle region), together with the local wall-to-coolant heat transfer coefficients (or alternatively the time-temperature data at the inner surface of RPV wall);
 - Primary circuit pressure.

3.1. Sequence analysis plan

The overall progression of accidents (referred to as a sequence) is calculated with advanced thermal-hydraulic system codes. The output from these is primarily the time variation of primary side pressure, coolant temperature and loop mass flow rates, and further the temperature and mass flow rate of the sub-cooled water injected by emergency systems into the primary circuit.

- Conservative sequences: Conservative assumption for the system TH analyses should be selected in such a way that the following general criteria are met:
 - Maximum coolant flow to downcomer from primary system in case of LOCA, or from secondary system in case of feed water line break and from ECCS tanks (including trays of bubble condenser);
 - Minimum temperature of water;
 - Maximum primary pressure.
- Best estimate sequences are only considered for very low probability events.

In case of non-symmetric cooldown and/or flow stagnation in the primary circuit, when buoyancy induced forces dominate the fluid flow behaviour in cold legs and the downcomer, the system code results are no longer reliable for calculation of the temperature fields. Further considerations regarding plumes and the associated thermal mixing calculations are given in section 3.6.3.

The role of the thermal hydraulic system codes is, in addition to the inner pressure calculations, to give the initial and boundary conditions for thermal mixing calculations. Based on these system codes results the initiation of primary side stagnation is estimated in the thermal mixing calculation. The calculation period of a transient should always exceed the critical time from the point of view of the RPV integrity assessment or to reach the termination of the PTS regime by operator action.

3.2. Calculation method requirements

The calculation methods should be validated for this purpose. Thermal hydraulic analyses of overcooling sequences include many features that are different from those in accident analyses performed with respect to core cooling. The utilized methods must be capable of modelling the normal operation systems, such as control systems, main feedwater system and make-up system because the proper operation of these systems usually leads to more severe overcooling. Heat losses from the systems should be modelled in system thermal hydraulic analyses. Direct ECCS injection into reactor vessel (especially into the downcomer) should be modelled. Plus, if flow baffles exist in the neighbourhood of hydro-accumulator line connections to the reactor downcomer, then these baffles must be modelled in the system thermal hydraulic and mixing calculation, as they can deteriorate a course of LOCA from the PTS point of view. The pressurizer modelling used in the code must be capable of calculating the pressure which can occur after the repressurization of the primary circuit.

² Overcooling transients are usually very complex and it is often not possible to define in advance conservative or limiting conditions for all system parameters. Thermal hydraulic, and in some cases even fracture mechanics, analyses are necessary for choosing those initiating events and scenarios that can be identified as limiting cases for a given group of events.

Non-uniform cooldown should be analysed with appropriate fluid mixing codes that are capable of taking into account thermal stratification of high pressure injection water in the cold leg. They should be able to determine the azimuthal, axial, and in some cases also radial fluid temperature distribution in the downcomer and the azimuthal and axial distribution of the heat transfer coefficient to the RPV wall (see Appendix C). Current quasi 3D methods applied in mixing codes based on engineering models or on the regional mixing model allow sufficiently accurate calculation of the extent of the thermal stratification integrated into the overall system response.

The exponential decay of the temperature in the mixing volume (mixing cup model) gives very simple presentation for transient cooldown. This approach can also be used when the mixing volume is properly defined and the heat transfer from the RPV wall is also added.

3.3. Boundary conditions

3.3.1. Plant operating conditions

The initial power of the reactor has always to be set to the most conservative value determined by the conditions of the overcooling transient. The following operating conditions should be analysed:

- Normal operation at nominal power;
- Hot zero power;
- Heat-up, cooldown;
- Cold shutdown regimes.

The value of the residual heat should be the lowest possible one, defined on the basis of the initial power level. For this reason the analyses are to be performed for the initial period of the fuel cycle (after longest planned outage). The estimated error of the residual heat calculation is to be taken into consideration with negative value. The determination of the residual heat might be based on actual operational measurement information except for cases of low power operation.

Other initial conditions such as reactor coolant flow rate, temperature as well as pressure and steam generator water level should be chosen conservatively. Concerning the parameters of the normal operation and control systems, the expected values based on the operational experience should be assumed as they usually tend to lead to more serious overcooling. Failure of components of these systems (when it is not a direct consequence of the initial event) should be considered only in cases that lead to more severe PTS loading. The loss of the external power supply has to be taken into consideration as an additional failure if it will further aggravate the analysis results.

The availability of the emergency core cooling systems should be taken into consideration in such a way as to produce the most intensive overall cooling or the most unsymmetric cooling.

Typically, the maximum thermal load on the cylindrical RPV part in core elevation is reached in case the most intensive overall cooling is applied. However, often a comparable thermal load can be reached on this RPV region applying unsymmetrical cooling. That is, plumes can have almost the same thermal load increasing effect as a quicker overall cooldown.

The most unsymmetrical cooling is applied in order to reach the maximum thermal load at the cold leg nozzle exit or inside the hot leg nozzle. This is because a higher ECC injection rate per leg can be reached in case of a small or medium leak scenario when only part of the ECC systems is injecting. Consequently maximum ECC injection rates are applied to reach the maximum thermal loads in all relevant RPV regions. It is assumed that the systems operate on maximum installed capacity (with corresponding head value taken according to maximum pump characteristics) and that they inject the lowest possible temperature cooling water to the primary circuit. Time variation of injected water temperature should also be conservatively evaluated (e.g. automatic switching from heated high to non heated low pressure tanks) along with considering a relevant single failure.

The stuck open safety valve should be considered as a consequential failure if the valve is not qualified for the discharged coolant (liquid or steam-water mixture) or if there is a demand for a large number of successive cycles.

The possible later reclosure of the opened and stuck open safety valve should be taken into account. The reclosure can lead to the repressurization by the normal operating make-up or safety injection pumps or, in case of the water solid primary system (completely filled by water), through thermal expansion of coolant volume. The time of the safety valve reclosure should be selected conservatively from the PTS severity point of view. In the case that operation of the secondary circuit steam and feedwater systems results in cooling and depressurization of the primary circuit, then those systems have to be taken into account.

3.3.2. Symmetric cooling

If forced or intensive natural circulation is maintained, homogeneous cooling of the whole primary circuit can be assumed (except for the pressurizer and reactor upper head). In these conditions the cooling of the reactor pressure vessel can be assumed axisymmetric.

According to the results of studies performed in the scope of the US PTS re-evaluation [2], for US reactor designs the simplifying assumption of uniform temperatures can be assumed in the downcomer, in the region adjacent to the core. It is only in this region that the vessel is embrittled. The top of the core is approximately 5 feet below the cold leg. This distance provides a mixing zone for cold fluid entering the downcomer from the cold legs before it reaches the embrittled zone of the reactor vessel. The uniform temperature distribution allows the fracture mechanics analysis to be treated with a one dimensional assumption regarding vessel wall temperature distribution, which greatly simplifies the calculations. A detailed justification for this conclusion is given in [3].

Symmetrical cooling can also be applied at primary side stagnation in case of relatively high cold side cold water injection rates e.g. for a double-ended guillotine break for German PWRs. The high injection rate leads to a quick cooldown to the cold water temperature, giving to a symmetrical thermal shock without plumes.

For WWER reactor designs, the downcomer width is less than in western designs, so that mixing of the injected ECCS water is less efficient and the role of plumes may be correspondingly greater.

3.3.3. Plume cooling

If flow stagnation occurs in the primary system, the cooling process has to be investigated in a significantly smaller volume. In such cases it has to be taken into account that below the cold legs with cold water injection plumes will exist causing the temperature and heat transfer coefficient distribution to be non-uniform.

In case of flow stagnation, thermal mixing and plume cooling of the RPV wall occurs when the downcomer and the cold legs are totally filled with water. A cold stream, caused either by ECCS water injection or by an increased heat removal from the primary to the secondary side in affected loops, flows in the cold loop towards the RPV inlet and falls into the downcomer forming a quasi-planar buoyant plume. In case of direct ECCS water injection into the downcomer, as applied in WWER, the plume origin is at the lower edge of the injection nozzle.

Condensation and strip cooling of the RPV wall takes place when the cold legs are partially filled with steam and the collapsed water level in the downcomer is below the lower edge of cold leg. A cold stream caused by ECC water injection flows at the bottom of the cold leg towards the RPV inlet and falls into the downcomer forming a strip directly in contact with the RPV wall. The stripe detaches from the RPV wall when higher cold leg ECC injection rates are applied. In case of direct ECC water injection into the downcomer, the ECC water impinges on the core barrel forming a water film which flows along the core

barrel. To account for these effects, sophisticated 3D computer codes that are able to treat two-phase flow phenomena or engineering calculation methods verified on experimental data are needed to account for the associated condensation processes.

The number of plumes depends on the break location and the configuration of the injection system. The most asymmetric situation of plumes around the RPV may be of importance for numerical fracture mechanics simulations. Additional information concerning analysis of plumes and associated mixing phenomena is given in Appendix C.

3.3.4. Failures

Failure of components of systems (when it is not direct consequence of the initial event) should be considered only in cases that lead to more severe PTS loading. Only single failure criteria need to be considered, in accordance with the safety analysis report .

3.4. Operator actions

Prior to the analysis, those operator's activities that are to be carried out in the case of a given overcooling transient should be determined, as specified in the safety analysis report (SAR). The estimated time of the operator's intervention is to be evaluated separately.

For WWER reactors, two different groups of operator actions can have a significant impact. The first group is where operator actions may turn an ongoing accident sequence into a PTS transient. Such adverse actions should be identified and removed from the operating procedures where possible. The second group includes actions that have a possible impact by mitigating the severity of an ongoing PTS transient. Further information is given in [4].

3.5. References

- [1] SIEVERS, J., SCHULZ, H., BASS, B.R., PUGH, C.E., KEENEY, J., CSNI Project for Fracture Analyses of Large Scale International Reference Experiments (Phase I), GRS-108, NEA/CSNI/R (NUREG/CR 5997), Washington (1994).
- [2] U.S. NUCLEAR REGULATORY COMMISSION, Technical Basis for Revision of the Pressurized Thermal Shock (PTS) Screening Limit in the PTS Rule (10 CFR 50.61): Summary Report, NUREG-1806, US NRC, Washington (2007).
- [3] U.S. NUCLEAR REGULATORY COMMISSION, Thermal-Hydraulic Evaluation of Pressurized Thermal Shock, NUREG-1809, US NRC, Washington (2005).
- [4] INTERNATIONAL ATOMIC ENERGY AGENCY, Guidelines on Pressurized Thermal Shock Analysis for WWER Nuclear Power Plants, IAEA-EBP-WWER-08 (Rev.1), IAEA, Vienna (2006).

4. TEMPERATURE AND STRESS FIELD CALCULATIONS

Temperature and stress distributions in the RPV wall during PTS transients are needed to assess the integrity of the vessel. This chapter describes the main input parameters used in the temperature and stress field calculations. These parameters include e.g. the physical properties of base/weld and cladding material, boundary conditions, stress-free temperature, and residual stresses. Generally accepted values of physical parameters are given for WWER and PWR plants to be used if plant specific data are not available.

4.1. Physical properties

In order to perform the corresponding thermal and thermal mechanic stress analysis for the RPV; different material properties have to be defined with their variation with temperature:

- The elastic modulus, E ;
- The thermal expansion coefficient, α_{ref} ;
- The thermal expansion coefficient corresponding the zero-stress-temperature, α_0 ;
- The thermal conductivity, λ ;
- The thermal diffusivity, $\lambda / \rho C$;
- The yield stress of the material, σ_y or $R_{p0.2}$.

For PWRs these values are generally provided in the construction codes (ASME Section II [1], RCC-M [2] or KTA [3]). For WWERs, reference values are also given in the VERLIFE procedure [4], and the Russian Standard MRKR-SKhr-2004 [5] contains physical and mechanical properties of the relevant materials. The analyst can propose alternative values if suitably justified.

Concerning the effect of irradiation on the tensile properties, it is noted that the beginning of life values are in most cases conservative and their influences are negligible compared to other uncertainties in PTS analyses. The irradiation effects can be taken into account if they are reliably known and required by the national code or the authority.

Stress-strain curves for WWER RPV base and weld metal are presented in Russian standard [6]. In this standard are also included recommendations on how to take into account irradiation effect for stress-strain curves (change in yield stress $R_{p0.2}$).

The following tables provide representative values of thermo-mechanical properties for the two broad classes of reactor types.

Table 4.1 – Representative thermo-mechanical properties for WWER-440 vessels [4]

Material	T [°C]	E [GPa]	α_{ref} [$10^{-6} K^{-1}$]	α_0 [$10^{-6} K^{-1}$]	ν	λ [$Wm^{-1}K^{-1}$]	C_p [$Jkg^{-1}K^{-1}$]	ρ [kgm^{-3}]	$\lambda / \rho C_p$ [$10^{-6} m^2 s^{-1}$]
Base material or weld	20	210		12.9	0.3	35.9	445	7821	10.32
	100	205	11.9	13.3	0.3	37.3	477	7799	10.03
	200	200	12.5	13.9	0.3	38.1	520	7771	9.43
	300	195	13.1	14.5	0.3	37.3	562	7740	8.57
Cladding	20	165		15.9	0.3	15.1	461	7900	4.15
	100	160	14.6	16.5	0.3	16.3	494	7868	4.19
	200	153	15.7	16.5	0.3	17.6	515	7830	4.36
	300	146	16.0	16.8	0.3	18.8	536	7790	4.50

Table 4.2 – Representative thermo-mechanical properties for WWER-1000 vessels [4]

Material	T [°C]	E [GPa]	α_{ref} [$10^{-6} K^{-1}$]	α_0 [$10^{-6} K^{-1}$]	ν	λ [$Wm^{-1}K^{-1}$]	C_p [$Jkg^{-1}K^{-1}$]	ρ [kgm^{-3}]	$\lambda / \rho C_p$ [$10^{-6} m^2 s^{-1}$]
Base material or weld	20	208		12.5	0.3	35	446.9	7830	10.00
	50				0.3	35.5	458.9	7822	9.89
	100	201	11.6	12.9	0.3	36.1	478.8	7809	9.66
	150				0.3	36.6	499.7	7795	9.40
	200	193	12	13.6	0.3	36.8	520.4	7780	9.09
	250				0.3	36.6	541.2	7765	8.71
	300	183	12.6	14.2	0.3	36.2	562	7750	8.31
	350	177.5			0.3	35.6	584.6	7733	7.87
Cladding	20	165		16.6	0.3	13.2	448.9	7900	3.72
	50				0.3	13.5	460.4	7889	3.72
	100	160	15.7	17	0.3	14.4	479.6	7870	3.82
	150				0.3	15.3	499.6	7851	3.90
	200	153	16.1	17.6	0.3	16.4	519.2	7830	4.03
	250				0.3	17.5	538.7	7809	4.16
	300	146	16.7	18.2	0.3	18.4	558.5	7788	4.23
	350	142			0.3	19.6	579.2	7766	4.36

Table 4.3 – Thermo-mechanic properties for PWR material [1]

Material	T [°C]	E [$10^3 MPa$]	α_{ref} [$10^{-6} K^{-1}$]	ν	λ [$Wm^{-1}K^{-1}$]	ρ [kgm^{-3}]	$\lambda / \rho C_p$ [$10^{-6} m^2 s^{-1}$]
Base material or weld	20	191		0.3		7800	
	50		11.78	0.3	40.8		11.47
	100	187	12.10	0.3	40.6		10.88
	150	184	12.43	0.3	40.4		10.33
	200	181	12.75	0.3	40.1		9.82
	250	178	13.08	0.3	39.5		9.32
	300	174	13.22	0.3	38.7		8.82
	350	171	13.54	0.3	37.8		8.32
Cladding	20	195		0.3		7900	
	50		15.64	0.3	14.6		3.64
	100	189	16.11	0.3	15.4		3.75
	150	186	16.57	0.3	16.1		3.86
	200	183	17.04	0.3	16.8		3.98
	250	179	17.40	0.3	17.6		4.11
	300	176	17.64	0.3	18.3		4.22
	350	172	17.86	0.3	19.0		4.33

4.2. Temperature and stress fields

4.2.1. Heat transfer analysis

The first step in the evaluation of RPV integrity during PTS transients is the assessment of thermal loads (temperature fields) in the vessel wall at different time steps during each transient. Generally, an uncoupled heat transfer analysis is carried out to assess the temperature distribution in RPV wall taking into account boundary conditions and the temperature dependency of material properties. Boundary conditions are generally nonlinear, for example, the film coefficient (heat transfer coefficient α or h) can be function of surface temperature and so the heat transfer analysis is also nonlinear. The distribution of cold plumes around the circumference of RPV should be taken into account when boundary conditions (symmetry of loading) and extend of the model in circumferential direction are defined. For the heat transfer analysis by FEM, a boundary without any prescribed boundary conditions corresponds to an insulated surface.

The thermal conductivity, specific heat and density of the materials must be defined for transient PTS problems. Thermal expansion coefficients are not meaningful in an uncoupled heat transfer analysis since deformations of the structure are not considered.

Most of the FEM codes use an iterative scheme to solve the nonlinear heat transfer problems. For PTS transients, fixed time incrementation or automatic incrementation can be used to solve the heat transfer analysis depending on the nonlinearity of the case. For fixed incrementation the timestep size Δt should be chosen depending on the “mesh size Δl ” to achieve convergence for nonlinear problems.

For highly nonlinear cases automatic time incrementation is recommended. Criteria for the convergence and the number of iteration cycles should be chosen carefully according to the FEM code manual recommendation to achieve reliable results.

In heat transfer transients, spurious oscillations due to small time increments with second-order elements can occur. If second-order elements are used, the time increment should comply with the following simple expression:

$$\Delta t > \frac{\rho c}{6k} \cdot \Delta l^2 \quad (4.1)$$

where Δt is the time increment, ρ is the density, c is the specific heat, k is the thermal conductivity, and Δl is a typical element dimension (such as the length of a side of an element).

In transient analyses using first-order elements the heat capacity terms are lumped, which eliminates such oscillations but can lead to locally inaccurate solutions especially in terms of the heat flux for small time increments. If smaller time increments are required, a finer mesh should be used in regions where the temperature changes occur. On the other hand, the time steps should be small enough to describe the transient in detail mainly in times with rapid changes of coolant temperatures and close to the expected critical time moment of the PTS transient.

4.2.2. Stress and strain analysis

Calculation of stresses and strains shall be carried out preferably using advanced numerical methods, e.g. finite elements method (FEM) which enable complex material and load response modelling. Simplified analytical calculations based on formulae can be applied if they are verified and their use is accepted by regulatory organizations.

The stresses due to internal pressure, temperature gradients, and residual stresses for both cladding and welds should be taken into account, including the beneficial effect of the first hydrotest if deemed useful. Plasticity effects should be also considered. It is common practice to choose the value of zero-stress-

temperature equal to normal operation coolant temperature in the downcomer. Alternatively the value of stress free temperature can be taken to provide stresses in the cladding at the level of yield stress at the room temperature used in the PTS analysis.

For simplified analytical solutions, the additional stresses due to plume or strip effects (if justified) can be considered as follows. Once a plume forms, the axial stresses increase and can lead to higher loading of postulated circumferential flaws in the case of a strong plume effect. An estimation of the thermally induced axial stress assuming the region of the vessel outside the plume is infinitely rigid:

$$\sigma_{tcv(z,t)} = E \cdot \alpha \cdot (T_{mean, outside\ plume(t)} - T_{mean, in\ plume(t)}) \quad (4.2)$$

where $\sigma_{tcv}(z,t)$ is the thermal axial stress component associated with circumferential coolant variation at height z , α is the coefficient of expansion, E is the elastic modulus, $T_{mean, outside(t)}$ is the time dependant average through-wall temperature outside of plume region and $T_{mean, inside(t)}$ is time dependant average through-wall temperature in plume region. If the plume width and location-specific material properties (outside plume, in plume) are considered, the value is given by:

$$\sigma_{tcv(z,t)} = \left(1 - \frac{\phi}{2\pi}\right) \cdot ((\alpha \cdot E \cdot T)_{outside\ plume(t)} - (\alpha \cdot E \cdot T)_{in\ plume(t)}) \quad (4.3)$$

Here ϕ is the plume width in radian, T is temperature and the material properties (coefficient of expansion α , Young's modulus E) are time dependent and are considered at crack tip depth (consideration of average through-wall properties leads to Equation 4.2), inside and outside the plume region. The highest value should be considered in the assessment. The additional stress is linearly superimposed on the time dependent stresses caused by the combination of the temperature gradient across the wall and the pressure. Figure 4.1 illustrates the effect from analyses performed in the WWER benchmark case in Appendix B. The reduction of fracture toughness caused by the lower temperatures in the plume affected region of the vessel should be taken into account in the fracture assessment.

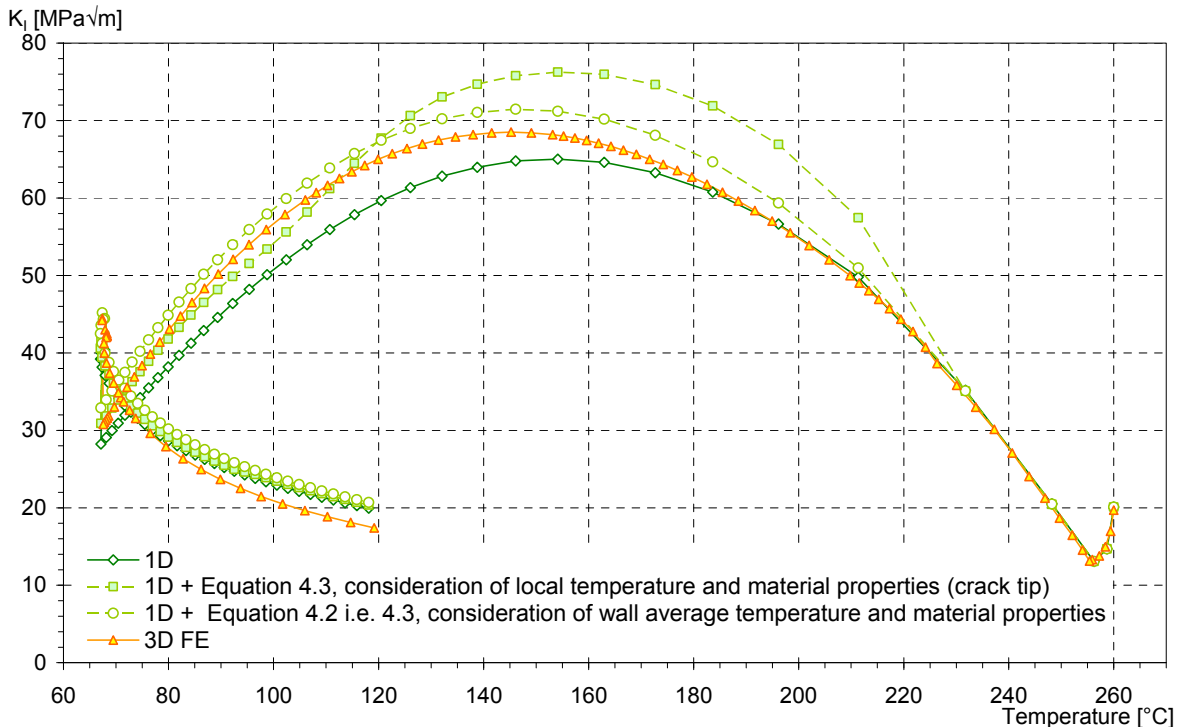


FIG. 4.1 – Example of the effect of including plume-induced stresses on the crack driving force from the WWER basic case benchmark (Appendix B, with circumferential crack), comparing the full 3D FE simulation with simplified solutions considering the thermally-induced axial stress as per equations 4.2 and 4.3.

Residual stresses can influence the integrity analysis results depending on how they are treated (see sections 4.3 and 4.4 below). Stress fields are calculated on the basis of temperature dependent material properties for base and/or weld materials and cladding. Changes of material tensile properties due to neutron irradiation can be taken into account in the stress field calculation.

As regards the suitability of chosen material model in connection to calculated stress values following observations and recommendations are available:

- Elastic-plastic models in compare with linear elastic model offer more realistic stress variations through the wall thickness; in cladding area elastic-plastic stresses are lower than elastic ones, in base metal these difference is opposite, but not such high as in the former case;
- The actual values of stress components and arisen differences are dependent on actual applied model parameters;
- Elastic-plastic models utilizing irradiated material properties seems to be more conservative in compare with elastic plastic models utilizing initial material properties in many cases (in areas without crack), i.e. they result in higher stresses in cladding.

The influence of above mentioned material models should be considered in calculation of J and K_I values. Criteria for the convergence and the number of iteration cycles should be chosen carefully to achieve valid results.

The following formula for thermal expansion coefficient correction should be used in the case where the FEM code used for elastic and elastic-plastic calculations does not correct it automatically to stress-free-temperature T_{sf} (this is different from reference temperature T_{ref} used for thermal expansion coefficient measurement):

$$\alpha_0(T) = \frac{\alpha_{ref}(T) \cdot (T - T_{ref}) - \alpha_{ref}(T_{sf}) \cdot (T_{sf} - T_{ref})}{(T - T_{sf}) \cdot [1 + \alpha_{ref}(T_{sf}) \cdot (T_{sf} - T_{ref})]} \quad (4.4)$$

4.3. Weld residual stresses

The core section of the RPV is manufactures from cylindrical forgings which are welded together by a circumferential weld. Before welding the forgings are covered with an austenitic cladding inside. After welding the rings together the RPV is heat treated to relieve the highest weld residual stresses. Thus the residual stresses in the vessel arise both during the welding process and clad manufacturing. This section considers the weld residual stress, while those associated with the clad are discussed in section 4.4.

The main factors that affect the level of the weld residual stress are:

- Welding technology;
- Welding sequence and the location of the weld root;
- Stress relieving temperature and time.

For the analysis, the shape of residual stress distribution in the weld is often assumed to be cosinusoidal. The level of the maximum residual stress depends on the parameters of the stress relieving heat treatment (temperature and time) and the material properties of the weld. Measurements from different manufacturing processes indicate that the magnitude (σ_{Rmax}) is between 50 and 100 MPa. Russian Standard MRKR-SKhR-2004 [5] contains recommendations how to perform the calculation of residual stresses due to welding and cladding manufacturing processes and heat treatment. Material properties required for such analysis are also presented in [6]. This also contains the results of residual stresses calculations for a basic case. For WWER vessels according VERLIFE the amplitude of the residual stress is taken to be 60 MPa, while for PWRs the value of 56 MPa is typically used.

For deterministic PTS analyses the residual stress distribution in the weld can be taken as follows:

$$\sigma_R = \sigma_{R\max} \cdot \cos\left(\frac{2\pi x}{s_w}\right) \text{ (MPa)} \tag{4.5}$$

where
 x is the coordinate in weld thickness direction starting from the cladding/weld material interface,
 s_w is weld thickness (wall thickness without cladding).

Similar formulae are prescribed in different standards or guidelines. If the distribution of the weld residual stresses (measured or simulated by FEM) is available, it can be used with safety margins to achieve a conservative approach. Equation 4.5 can be used only in the case when the heat treatment of the weld joint was performed after welding. In probabilistic PTS analyses a best estimate residual stress distribution should be used.

In Figure 4.2, the K_I distribution along the crack front as a function of elliptic angle is shown. The crack is an elliptical underclad crack with depth of 15 mm in weld and with aspect ratio 0.3. The maximum residual stress level is 60 MPa.

For finite element calculations, the residual stresses can be defined as an initial stress distribution (e.g. ABAQUS code) or as an initial strain distribution (e.g. SYSTUS and ADINA codes). In the first step of the analysis, the balance of internal forces is calculated. Alternatively a specially defined temperature load can be imposed that gives the required stress and plastic strain distribution.

A conservative way to include weld residual stresses is to apply an additional pressure corresponding to the residual stress amplitude (elastic-plastic analysis). In an elastic analysis the predefined K_I values estimated by analytical formulae for loading due to residual stress can be added to the calculated K_I-value.

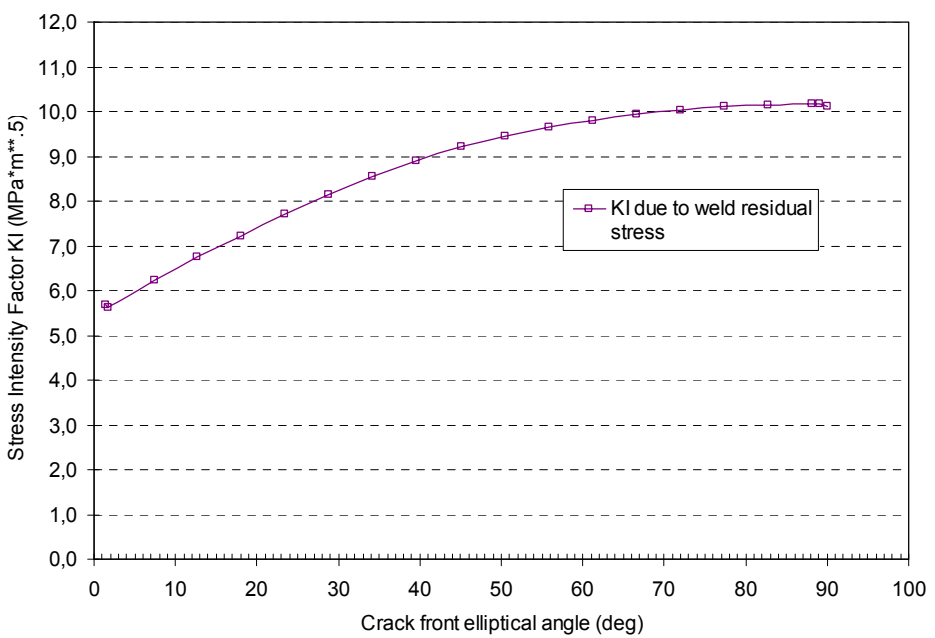


FIG. 4.2 – Example of the values of crack driving force obtained along the front of an elliptical crack (a = 9 + 15 mm, aspect ration =0.3) due to a weld residual stress of 60 MPa. with the cosine formula.

4.4. Cladding residual stresses

The cladding residual stresses should be taken into account. One way to do this is to apply a stress free temperature (T_{sf}), which should be chosen to produce appropriate levels of residual stress at room temperature (in any case not above the yield stress of the cladding). The value depends on material properties, the manufacturing procedure and the influence of the hydro test. In connection to T_{sf} , a corrected value of thermal expansion coefficient should be used if necessary (this depends on the finite element code used).

When measured data of cladding residual stresses are available (experimental data) they can be considered in defining the initial stress distribution in the cladding. The hydro test is known to have positive effect on cladding residual stresses in low temperatures. The effect of hydrotest should be quantified by elastic-plastic calculations taking into account the test temperature and the hydro test pressure. It is noted that Russian Standard MRKR-SKhR-2004 [5] contains recommendations on how to define the residual stresses in the cladding after the hydro test.

4.5. References

- [1] AMERICAN SOCIETY FOR MECHANICAL ENGINEERS, ASME Boiler and Pressure Vessel Code, Section II, "Materials", Part D, "Properties", New York (2004).
- [2] ASSOCIATION FRANÇAISE POUR LES REGLES DE CONCEPTION ET DE CONSTRUCTION DES MATERIELS DES CHAUDIERES ÉLECTRONUCLEAIRES, Design and Construction Rules for Mechanical Components of PWR Nuclear Islands, RCC-M, Section II, Paris (1998).
- [3] SICHERHEITSTECHNISCHE REGEL DES KTA, Teil 2 Komponenten des Primärkreises von Leichtwasserreaktoren, KTA 3201, Cologne (1996).
- [4] UNIFIED PROCEDURE FOR LIFETIME ASSESSMENT OF COMPONENTS AND PIPING IN VVER NPPS "VERLIFE", Řež (2008).
- [5] CALCULATION PROCEDURE FOR EVALUATION OF BRITTLE STRENGTH OF VVER RPV DURING OPERATION, MRKR-SKhR-2004, RD EO 0606-2005, St. Petersburg, Moscow (2004).
- [6] PROCEDURE FOR DETERMINATION OF FRACTURE TOUGHNESS TEMPERATURE DEPENDENCE FOR RPV MATERIALS OF VVER-440 AND VVER-1000, MKc-KR-2000, RD EO 0350-02, Saint-Petersburg, Moscow (2001).

5. CRACK TIP LOADING

This chapter describes the steps used to assess the crack driving force experienced at a postulated flaw due to the loads arising from a PTS transient.

It deals with two main aspects:

- a) the selection of an appropriate flaw geometry, size and location; and
- b) the fracture mechanics methods used to determine a driving force value at the crack front.

5.1. Postulated flaws

Postulation of defects is one of the most important parts of used in RPV integrity assessment under PTS transients. Postulated defect is usually exactly defined in the applied standard, in some cases in relation to the status of non-destructive testing used in the assessed RPV. The aim of this section is therefore not to define values for the flaw parameters themselves, but to illustrate their influence on the assessment using the results of sensitivity studies.

5.1.1. *Underclad vs. surface cracks*

The position of postulated defect should be based on the standard used. This position through the wall thickness is usually postulated as surface one or underclad one (Figure 5.3). The surface position is more conservative than the underclad one, but it is known that no flaws in base or weld metal extended up to the inner surface of the RPV (i.e. penetrating the cladding) were found in real clad RPVs. Moreover, for multilayer claddings, the probability of presence of surface crack is still lower. The bands of multilayer cladding are usually welded in such manner to be overlapped. Underclad defects exhibit much smaller K_I values and, as consequence of it, much higher allowable index temperatures (i.e. less conservative solution) than the surface breaking defects exhibit. In the benchmark performed (see Appendix B), postulating of underclad defect brings the benefit about 40 MPa \sqrt{m} in terms of K_I (reduction on more than 50%) and significant benefit in terms of RT_{PTS} . A similar trend was found in the ICAS study [1] and in sensitivity studies performed within the IAEA WWER PTS benchmark.

For some standards postulating an underclad defect can be accepted when cladding integrity is assured both before the transient, but also during the PTS transient through appropriate toughness data (J_R curve). In addition, it should be noted that an elastic evaluation of the underclad defect is not conservative since an amplification of K_I due to plasticity in the cladding may be encountered.

5.1.2. *Effect of flaw depth*

The maximum depth of the postulated crack is very important parameter of the RPV integrity assessment. It should be prescribed by the standard applied. It is usually prescribed directly in the standard (e.g. as $\frac{1}{4}$ of the wall thickness). According to some recent standards the original (large) prescribed maximum depth of the postulated crack can be significantly reduced on the basis of qualified non-destructive testing results. The crack depth is in this case connected to the plant specific non-destructive testing qualification criteria, along with application of some safety margin.

Concerning the effect of postulated crack depth on the results of PTS analyses, it could seem that the deeper crack is postulated the more conservative solution is obtained, but the situation is not so simple. When assessing the deepest point of the crack only (which is sufficient according to some older standards), the K_I values increase in most cases with increasing crack depth, but at the same time the temperature at the deepest point of the crack also increases with increasing crack depth (and, consequently, also fracture toughness of the material is increasing). Before the calculation, it is not clear which effect prevails. Moreover, if attenuation of the fluence is taken into account, the deeper points may not be so dangerous as points more close to the inner surface. Due to this fact, the standards usually prescribe analysing a set of postulated defects with varying depths.

A little different situation is in case of assessment of the (near) interface point of the crack. The temperature in this point is not changing with increasing crack depth; while the K_I values are increasing, so postulating deeper crack is conservative (from the point of view of assessment of the (near) interface point).

It was shown in some examples (see Appendix B) that as crack depth is increased the assessment of the deepest point gives less conservative results, i.e. some point closer to the clad interface becomes more critical. The assessment at this point gives more conservative results for deeper crack. In summary, the assessment is performed for the whole crack front (not only for the deepest point), deeper cracks always give more conservative predictions. Some standards (e.g. VERLIFE) allow assessment of only the crack with maximum depth, which is allowed in the case when the whole crack front is assessed. Assessment of the entire crack front for the set of postulated cracks with varied depth is described in [2].

5.1.3. Effect of defect shape

Another important parameter entering the assessment is shape of the postulated defect. Different crack shapes are seen in Figure 5.1. The most usual shape is semi-elliptical one. Some standards prescribe elliptical defects (underclad or partially penetrating the cladding). It has to be mentioned that modelling the elliptical underclad defects in finite element models is difficult task compared to assessing them using simplified codes. Under the term “crack shape” we can also understand the aspect ratio. For semi-elliptical crack we can also distinguish two positions of main axis.

Aspect ratio effect

The exact shape of the crack is expressed by the aspect ratio parameter, a/c , which means the ratio of the minor semi-axis of the (semi)ellipse, denoted by a , to the crack half length (the major semi-axis of the (semi)ellipse), denoted by c . In some standards, the reverse value, i.e. c/a or $2c/a$, is used as aspect ratio. It has to be mentioned that the semi-elliptical and elliptical cracks with the same depths and aspect ratios have different lengths.

Sensitivity studies and tables of influence coefficients show that for the deepest point of the semi-elliptical crack (both surface and underclad), smaller aspect ratios (i.e. the longer crack) produce higher K_I values and, consequently, more conservative solution (lower maximum allowable transition temperature). For near interface point, the situation is not so clear and usually smaller aspect ratios produce smaller K_I values. Since in most cases it is not clear (before performing the analyses) which aspect ratio is more conservative, some standards require assessment of several postulated cracks with different aspect ratios selected from prescribed range.

Elliptical vs. semi-elliptical underclad crack

It was shown during sensitivity studies that elliptical and semi-elliptical underclad cracks of the same depths and lengths give similar values of K_I in the deepest point. On the other hand, the K_I values in the near interface point differ significantly and more conservative results are obtained for elliptical cracks (also in dependence on aspect ratio).

Surface semi-elliptical crack — two shapes

Two shapes of crack front can be distinguished for surface semi-elliptical cracks (Figure 5.1). “Shape 1” is characterized by the main axis of the semi-ellipse lying on the cladding/base material interface, while “shape 2” is characterized by the main axis on the RPV inner surface. Having the same dimensions (depth, length) the resulting K_I values are very close in the deepest point but different in the near interface point (in base material), see also the results of sensitivity studies in Appendix B. At the deepest point, shape 1 produces a slightly higher K_I (probably due to slightly higher area of the crack). At the near interface point, shape 2 produces significantly higher K_I values (due to different curvature of the crack front in this position). It has to be underlined that some formulae used in analytical calculation of K_I are developed for shape 1 and some formulae are developed for shape 2. In

this way, the crack shape can be source of discrepancies when comparing different results, mainly in the assessment of the near interface point or for the analysis all along the crack front.

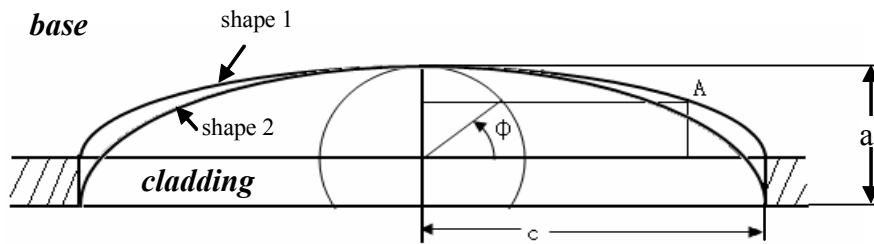


FIG. 5.1 – Postulated defect geometries.

5.1.4. Orientation and position (axial/circumferential)

Orientation of postulated defect (axial or circumferential) is very important parameter affecting the results of the assessment. Which orientation is more conservative is strongly dependent on the transient assessed. For transients with no cold plume (axisymmetric cooling) the axial crack is always more conservative due to twice larger circumferential stresses due to pressure (while the thermal stresses are of the same magnitude in both orientations). On the other hand, cold plumes (or other types of non-axisymmetric cooling) give additional axial thermal stresses below the cold plume that may cause that circumferential crack becomes the most conservative one. The ratio between higher circumferential stresses due to pressure and higher axial stresses due to non-axisymmetric cooling cannot be (generally) known before performing the analyses.

Also the position close to large geometry change of the RPV (e.g. change of thickness of RPV wall between beltline and nozzle rings) can affect behaviour of axial and circumferential cracks. For axial crack postulated in thinner part of RPV in the vicinity of its thicker part, the K_I values due to inner pressure are reduced in comparison to crack postulated far from the thickness change. The effect of geometry change on K_I due to thermal shock is not very significant for axial crack. For circumferential crack postulated in thinner part of RPV in the vicinity of its thicker part, the K_I values due to thermal shock are increased. The effect of geometry change on K_I due to inner pressure is not very significant for circumferential crack.

For the reasons mentioned above, most of standards require assessment of both crack orientations.

It can be presented as a comment the question of the potential presence (existence) of flaws of both orientations in the RPV. In base material, both orientations of embedded flaws can be usually expected. Concerning flaws arisen during the process of welding the cladding (underclad cracks), they are usually oriented perpendicularly to the direction of welding of the cladding bands (i.e. axial cracks). Concerning the flaws embedded in welds, they have usually the same orientation as the weld. The flaws in welds are usually of the type of lack of fusion between adjacent weld beads or between weld bead and base material or of the type of root not properly welded through. This means that in the case of circumferential weld the flaws are circumferential ones. The orientation of defects postulated in the assessment should be prescribed in the standard applied.

5.1.5. Characterization of NDE indications

A different task to PTS assessment is to analyse flaw indications found during in-service inspections by non-destructive testing. The standard should prescribe the way, how to schematise the indication found, safety margins applied to the schematised flaw dimensions and the procedure for assessment of

its allowableness. Fatigue crack growth during the RPV operation is usually also taken into account. The standard usually contains tables of allowable flaw sizes that can serve as the screening criteria. Flaws sizes of which exceed the limits given in the standard should be assessed according to the appropriate procedure described in the standard. The procedure is usually similar to that one used in PTS analyses with postulated defect. The most severe transients found during PTS analyses should be taken into account during assessment of the flaw found during in service inspections.

5.2. Crack tip stress intensity factor

The parameter used to characterise the loading condition at the postulated flaw is the crack driving force (CDF) or stress intensity factor (SIF), denoted by K_I for elastic analysis or K_J when derived from elastoplastic evaluation of the J integral³. For many defect and transient combinations, a linear elastic fracture mechanics is sufficient. However for more severe conditions characterized by significant plasticity and especially for vessels with cladding, elastic-plastic fracture mechanics based on the J-integral should be used.

To calculate the SIF, two basic options are considered here:

- a) engineering methods, whereby use is made of analytic formulae or tabulated collections of stress intensity values for given defect and vessel geometries
- b) cracked body finite element analyses, in which the crack is directly modelled in the mesh and subjected to the appropriate loadings.

While latter allows detailed analysis of a specific defect, vessel geometry, material properties and transient conditions, the specialised engineering solutions now available for RPV applications that have been developed from detailed cracked body FE analyses are highly accurate, and provide a rapid and essential tool for considering many transients and postulated defect geometries/orientations. This can be used for example in the frame of worth transient determination or in probabilistic approaches.

5.2.1. Engineering methods

The application of these methods requires:

- a) Through-wall stress distributions at the flaw location and in the direction perpendicular to the crack plane. These are typically available from coupled thermal and stress analyses, as described in the previous chapter. The severity of some PTS transients means that plasticity may occur at the inner surface region. However, the calculation of K_I must rely on elastically calculated stresses. In case of important plastic effects, the plasticity should be taken into account by an appropriate plastic correction (such as $k\beta$ correction of the RSE-M for example);
- b) Details of residual stresses arising from either the clad or welds (see sections 4.3 and 4.4 above);
- c) Details of the postulated elliptical or semi-elliptical flaw (aspect ratio, location and orientation) as discussed in the preceding section. The basic configurations for which formulae are available are shown in Figure 5.3;
- d) Stress intensity factor solutions relevant to flaw and vessel geometry. These typically provide K_I values at the deepest and near surface points.

The calculation of the SIF is typically based on influence functions:

$$K_I = \sqrt{\frac{\pi a}{Q}} \cdot \left[b_0 \cdot i_0 + b_1 \cdot i_1 \cdot \frac{a}{t} + b_2 \cdot i_2 \cdot \left(\frac{a}{t}\right)^2 + b_3 \cdot i_3 \cdot \left(\frac{a}{t}\right)^3 + b_4 \cdot i_4 \cdot \left(\frac{a}{t}\right)^4 \right] \quad (5.1)$$

³ Considerable research has been carried out on more advanced methods of describing the crack tip loading, for example the two-parameter constraint-based approach or the so-called local approach, using the Weibull stress. Further details are given in section 6.2.

where:

a is the crack depth,

x is a variable indicating the distance across the wall thickness, t ;

b_0, b_1, b_2, b_3 and b_4 are coefficients for the polynomial approximation of the stresses (also named nominal stresses) and are fitted to the stress distribution through the wall thickness for

$$0 \leq x \leq u \quad (u \in [a, t])$$

$$\sigma = b_0 + b_1 \frac{x}{t} + b_2 \left(\frac{x}{t}\right)^2 + b_3 \left(\frac{x}{t}\right)^3 + b_4 \left(\frac{x}{t}\right)^4, \quad (5.2)$$

i_0, i_1, i_2, i_3 and i_4 are influence coefficients which depend on the crack depth/thickness ratio, a/t , on the shape of the crack, a/c , and on the location along the crack front and crack orientation,

Q is a crack shape correction factor (used in some formulae and function of aspect ratio a/c)

Concerning the discontinuity of the stress profile for clad vessels under severe transients, the distributions in the clad and the ferritic base material are in new compendiums treated separately, as indicated in Figure 5.2. It has to be noted that the contribution of stresses in the cladding is in general significant for surface cracks and thus approximate calculation neglecting this contribution are inadequate.

A linear description of stresses in the cladding is generally used (Figure 5.2). Other approximations fitting the whole stress field in the same formula (base metal + cladding) must be validated when used in formulae that don't take into account the stress discontinuity.

For the calculation of the nominal stresses (i.e. b_0 to b_{1r} coefficients), two approaches may be used:

- a) Finite element calculation: in this case, the stresses are determined for the crack free structure with an appropriate model for the studied transient: 1, 2 or 3D elastic models, depending on the assumptions. The absence of crack makes this calculation relatively easy to perform in comparison to calculation of the cracked body;
- b) Simplified analytical approaches, which allow a reasonably good estimation of the stresses during the transient.

To define the influence function values, use should preferably be made of purpose-made methods for clad RPVs, such as those developed for the French RSE-M [3] code by CEA [4] or formulae used in FAVOR code [5]. Recent benchmark exercises, including this CRP, have shown that these provide K_I estimates in good agreement with those obtained by 3-D FE cracked body analysis. It is noted that the available solutions cover semi-elliptical crack geometries only.

Other SIF solution compendiums, such as that in ASME Section XI [7], R6 [8] or VERLIFE [9], can be applied with elastic stresses distribution and an appropriate plasticity correction. Further details are given in Appendix D. These methods however do not consider the effect of the cladding on crack behaviour. Hence the following limitations need to be taken into consideration: firstly, for underclad, subsurface or partly through the interface cracks for which influence function are not available, the methods cannot be applied without complementary analyses and justification; secondly the plastic zone correction can be non-conservative for large plasticity or at the clad/base metal intersection point.

In general case, if no formulae is available for the underclad crack, it is noted that the case of a semi-elliptical subsurface crack in the interface of cladding and base metal is covered by a surface crack of the same depth, independent of linear elastic or elastic plastic material behaviour for the loading cases under investigation.

5.2.2. FE cracked-body models

Direct finite element analysis of cracks allows accurate analysis of the stress intensity factor considering a range of factors specific to the defect, material condition and loading transient of interest. The main parameters to be considered in making such analyses are as follows:

a) Component model

In general the FE analysis will address the entire RPV shell, using the same model as that for the temperature and stress analyses. The cladding at the inner surface is explicitly modelled.

b) FE meshing of the crack

The selected defect geometry is modelled using appropriate meshing techniques. Guidance on this is given in FE software user manuals and in other literature. Quadratic element types are recommended. Attention is needed to ensuring sufficient mesh refinement to handle the strong stress gradients induced by the combination of the crack tip and the imposed thermal loads, particularly at the base-clad interface.

c) J-Integral and SIF

There are several different ways of calculating J, depending on the FE software being used. Direct J-Integral: In the direct method a domain integral is performed over a series of paths ahead of the crack tip, in plans perpendicular to the crack front. This approach has been widely implemented in commercial software packages and has been shown to be reliable for PTS analysis in numerous benchmark exercises. Virtual Crack Extension, in which the energy variation is determined for a virtual crack advance G-theta approach consisting in the calculation of the energy release rate associated with a virtual crack growth [10].

Independence of results in J on the integration path or theta field in these formulations should be verified. In many cases it is sufficient to evaluate J for the deepest point of the crack front and for the point of intersection of the crack front with the free surface (for unclad RPV), or for the point close to intersection of the crack front with the boundary between cladding and base or weld metal (for clad RPV). The SIF is calculated from the J-integral value according to one of the following formulae:

$$K_J = \sqrt{J \cdot E} \quad \text{for plane stress (only for surface point)} \quad (5.3)$$

$$K_J = \sqrt{\frac{J \cdot E}{1 - \nu^2}} \quad \text{for plane strain assumption (other points)} \quad (5.4)$$

It should be noted that for the integral approach applicable in Master Curve or the Russian approaches, it is required to integrate the stress intensity over the full crack front. In these cases, K_J should be determined in a sufficient description of the crack front, paying particular attention to the location just below the clad interface where strong gradients are present.

In summary, if the precision of the mesh is accurate enough, the 3-D FE analysis of a postulated crack is considered the best estimate approach. However as discussed above, for semi-elliptical defects and for a known fluid temperature loading, the customised analytical stress calculation and influence function solutions can provide good estimations.

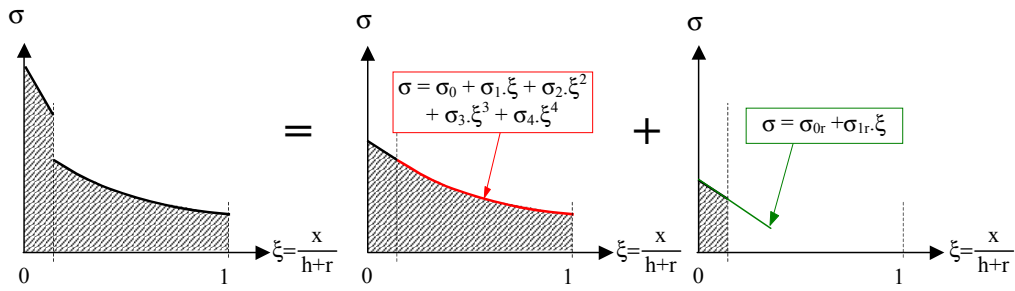


FIG. 5.2 – Stress decomposition for a clad vessel.

<p>a) unclad vessel, surface breaking semi-elliptic flaw</p>	
<p>b) clad vessel, subsurface elliptic flaw</p>	
<p>c) clad vessel, subsurface semi-elliptic flaw</p>	
<p>d) clad vessel, surface breaking semi-elliptic flaw</p>	

FIG. 5.3 – Elliptical and semi-elliptical crack models.

5.3. References

- [1] SIEVERS, J., SCHULZ, H., BASS, B. R., PUGH, C. E., KEENEY, J., CSNI Project for Fracture Analyses of Large Scale International Reference Experiments (Phase I), GRS-108, NEA/CSNI/R, NUREG/CR 5997, (1994).
- [2] CALCULATION PROCEDURE FOR EVALUATION OF BRITTLE STRENGTH OF VVER RPV DURING OPERATION, SKhR-2004, RD EO 0606-2005, St. Petersburg, Moscow, (2004).
- [3] ASSOCIATION FRANÇAISE POUR LES REGLES DE CONCEPTION ET DE CONSTRUCTION DES MATERIELS DE CHAUDIERES ELECTRONUCLEAIRES, Règles de conception et de construction de matériels mécaniques des îlots nucléaires, Paris (2005).
- [4] CHAPULIOT, S., MANAGER, Y., MARIE, S., Stress intensity factors for underclad and through clad defects in a reactor pressure vessel submitted to a pressurized thermal shock, p. 746–760 in International Journal of Pressure Vessels and Piping, Vol. 82 (2005).
- [5] FRACTURE ANALYSIS OF VESSELS – OAK RIDGE FAVOR, v.04.1 - Computer Code. User's Manual, NUREG/CR-6885, Oak Ridge (2007).
- [6] AMERICAN SOCIETY OF MECHANICAL ENGINEERS, ASME Boiler and Pressure Vessel Code, Section XI, "Rules for in-service inspection of nuclear power plant components", New York (2004).
- [7] R6 PROCEDURE REV 4, British Energy (2001).
- [8] INTERNATIONAL ATOMIC ENERGY AGENCY, Guidelines on Pressurized Thermal Shock Analysis of WWER Nuclear Power Plants, IAEA-EBP-WWER-08, IAEA, Vienna (2005).
- [9] AMERICAN SOCIETY FOR TESTING AND MATERIALS, Standard Method for Conducting Drop-Weight Test to Determine Nil-Ductility Transition Temperature of Ferritic Steels, E208, Annual Book of ASTM Standards, ASTM International, West Conshohocken (2002).
- [10] U.S. NUCLEAR REGULATORY COMMISSION, Title10 Code of Federal Regulations, Part 50.61 (10 CFR 50.61), Fracture Toughness Requirement for Protection Against Pressurized Thermal Shock Events, US NRC, Washington (1995).

6. INTEGRITY ASSESSMENT

6.1. Definition of material toughness

6.1.1. Design fracture toughness curves

The approach taken in defining the fracture toughness curves is very similar between the various approaches. The differences between the curves are not large, but the indexing approaches for using the curves can differ substantially. The general shape of the fracture toughness curves can be expressed as:

$$K_{IC} = A + B \exp [C (T - TT_{ref})] \quad (6.1)$$

where A is the lower shelf asymptote, B and C are parameters defining the shape of the exponential curve, and TT_{ref} is the reference transition temperature used to index the fixed curve. The same general equation is also used for defining the crack arrest toughness (K_{Ia}) as defined in the ASME approach. The specific coefficients are listed in Table 6.1 along with the parameters that are needed to utilize the fracture toughness curves.

6.1.2. Indexing of fracture toughness curves

TT_{ref} is defined in the ASME approach as RT_{NDT} , reference temperature for Nil Ductility Transition (NDT). The initial start of life value of RT_{NDT} is defined in the ASME Section III [1], Subsection NB-2300. Essentially, initial RT_{NDT} is defined as the minimum of the drop weight NDT temperature (T_{NDT}) following ASTM E 208-95a(2000) [2] and $\{T_{cv} - 33^{\circ}C\}$, where T_{cv} is the 68 J (or 0.89 mm lateral expansion) temperature evaluated as the minimum of at least three Charpy V-notch impact tests. Irradiated RT_{NDT} is not directly measured; instead, the irradiated value of RT_{NDT} is determined from the shift due to irradiation at the CVN 41 J temperature (ΔT_{41J}) added to the initial value:

$$\text{Irradiated } RT_{NDT} = \text{initial } RT_{NDT} + \Delta T_{41J} \quad (6.2)$$

The indexing temperature for the reference toughness curves is termed the Adjusted Reference Temperature (ART). ART is the irradiated RT_{NDT} plus a Margin to account for uncertainties and regulatory comfort:

$$\text{ART} = \text{Irradiated } RT_{NDT} + \text{Margin} = \text{initial } RT_{NDT} + \Delta T_{41J} + \text{Margin} \quad (6.3)$$

Margin is defined later based on estimates of the uncertainties in ΔT_{41J} and initial RT_{NDT} .

Alternatively, the ASME Code through Code Cases N-629 [3] and N-631 [4] allows the use of RT_{T_0} , the reference temperature using T_0 from the Master Curve fracture toughness approach in ASTM E 1921-05 [5]. RT_{T_0} is defined as:

$$RT_{T_0} = T_0 + 19.4^{\circ}C \quad (6.4)$$

where T_0 is the temperature at the 100 MPa-m^{1/2} adjusted median fracture toughness level. The effect of irradiation can be measured directly when the irradiated test material corresponds to the fluence of interest for the RPV material. A Margin term is also required to define the index temperature for the reference toughness curves, although there is currently no regulatory requirement or definitive guidance on the Margin term for RT_{T_0} .

The French approach is very similar to the USA method except that an ISO Charpy machine is used rather than an ASTM machine. The main difference is in the striker (tup) between these two machines (and standards). At low levels of CVN impact energy there are very small, if any, differences in the

CVN results. The French requirements do not reference the ASME Code requirements; instead the RCC-M Code is used [6]. The shift in transition temperature is measured using the CVN energy or lateral expansion change, whichever is larger.

The approach for German vessels is again essentially the same as the USA method using initial RT_{NDT} and $\Delta RT_{NDT} = \Delta T_{41J}$ for radiation embrittlement. German standards are used as defined in the recently revised KTA 3203 [7]. The ISO tup is used for Charpy tests, like the French method. In the latest version of KTA 3203, the use of RT_{T0} is allowed following the ASME Code Cases.

In Japan, the approach is again very similar to the USA method. The definition of RT_{NDT} is the same as in the ASME Code. $\Delta RT_{NDT} = \Delta T_{41J}$ for radiation embrittlement is used where the CVN test follows ASTM standards.

In the Russian approach for WWER type reactors, brittle fracture transition temperature T_k is used as an index for the curve. This temperature is determined from mean values of at least three Charpy V-notch impact tests performed in several temperatures; CVN energy level is a function of proof stress (yield strength) in the initial condition, at the same time, additional requirements for CVN level (1.5-times larger than at T_k) and 50% ductile fracture appearance must be fulfilled at temperature $T_k+30^\circ\text{C}$ as defined in PNAE-G-7-002-86 [8]. The direct measurement of irradiated T_k as TT_{ref} is required by this Code, where irradiated T_k is defined as the temperature at a CVN energy level that is also a function of proof stress (yield strength) in the irradiated condition. The shift due to irradiation is made relative to T_{k0} .

In the VERLIFE procedure, the same approach is required for the determination of T_{k0} , while T_k in irradiated conditions uses a constant CVN energy level equal to 41 J. VERLIFE procedure [9] prefers to use T_0 instead of T_k as reference temperatures.

6.1.3. Master Curve approach

RPV integrity assessment can be also performed using “Master Curve” approach. In such a case, allowable stress intensity factor values are determined with the use of an experimentally determined transition temperature T_0 (instead of any transition temperature from Charpy V-notch impact tests – RT_{NDT} or T_k) obtained from testing static fracture toughness of surveillance specimens. Neutron fluence of these specimens should be close to the analysed state of the RPV; in this case no initial values of any transition temperature of tested material are necessary. Transition temperature T_0 for the analysed state of the RPV is determined using single or multiple temperature method in accordance with the ASTM standard E 1921-05 [5].

The Master Curve method has in general shown to be applicable in its basic form for a variety of ferritic base and weld metals with microstructures and properties which may result from very different manufacturing and operation history including special heat treatments and exposure to thermal ageing and/or neutron irradiation. The transition range fracture toughness is also relatively insensitive over a wide range of mechanical properties and microstructure characteristics. This means that a similar fracture toughness vs. temperature dependence, as it is assumed in the basic Master Curve model, can be used in most cases. Even measures decreasing the toughness of the steel, like special heat treatments or neutron irradiation, do not generally degrade the consistency of the measured fracture toughness vs. temperature behaviour with that predicted by the model.

Although the model has been applied mainly to quenched and tempered low-alloy structural steels, normally with high strength and at least moderate toughness, more specific and/or more alloyed steel types like ferritic stainless steels or steels with low ductility have followed, at least moderately, the Master Curve estimation.

Even ferritic steels with very high ductile-to-brittle transition temperatures following, for example a tempering treatment or a high neutron fluence, have usually shown quite "normal" fracture behaviour

in regard to both scatter and temperature dependence, confirming the general validity of the basic Master Curve model. In general, the model has been applied successfully to the most common Western and several WWER-440 and WWER-1000 type reactor pressure base and weld metals, including surveillance data measured with miniature fracture mechanics specimens.

Fracture toughness K_{Jc} values tend to conform to a common toughness versus temperature curve shape expressed by Equation 6.4.

$$K_{Jc(\text{median})|T} = 30 + 70 \exp[0.019(T - T_0)] \quad (6.5)$$

The lower and upper tolerance bound ($K_{Jc(0.xx)}$) for the estimated fracture toughness in $K_{Jc} = f(T)$ is calculated from a revised T_0 ($T_{0(\text{margin})}$) as follows:

$$T_{0(\text{margin})} = T_0 + \Delta T_0 \quad (6.6)$$

$$K_{Jc(0.xx)} = 20 + \left[\ln \left(\frac{1}{1 - 0.xx} \right) \right]^{1/4} \left\{ 1 + 77 \exp[0.019(T - T_{0(\text{margin})})] \right\} \quad (6.7)$$

where,

0.xx is the selected cumulative failure probability (in %/100).

For 1%, 2% and 5% cumulative failure probability the bounds are as follows:

$$K_{Jc(0.01)} = 23.5 + 24.4 \exp[0.019(T - T_{0(\text{margin})})] \quad (6.8)$$

$$K_{Jc(0.02)} = 24.1 + 29.0 \exp[0.019(T - T_{0(\text{margin})})] \quad (6.9)$$

$$K_{Jc(0.05)} = 25.2 + 36.6 \exp[0.019(T - T_{0(\text{margin})})] \quad (6.10)$$

The uncertainty in determining T_0 depends on the number of specimens used to establish the value. The uncertainty is defined according to a standard two-tail normal distribution with two basic variables, i.e. the test temperature and the number of specimens used for the T_0 determination, as follows:

$$\Delta T_0 = \frac{\beta}{\sqrt{r}} \cdot Z \quad (6.11)$$

where:

$\beta = 18-20^\circ\text{C}$, depending on the value of $T - T_0$ (single-temperature data; when $K_{Jc(\text{med})}$ is equal to or greater than $83 \text{ MPa}\sqrt{\text{m}}$, $\beta = 18^\circ\text{C}$)

r is the number of valid (uncensored) test results used to determine T_0

Z is the confidence level ($Z_{85\%} = 1.44$).

Alternatively, $\beta = 20^\circ\text{C}$ can be used for all values of $K_{Jc(\text{med})}$ not less than the minimum ($58 \text{ MPa}\sqrt{\text{m}}$).

The exact value of β can be determined from $K_{Jc(\text{med})}$ according to ASTM E 1921-05.

Usually, 5% lower boundary is used for RPV integrity assessment. This choice is based on the results from comparison of design fracture toughness curves – K_{IC} according to ASME or $[K_{IC}]_3$ according to Russian Code. In both cases, this 5% lower boundary is very close to design fracture toughness curves if reference temperature RT_{T0} is used, as it is seen from Figure 6.1.

Despite the general good applicability, special cases have been recognised where the Master Curve method should be adjusted or modified, or the method should not be applied at all.

The following cases have been identified:

- a) Inhomogeneous materials or materials with a dual or multiphase microstructure which consists of large areas of phases with very different properties. These cases can usually be estimated with the Master Curve by adopting a modified scatter band model for fracture probability;

- b) Materials which are susceptible to grain boundary fracture may exhibit fracture behaviour which do not follow the Master Curve prediction if the proportion of grain boundary fracture is high.

The fracture behaviour outside the standard temperature region ($-50^{\circ}\text{C} \leq T - T_0 \leq 50^{\circ}\text{C}$) will often, but not always, follow the Master Curve model. In certain cases these extrapolations may be used, although this option is not included in the ASTM E 1921-05 standard. Deviations from the predicted behaviour are often associated with special situations that should be recognised before the extrapolation.

6.1.4. Russian standards for fracture toughness temperature dependence $K_{IC}(T)$

Fracture toughness temperature dependence $K_{IC}(T)$ for base and weld metals of RPV is determined according to the procedures given in Russian Standard [10]. Russian Standard Procedure [10] consisting of two parts foresees determination of $K_{IC}(T)$ curve for the case when the lateral shift condition is valid (Part I) and for the case when the lateral shift condition is invalid, i.e. a shape of $K_{IC}(T)$ curve varies due to the irradiation effect. Part I is the Basic Curve concept. Part II is based on Prometey local approach to brittle fracture. The main features of the procedures in [10] are given in Appendix E.

6.1.5. Material (base and weld) non-homogeneity and property gradients

RPV materials are, as a rule, characterized by properties of tested specimens cut from one quarter of the semi-product thickness, either plate or forging. These specimens are located usually on one end of the ingot, either A or Z, depending on Code requirements and/or distribution of chemical properties through the vessel ingot. These properties are usually conservative as near surface areas are cooled during manufacturing heat treatment faster than the middle part of the thickness and thus their tensile properties as well as toughness properties are higher – transition temperature is lower. Typical distribution of tensile properties (yield strength and ultimate tensile strength) and transition temperatures (T_{41j}) for typical ASTM A 533-B type plate are shown in Figure 6.2.

In the case of welds, specimens are usually taken from the whole thickness of the weld excluding near surface and weld root areas. As no specimens can be cut directly from the weldment of the RPV, special weld coupons are prepared before the real welding, they must be manufactured with the same technology, welding parameters and welding consumables including pre- and post weld heat treatment as appropriate welds in the RPV. Usually, weld coupon for surveillance specimens is manufactured from additions to the beltline materials – plates or forgings – and with the same procedure as typical weld coupons. Its heat treatment should have to represent number and type of all heat treatments of given critical weld in the RPV beltline region.

As it is seen, results of acceptance tests (and also of surveillance specimen tests) are conservative with respect to the near surface properties but they well characterize properties of the middle half of RPV thickness in the initial condition. This approach is supported by the fact that scatter of all mechanical properties as well as chemical composition exists not only through RPV wall thickness, but also along the height of the RPV rings (or plate length) due to the segregation and crystallization properties during ingot cooling and in some level, also in circumferential direction of the rings. Additionally, scatter in content of most deterioration element contents (copper and phosphorus) exists along and through welds, at least for old generation of RPVs.

All these facts lead to the requirement of adding some Margins to real mechanical properties of critical evaluated materials. These margins can be different in cases when guaranteed mechanical properties are used in evaluation or when real values e.g. from Acceptance or Surveillance specimen tests are used.

Special situation is obtained for evaluation of the behaviour of beltline region of RPVs during operation – radiation embrittlement and radiation hardening results from material irradiation by a

strong field of reactor radiation – neutrons and gamma. Resulting damage depends on neutron fluence, neutron flux, irradiation temperature and content of chemical elements like copper and phosphorus as the most important ones, but also others like nickel, manganese, silicon etc. These effects are usually implemented into predictive formulae in individual codes – see Table 6.1.

Regarding the effect of neutron fluence, two different threshold energies are taken for its characterization – 1 MeV for PWR type RPVs and 0.5 MeV for WWER type RPVs. Moreover, neutron energy spectrum is important in final damage value, thus irradiation in other type of reactors (including experimental ones) cannot be easily transferred into evaluation of RPV of power reactors. Results from Surveillance specimen tests are usually required, either they are basis for Predictive formulae or their exact values can be used for RPV material evaluation.

Neutron field in the RPV has a very complicated form – in azimuthal direction it depends on active core design (quadratic for PWR or hexagonal for WWER) and real fuel loading, in axial direction on core height and movement/position of control rods, and in RPV wall thickness on attenuation effect of neutron flux and changes in neutron energy spectrum through the RPV wall.

Conservatively, attenuation through RPV wall is usually not taken into account in PTS calculations when initiation is only evaluated, as its effect for small postulated defects is very small (up to 10°C). Attenuation effect must be taken into account, if crack arrest is applied or defects in outer surface are evaluated (external flooding).

Similarly, conservative approach is usually taken for evaluation of beltline region in azimuthal/circumferential direction – maximum value is used in calculation of radiation embrittlement. Regarding axial distribution, calculation for critical welds and appropriate base materials, including beltline centre are performed and used in calculations without any detailed distribution between these locations.

Changes in tensile properties, i.e. radiation hardening resulting in increase of yield strength and ultimate tensile strength and decrease of elongation (mainly uniform) and reduction in area as well as changes in stress-strain diagrams usually are not taken into account due to the principal that any improvement of material properties due to operation should be neglected. It can be shown that real changes in stress-strain diagrams as an effect of radiation hardening in RPV ferritic materials lead to some conservatism.

6.1.6. Cladding toughness

RPVs are given an austenitic cladding on their inner surface. This is mostly performed by automated strip welding under flux using different strip width, and in some special cases or locations (nozzle radius etc.) by manual welding. In principle, two layers are used for cladding, 1st layer is usually of 24/13Nb 23/12 Nb for PWR and 25/10 for WWER while 2nd layer is welded from 19/9 Nb for PWR (21/10 Nb for manual welding) and 18/10 Nb for WWER RPVs While 1st layer is obtained by one pass, 2nd layers are manufactured by several (normally 1 for PWR and 3 for WWER) passes up to 6 mm (PWR) and 8–9 mm for WWER. Thus, effect of cladding can be different for both types of vessels due to different thermal conductivity of austenitic cladding and ferritic material and also due to different tensile and toughness properties.

Cladding materials are characterized by relatively lower toughness in comparison with austenitic materials of the same type as they are not austenized after welding: they are heat treated only for removal of residual stresses (post-heat weld treatment).

Both layers are of different chemical composition and also different tensile and toughness properties; 1st layer is mostly more important for PTS evaluation. Both properties are also affected by neutron irradiation even though in smaller way than RPV ferritic materials. The Russian standard [10]

provides the dependence of fracture toughness J_C and yield strength on neutron fluence for the cladding.

6.1.7. Thermal ageing

Thermal ageing embrittlement is a time and temperature dependent degradation mechanism. It is caused by the thermally activated movement of lattice atoms over a long time period, a process that can occur without external mechanical load. Changes in material properties (e.g. a decrease in ductility and toughness and an increase in strength properties and hardness) are the consequence of these diffusion processes.

The significant parameters responsible for these ageing processes are:

- Temperature;
- Material state (microstructure and content of elements);
- Time.

Thermal ageing is usually pronounced by embrittlement while hardening usually does not take place. Only WWER codes strictly require inclusion of thermal embrittlement into RPV integrity evaluation: WWER codes (Russian and VERLIFE) contains parts with description of thermal ageing effect into RPV material degradation effect. According to Russian codes a thermal ageing effect should be considered only outside the irradiated part of RPV.

A mandatory part of all WWER Surveillance specimen programme are specimens determined for evaluation of thermal ageing/embrittlement of RPV materials; such specimens are located in containers in places over and far from the active core, usually in front of the upper nozzle ring (i.e. at outlet water temperature) located on or close to RPV inner wall. While 15Kh2MFA type materials usually show no thermal ageing, testing of surveillance specimens of 15Kh2NMFA type steel shows a T_k temperature shift of up to 30 °C due to thermal ageing (for base and weld metal).

ASME Code does not require, in principle, any evaluation of thermal ageing of RPV materials, there are also no part of RPV Surveillance specimen programme concentrated on thermal ageing effect. In the same time, some experimental results show that some thermal ageing/embrittlement exist in PWR type steels at 300°C for long term operation.

Table 6.1 – Comparison of design fracture toughness curves and irradiation effects correlations

SI Method	K _{IC} Curve	K _{Ia} Curve	Indexing Approach (T _{Tref})	Irradiation Effects and Correlation(s)	Comments
USA	A = 36.48 B = 22.783 C = 0.036 K _{IC(max)} =200	A = 29.45 B = 13.675 C = 0.0261	ASME Code RT _{NDT} or RT _{T0}	US NRC Reg. Guide 1.99, Rev. 2: shift in CVN T _{41J} ; Cu, Ni, and Φ (E > 1 MeV) or direct measurement of irradiated RT _{T0}	New mechanistic-guided embrittlement correlation has been developed and approved as ASTM E 900-02, US NRC Reg. Guide 1.99, Rev.3 is under preparation
Russian	<i>WWER-440 Base Metal/ Emergency:</i> A = 35 B = 45 C = 0.02 <i>WWER-1000 Base Metal:</i> A = 74 B = 11 C = 0.0385 <i>WWER-440/-1000 Welds:</i> A = 35 B = 53 C = 0.0217 <i>Generic Curve:</i> A = 26 B = 36 C = 0.02	None	Russian Norm, PNAE-G-7-002-86: T _k	Russian Norm, PNAE-G-7-002-86: direct from irradiated CVN curve depending upon material yield strength; Prediction formulae for ΔT _k for all mentioned materials Cu, P, Φ (E > 0.5 MeV) based on data from experimental reactors irradiation;	
	<i>Base Curve</i> A = 23 B = 48 C = 0.019		Russian Procedure MPKP – CXP – 2004		New local fracture approach has been developed that has similarities to the Master Curve
VERLIFE	<i>Master Curve 5 % lower boundary A = 25.2</i> B = 36.6 C = 0.019	A=26 B=36 C=0.02	Master Curve approach is preferred for the use in priority to T _k	Direct from irradiated CVN curve for CVN=41 J; Prediction formulae for ΔT _k for all mentioned materials Cu, P, Φ (E > 0.5 MeV) based on data from experimental reactors irradiation;	T _k in accordance with Russian Norm, ΔT _k criterion is 41 J
	<i>Generic Curve:</i> A = 26 B = 36 C = 0.02 K _{IC(max)} =200	T _{TREF} =T _k -30°C K _{IC(max)} =200			
French	A = 36.5 B = 22.86 C = 0.036	A = 29.43 B = 13.792 C = 0.0261	RCC-M RT _{NDT}	<i>Design:</i> RCC-M, App. ZG; Cu, P, and Φ (E > 1 MeV) <i>Surveillance:</i> RSE-M Code, Article B7212; Cu, Ni, P, and Φ (E > 1 MeV)	All correlations use shift in CVN T _{41J}
Japanese	<i>For 1-pass bead Method:</i> Base Metal: A=33.46 B=65.29 C=0.0332 Welds: A=32.55 B=32.64 C=0.0378 <i>For 2-pass bead Method:</i> Base Metal: A=32.91 B=43.40 C=0.0343 Welds: A=32.60 B=32.12 C=0.0340	<i>For 1-pass bead Method:</i> A=29.46 B=15.16 C=0.0274 <i>For 2-pass bead Method:</i> A=29.43 B=13.68 C=0.0261	MITI Notification No. 501: RT _{NDT} equivalent to ASME Code	JEAC4201: shift in CVN T _{41J} ; Base Metal: Cu, Ni, P and Φ (E > 1 MeV) Welds: Cu, Ni, Si and Φ (E > 1 MeV)	

Table 6.1 – Comparison of design fracture toughness curves and irradiation effects correlations (continued)

SI Method	K_{IC} Curve	K_{Ia} Curve	Indexing Approach (TT_{ref})	Irradiation Effects and Correlation(s)	Comments
German	A = 36.5 B = 22.86 C = 0.036	A = 29.43 B = 13.792 C = 0.0261	ASME Code RT_{NDT} or RT_{T0}	KTA 3203 (graphical); considers Cu, P, and Φ ($E > 1$ MeV) in RT_{Limit}	Latest version includes provision for using RT_{T0}
IAEA	A = 26 B = 36 C = 0.02 $K_{IC(max)}=200$		Russian Norm, PNAE-G-7-002- 86: T_k	Prediction formulae for ΔT_k for all mentioned materials Cu, P, Φ ($E > 0.5$ MeV) for 15Kh2MFA materials based on surveillance data, for 15Kh2NMFA materials based on data from experimental reactors irradiation;	Master Curve approach is also allowed

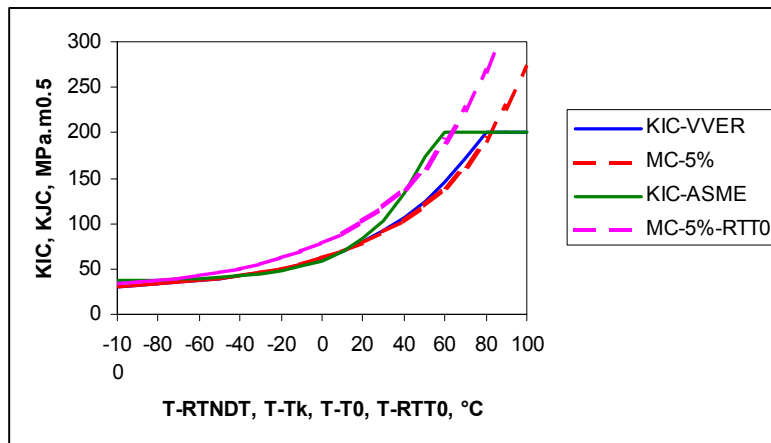


FIG. 6.1 – Comparison of design fracture toughness curves and Master Curve.

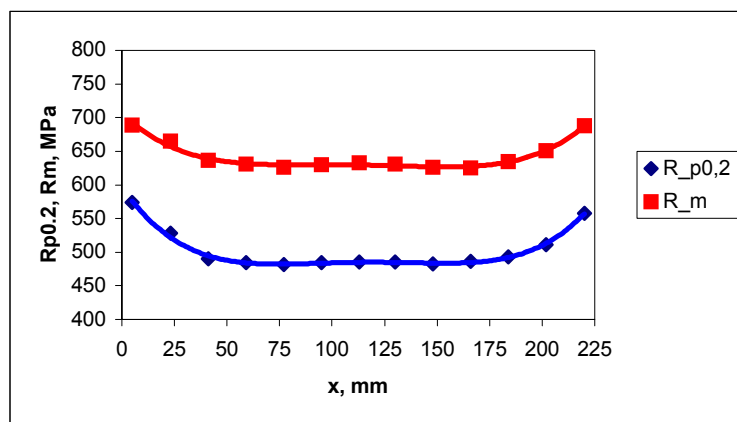


FIG. 6.2 – Distribution of tensile properties through a ASTM A 533-B plate thickness.

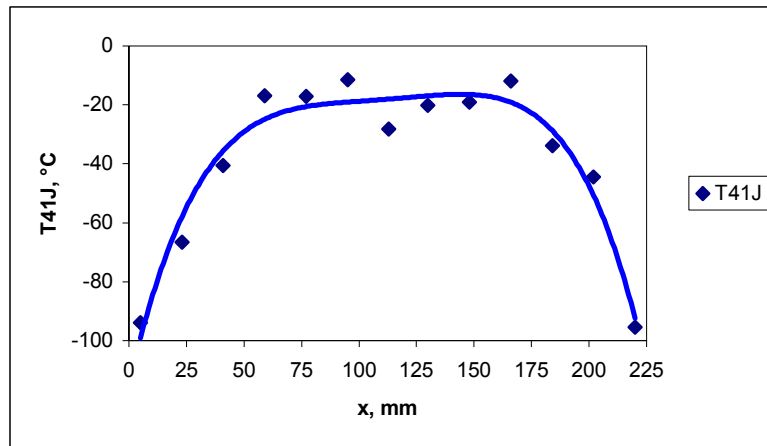


FIG. 6.3 – Distribution of transition temperature through a ASTM A 533-B plate thickness.

6.2. Comparison of applied loading and material resistance

6.2.1. Basic assessment principle

The assessment of integrity according to fracture mechanics principles follows the scheme shown in Figure 6.4. Steps 1–4 have been covered in the previous sections. Step 5 – the applied crack tip loading with the local material resistance allows to predict crack growth behaviour, i.e. non-initiation or initiation of postulated cracks (step 6) or arrest behaviour after initiation (step 7). Such analyses have to be done for the leading embrittled zone of the core weld and for other positions in the RPV being in the path of the injected coolant. Further lines of defence can be demonstrated from the residual resistance against wall penetration (step 8). The results of the analyses in the framework of relevant Codes and Standards deliver the safety proof (step 9). In the same time, it is necessary to stress that while most of PWR Codes allow to apply crack initiation and subsequent arrest, Russian Code for WWER vessels is strictly based on prevention of any crack initiation, i.e. without step 7.

In step 5 for each individual analysed PTS sequence, the material behaviour in terms of allowable stress intensity factor, and the crack loading path in terms of stress intensity factor are considered as a function of temperature and should be presented in a stress intensity factor respectively allowable stress intensity factor vs. temperature diagram. A schematic description of the assessment is provided in Figure 6.5.

The maximum allowable transition temperature for analysed sequence corresponds to the allowable stress intensity factor curve shifted horizontally up to the point where it becomes a tangent to the crack loading path of the i^{th} sequence of PTS or intersect it at a certain point relative to the maximum value of K_I (e.g. 1, 0.9 or 0.8) during the PTS event if Warm Prestressing (WPS) approach is applied. The vessel maximum allowable critical brittle fracture temperature T_k^a (for WWER) or maximum allowable transition temperature RT_{NDT}^a is equal to the minimum value of the set of obtained $T_k^a(i)$ or $RT_{NDT}^a(i)$ values for all sequences analysed, respectively.

The difference between the vessel maximum allowable transition temperature and the vessel material transition temperature (for its determination see chap. 7.1) determines the safety margin. The value of this safety margin should be larger than or equal to zero depending on the national regulatory requirements and considering the reliability of individual input data, such as material properties and effectiveness of NDE.

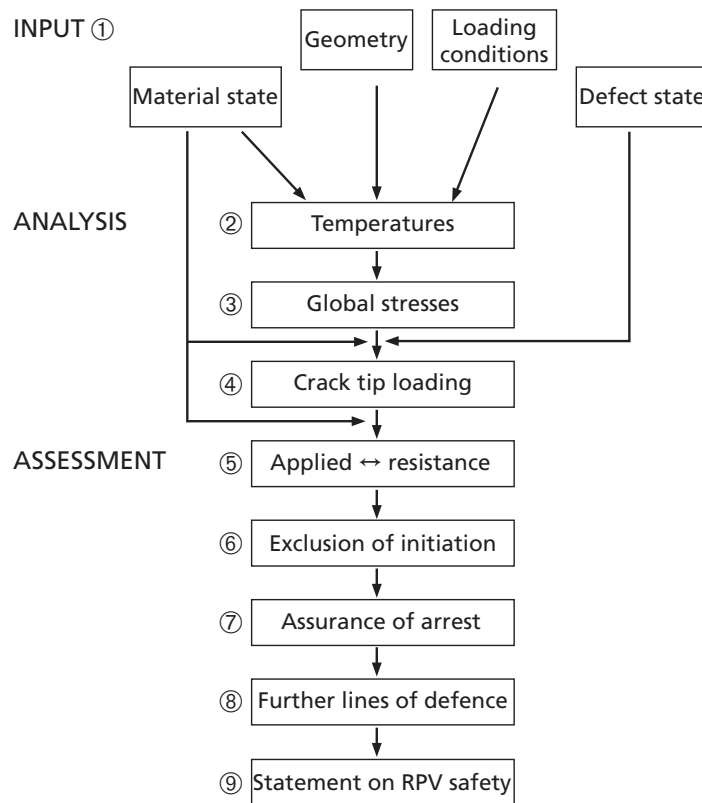


FIG. 6.4 – General procedure for fracture mechanics based PTS analysis.

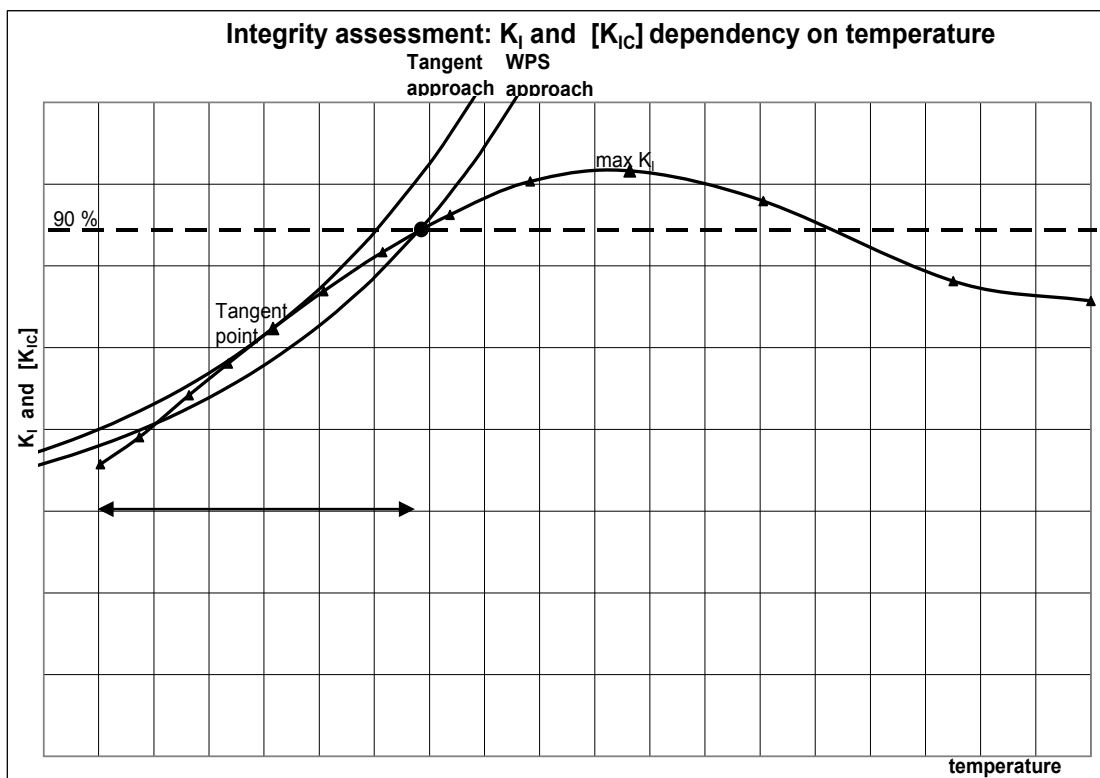


FIG. 6.5 – Scheme of the approach for establishing the allowable indexing parameter for fracture toughness, on the basis of a) the tangent point and b) the 90% maximum K_I intersection point between the K_{IC} and crack driving force (K_I) curves (exclude 90% line x%).

If crack initiation for a postulated defect cannot be excluded for an accident sequence with sufficient margin, some codes allow application of a crack arrest approach to demonstrate, that the initiated crack will arrest within the vessel wall thickness (related material crack arrest data are needed).

It is not a priori clear that the vessel belt line region represents the only and the most critical situation concerning loading and material conditions in the vessel. The cooling stresses are more severe for regions closer to the coolant injection and increased constraint of the flange ring or of the nozzles themselves could induce a major stress concentration for a postulated defect. Although in general more favourable material properties can be expected because of reduced irradiation exposure away from the core, it has to be checked whether such situations are safe from crack initiation under all transients and for all times. The procedure for the fracture mechanics assessment will in principle be the same as for the core weld, but additional complexities can arise because the situation now is three-dimensional from the beginning and extended plastic deformation covering the crack may require specific analytical tools.

The results of the analyses for different PTS-transients have to be summarized and assessed in the framework of the relevant national codes as part of a final safety report. The reliability of the input data concerning material data, defect status and sequence of thermal-hydraulic events will determine the partial safety factors to be applied and the acceptability of the predictions.

6.2.2. Uncertainty of results

In the analysis, the source of uncertainties could be associated with the following aspects:

- Material properties including fracture toughness in initial as well as end-of-life states;
- Neutron fluence;
- Transient description (gradient, final temperature, pressure);
- Fluid temperature and heat transfer coefficients;
- Assumptions of the structural analysis model including boundary and initial conditions;
- Method of calculation of stress intensity factors;
- Crack geometry and size with respect to NDE effectiveness;
- Operator action.

Therefore, careful consideration should be given to these aspects and if necessary, sensitivity studies should be carried out. Further, computer codes used should comply with the specific requirements discussed in Chapter 8.1.

6.2.3. Crack front length effect

The initiation of brittle fracture in ferritic steels or welds such as those used for RPVs is linked the distribution of carbide particles at the crack tip; as a result the likelihood of brittle failure is intrinsically dependent on the length of the crack front i.e. for given load conditions, the larger the volume of material sampled by the crack front, the greater the chance of encountering a potential crack initiation site. Design fracture toughness curves (see section 6.1.1) have been derived as lower bounds to fracture test data covering a wide range of specimen sizes and as such are considered to implicitly include crack length effects. N.B. An exception is the French RCC-M code which takes into account the associates the ASME toughness curve with a reference crack length of 100 mm; for shorter crack lengths the toughness value may be increased by $(100/B)^{1/4}$.

However both the Master Curve approach and the Prometey method [10] are based on Weibull weakest-link statistics, so the value of fracture toughness is directly linked to the crack front length. The standard curves assume a uniformly loaded 25 mm crack front. Therefore for assessment of postulated RPV defects, an allowance is required for the actual length of the defect. The situation is further complicated by the fact that under PTS transients the crack driving force K_I varies over the crack front, as does the local temperature.

According to the Master Curve approach, the crack growth initiation probability is proportional to the loading level and to the volume of potential initiation locations. That is why the crack front length (size) has an effect on the allowable transition temperature (T_{0_all}). The size effect can be taken into account in the material fracture toughness (K_{IC}) by applying formulae:

$$K_{IC} = K_{min} + (K_{IC_25mm} - K_{min}) \times \left(\frac{25mm}{B} \right)^{1/4} \quad (6.14)$$

Or if the temperature and stress intensity factors vary along the crack front, the effect of these parameters can be taken into account by applying the integral approach. In the integral approach, the effective stress intensity factor K_e is evaluated applying the following formulae:

$$K_e = K_{min} + (K_{0Tref} - K_{min}) \cdot \left\{ \int_0^s \left(\frac{K_{I\Phi} - K_{min}}{K_{0\Phi} - K_{min}} \right)^4 \cdot \frac{ds}{B_0} \right\}^{1/4} \quad (6.15)$$

$K_{I\Phi}$ is obtained from the stress analysis as a function of crack front location (Φ). K_{0Tref} is the standard, high constraint, Master Curve K_0 , corresponding to a reference temperature along the crack front and it has the form

$$K_{0Tref} = 31 + 77 \cdot \exp[0.019 \cdot (T_{ref} - T_0)] \quad (6.16)$$

$K_{0\Phi}$ is the local K_0 value, based on local temperature and constraint.

In the formulas:

s is the length of the crack front

B_0 25 mm (thickness of the standard fracture specimen)

K_{min} 20 MPa \sqrt{m} .

The allowable transition temperature T_{0_all} is defined by comparing K_e to the material fracture toughness K_{IC} curve (Master Curve 5% lower bound).

According to the Russian standard [10] the resistance against brittle failure taking into account the effect of the crack front length may be presented as:

$$\frac{1}{B} \int_0^B \left(\frac{(K_I(L))_i - K_{min}}{\bar{K}_{IC}(L) - K_{min}} \right)^4 dL \leq 1, \quad (6.17)$$

where::

$(K_I(L))_i$ is the distribution of $(K_I)_i \equiv n_i \cdot K_I$ along crack front which is located in base and (or) weld metal,

n_i is the safety factor,

$\bar{K}_{IC}(L)$ is the distribution of \bar{K}_{IC} along crack front which is located in base and (or) metal that is caused by non-uniform distribution of temperature or fluence,

L is a curvilinear coordinate (see Figure 6.6),

dL is part of the crack front,

B is crack front length locating in ferritic material,

K_{min} is 20 MPa \sqrt{m} .

\bar{K}_{IC} is the reference temperature dependence of fracture toughness for the crack front length $\bar{B} \equiv 150$ mm and the fracture probability $P_f = 0.05$. \bar{K}_{IC} is determined according to Russian Standard (see also Appendix E).

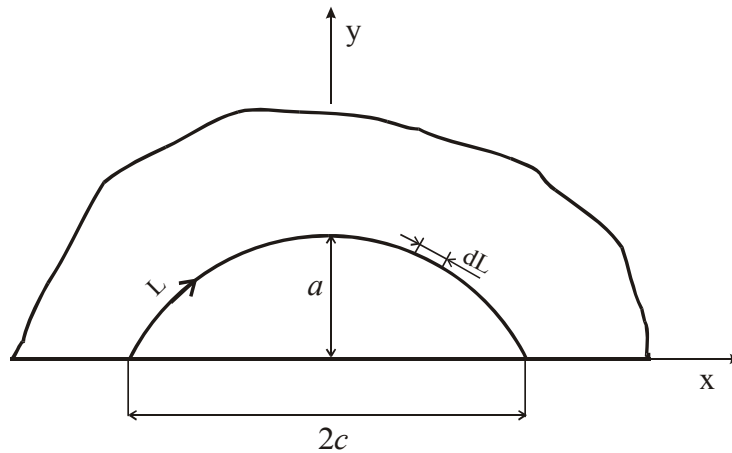


FIG. 6.6 – Curvilinear coordinate system for surface semi-elliptical crack.

6.2.4. Constraint effects

The pattern of crack-tip stresses and strains causing plastic flow and fracture in components can be different to that in test specimens. This gives rise to the so-called constraint effect. For example, the effective toughness applicable to shallow cracks (low constraint) can be higher than that associated with deep cracks (high constraint). However under PTS conditions, the thermal, pressure, and residual stresses in the reactor pressure vessel (RPV) combine to form a complex, biaxial, non-linear state of stress. Included in this stress field are significant tensile out-of-plane stresses aligned parallel to possible surface or embedded flaws oriented in either the longitudinal or circumferential directions. While the behaviour of shallow flaws is of prime concern in PTS analyses, the low crack-tip constraint associated with them is offset by the effect of biaxial loading (which tends to increase crack-tip constraint).

At present no American, European or Asian national PWR codes specifically include constraint – based fracture mechanics approaches. The development of constraint-based fracture mechanics approaches for application to PTS assessment has been the subject of research. The VOCALIST project (validation of constraint-based methodology in structural integrity) was completed in 2004. The results improved confidence in the use of $K_J - T_{\text{stress}}$ and $K_J - Q$ approaches to assessments of cleavage fracture where the effects of in-plane constraint are dominant. Cleavage fracture models based on the Weibull stress, σ_w , have been shown to be reliable, although current best practice advice suggests that σ_w should be computed in terms of hydrostatic stress (as distinct from maximum principal stress) for problems involving out-of-plane loading. Correspondingly, the results suggest that the hydrostatic parameter, Q_H , is the appropriate one with which to characterize crack-tip constraint in analysing such problems. The materials characterization test results generated as part of VOCALIST provided added confidence in the use of sub-size specimens to determine the Master Curve reference temperature, T_0 , for as-received and degraded ferritic RPV materials. The usefulness of correlating the Master Curve reference temperature, T_0 , with the constraint parameter, Q , has been demonstrated; however, the trend curves derived require further development and validation before they can be used in fracture analyses.

Russian standard [10] allows consideration of shallow crack and biaxial loading effects on fracture toughness (see Appendix E). The shallow crack effect and the biaxial loading effect should be considered for the cracks with depth less than 15% of the RPV wall thickness.

6.2.5. Warm prestressing

The warm prestress effect can be generally defined as follows: A warm prestress (WPS) is an initial preloading applied to a ferritic steel containing a pre-existing flaw which is carried out at a temperature above the ductile-brittle transition temperature, and at a higher temperature or in a less-embrittled state than that corresponding to the subsequent service assessment. The phenomenon is well known in regard the risk of RPV brittle failure for ferritic steels during possible overcooling PTS transient.

From a practical point of view, it has two major consequences:

- Brittle failure can be excluded during monotonic unloading (decreasing of the stress intensity factor);
- In case of a reloading of the vessel at lower temperature, there is an additional margin against brittle failure compared with respect to the nominal material fracture toughness at that temperature.

Inclusion of warm prestress concept in codes and standards, as well as effective practice in RPV safety assessment, is variable according to codes and national requirements, as shown below.

When credit is being given to warm prestress, its applicability in particular for materials with higher embrittlement rate should be carefully considered since it may not be fully applicable in the highly embrittled materials. The national regulatory requirements may not allow use of this approach directly and further justification may be needed. Additionally, it must be mentioned that WPS does not restore material properties, i.e. cannot remove radiation embrittlement; its effect is pronounced through the crack tip blunting.

US, ASME

For flaws found during ISI, Appendix A of Section XI, Article A-5400 Emergency and faulted conditions (very low probability postulated incidents whose consequences are such that subsequent plant operation is not required and safe system shutdown is the only consideration), WPS is applicable to those transients where K_I is monotonically decreasing with time (e.g. where system repressurization is limited), allows warm prestressing to be credited to preclude flaw initiation or reinitiation at times in the transient beyond the time of the peak stress intensity factor. WPS concept is included in probabilistic code FAVOR for the calculation of the failure probability of US RPVs.

German KTA rule

WPS concept is included in German KTA Rule 3201.2, paragraph 7.9 'Brittle failure analysis' and has been applied in flaw assessment. There is no limitation for preloading. The criterion for WPS is "for transients which upon attainment of the load path maximum show a stress intensity being strictly monotonic declining versus time, crack initiation can be excluded for the crack postulated by the calculation if the crack tip has been subjected beforehand to warm preloading (warm prestress WPS) in the course of the actually considered transient".

United Kingdom

The flaw assessment is based on the failure assessment diagram (FAD) in R6 procedure, there is no direct comparison between the material fracture toughness and the stress intensity factor (or driving force). The warm prestress effect is included in R6 flaw assessment procedure, the advice in British Standard flaw assessment document BS7910 taken from R6. The WPS is not included in UK design codes. No use has been made of a quantitative WPS model, the only use has been of the conservative WPS principle. The UK regulator, NII, has accepted cases made according to this conservative WPS principle.

France (RCC-M and RSE-M Codes)

WPS concept is not included in present Codes RCC-M (Design) and RSE-M (In-service assessment) and still cannot be used in RPV assessment even though its inclusion into the RSE-M is in preparation.

VERLIFE Procedure

The VERLIFE allows consideration of the WPS effect according to the following criterion:

- If the tangent point for the fracture assessment is found on a continuously decreasing (here “decreasing” means decreasing in time) path of temperature dependence of K_I below 90% of its global maximum value $K_{I_{maxj}}$, temperature [Tt] is determined using the value of stress intensity factor equal to $0.9 K_{I_{maxj}}$ instead of value corresponding to the tangent point (warm prestressing approach);
- In the case of reloading, i.e. when the path of temperature dependence of K_I is not continuously decreasing, a maximum allowable transition temperature for static crack initiation, [Tt] can be determined using the most conservative value from all 90% of local maxima of stress intensity factor K_I .

Russian Standard MRKR-SKhR-2004

Russian standard [10] allows to use WPS effect by the following way:

- global maximum $K_{I_{max}}$ value is defined for all time period of considered PTS transient;
- strength criteria is checked only for $K_I \geq 0,9 K_{I_{max}}$ and it is automatically satisfied for $K_I < 0,9 K_{I_{max}}$.

6.3. Crack arrest

Several codes allow consideration of crack arrest and possible reinitiation scenarios usually only in cases where reloading is excluded.

6.3.1. Simplified approach

After initiation of the postulated crack, it is supposed that the crack propagates immediately to infinite length and, if the postulated crack was subcladding, propagates also through the cladding (i.e. becomes the surface one). The arrest – reinitiation analysis described below is performed for this surface, infinite length crack.

Using transient histories such as pressure, temperature and heat transfer coefficient, the temperature distribution in the vessel wall is computed and stresses due to the temperature and pressure are determined. For various penetration depths, the stress intensity factors for surface, infinite length cracks are calculated. The flaw arrest K_{Ia} and flaw initiation K_{Ic} fracture toughness profiles are also determined. Thus, for each time during the transient, the variations of K_I , K_{Ic} and K_{Ia} through the thickness are determined. The flaw penetration at which the calculated stress intensity factor exceeds the K_{Ic} profile corresponds to the critical flaw size for initiation a_i , and the penetration at which the stress intensity factor goes below the K_{Ia} curve corresponds to the critical flaw size for arrest a_a . This comparison is illustrated in Figure 6.7 for both an arrest and a non-arrest situation. This situation depends on the shape of K_I , K_{Ic} and K_{Ia} curves for individual time steps. Curves such as Figure 6.7 are prepared for a number of selected times following the postulated accident to establish the critical time.

A critical crack depth diagram consisting of graphs of a_i and a_a versus time can be prepared based on figures like Figure 6.7 for all time steps as shown in Figure 6.8 for the analysed transient. The behaviour of flaw initiation and arrest can be predicted from the critical crack depth diagram. For example, if the postulated crack with $a/t = 0.25$ initiated like in Figure 6.8a, it is initiated twice following the dotted line resulting in an arrest with $a/t = 0.54$. But if an arrest is not considered, it is initiated once following the dotted line resulting in Figure 6.8b resulting in the through-wall propagation.

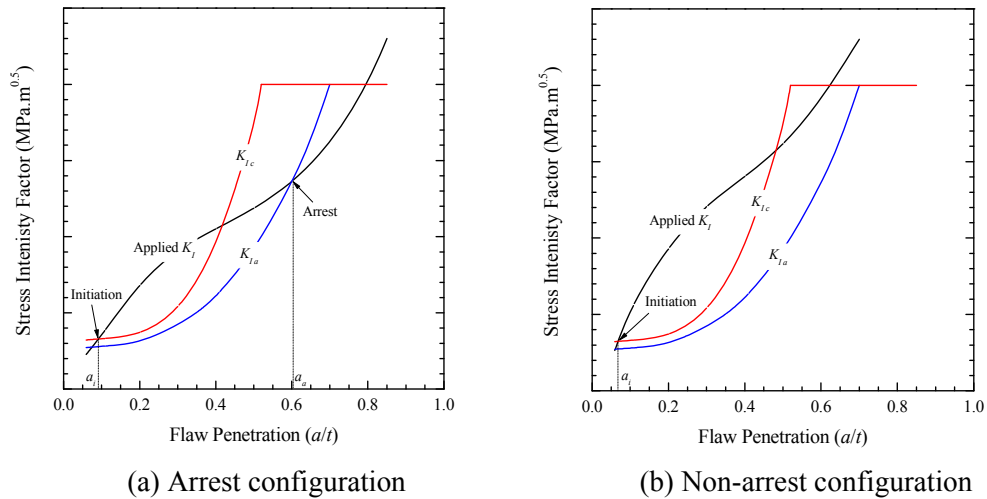


FIG. 6.7 – Determination of critical flaw sizes a) considering crack arrest and b) without crack arrest.

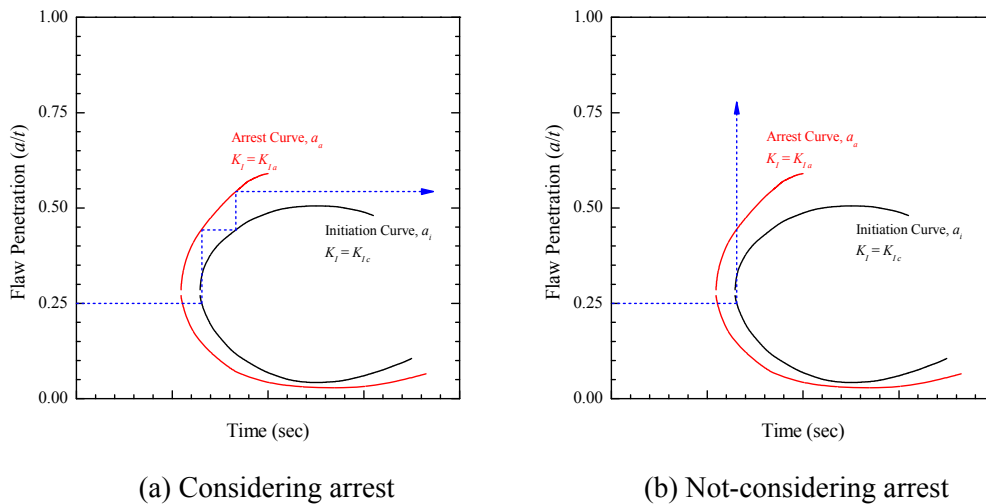


FIG. 6.8 – Critical flaw depth diagram for crack arrest analysis.

If crack initiation cannot be excluded for all relevant postulated defects and transients for the full life time of the vessel or if the demonstration of a second safety barrier is wanted then crack arrest has to be considered. The relevant Codes require that any initiated brittle fracture has to be “stably” arrested (i.e. without further reinitiation) within e.g. $\frac{3}{4}$ of the wall thickness. A linear elastic fracture mechanics calculation using analytical formulae is proposed for this purpose because of the necessity to analyse a large set of cracks with different crack depths. The temperature dependence of the arrest fracture toughness K_{Ia} can be derived from the corresponding K_{Ic} -curve through a conservative shift of ~ 30 to 40°C [9].

Obviously there is an inherent arrest capability of the RPV during thermal shock with low pressure because the driving force as a consequence of the transient thermal stresses increases through the wall thickness slowly and the material resistance increases through the wall thickness as a consequence of the increasing temperatures and decreasing irradiation effects.

6.3.2. Complex approach

The same procedure as given in the previous Chapter 6.3.1 is applied, only the crack configuration is changed. By means of available results for the stress intensity factor along the whole crack front and a variety of crack sizes, the very stringent requirement of an infinite crack length and a through the clad crack is modified. The crack shape is calculated more realistically by extending Figure 6.8 and analysing not only the deepest point, but all points along the crack front. As long as only the deepest point of the crack has initiated, the crack shape remains constant for the deeper cracks. Otherwise the crack shape will be changed during the analysis.

6.4. Fatigue crack growth assessment

Fatigue crack growth only needs to be considered for large flaws in the cylindrical part of the vessel or for flaws in nozzles. More details are given in Appendix F.

6.5. Mitigation of PTS risks

The integrity of RPV has to be guaranteed in all operation conditions and in anticipated accidents. If the PTS analyses cannot demonstrate the vessel integrity, corrective actions are required to extend the plant life. These actions include more detailed definition of material properties and load conditions, moderation of embrittlement rate and if necessary annealing of the RPV. The qualification of in-service inspection procedures can provide a basis to remove the possible over-conservativeness included in the original vessel assessment practices. The qualification of inspection procedures includes the proper technical justification and actual demonstration of the inspection capability for the RPV in question.

6.5.1. Reduction of flux and annealing

As a corrective action, the embrittlement rate of the RPV materials can be moderated by reducing the neutron flux on the RPV wall or the material properties may be restored by thermal annealing.

The flux reduction measures include the use of low leakage core loading pattern, use of partial shielding assemblies with outer fuel pins replaced by steel pins, insertion of dummy shielding assemblies and use of fuel with poison at the core periphery. The benefits of flux reduction depend on the time of implementation, original flux level and chemical composition of the vessel material. The implementation of flux reduction measures may result in plant power reduction.

Mechanical properties of embrittled vessel may be restored by thermal annealing, i.e. heating up of the critical vessel section to temperatures higher than the irradiation temperature. Two small non-commercial PWR RPVs were annealed using the "wet" low temperature annealing at 345°C, resulting in relatively low recovery of the material properties. The "dry" high temperature annealing at 460°C to 475°C has been applied to WWER-440 reactors and produced substantial or even almost complete recovery of the embrittled vessel weld.

The degree of recovery and re-embrittlement behaviour with respect to transition temperature shift have to be evaluated on plant specific basis. Further consideration of upper shelf drop and of other impacts on the vessel itself and on other structures of the plant may be also necessary.

6.5.2. Reduction of PTS loads

The reduction of vessel loading could be achieved by plant design modifications or by modification of operational procedures. Plant design modification include for example heating up of the ECCS water tanks or sumps, operator or automatic control of ECCS heat exchanger, modification of high pressure injection capacity and shut-off head, redirection of the safety injection in the downcomer to improve

mixing, implementation of low temperature overpressure protection system, modification of steamline isolation criteria, reduction of hydroaccumulator pressure, especially for the hydroaccumulators connected to downcomer, and others.

The modification of operational procedures involves operator training and establishing operational actions based on integrated systematic evaluation of PTS events. These include instructions to avoid isolation of breaks, high pressure injection pumps throttling etc. System responses need to be thoroughly understood by operators and detailed guidelines for operator actions developed. Such steps could reduce the probability of severe overcoolings or reduce the overcooling severity itself (in terms of thermal stresses).

The change of safety valves to qualified (for steam, water and mixture) valves or requalifying the existing safety valves gives a possibility to exclude the safety valve opening/closure transient from the PTS sequences. The exclusion is also possible if the safety valve can be fixed in open position with high reliability. These modifications need to be based on a detailed plant specific PTS analysis; the impact of modifications proposed on the core cooling in general has to be also evaluated.

6.5.3. Improvement of ISI performance

The crack size is known to be the key factor in the PTS results. The reactor pressure vessel and especially the weld in core region are inspected by NDE methods several times during the plant lifetime. So it's justified to use smaller crack sizes than a crack having depth equal to quarter of the wall thickness generally used for the preliminary licensing analyses according to the design codes and thus leading to over-conservative PTS results.

The ISI procedures have to be qualified according to national or international rules. The procedures should demonstrate the capability of detecting all the cracks placed in the blind specimens used in qualification with high reliability. The qualified inspection procedures should have a high reliability of both flaw detection and sizing. Based on the results a postulated flaw size can be defined by applying an appropriate safety factor.

6.6. References

- [1] AMERICAN SOCIETY OF MECHANICAL ENGINEERS, ASME Boiler and Pressure Vessel Code, Section III, "Nuclear Power Plant Components", New York (1995).
- [2] AMERICAN SOCIETY FOR TESTING AND MATERIALS, Conducting Drop-Weight Test to Determine Nil-Ductility Transition Temperature of Ferritic Steels, ASTM E208, West Conshohocken (2006).
- [3] AMERICAN SOCIETY OF MECHANICAL ENGINEERS, ASME Boiler and Pressure Vessel Code, Section III, Division 1, Code Case N-631, Use of Fracture Toughness Test Data to Establish Reference Temperature for Pressure Retaining Materials Other Than Bolting for Class 1 Vessels, New York (1999).
- [4] AMERICAN SOCIETY FOR TESTING AND MATERIALS, Standard Test Method for Determination of Reference Temperature, T_0 , for Ferritic Steels in the Transition Range, E1921-05, Annual Book of ASTM Standards, ASTM International, West Conshohocken (2005).
- [5] ASSOCIATION FRANÇAISE POUR LES REGLES DE CONCEPTION ET DE CONSTRUCTION DES MATERIELS DES CHAUDIERES ÉLECTRONUCLEAIRES, Design and Construction Rules for Mechanical Components of PWR Nuclear Islands, RCC-M, Paris (1988).

- [6] SICHERHEITSTECHNISCHE REGEL DES KTA, Überwachung des Bestrahlungsverhaltens von Werkstoffen der Reaktordruckbehälter von Leichtwasserreaktoren, KTA 3203, Cologne (2001).
- [7] RULES FOR DESIGN AND SAFE OPERATION OF COMPONENTS AND PIPING, PNAE-G-7-002-86, Calculation Standard for Strength of Equipment and Pipes of Nuclear Power Units, Energoatomizdat, NGA-01-85-1, NIKIET, Moscow (1989).
- [8] UNIFIED PROCEDURE FOR LIFETIME ASSESSMENT OF COMPONENTS AND PIPING IN VVER NPPS “VERLIFE”, VERSION 5 – FINAL, Řež (2003).
- [9] PROCEDURE FOR DETERMINATION OF FRACTURE TOUGHNESS TEMPERATURE DEPENDENCE FOR RPV MATERIALS OF VVER-440 AND VVER-1000, МКс-KR-2000, RD EO 0350-02, St. Petersburg, Moscow (2001).
- [10] CALCULATION PROCEDURE FOR EVALUATION OF BRITTLE STRENGTH OF VVER RPV DURING OPERATION, MRKR-SKhR-2004, RD EO 0606-2005, St. Petersburg, Moscow (2004).

7. ANALYSIS OF NOZZLES

Within PTS analysis it is necessary to show that the strength criteria are satisfied for the postulated defects located at the elements of RPV with the worst properties, highest neutron fluence and with maximum tensile stresses. The coldest water temperatures as well as the maximum heat transfer coefficient under PTS occur at the lower region of the nozzle, leading to maximum tensile stresses (see the examples presented in Appendix G for WWER-1000 and PWR RPVs). For these reasons PTS analysis also needs to be performed for this part of the RPV.

Irradiation effects are not considered for nozzle area due to negligible fluence values at this location. The integrity assessment results for the RPV nozzles area are the governing ones for unirradiated parts of RPV⁴. The following sections provide recommendations on nozzle integrity assessment.

7.1. *Governing transients*

Based on experience of PWR and WWER nozzle area calculations the small primary side break LOCA transient leads to the most severe results due to the high inner pressure during the transient. Situations with maximum temperature gradients in the RPV nozzle area should also be analysed. Therefore the governing transients to be considered for the nozzle integrity assessment are not necessary the same as for the beltline region, and specific transient selection should be performed.

7.2. *Postulated defect location*

The postulated defect should be located in the region submitted to maximum tensile stresses as well as the coldest water temperatures during the selected transient. Based on the experience of nozzle integrity assessment on PWR and WWER (with and without cladding) the defect location at the 6 o'clock position parallel to the nozzle axis, in the lower nozzle corner (inlet nozzle for PWR, inlet and outlet nozzle for WWER) leads to the most severe results however the highest stress location in the nozzle can slightly change during the transient. The highest stresses during cooling transient acting on the outlet nozzle of PWR are located at the lower nozzle area (in the MSL direction and not at the corner, due to the outlet nozzle geometry of PWR). More details can be found in Appendix G.

The size of the postulated defect could be selected with respect to the size of a realistic manufacturing defect probable to exist in the considered nozzle region or according to standards if available. According to [5] the crack depth can be also connected to the plant specific non-destructive testing qualification criteria, along with specification of safety margins.

7.3. *Temperature and stress field*

The recommendations in section 4 are also valid for the nozzle area, with some specific considerations. Stratification in the nozzle occurs for transients with ECCS water injection. This has to be taken into account in the thermal load description (T fluid, HTC), in addition to the mechanical loading due to pressure variation and other loadings due to the attached piping system.

The residual stress in the cladding due to the cladding manufacturing should be considered in the calculation. This stress is usually simulated with the use of the stress-free temperature in the FE code.

⁴ The integrity assessment results for the cylindrical part of RPV are the governing ones for the irradiated part of RPV due to of the worst material properties, large values of neutron fluence and high rates of embrittlement

7.4. K_I estimation methods and integrity assessment

Numerical methods of K_I calculations are preferable if no validated and solid analytical solution is available. According to the Russian and German experience, the WPS effect as well as shallow crack and biaxial loading effects can be taken into account in calculations. Also the calculations with the integral approach and evaluation of ductile tearing risk should be performed for nozzles. Consideration of crack arrest can be seen as a safety barrier redundancy, to supplement exclusion of initiation.

8. OTHER ISSUES

8.1. Management system and quality assurance

The overall PTS analysis including its individual parts should be subject to formally established management and quality assurance procedures in line with applicable national standards and the IAEA Safety Standards for Management Systems [1].

As outlined in [2], such procedures should consider the following general principles:

- The responsibility of any individual working in the organization involved in the analyses should be clearly specified;
- The qualification of experts should be sufficiently high and adequately documented;
- Calculational notes and results should be documented to the extent needed to allow their independent checking by qualified reviewers;
- Only validated methods and tools should be used;
- Procedures and results should be independently reviewed both from a technical as well as a procedural point of view;
- All differences found during the review should be resolved before the final use of the results.

These principles may be expressed more specifically as follows:

- Selection of initial data and boundary conditions, computer codes and users, influence the quality of results, therefore all of them should be subject to quality assurance procedures;
- Any activity should be performed only by qualified personnel. A record documenting the qualification should be maintained;
- The origin and version of computer codes used should be clearly documented and must be referenced in order to allow a meaningful evaluation of a specific accident analysis. Computer codes should be verified and validated for the relevant area of their application; verification and validation should be documented;
- All sources of primary plant data should be clearly referenced. Derivation of input data for the analysis from primary information should be documented in such way to permit adequate control, review, check and verification. A form should be used which is suitable for reproduction, filing and retrieval. Notes should be sufficiently detailed such that a person technically qualified in the subject can review, understand and verify the results;
- It is advantageous to have one "master" input deck. All calculations should be done introducing the necessary changes (e.g. initial conditions, functioning of safety systems) with respect to this "master". All such changes should be documented so that it can be traced to the date in which improvements/error corrections have been done. Inputs should be designated in a way that permits later checking. Data permitting reconstruction of calculated results must be archived (including relevant parametric studies);
- For each case analysed a sufficient description of input data, basic assumptions and process and control system operational features should be provided giving a possibility of a unique interpretation and reproducibility of the results. It is recommended to follow the same format for all cases analysed;
- "User effects" should be reduced to minimum. This implies that guidelines should be developed at the institution performing the analyses, permitting each member of the staff to benefit from the experience accumulated in applying a given computer code. For the same reason, data transfer between computer codes should either be automatic or it must be assured that they are defined in an unequivocal way;
- Results should be presented in such quality and detail to allow the reviewer to check the fulfilment of all acceptance criteria and to understand properly all elements and in particular the interdisciplinary aspects (interfaces) of the PTS analysis. The same format for presentation of results for all cases under consideration is recommended. Results of analysis should be archived for a sufficiently long period of time;

- All calculations and analyses should be checked by a competent individual other than the author. The following methods may be used for checking the adequacy and correctness of calculations:
 - Independent review and checking of calculations;
 - Comparison with results of other methods such as simplified calculations or alternative computational methodologies;
 - Other appropriate methods may be also used;
 - The review process and all comments as well as deficiencies found by the reviewer should be adequately documented. Specifically it must be documented which parts of calculations and results have been checked and which methods have been adopted;
 - In response, the author should properly address all comments and remove all deficiencies to the satisfaction of the reviewer;
 - All input data for structural analysis (like RPV geometry, material properties etc.) should be documented according to the QA manual prepared for the PTS analysis.

8.1.1. Use of computer codes

Computer codes play a crucial role at several stages of PTS assessment. The confidence in the results depends strongly on the capability of the code to model the pertinent physical phenomena and on the judicious preparation of input data for the calculations. In order to ensure consistency of results and permit independent review of the analysis, a comprehensive documentation of the code(s) used should be developed.

All models and correlations used in the code should be explained. The applicability range of correlations must be stated and they should not be used outside that range. It should be ensured, that the numerical scheme is suitable and convergent. Truncation errors and numerical diffusion should be kept within an acceptable level.

Since the user of codes may not have been involved in the code development and testing, code documentation should include detailed user guidelines. These should include, among others, guidance on modelling for each specific component or sub-model. It is recommended to perform uncertainty and sensitivity analyses to identify the main influence factors on the relevant results to support the assumptions for PTS analysis.

To ensure consistency of the analysis results of the computer codes used for integrity assessment, a comprehensive documentation of the methods and user guidelines including simple verification examples should be available. Furthermore the users of the codes should be well-trained, which can be achieved by participation in round robin exercises or by using benchmark results for training purposes. Due to the common practice that structural and thermal hydraulic calculations are performed separately, the adequacy of the coupling should be assessed for each specific application. The international cooperation in benchmarking and methods qualification is recommended.

Thermal Hydraulic Codes

The applied thermal hydraulic system code and fluid flow mixing code are required to provide input for the structural analysis in terms of the downcomer temperature field, heat transfer coefficient field, and the primary pressure during selected transients and accidents.

A basic requirement is the adequacy of the physical model being used to represent plant behaviour realistically. The choice of the model also depends on the accident being evaluated. The models should include an accurate presentation of the pertinent part of the primary and secondary systems. Particular attention should be given to the modelling of control systems.

The thermal hydraulic models should be capable of predicting system behaviour and critical flow in single and two-phase flow conditions. The models should be capable of predicting plant behaviour for LOCA, steam line breaks, primary-to-secondary leakage accidents, and various overcooling transients. In general, a one dimensional lumped parameters code is suitable for most overcooling sequence

calculations (except for thermal stratification as discussed below). In case it is likely that the non-uniform temperature and velocity fields in reactor downcomer can influence overall system behaviour (especially circulation rates in individual loops), the application of system TH codes with 2D/3D capabilities is more appropriate than a simple 1D system TH calculation.

The models should be capable of predicting condensation at all steam-structure and steam-water interfaces in the primary system, especially in the pressurizer during the repressurization phase of an overcooling event or during refilling of the primary system with safety injection water. The effects of non-condensable gases (if present) on system pressure and temperature calculations should be included. In special cases the thermal hydraulic models should be coupled with appropriate neutronic models that have the capability to analyse pressure surges resulting from sequences involving recriticality. Adequate modelling of natural circulation and validation is important. Fluid flow mixing codes should be able to describe the phenomena like mixing near the injection location, stratification in the cold leg and mixing in the downcomer.

An important feature of some PTS transients is flow stagnation in the primary circuit. It occurs when the flow distribution is governed by buoyancy forces (i.e. thermal stratification and mixing of cold high pressure injection water in the cold legs and the downcomer become the dominant effects). These phenomena can also be influenced by the loop seals behaviour. Since these may not be predicted correctly with the existing thermal hydraulic system codes, specific fluid-fluid mixing calculations may be needed, as discussed above in Chapter 4.

Structural Calculation Codes

For the RPV integrity assessment a three step structural analysis is necessary:

- structure temperature field;
- structure stress-strain fields;
- loading of postulated defects in terms of stress intensity factor.

For the determination of temperature distribution and the structural response the finite element method is normally used. Crack loading can be calculated using analytical engineering methods or by finite element analysis with postulated cracks generated in the FEM mesh. The choice between linear elastic or elastic plastic 2D or 3D FEM analysis, with or without postulated cracks generated in the FEM mesh depends on several factors such as: the degree of accuracy required in the results, the complexity and severity of the loading conditions, the existence of RPV inner surface cladding, and the computation time.

8.1.2. Code validation

The quantification of the status of validation⁵ can be expressed in terms of the accuracy of the code predictive capabilities for specific output quantities, which can be derived by theoretical formula or measured in the frame of experiments or plant monitoring. In practical sense the validation process includes the comparison between experimental and analysis results which could effect (if necessary) a reformulation of the analytical model. Sometimes a code can predict a set of parameters with high degree of accuracy and still be inaccurate for other ones. This has led to the need to develop a validation matrix with respect to different types of experimental facilities and different sets of conditions in each facility. In that sense experiments influence the code development and vice versa.

Inter-comparison exercises between codes (round robins) and direct comparison of predictions with integral or single-effect results from experimental simulations are an important part of the validation process. For thermal hydraulic codes, results are available from international round-robins for WWER designs conducted under the auspices of IAEA [3, 4] and for a western type RPV in the OECD ICAS project [5]. Fluid flow mixing models should be validated against data bases such as [6].

⁵ Assessing the status of validation of any computer code is difficult because there has not been a formal consensus on what constitutes a validated code.

Benchmarking exercises for structural and fracture mechanics analysis codes include the OECD ICAS project [6] and the NESCE project [7, 8]. Also the OECD FALSIRE project [9, 10] compiled results from 84 analyses of 13 large-scale tests. The data base is available on request from GRS, Germany [11].

8.2. International research and development

This section provides a brief summary of recent international R&D work aimed at improving the reliability of PTS analyses.

8.2.1. IAEA Coordinated Research Projects on RPV integrity

The IAEA has sponsored a series of Coordinated Research Projects (CRPs) that have led to a focus on reactor pressure vessel (RPV) structural integrity application of measured best irradiation fracture parameters using relatively small test specimens.

The first project (or CRP Phase 1), "Irradiation Embrittlement of Reactor Pressure Vessel Steels," focused on standardization of methods for measuring embrittlement in terms of both mechanical properties and the neutron irradiation environment. The main results were published in 1975 in Report IAEA-176 [12].

CRP Phase 2, "Analysis of the Behaviour of Advanced Reactor Pressure Vessel Steels under Neutron Irradiation," involved testing and evaluation of so-called advanced RPV steels that had reduced residual compositional elements (copper and phosphorus). The results were summarized in IAEA Technical Report Series (TRS) No. 265 [13].

CRP Phase 3 "Optimising Reactor Pressure Vessel Surveillance Programmes and Their Analyses" addressed the direct measurement of fracture toughness using irradiated surveillance specimens. A key achievement was the acquisition a series of RPV steels for radiation embrittlement research. The JRQ reference material was documented in IAEA TECDOC-1230 [14].

The main emphasis during CRP Phase 4 was the experimental verification of the Master Curve approach for surveillance size specimens. Application included a large test matrix using the JRQ steel and other national steels including WWER materials. No differences in laboratories were identified, and results from dynamic data also followed the Master Curve.

Guidelines were developed and additional Master Curve testing was performed under CRP Phase 5, "Surveillance Programme Results Application to Reactor Pressure Vessel Integrity Assessment." The large CRP group consisted of 20 testing laboratories representing 15 Member countries. This CRP had two main objectives: 1) develop a large database of fracture toughness data using the Master Curve methodology for both precracked Charpy size and one-inch thick (25.4 mm) compact tension (1T-CT) specimens to assess possible specimen bias effects and any effects of the range of temperatures used to determine T_0 , either using the single temperature or multi-temperature assessment methods and 2) develop international guidelines for measuring and applying Master Curve fracture toughness results for RPV integrity assessment. The results were documented in IAEA TECDOC-1435 [16] and IAEA Technical Report Series (TRS) No. 429 [15].

CRP Phase 6 "Effects of Nickel on Irradiation Embrittlement of Light Water RPV Steels" comprised procurement of materials, determination of mechanical properties, irradiation and testing of specimens and microstructural characterization. The results clearly show the significantly higher radiation sensitivity of the high nickel weld (1.7 wt%) compared with the lower nickel base metal (1.2wt%), as documented in IAEA TECDOC-1441[16].

CRP Phase 7 was focused on WWER-440 steels and the need for an improved predictive embrittlement correlation. In this study, a group of eight representatives from seven member states developed new correlations for WWER-440 RPVs that provides better predictive capabilities based upon chemical content and neutron exposure. This new correlations were developed in a framework

that better simulates the known embrittlement mechanisms for these steels, and was published in IAEA TECDOC-1442 [17]. The CRP was accomplished through the completion of four tasks: (1) collection of WWER-440 surveillance and other relevant data and input into the IAEA International Database on RPV Materials (IDRPVM), (2) analysis of radiation embrittlement data of WWER-440 RPV materials using the IDRPVM database, (3) evaluation of predictive formulae depending on material chemical composition, neutron flux and fluence, and (4) guidelines for prediction of radiation embrittlement of operating reactor pressure vessels of WWER-440 including methodology for evaluation of surveillance data of a specific operating unit.

CRP Phase 8 is an ongoing extension of CRP-5 in that some of the outstanding issues associated with use of the Master Curve fracture toughness methodology are being studied in more detail. The overall objectives of CRP-8 include: (1) better quantification of fracture toughness issues relative to testing surveillance specimens for application to RPV integrity assessment, and (2) development of approaches for addressing MC technical issues in integrity evaluation of operating RPVs. Since the Master Curve approach is applicable to all nuclear power plant ferritic steel components, including the RPV, the scope of materials to be addressed will include both RPV and non-RPV materials.

8.2.2. NEA/CSNI Projects

The Nuclear Energy Agency's Committee on the Safety of Nuclear Installations (CSNI) has organized a series of international cooperative activities relating to PTS assessment.

ICAS (1996 to 1999)

The International Comparative Assessment Study of Pressurized-Thermal-Shock in Reactor Pressure Vessels (RPV PTS ICAS) brought together an international group of experts to perform a comparative evaluation of analysis methodologies employed in the assessment of RPV integrity under PTS loading conditions. The problem statement defined a Western type four-loop RPV with cladding on the inner surface. The task matrix included a set of transient thermal-mechanical loading conditions postulated to result from loss-of-coolant accidents. The assessment activities were divided under three tasks: deterministic fracture mechanics (DFM), probabilistic fracture mechanics (PFM) and thermal-hydraulic mixing (THM).

Within the DFM task, reasonable agreement was obtained in linear-elastic and elastic-plastic analysis results. Linear elastic analyses and J-estimation schemes were shown to provide conservative estimates of peak crack driving force when compared with those obtained using complex three-dimensional (3D) finite element analyses. Predictions of RT_{NDT} generally showed less scatter than that observed in crack driving force calculations due to the fracture toughness curve used for fracture assessment in the transition temperature region. Observed scatter in some analytical results could be traced mainly to a misinterpretation of the thermal expansion coefficient data given for the cladding and base metal.

Also, differences in some results could be due to a quality assurance problem related to procedures for approximating the loading data. For the PFM task, linear-elastic solutions were again shown to be conservative with respect to elastic-plastic solutions (by a factor of 2 to 4). Scatter in solutions obtained using the same computer code was generally attributable to differences in input parameters, e.g. standard deviations for the initial value of RT_{NDT} , as well as for nickel and copper content. In the THM task, while there was a high degree of scatter during the early part of the transient, reasonable agreement in results was obtained during the latter part of the transient. Generally, the scatter was due to differences in analytical approaches used by the participants, which included correlation-based engineering methods, system codes and three-dimensional computational fluids dynamics codes. Some of the models used to simulate condensation effects, especially those in the systems codes, showed a weakness in recognizing the flow regime at the water-stripe discharge in the downcomer.

PROSIR (2003-2007)

The objective of the PROSIR (Probabilistic Structural Integrity of a PWR Reactor Pressure Vessels) Round Robin is to issue some recommendations regarding best practices in the area of probabilistic fracture mechanics applied to RPV structural integrity evaluation and to assure an understanding of the key parameters that characterise such an approach, such as the thermal transient, the defect type and distribution, the fracture mechanics approach, etc. Organizations from 9 countries are participating. The exercise consists of a prerequisite deterministic calculation based on mean values of each relevant random parameter, and of a set of probabilistic assessments, constituting the essence of the round robin. The main results were presented a final report is under preparation.

8.2.3. EURATOM Supported Projects

The European Commission has supported a series of R&D projects relevant to PTS assessment as part of recent EURATOM framework programmes. The results are summarised in the proceedings of the FISA conference series. In addition the Joint Research Centre has coordinated several projects via the European Networks AMES (Ageing Materials European Strategy), ENIQ (European Network for Inspection and Qualification) and NESC (Network for Evaluating Structural Components). In particular the NESC-I spinning cylinder test provided a large-scale demonstration of the capability of a degraded component to resist a severe thermal shock transient and of the considerable safety margins in code-based assessment procedures.

8.3. References

- [1] INTERNATIONAL ATOMIC ENERGY AGENCY, Management Systems Safety Requirements, NS-R-3, IAEA, Vienna (2005).
- [2] INTERNATIONAL ATOMIC ENERGY AGENCY, Guidelines on Pressurized Thermal Shock Analysis of WWER Nuclear Power Plants, IAEA-EBP-WWER-08, IAEA, Vienna (2005).
- [3] INTERNATIONAL ATOMIC ENERGY AGENCY, WWER-440/213 RPV PTS Analysis Benchmark Exercise. Results of Phase I: Thermal Hydraulic System and Mixing Analysis, WWER-SC-211, IAEA, Vienna (1998).
- [4] SIEVERS J., SCHULZ, H., BASS, B. R., PUGH, C., Final Report on the Reactor Pressure Vessel Pressurized thermal Shock International Comparative Assessment Study, RPV PTS ICAS, GRS-152, NEA/CSNI/R(99) 3, (1999).
- [5] THEOFANOUS, T. G., YAN, H., A Unified Interpretation of One-Fifth to Full Scale Thermal Mixing Experiments related to Pressurized Thermal Shock, NUREG/CR-5677, Washington (1991).
- [6] INTERNATIONAL ATOMIC ENERGY AGENCY, WWER-440/213 RPV PTS Analysis Benchmark Exercise (WPB). Results of Phase II: Structural Analysis and Fracture Mechanics Analysis (Revision 3), WWER-SC-216, IAEA, Vienna (1999).
- [7] BASS B. R, WINTLE, J., HURST, R., TAYLOR, N., NESC-1 Project Overview, European Commission Report, EUR 19051 EN (2001).
- [8] STUMPFROCK L. et al, NESC-II Final Report, European Commission report EUR 20696 EN (2003).
- [9] SIEVERS, J., SCHULZ, H., BASS, B.R., PUGH, C.E., KEENEY, J., CSNI Project for Fracture Analyses of Large Scale International Reference Experiments (Phase I), GRS-108, NEA/CSNI/R, NUREG/CR 5997 (1994).

- [10] BASS, B.R., PUGH, C.E., KEENEY, J., SCHULZ, H., SIEVERS, J., CSNI Project for Fracture Analyses of Large Scale International Reference Experiments (FALSIRE II), US NRC, NUREG/CR-6460, ORNL/TM-13207, Washington (1996).
- [11] DEFFRENNES, M., HUGON, M., MANOLATOS, P., VAN GOETHEM, G., WEBSTER, S., Euratom research framework programme on reactor systems (2006), Proceedings from the International Conference on Nuclear Engineering, Miami (2006).
- [12] INTERNATIONAL ATOMIC ENERGY AGENCY, Co-ordinated Research Programme on Irradiation Embrittlement of Pressure Vessel Steels, Report of a Research Co-ordination Meeting, IAEA-TECDOC-176, IAEA, Vienna (1975).
- [13] INTERNATIONAL ATOMIC ENERGY AGENCY, Analysis of the Behaviour of Advanced Reactor Pressure Vessel Steels Under Neutron Irradiation, IAEA-TRS-265, IAEA, Vienna (1986).
- [14] INTERNATIONAL ATOMIC ENERGY AGENCY, Reference Manual on the IAEA JRQ Correlation Monitor Steel for Irradiation Damage Studies, IAEA-TECDOC-1230, IAEA, Vienna (2001).
- [15] INTERNATIONAL ATOMIC ENERGY AGENCY, Guidelines for Application of the Master Curve Approach to Reactor Pressure Vessel Integrity in Nuclear Power Plants, IAEA-TRS-429, IAEA, Vienna (2005).
- [16] INTERNATIONAL ATOMIC ENERGY AGENCY, Effects of Nickel on Irradiation Embrittlement of Light Water Reactor Pressure Vessel Steels, IAEA-TECDOC-1441, IAEA, Vienna (2005).
- [17] INTERNATIONAL ATOMIC ENERGY AGENCY, Guidelines for Prediction of Irradiation Embrittlement of Operating WWER-440 Reactor Pressure Vessels, IAEA-TECDOC-1442, IAEA, Vienna (2005).

9. CONCLUSIONS AND RECOMMENDATIONS

The handbook presents the current status on the main technical issues for deterministic PTS assessment for pressurized water reactors:

- Benchmark calculations were performed to improve the user qualification and to reduce the user effect on the results of the analysis. This addressed generic PWR and WWER reactor vessels types, as well as sensitivity analyses to check several points. For well-defined boundary conditions (vessel geometry, transient parameters, material properties, postulated flaw) the participating organizations produced very consistent results. The complementary sensitivity analyses showed that the following factors significantly influenced the assessment: flaw size, shape, location and orientation, thermal hydraulic assumptions, material toughness. Factors which proved to be of less importance included: the vessel steel stress-strain curve, fatigue crack growth, profile of weld residual stresses and (for assessment at the deepest point) whether the form of sub-clad flaws is semi-elliptical or elliptical;
- Benchmarks such as that developed in CRP-9 are important for future training for assessments of operating plants and for design of new plants;
- Applying national codes and procedures to the benchmark cases produced significantly different results in terms of allowable material transition temperature. This is mainly related to the safety factors used and approaches to postulated defects, postulated transients and representation of material toughness. In this respect the situation appears largely unchanged since the 1990s ICAS study;
- For estimating crack driving force for flaws on clad vessels, estimates from advanced handbook methods provided equivalent results to 3-D FE calculations;
- For symmetrical cooling of the core weld with 1-D temperature distributions, simplified fracture mechanics assessment methods can be applied.

For the continued development of PTS assessment technology, the following priorities are identified:

- Continue in development of international consensus on good practices for PTS assessment and associated safety margins;
- Improve consistency between PTS assessment, flaw evaluation, P-T curves, screening criteria and ISI performance;
- Development of associated training material, in particular benchmarks, recognising the multidisciplinary nature of PTS assessment and the part it plays in the overall plant life management programme;
- Future studies should focus on thermal hydraulic aspects, transient selection and on nozzle assessment;
- Improve use of harmonised probabilistic methods (transient selection, safety factors etc.) in the context of the assessment procedure;
- Need to have common approach to efficient selection of transients.

APPENDIX A
NATIONAL PRACTICES FOR PTS ASSESSMENT

Table A1 – National practices for RPV structural integrity assessment for design and operation for CRP-9 participants

	China	Czech Rep.	Finland	France	Germany	Hungary	Korea	Slovakia	Russia
Reactor Type	PWR	WWER	WWER and PWR	PWR	PWR	WWER	PWR	WWER	WWER
Codes/ Approaches	ASME XI PNAE G-7-002-86	VERLIFE	ASME III, XI, VERLIFE	RSE-M	KTA	VERLIFE	ASME XI	VERLIFE (details described in country report)	MRKR-SkR-2004
Critical Transients									
Transients	SB-LOCA LB-LOCA Over-cooling with repressurization based on PRA	LB LOCA, PRZ SV opening + reclosure	Large LOCA Safety valve opening and reclosure Cold pressurization External cooling	LB-LOCA & SB-LOCA SLB-SSLB	SB-LOCA and critical transient selected by fracture mechanics	LB LOCA SLB Overcooling with repressurization	SGTR SBLOCA MSLB	Case to case, mainly transients with pressurization under low temperature as Small LOCA, Primary to secondary leakage	WWER-1000: Primary Small LOCA, Primary to Secondary Leakage WWER-440: Primary Small LOCA, Secondary Leakage

⁶ Chinese WWER: calculations were performed for design stage in 1998-1999

	China	Czech Rep.	Finland	France	Germany	Hungary	Korea	Slovakia	Russia
Thermal Hydraulic Computation									
Tools for global system	RELAP 5	RELAP 5	APROS, RELAP5	Cathare	S-RELAP5 Version V311 PTS	RELAP5 ATHLET	RETRAN-3D RELAP5/M OD3.2	RELAP4	TRAP code
Plumes and mixing (Y/N)	No	Yes	Yes	Yes	Yes	Yes	Yes	Yes	Yes
Tools for mixing analysis	No	REMIX/NE WMIX, CATHARE	REMIX	SATURNE SYRTHES	KWU-MIX	REMIX	PHOENICS	EBOMIX	OKBMIX code
Fluence									
Measurement via monitoring (Y(position)/N)	Yes	Y, surveillance capsules, outer surface	Y (samples outside RPV, max fluence)	Yes	Yes	Yes (surveillance capsules)	Yes	Yes	Yes (surveillance capsules, templates, outer surface)
Calculation	Yes	Yes	Yes	Yes	Y 3D	Yes	Yes	recalculation based on measured values	Yes
Attenuation through the thickness (Y/N)	No	Yes	Yes	Yes	No	Yes	Yes	Yes	Yes

	China		Czech Rep.	Finland	France	Germany	Hungary	Korea	Slovakia	Russia
Vessel Temperature and Stress Evaluation										
FE (tools) or analytical	MSC.MA RC	MSC.MARC	FE, SYSTUS	FE (FLUENT, ABAQUS)	FE (ASTER, CUVEID, CASTEM, SYSTUS analytical)	FE	MSC.MARC	FE (ABAQUS, ANSYS)	FE - ADINA	FE
Elastic or elastic/plastic	Both	Elastic	Elastic-plastic	Elastic-plastic	Elastic-plastic FE or elastic + plastic correction	Elastic-plastic	Elastic, Elastic-plastic	Elastic, Elastic-plastic	Elastic-plastic	Elastic-plastic
Safety factor on loading	No	No	No	Level A Service limits 2 (primary), 1 (secondary)	Level A: 2 Level C: 1.6 Level D: 1.2	1	No	No	No	Yes
Weld residual stress (Y/N)	Yes	Yes	Yes	Yes	In clad: Yes In weld: No	Yes	Yes	Yes	Yes	Yes
Crack Driving Force										
Postulated surface defects (depth and aspect ratio, shape 1 or 2)	Shape 2 Depth=0.1t or based on NDE a/c=1/3	Depth up to 0.25t a/c=2/3 Surface semi-elliptical crack in the base or weld metal	No	Shape 1 15 mm, aspect ratio 1 (Loviisa)	design: a= 20 mm a/c=0.3	No	Depth up to 0.1t; a/c=1/3 Shape 1 Inelastic	0.1t or based on NDE a/c=1/3 shape 2	a=0.1, a/c=0.3, 0.7, shape 2	0,07t+cladding thickness, shape 2, a/c=1/3 ⁷
Postulated sub-surface defects (depth and aspect ratio)	Depth=15 mm or based on NDE a/c=1/3	No	a = 0.1* ^s , a/c = 0.3 and 0.7	No	Operation: a = 6 mm, 2c=60 mm	Depth=NDE x2 (10 mm) Ratio a/2c=1/6	Depth up to 0.1t; a/c=1/3 Shape 1 Inelastic	N0	a=0.1, a/c=0.3, 0.7, shape 2	0,07t, a/c=1/3

⁷ Russian approach: postulated defect is selected according to the size of a realistic manufacturing defect i.e. which could probably exist (with appropriate margins)

	China	Czech Rep.	Finland	France	Germany	Hungary	Korea	Slovakia	Russia
Cladding considered (Y/N)	Yes Cladding considered only in temperatures and stresses calculations	Yes	Yes	Yes	Yes	Yes	Yes	Yes	Yes
K estimation method (handbook, plasticity correction, FE)	FE, ASME XI with plasticity correction Analytical formula, no plasticity correction	FE, G-theta method	FE	Elastic un-cracked model Handbook + plasticity correction	FE	Handbook for elastic; FE for elasto-plastic	FE, Handbook	FE	FE, Handbook
Safety factor on K_I	No	No	No	No (on load)	No	No	No	No	1.1
Material Fracture Resistance									
Crack initiation parameter (RT_{NDT} , T_k , T_0)	T_k	T_0 or T_k	T_0 , (T_k)	RT_{NDT}	RT_{NDT}	T_0 or T_k	RT_{NDT} , T_0	T_k	T_k
Crack Arrest (Y/N)	No If required	Not until now	Yes	No	Yes	Not utilised	Yes	No	No
Shift formula for radiation embrittlement (code, surveillance)	R.G 1.99 and surveillance test Code (PNAE G-7-002-86)	design – code operation – surveillance results	Direct measurement on toughness of irradiated specimens and Russian code	- CVN shift - from all the surveillance programs of 58 plants	Surveillance	Surveillance results	RG1.99, surveillance	surveillance	Code+ Surveillance
Safety factors	$2^{0.5}$	On predicted T_0 or T_k	10°C	lower bound	1	On predicted T_k or T_0	$2^{0.5}$	according to VERLIFE	Yes

	China	Czech Rep.	Finland	France	Germany	Hungary	Korea	Slovakia	Russia
Integrity Evaluation Criteria									
Cleavage (Y/N)	Yes	Yes	Yes	Yes + ductile with thermal ageing considering surface content	Yes	Yes	Yes	Yes	Yes
Ductile in cladding (Y/N)	No	Not up to now (yes in future)	No	Yes	Yes	Not up to now (yes in future)	No	Yes	Yes
Crack arrest (Y/N)	Yes	Not until now	Yes	No	Yes	Not until now	Yes	No	No
Crack length correction (Y/N)	No	Y for T_0 approach only	Yes	Yes, reference toughness curve length = 100 mm	No	No	No	No	Yes
Fatigue crack growth correction (Y/N)	Yes	N for postulated defect Y for real defect (from ISI) assessment	No	Yes (but negligible in vessel wall)	No	No	No	No	Yes
WPS (Y/N)	No	Yes (monotonical unloading only)	Yes (Large LOCA, external)	No	Yes	Yes	No	Yes	Yes
Shallow crack effect loss (Y/N)	No	No	No	No	No	No	No	No	Yes
Biaxial Effects (Y/N)	No	No	No	No	No	No	No	No	Yes

	China	Czech Rep.	Finland	France	Germany	Hungary	Korea	Slovakia	Russia
Nozzles									
Nozzle Considered (Y/N)	Yes	No	Yes	Yes	Yes	Yes	No	Yes	Yes
Postulated crack, size, shape	Depth=(0.025-0.1)t Elliptical Only performed during design	Depth up to 0.25t a/c=2/3 Surface semi-elliptical crack in the base or weld metal	Based on NDE; sub-surface (10x18 mm)	- circular - 20 mm depth	Inlet: nozzle corner, 6 o'clock, straight crack front, size: NDEx2 (10mm) Outlet nozzle: cylindrical part, 6 o'clock, semi-elliptical, a/2c=1/6, size NDEx2 (10mm)	Surface and underclad flaws in lower nozzle, a=0.1t, a/c = 1/3		surface and underclad cracks in radius, a=0.1-0.25, a/c=1	Initial depth 0,07t, fatigue crack growth is considered, a/c=1/3

APPENDIX B

RESULTS OF THE ANALYSIS BENCHMARK

1. INTRODUCTION

This report describes the results of the PTS benchmark performed within Phase 1 “Benchmark calculations” of the IAEA Coordinated Research Project 9 (CRP-9) “Review and Benchmark of Calculation Methods for Structural Integrity Assessment of RPVs During PTS”. The benchmark discussed here concerns the assessment of the reactor pressure vessel (RPV) resistance against fast fracture for events in the NPP leading to pressurized thermal shock (PTS). This assessment is based on the stress intensity factors K_I for a postulated crack.

The aim of the benchmark was to compare the results obtained by individual participants for well-defined task, to compare the results obtained when applying national codes requirements and to assess the influence of individual parameters entering to the analysis when performing a large set of sensitivity studies. The further aim of this benchmark was to create data, which can be used for training of young specialist and for validation of their approach.

2. BENCHMARK DEFINITION

To enable the participants solving problems close to that ones, they solve in their countries for their types of NPPs, it was agreed to split the benchmark into two cases, i.e. PWR and WWER ones. For both cases similar transient with repressurization was selected. Also the postulated crack for both cases (for the “basic” case) was similar – axial semi-elliptical surface crack.

2.1. Basic case

The basic (mandatory) case was defined uniquely (all input parameters precisely defined) to enable comparison of the results. Only effect of different models, methods of solving the problems or user effect can be source of the differences in the results, but not the difference in the input data (e.g. material properties, crack geometry, safety margins etc.).

2.1.1. WWER case

The given scenario describes a PTS regime for a reactor pressure vessel of the WWER 440/213 type. As the initiating event, the “Pressurizer safety valve inadvertent opening with reclosure at 3600 s” is assumed. The scenario was selected for the benchmark, because it was used for an older benchmark „WPB“ organized by IAEA in the past [1, 2, 3]. The aim of the CRP-9 benchmark was to reanalyse this scenario. The same scenario was simultaneously analysed (but with rather different postulated crack and other input data) within a benchmark run in parallel under the COVERS project of 6th EURATOM framework programme [12].

The selected PTS scenario results in two opposite cold plumes below the cold legs in the downcomer of the RPV, which suddenly cool the inside surface of the RPV. The undercooled region includes the core weld that is supposed to be one of the most embrittled regions of the RPV due to neutron radiation. Additionally, welds are also likely locations for cracks or flaws. Therefore, the axially oriented semi-elliptical surface crack was postulated. The axial orientation is chosen, since maximum principal stress in a pressurized cylindrical vessel is acting in hoop direction and so perpendicular to the faces of the postulated crack. The undercooled inner surface of the RPV and the crack are exposed to tensile stress. Re-pressurizing the RPV after 3600 seconds by closing the safety valve will suddenly increase the tensile stress and is assumed to be the critical phase of the scenario. After reclosing the pressurizer safety valve, the temperature of coolant in the downcomer starts to increase.

The whole set of input data as prescribed in the benchmark proposal, is presented in Appendices B1 and B2. The data consist in thermal hydraulic input data (time variations of pressure, water temperature and heat transfer coefficient, and geometry of the cold plume), RPV geometry, material properties, residual stresses, design fracture toughness curve, postulated defect, etc. Time variations of both pressure and coolant temperature in the downcomer (in different locations) according to the benchmark definition are drawn in figures B1 and B2. Totally, 7 participants analysed at least some tasks of WWER case.

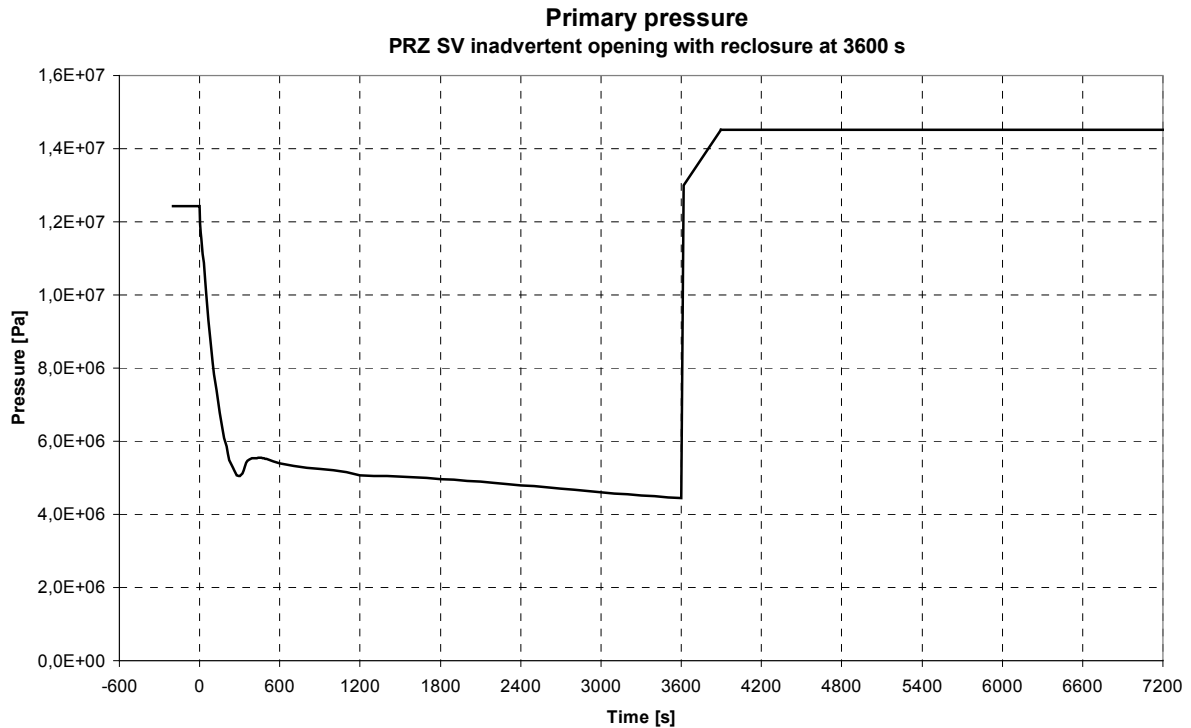


FIG. B1 – WWER case, primary pressure.

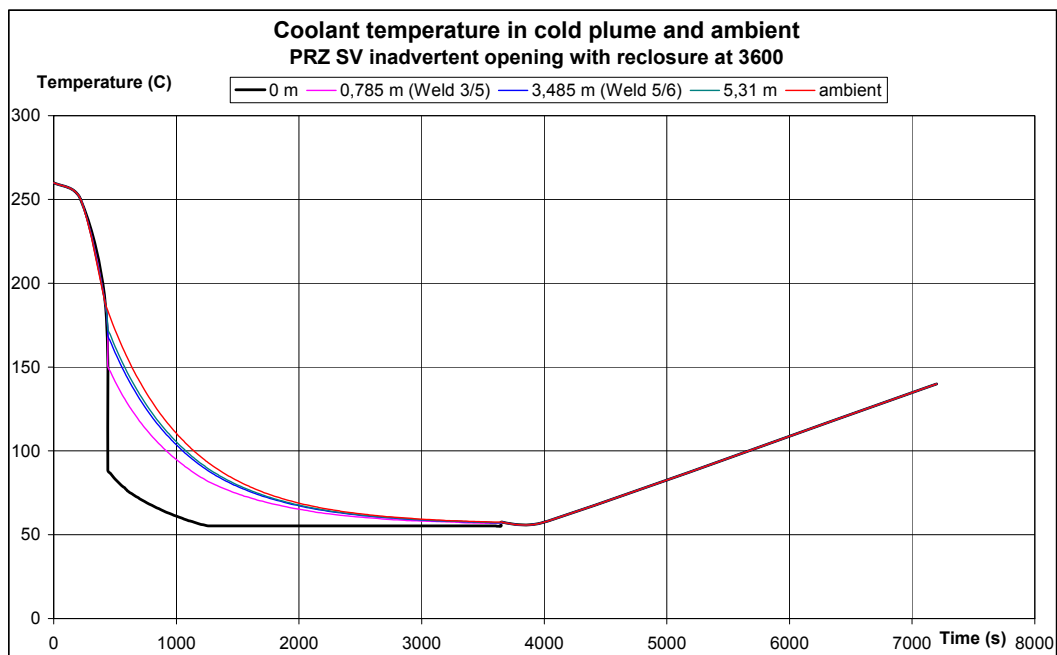


FIG. B2 – WWER case, coolant temperature.

2.1.2. PWR case

The given scenario describes PTS regime for a reactor pressure vessel of the 3 loop typical French PWR. Similarly as for the WWER case, the PTS scenario with repressurization (possibly also “Pressurizer safety valve inadvertent opening with reclosure”) was selected. The scenario was selected for the benchmark, because it was used for an older benchmark „PROSIR“ organized recently by OECD NEA [4], where it was named “TR 3”. The main purpose of the PROSIR project, in contrary to this CRP-9, was the probabilistic assessment of RPV integrity.

The course of the selected transient is similar as for WWER case. The reclosure happened at time 7185 s. The coolant temperature starts slightly increase in 6000 s. The significant difference between both cases consists in the fact, that for PWR case uniform cooling of the whole downcomer (i.e. no cold plumes creation) is supposed. The whole set of input data as prescribed in the benchmark proposal, is presented in appendices B1 and B3. Time variations of both pressure and coolant temperature in the downcomer according to the benchmark definition are drawn in figures B3 and B4.

Totally, 13 participants analysed at least some tasks of PWR case. Some participants analysed both WWER and PWR cases.

The required data to be reported by the participants were as follows:

- Variation of temperature through the RPV wall thickness
 - WWER: $t = 1,200; 2,400; 3,600$ s
 - PWR: $t = 3,600$ s, $7,200$ s
- Variation of axial and hoop stresses through the RPV wall thickness in crack free region
 - WWER: $t = 1,200; 2,400; 3,600; 3,895$ s
 - PWR: $t = 3,600$ s, $7,200$ s
- Variation of stress intensity values K_I as a function of temperature for
 - WWER: deepest point and at point 2 mm below the interface
 - PWR: deepest point and at point 2 mm below the interface
- Maximum allowable transition temperature
 - WWER: T_k^a for both positions
 - PWR: RT_{PTS} for both positions.

Additional request (during the project period) was defined as follows:

- K_I variation along the crack front (in dependency on elliptical angle)
 - WWER at 3895 s
 - PWR at 7200 s.

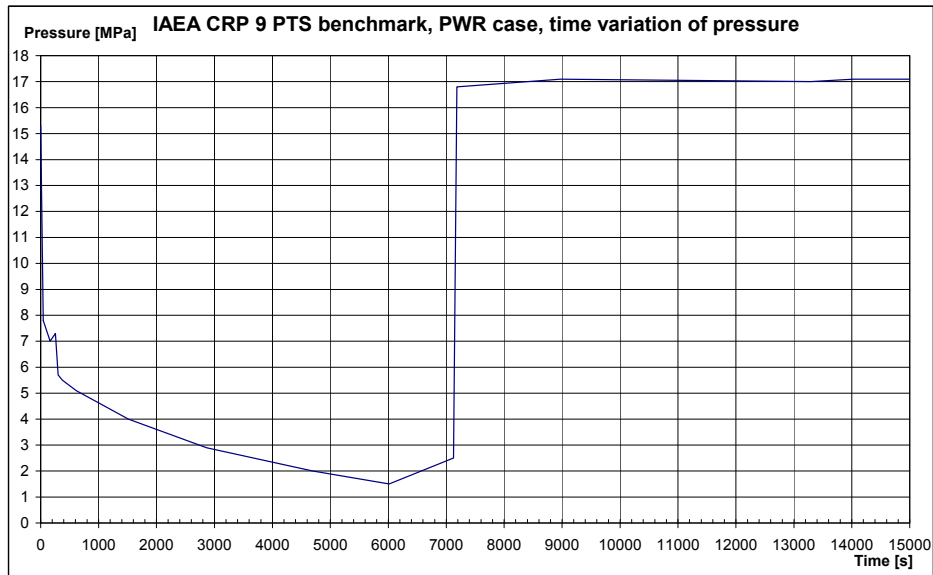


FIG. B3 – PWR case, primary pressure.

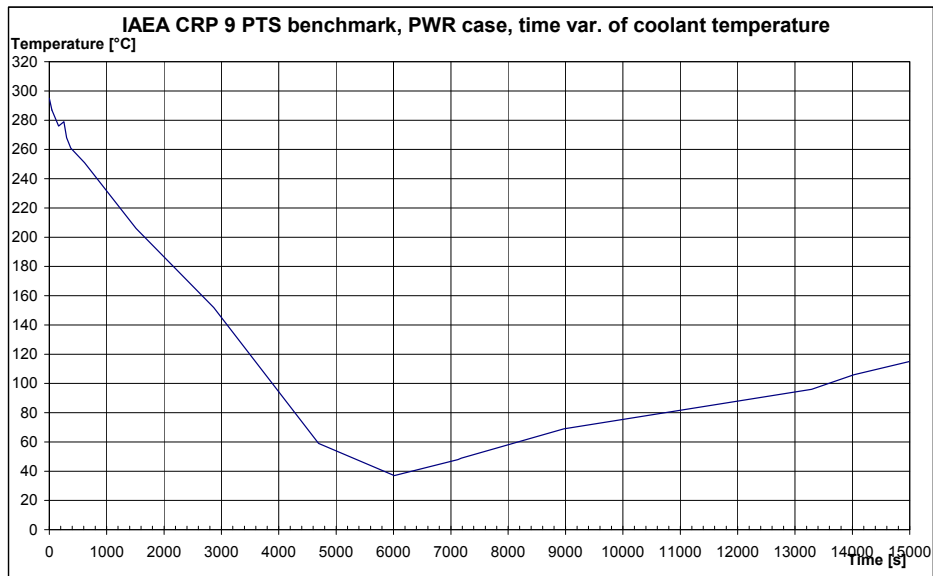


FIG. B4 – PWR case, coolant temperature.

2.2. National codes

The second task of the benchmark was application of the national codes, which are used by the participants for RPV integrity assessment in their home countries. The participants had to analyse the same transient as in the “basic case” but following the requirements of the appropriate national code. Full comparison of the results is impossible in this task. The purpose of it was to compare the approaches of individual national codes and mainly their conservativeness. Two subtasks were defined:

- Applying the national code, but with the same postulated defect as in the basic case (the purpose of this subtasks was to assess the other requirements of the codes with exception of the postulation of the defect);
- Applying the national code fully (mandatory subtask).

The required data to be reported by the participants were as follows:

- Similar to the basic case:
 - Variation of axial and hoop stresses through the RPV wall thickness in crack free region
 - WWER: $t = 3,895$ s
 - PWR: $t = 7,200$ s
 - Variation of stress intensity factor values K_I as a function of temperature for:
 - WWER : deepest point and at point 2 mm below the interface
 - PWR: deepest point and at point 2 mm below the interface
 - Maximum allowable transition temperature for:
 - Initiation
 - Arrest (if required)
- both results with and without safety factors
- Description of the methodology used
 - Description of the input data used.

2.3. Sensitivity studies

Several sensitivity studies were defined at the beginning of the project (see Table B1) and split among the participants. During the project period, the list of sensitivity studies was a little changed. The original whole list of sensitivity studies is attached in Appendix B4.

The required data to be reported by the participants were as follows:

- Similar to the basic case:
 - Variation of axial and hoop stresses through the RPV wall thickness in crack free region
- Variation of stress intensity factor values K_I as a function of temperature for:
 - WWER : deepest point and at point 2 mm below the interface
 - PWR : deepest point and at point 2 mm below the interface
- Maximum allowable transition temperature for:
 - Initiation
 - Arrest (if required)
- Description of the methodology used
- Description of the input data used.

Table B1 – Proposed sensitivity studies

Sensitivity study	Comment
1. THERMAL HYDRAULIC INPUTS	
— Heat transfer coefficients in symmetrical case (by factor 2)	semi-analytical
— Plumes	
— Cold plumes vs. symmetrical case	
— Number of plumes (3 or 2 vs. 1)	
— Width and shape of the plumes	old results ICAS
— OKB Gidropress mix	
2. PHYSICAL PROPERTIES	
— Thermal conductivity coefficient	
— Thermal expansion coefficient	old results ICAS
— Young modulus of cladding	
3. STRESS FIELD	
— Linear elastic vs. elastic-plastic	comparison of basic and national
— Surface crack	
— Underclad crack	
— Initial vs. irradiated stress strain curves	
4. RESIDUAL STRESSES IN WELDS	
— YES vs. NO	old results ICAS
— Cos shape vs. constant	
5. RESIDUAL STRESSES IN CLADDING	
— Stress free temperature	old results ICAS
— Special shape (experimental)	
— After hydrotest – OKB Gidropress	
6. POSTULATED DEFECT	
— Underclad vs. surface	comparison of basic and national
— Effect of defect depth	
— Effect of defect shape – aspect ratio	
— Elliptical vs. semi-elliptical underclad crack	old results
— Surface semi-elliptical crack – two shapes	
7. FRACTURE MECHANICS	
— Comparison of formulae with 3D modelling	ASME
— Different ways for J/K calculations	different parameters
— Effect of mesh density	
— Interface problem including cladding toughness criteria	semi-elliptical
— Effect of cladding thickness	old results ICAS
8. INTEGRITY ASSESSMENT	
— Design fracture toughness curves	
— Master Curve – 1%, 5%	
— Integral (IAEA/VERLIFE – Russian) vs. point by point	
— Base Curve	
— Arrest vs. initiation	
— Warm prestressing (first part of PTS before reclosure vs. Russian approach)	
— Constraint effect	
9. NOZZLE PROBLEMS	

3. THE PARTICIPANTS AND THEIR APPROACHES TO THE ANALYSES

14 organizations from 9 different countries participated in the benchmark:

- AREVA NP GmbH, Germany (AREVA);
- CEA, Saclay, France (CEA);
- EdF, BPI/SEPTEN, France, (EdF) ;
- Fortum Nuclear Services, Finland (FNS);
- KFKI, Hungary, (KFKI);
- Nuclear Research Institute Řež, plc, Czech Republic (NRI);
- OKB Hidropress, Russia (OKB);
- Shanghai Nuclear Engineering Research and Design Institute, China (SNERDI);
- VUJE, Slovakia (VUJE);
- Korea Institute of Nuclear Safety, Korea, (KINS) – representing also 4 other Korean participants:
 - Sungkyunkwan University (SKKU);
 - Korea Advanced Institute of Science and Technology (KAIST);
 - Korea Atomic Energy Research Institute (KAERI);
 - Korea Power Engineering Company (KOPEC).

Some Korean participants used more than one method; so finally 7 Korean solutions denoted by P1 – P7 are available.

In the following tables B2 to B10 are described details of approaches used by individual participants, namely scope of analysed tasks, computer codes, finite element models, stress free temperature, methods used for stress intensity factor calculation, details on postulated cracks, information on applied national codes, details of results presentation, treatment of residual stresses. We can state that the participants used for temperature and stress analyses different FEM codes (ADINA, SYSTUS, ABAQUS, ANSYS, MARC, CUVE-ID). Most of participants used 3D model with crack involved in the mesh and elastic-plastic analysis. Some participants used analytical tools. The FEM meshes for the basic case are seen in figures B5–B11. For J or G calculation participants used virtual crack extension method, G -theta method or direct calculation of J by path integration (Rice J -integral in 2D sections). Some participants using analytical tools used influence functions for K_I calculations.

Table B2 – Scope of structural analyses performed by benchmark participants

Participant	WWER		PWR	
	Basic case	Nat. codes A)	Nat. codes B)	Nat. codes A)
VUJE	+	+	+	-
NRI	+	+	+	-
AREVA	+	-	-	+
FNS	+	+	+	-
OKB GP	+	+	+	-
SNERDI	-	-	-	+
Korea P1	-	-	-	-
Korea P2	-	-	-	-
Korea P3	-	-	-	-
Korea P4	-	-	-	-
Korea P5	-	-	-	-
Korea P6	-	-	-	+
Korea P7	-	-	-	-
EdF	-	-	-	-
KFKI	+	-	+	-
CEA	+	-	-	-

Table B3 – Computer codes and methods used for temperature and stress analysis

Participant	Computer code name	Method	Model	Type of thermal analysis	Type of mech. analysis (for national codes)
VUJE	ADINA	FEM	3D	nonlinear	elastic-plastic
NRI	SYSTUS	FEM	3D	nonlinear	elastic-plastic
AREVA	Company code ABAQUS	Semi-analytical FEM	1D 3D	nonlinear	elastic elastic-plastic
FNS	ABAQUS	FEM	3D	nonlinear	elastic elastic-plastic
OKB GP	MSC. Marc	FEM	3D	nonlinear	elastic-plastic
SNERDI	MSC. Marc	FEM	3D	nonlinear	elastic-plastic
Korea P1	Analytical	Analytical	1D	linear	elastic
Korea P2	ABAQUS	FEM	2D	nonlinear	elastic
Korea P3	ANSYS	FEM	2D	nonlinear	elastic
Korea P4	ABAQUS	FEM	3D	nonlinear	elastic
Korea P5	VINTIN	Analytical	1D	nonlinear	elastic
Korea P6	ABAQUS	FEM	3D	nonlinear	elastic
Korea P7	FAVOR	Analytical	1D	linear	elastic
EdF	CUVE-ID	FEM	1D	nonlinear	plasticity correction
KFKI	MSC. Marc	FEM	3D	nonlinear	elastic
CEA	Own code	Analytical	1D	linear	Elastic + plastic correction

Table B4 – Description of finite element model

Organization	Full vessel / Cylindrical part	circumf. angle of segment (for 3D model)	symmetry conditions in axial direction	length of the model (m)	boundary conditions on end without crack	Pressure loading on crack face (surface crack only)	cold plume included (WWER case only)	axial variation of plume width	sharp or smooth transition to ambient
VUJE	Cylindr.	180 degree	Yes	1.5	free	Yes	Yes	Yes	sharp
NRI	Cylindr.	180 degree	Yes	2 WWER/2.5 PWR	free	Yes	Yes	Yes	sharp
AREVA	Cylindr.	N/A	Yes	N/A	free generalised plain strain	No	No	-	-
FNS	Cylindr.	90 degree	Yes	~ 2	free	Yes	Yes	Yes	sharp
OKB GP	Cylindr.	90 degree	?	>1,5	free	Yes	Yes	Yes	sharp
SNERDI	Cylindr.	90 degree	Yes	1.5	free	Yes	-	-	-
Korea P1	Cylindr.	N/A	Yes	N/A	N/A	No	N/A	N/A	
Korea P2	Cylindr.	N/A	Yes	4	free	No	N/A	N/A	
Korea P3	Cylindr.	N/A	Yes	N/A	free	No	N/A	N/A	
Korea P4	Cylindr.	180 degree	Yes	2.7	free	Yes	N/A	N/A	
Korea P5	Cylindr.	N/A	Yes	N/A	N/A	No	N/A	N/A	
Korea P6	Cylindr.	180 degree	Yes	2	free	Yes	N/A	N/A	
Korea P7	Cylindr.	N/A	Yes	N/A	N/A	Yes	N/A	N/A	
EdF	ID								
KFKI	Cylindr.	90 degree	Yes	2.5	free	Yes	Yes	No	sharp
CEA	ID	N/A	Yes	N/A	fixed	Yes	N/A	N/A	??

Table B5 – Treatment of reference temperature for thermal expansion coefficient and stress free temperature

Organization	Reference temperature of α [°C]	Correction to stress free temperature	Stress free temperature [°C]	Initial temperature [°C]
VUJE	20	Yes	according to agreed input.	according to agreed input.
NRI	20	Yes	WWER: 267 PWR: 300	WWER: 260 PWR: 295
AREVA	20	Yes	WWER: 267 PWR: 300	WWER: 260 PWR: 295
FNS	20	Yes	267	260
OKB GP	20	Yes	according to agreed input.	according to agreed input.
SNERDI	20	Yes	295	295
Korea P1	20	Yes	295	295
Korea P2	20	Yes	300	295
Korea P3	20	Yes	295	295
Korea P4	20	Yes	295	295
Korea P5	20	Yes	295	295
Korea P6	20	Yes	295	295
Korea P7	20	Yes	295	295
EdF	20	Yes	600 ?	295
KFKI	20	No (temperature dependent instantaneous α curve was used)	267.	260
CEA	20		295	295

Table B6 – Methods used by benchmark participants for stress intensity factor calculation

Participant	Crack included into FEM model	Method of K_I calculation, (in case of influence coefficient write the reference)
VUJE	Yes	J-integral converted to K_I (virtual crack extension)
NRI	Yes	G-theta method in SYSTUS, G converted to K_I
AREVA	No	Influence coefficient method (Chapuliot, plasticity correction, stress discontinuity considered)
FNS	Yes	J-integral, J converted to K_I
OKB GP	Yes	J-integral, J converted to K_I
SNERDI	Yes	Virtual crack extension
Korea P1	No	Influence coefficient method
Korea P2	No	Influence coefficient method
Korea P3	No	Influence coefficient method
Korea P4	Yes	Energy release method
Korea P5	No	Influence coefficient method
Korea P6	Yes	J-integral method in ABAQUS, $J(=G)$ converted to K_I
Korea P7	No	Influence coefficient method
EdF	No	Influence coefficient method (elastic K_I handbook + plasticity correction)
KFKI	No	Influence coefficient method
CEA	No	Influence coefficient method (elastic K_I handbook + plasticity correction)

Table B7 – Postulated crack

Participant	basic case	shape	nat. codes B)	Total depth (mm)	aspect ratio
	shape in cladding		position		
VUJE	semi-elliptical	semi-elliptical	underclad	15	0.3; 0.7
NRI	semi-elliptical	semi-elliptical	underclad	15	0.3
AREVA	straight	semi-elliptical in B/W metal	underclad	15	0.3
FNS	semi-elliptical	semi-elliptical (main axis in interface)	surface	9+15=24	0.3
OKB GP	semi-elliptical	semi-elliptical	surface + underclad	19 mm – surface 10 mm - underclad	1/3
SNERDI	straight line	semi-elliptical	underclad	15	0.3
Korea P1	semi-elliptical	N/A	N/A	N/A	N/A
Korea P2	semi-elliptical	N/A	N/A	N/A	N/A
Korea P3	semi-elliptical	N/A	N/A	N/A	N/A
Korea P4	semi-elliptical	N/A	N/A	N/A	N/A
Korea P5	semi-elliptical	N/A	N/A	N/A	N/A
Korea P6	semi-elliptical	semi-elliptical	underclad	15	1/3
Korea P7	semi-elliptical	N/A	N/A	N/A	N/A
EdF	-	-	-	-	-
KFKI	semi-elliptical	semi-elliptical	Surface, circumferential	19	1/3
CEA	straight line	semi-elliptical	Underclad / surface	Bench spec.	Bench spec.

Table B8 – Details of results presentation

Organization	Position where stresses taken (axial distance from crack, m)	Position of near interface point (distance from interface, mm)
VUJE	0.2	basic case: 2.32; national code: 0.62
NRI	0.5	basic case: 2.57; national code: 2.4
AREVA	uncracked vessel	interface region (in B/W metal)
FNS	0.14	~2.0
OKB GP	crack free model for this task	2.0
SNERDI	crack free model for this task	2.0
Korea P1	N/A	N/A
Korea P2	N/A	N/A
Korea P3	N/A	N/A
Korea P4	0.93	2.46
Korea P5	N/A	N/A
Korea P6	1	2
Korea P7	N/A	N/A
EdF	0	not done (2 mm)
KFKI	1.25	Interface region
CEA	crack free model	Interface region

Table B9 – National codes

Organization	Name of code	index temperature	Safety margin on K_I	Safety margin on index temperature	WPS applied	Crack size correction	Specific feature of the code
VUJE	VERLIFE	T_k	No	No	No	No	-
NRI	VERLIFE	T_k	No	No	No	No	-
AREVA	KTA 3201.2 (06.96)		No	No	No	No	-
FNS	VERLIFE minor modifications	T_0	No	10°C	No	Integral	Master Curve application
OKB GP	MPKP-CXP-2004	T_k	1,1	No	Yes	Yes	Base curve approach
SNERDI	ASME XI, App. A, 2004	RT_{NDT}	$\sqrt{2}$	No	No	No	-
Korea P1	N/A	N/A	N/A	N/A	N/A	N/A	N/A
Korea P2	N/A	N/A	N/A	N/A	N/A	N/A	N/A
Korea P3	N/A	N/A	N/A	N/A	N/A	N/A	N/A
Korea P4	N/A	N/A	N/A	N/A	N/A	N/A	N/A
Korea P5	N/A	N/A	N/A	N/A	N/A	N/A	N/A
Korea P6	ASME XI, App. A, 2004	RT_{NDT}	$\sqrt{2}$	No	No	No	
Korea P7	N/A	N/A	N/A	N/A	N/A	N/A	N/A
EdF	RSE-M	RT_{NDT}	2 (level A) 1.6 (level C) 1.2 (level D)	No	No	YES	crack length correction underclad toughness properties
KFKI	VERLIFE minor modifications	T_k	No	No	No	No	

Table B10 – Treatment of residual stresses

Organization	Residual stresses in cladding by setting of stress free temperature T_{free}	Residual stresses in weld (profile, amplitude)	Residual stresses in weld (description of way of including)
VUJE	Yes	constant value, 60 MPa	K_{res} calculated separately in an analytical way
NRI	Yes	cos, 60 MPa	corresponding strains included into elements
AREVA	Yes	cos, 56 - 60 MPa	elastic, {cos shape; 0}
FNS	Yes	cos, 60 MPa	input as stress distribution, integration of balance of forces
OKB GP	Yes	constant value, 60 MPa	Additional pressure loading
SNERDI	No	cos, 60 MPa	included into elements
Korea P1	N/A	N/A	N/A
Korea P2	N/A	N/A	N/A
Korea P3	N/A	N/A	N/A
Korea P4	N/A	N/A	N/A
Korea P5	N/A	N/A	N/A
Korea P6	Yes	cos, 60 MPa	
Korea P7	N/A	N/A	N/A
EdF	600°C stress free	No	
KFKI	Yes	cos, 60 MPa	K_{res} calculated separately
CEA	no	no	

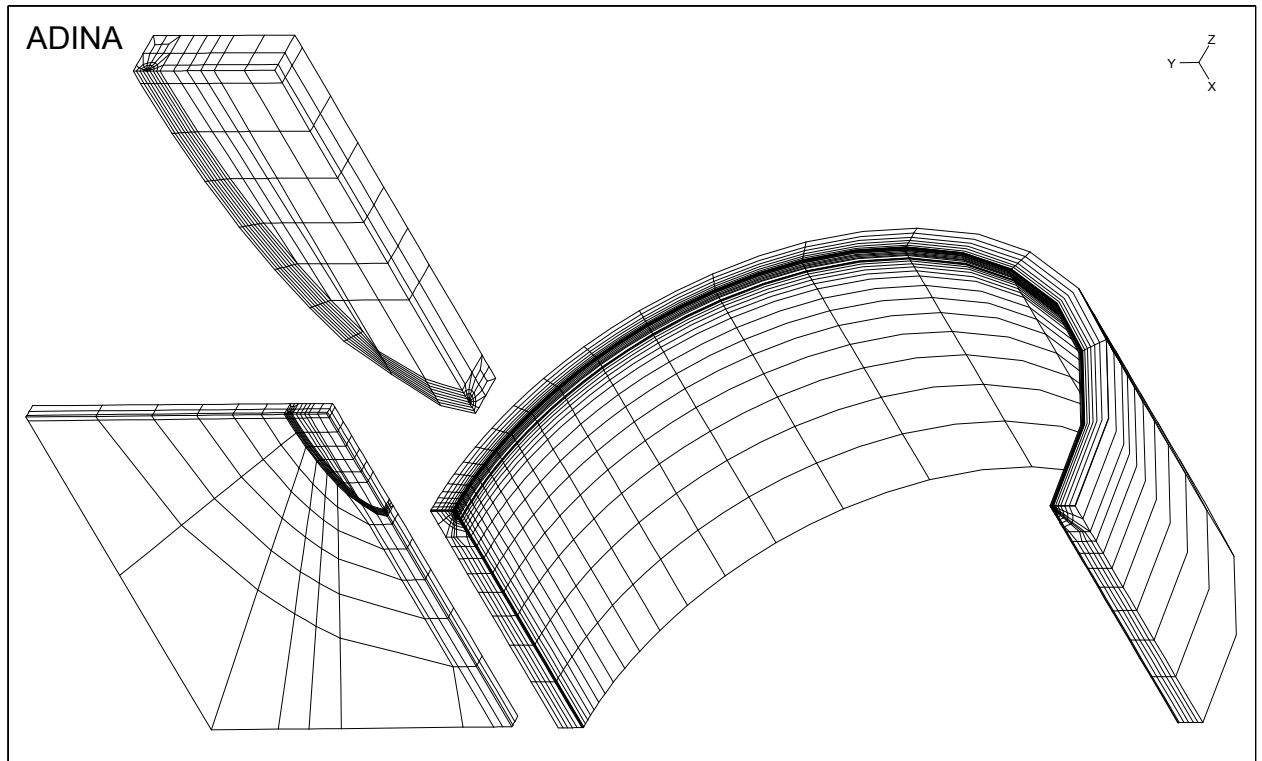


FIG. B5 – FEM mesh – VUJE, WWER case, basic case.

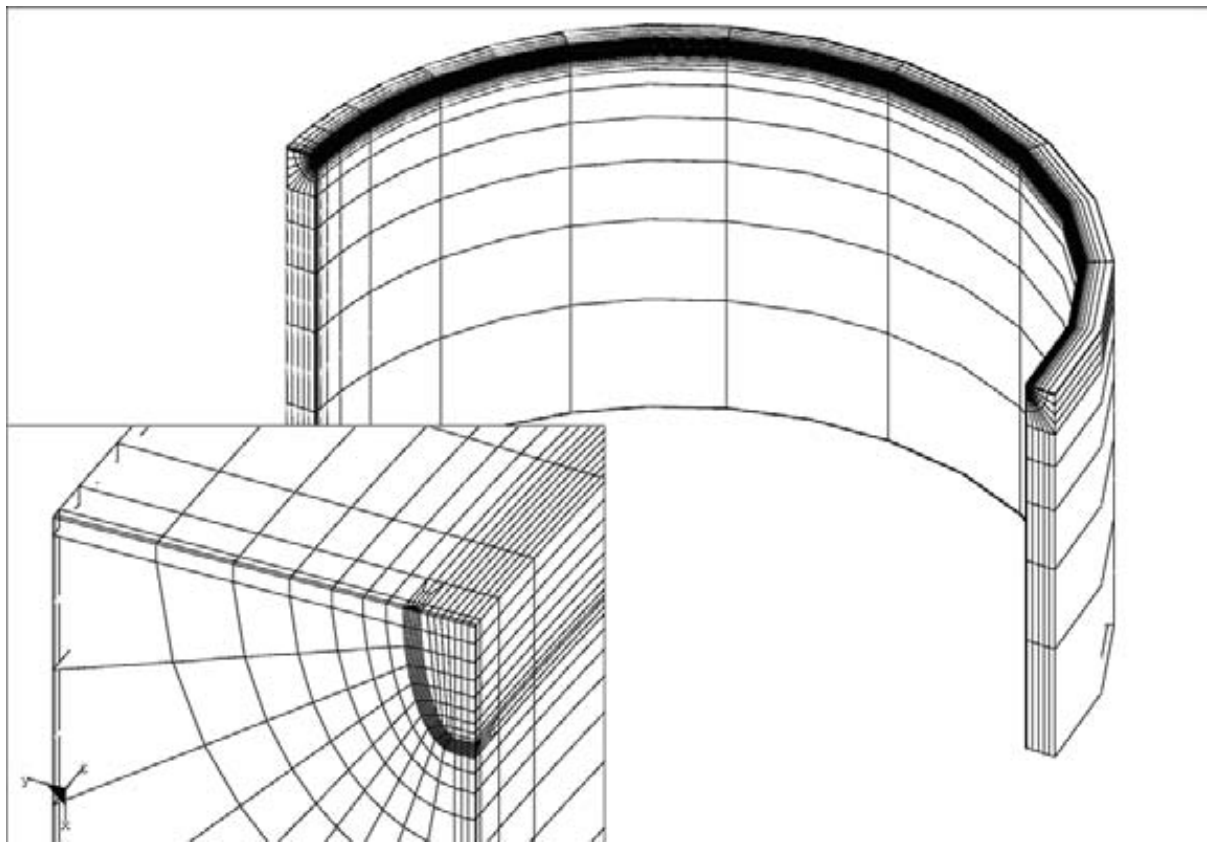


FIG. B6 – FEM mesh – NRI, WWER case, nat. codes.

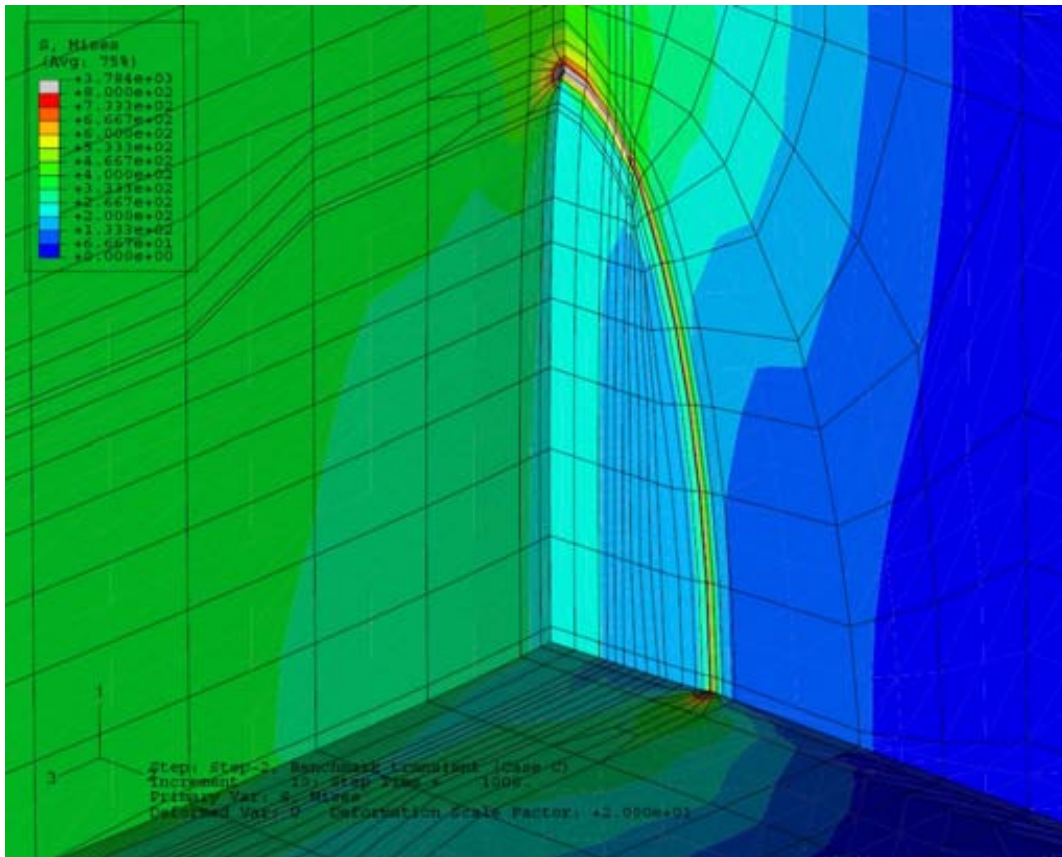


FIG. B7 – FEM mesh – FNS, WWER case, basic case.

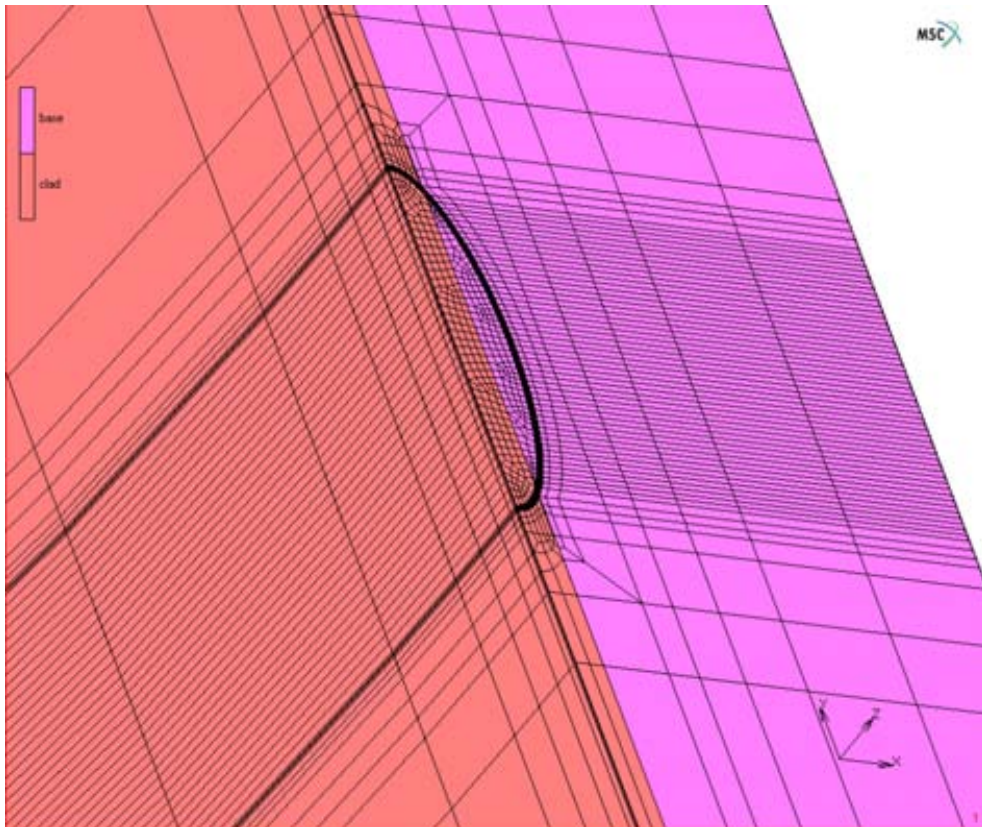


FIG. B8 – FEM mesh – OKB, WWER case, basic case.

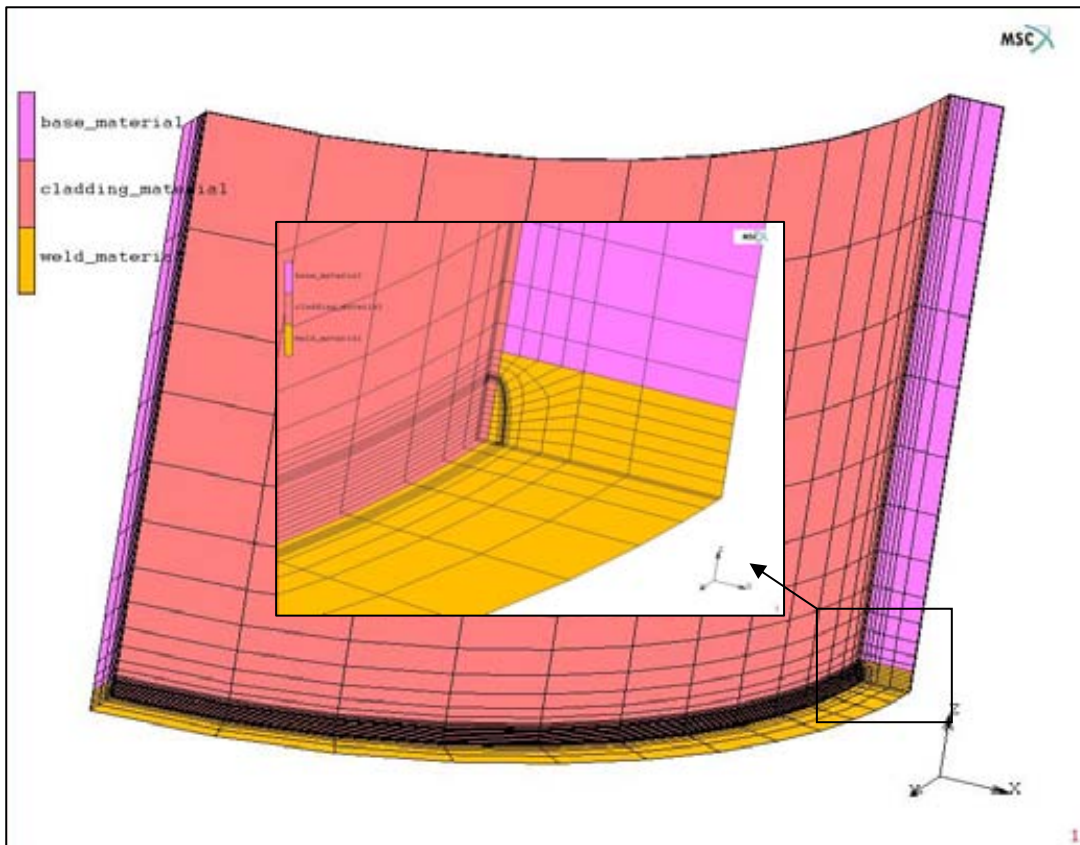


FIG. B9 – FEM mesh – SNERDI, PWR case, basic case.

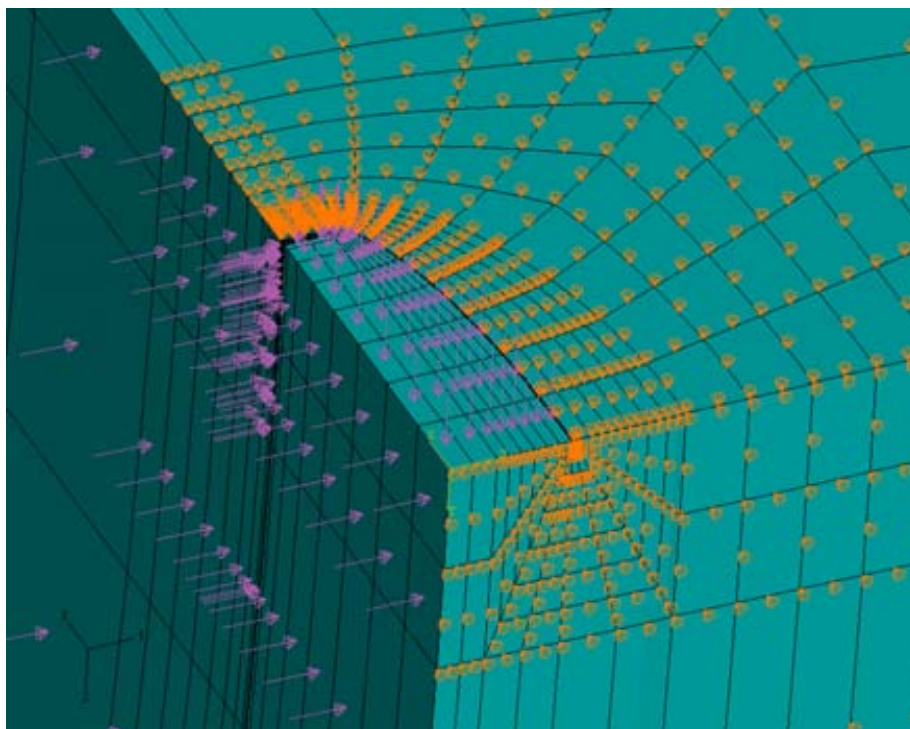


FIG. B10 – FEM mesh – Korea P4, PWR case, basic case.

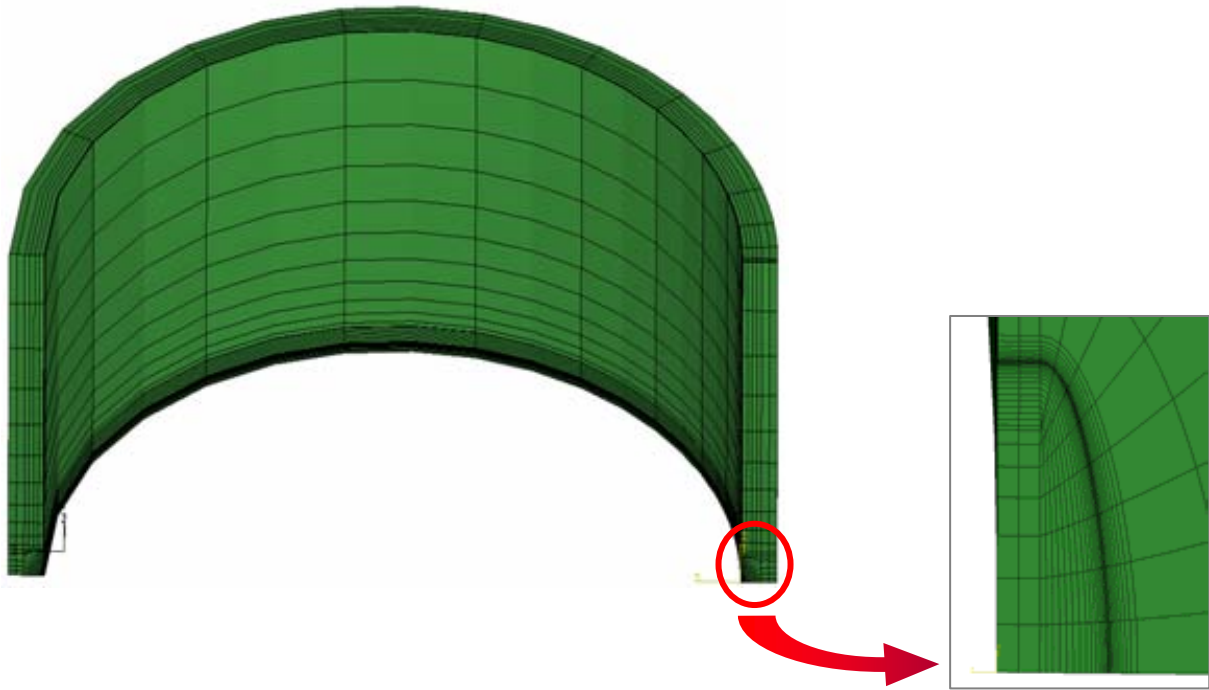


FIG. B11 – FEM mesh – Korea P6, PWR case, basic case.

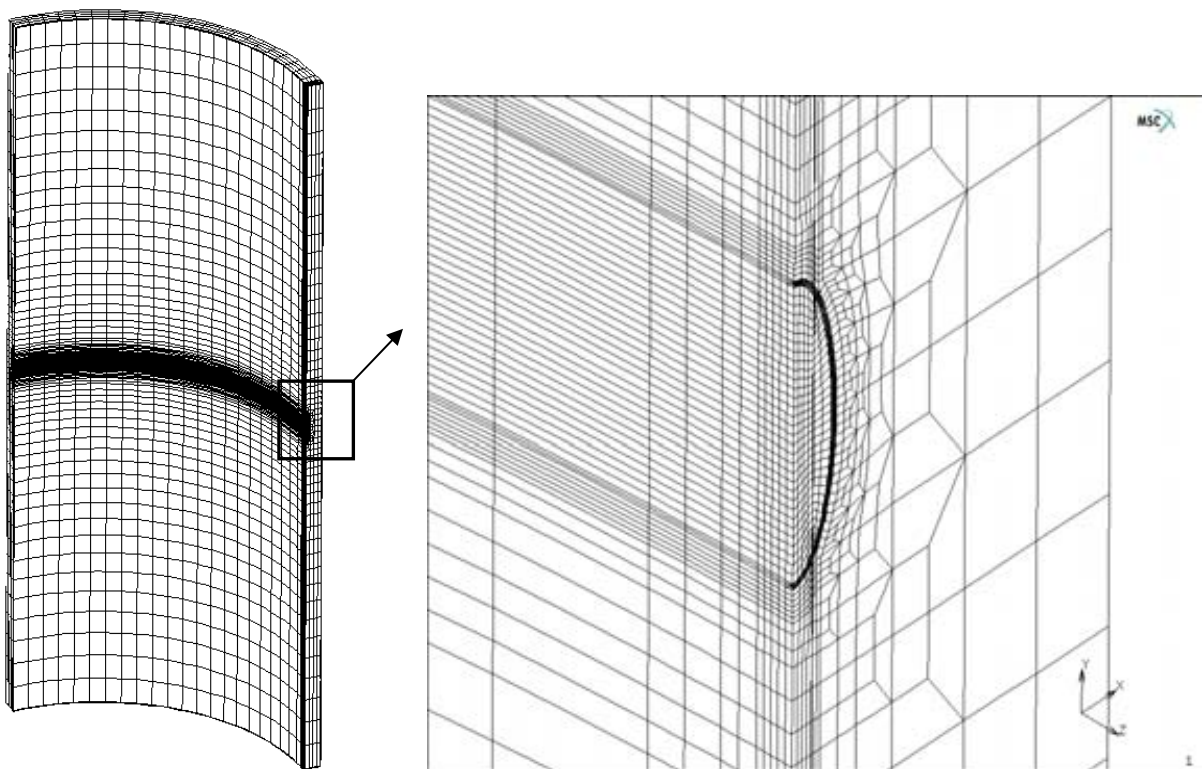


FIG. B12 – FEM mesh – KFKI, WWER case, basic case.

4. COMPARISON OF THE RESULTS, BASIC CASE

The results required by the benchmark definition (see Chapter 2) were provided by all participants in EXCEL format. The data were put in common files for individual cases to create the comparative plots. They are presented in the following figures.

4.1. Temperature fields

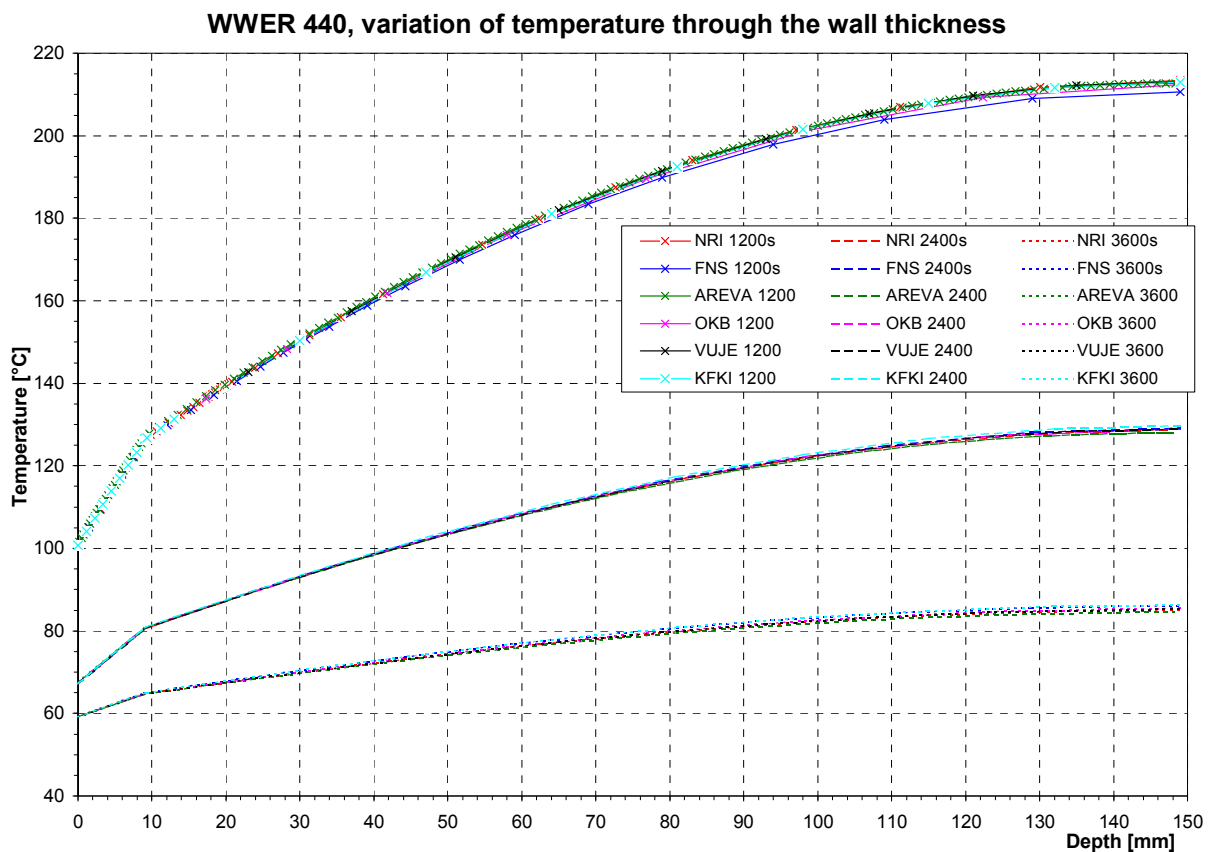


FIG. B13 – Variation of temperature through the RPV wall thickness, WWER case, $t = 1200s; 2400s; 3600s$.

PWR, variation of temperature through the wall thickness

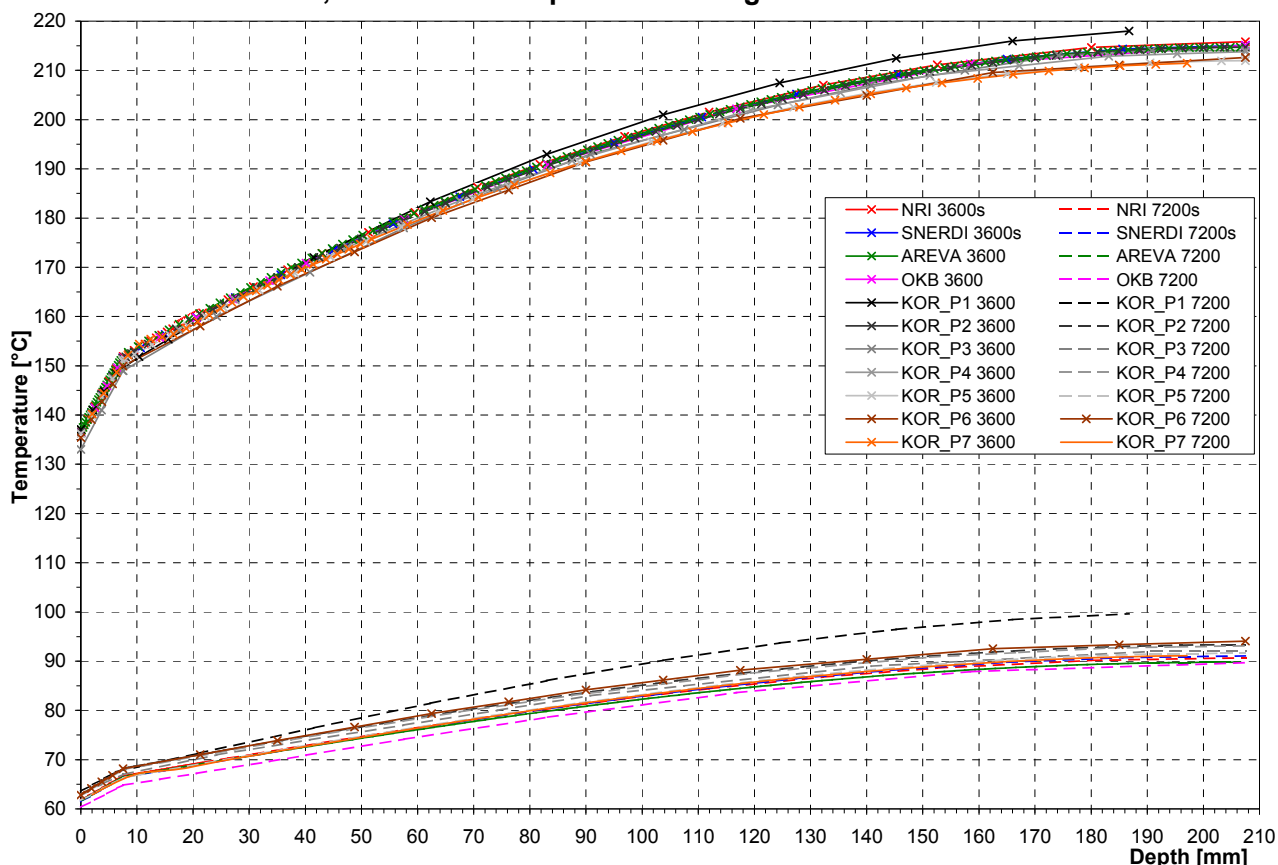


FIG. B14 – Variation of temperature through the RPV wall thickness, PWR case, $t = 3600\text{ s}; 7200\text{ s}$.

Comments to the results

We can see excellent accordance among all participants, namely for WWER case. For PWR case, one participant (Korea, P1) is an outlier, possibly due to using too simplified analytical method. With this exception, the differences in temperatures are below 3 °C or 5 °C for WWER or PWR case, respectively.

Concerning the temperature results themselves, it is seen for both cases, that due to the reduced thermal conductivity of the cladding material, the temperature gradient is steeper in the cladding (first 9 mm or 7.5 mm of the RPV thickness for WWER or PWR cases, respectively) than in the base material. The high temperature gradient through the wall thickness after the transient initiation is during the time course decreasing.

4.2. Stress fields

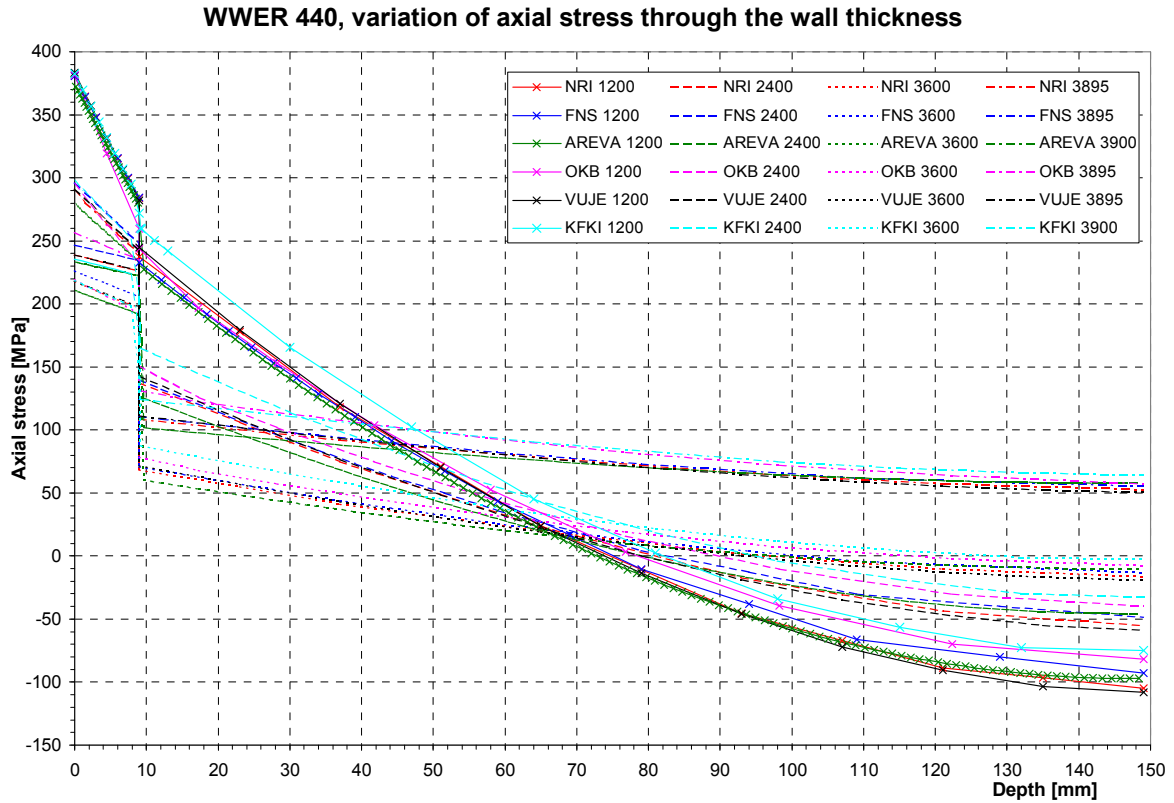


FIG. B15 – WWER case, variation of axial stress through the RPV wall thickness in crack free region.

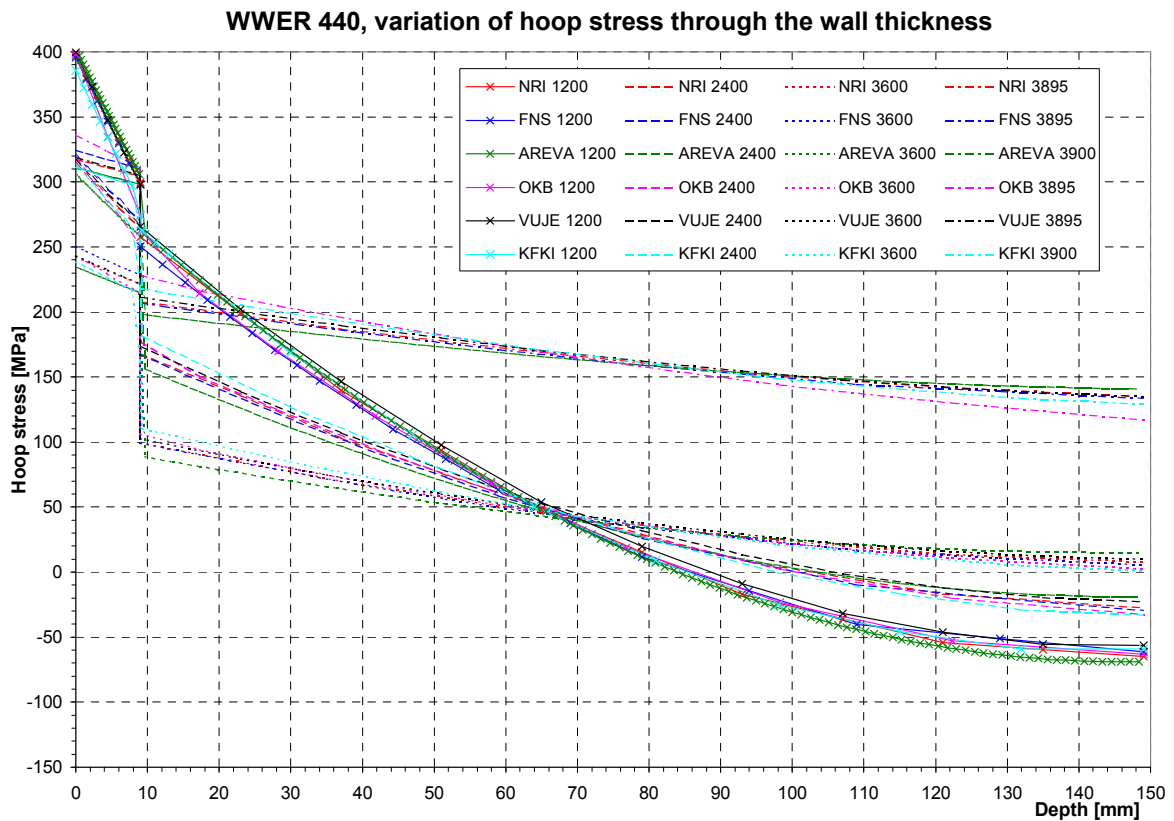


FIG. B16 – WWER case, variation of hoop stress through the RPV wall thickness in crack free region.

PWR, variation of axial stress through the wall thickness, time 3600 s

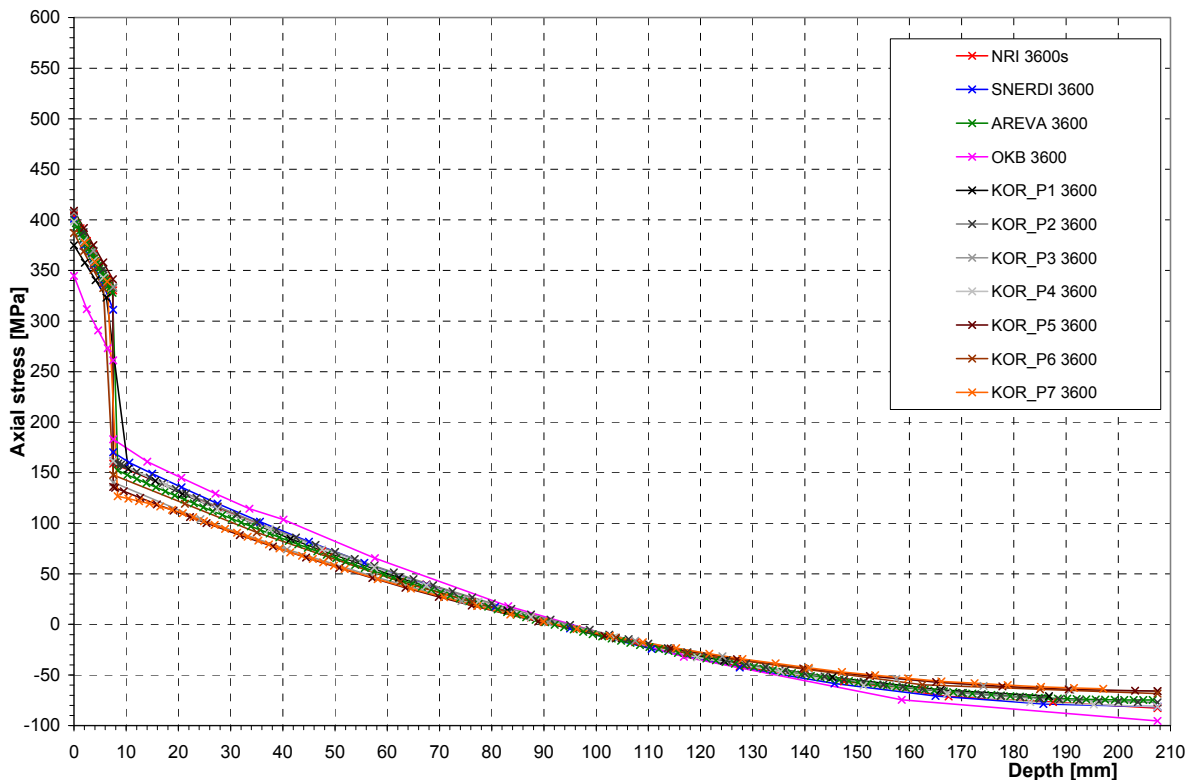


FIG. B17 – PWR case, variation of axial stress through the wall thickness in crack free region, $t=3600s$.

PWR, variation of axial stress through the wall thickness, time 7200 s

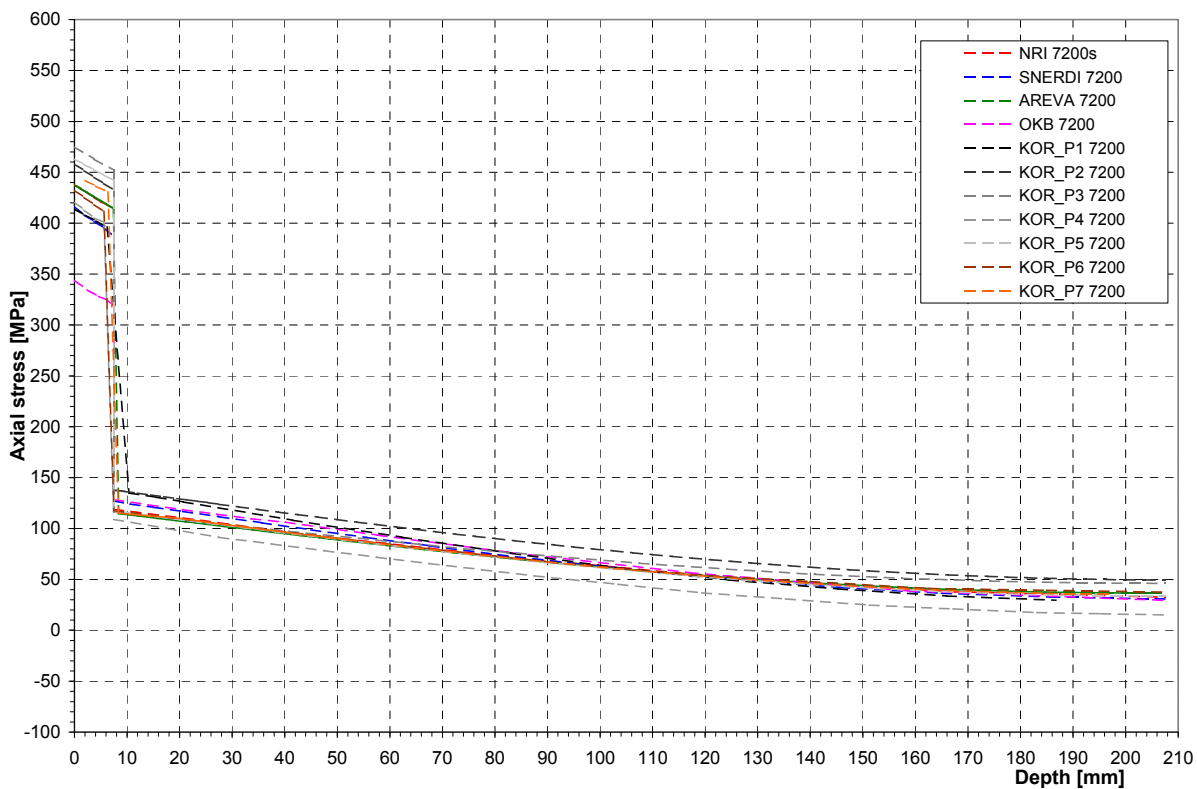


FIG. B18 – PWR case, variation of axial stress through the wall thickness in crack free region, $t=7200s$.

PWR, variation of hoop stress through the wall thickness, time 3600 s

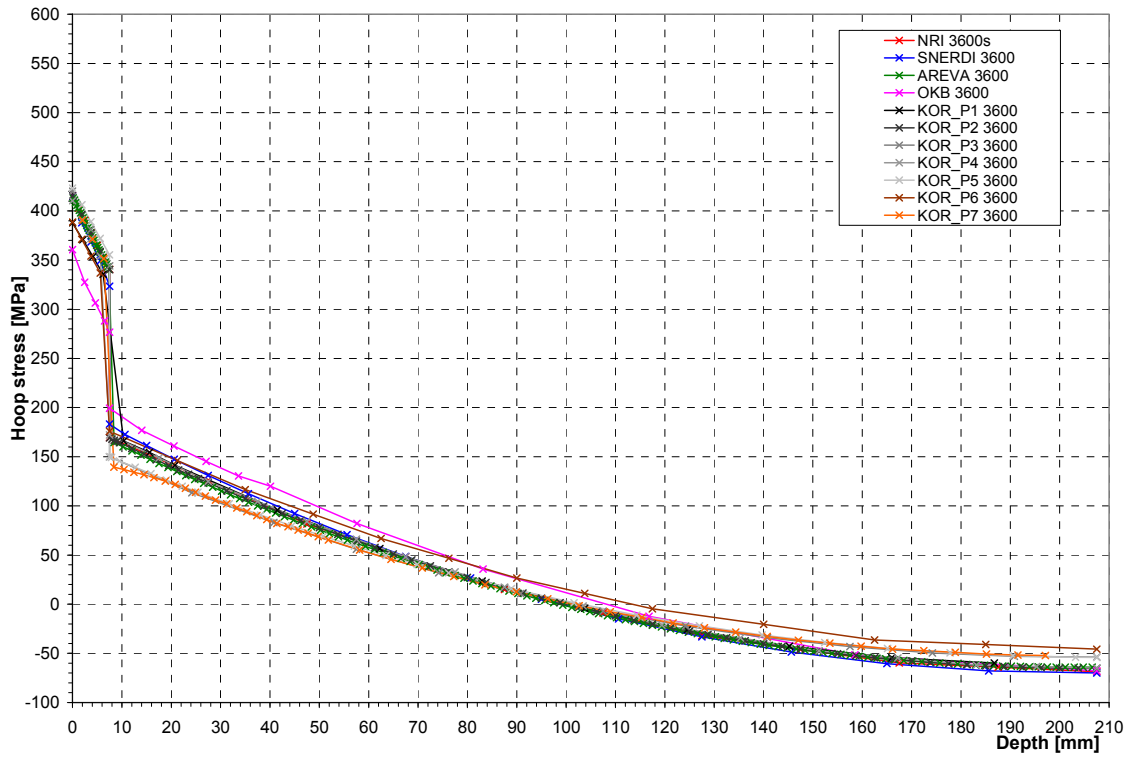


FIG. B19 – PWR case, variation of hoop stress through the wall thickness in crack free region, $t=3600$ s.

PWR, variation of hoop stress through the wall thickness, time 7200 s

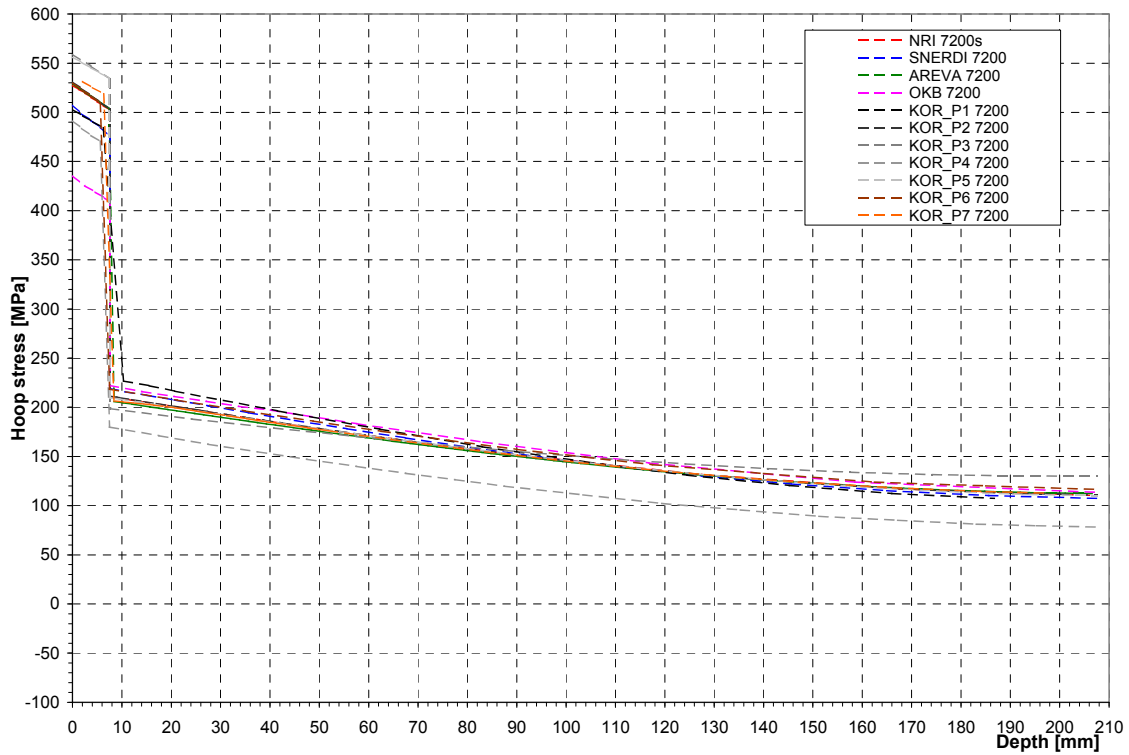


FIG. B20 – PWR case, variation of hoop stress through the wall thickness in crack free region, $t=7200$ s.

Comments to the results

We can see relatively good accordance among the participants. The better accordance is for WWER case, possibly due to smaller number of participants.

For WWER case, there are some differences in axial stresses (up to 23 MPa in cladding, up to 30 MPa in base material close to interface and up to 33 MPa in base material close to outer surface). Taking the results at long distance from the crack, where effect of the free end is in place, and moreover by simplified modelling of cold plume, causes a little bit higher values obtained by KFKI. For the circumferential stresses, the difference is up to 26 MPa in cladding, 30 MPa in base material close to interface, and 24 MPa in base material close to outer surface.

For PWR case, the highest difference for base material is about 50 MPa and for cladding up to 130 MPa (axial stress, 7200 s; here OKB seems to be outlier in cladding).

Concerning the stress results themselves, it is seen that very high stresses (reaching plasticity) are in cladding, due to different thermal expansion coefficients of base/weld material and cladding. Through the base material, the stresses decrease up to compressive stresses close to the outer surface (for time before repressurization). For WWER case, the stresses are highest (among investigated time steps) at time 1200 s, later they are decreasing due to decreasing temperature gradient. For both cases, after repressurization the stresses increased. The hoop stresses are higher than the axial ones. It confirms the well-known theoretical finding that in cylindrical vessel the hoop stresses due to inner pressure are twice higher than axial ones while the thermal stresses of both orientations are practically identical.

4.3. Stress intensity factors K_I

In the following figures, stress intensity factors are presented as variations of K_I with temperature during the transient. Moreover, the temperature variations of allowable values of stress intensity factor are presented in these figures according to the following formulae:

$$K_{IC} = 26 + 36 \cdot \exp[0,02 \cdot (T - T_k)] \quad \text{for WWER case (VERLIFE formula),} \quad (\text{B1})$$

$$K_{IC} = 36,5 + 3,1 \cdot \exp[0,036 \cdot (T - RT_{NDT} + 55.5)] \quad \text{for PWR case (ASME formula).} \quad (\text{B2})$$

The diagrams are presented for that value of T_k or RT_{NDT} , for which K_I and K_{IC} curves are touching, i.e. for maximum allowable transition temperature. For lucidity, only for the highest value of maximum allowable transition temperature among all participants, the K_{IC} curve is drawn. The diagrams are drawn separately for the deepest point of the crack and for the near interface point (2 mm below cladding / base or weld material interface). In all cases, the figure is drawn for the whole transient and detailed plot for the situation near the critical time (which was found early after repressurization). The values of K_I at the first maximum during the transient (before repressurization) as well as the values of K_I for the critical time are compared in separate plots.

WWER case

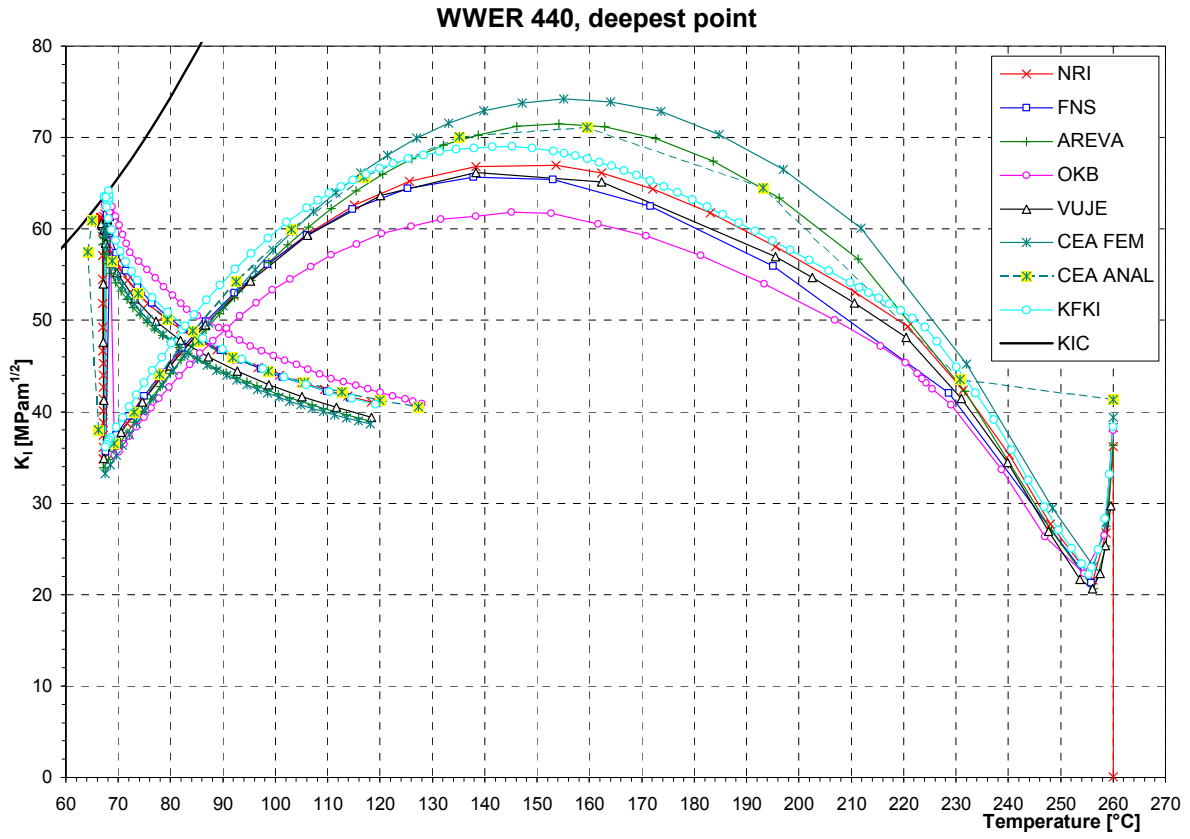


FIG. B21 – WWER case, K_b , K_{IC} vs. temperature, the deepest point, the whole transient.

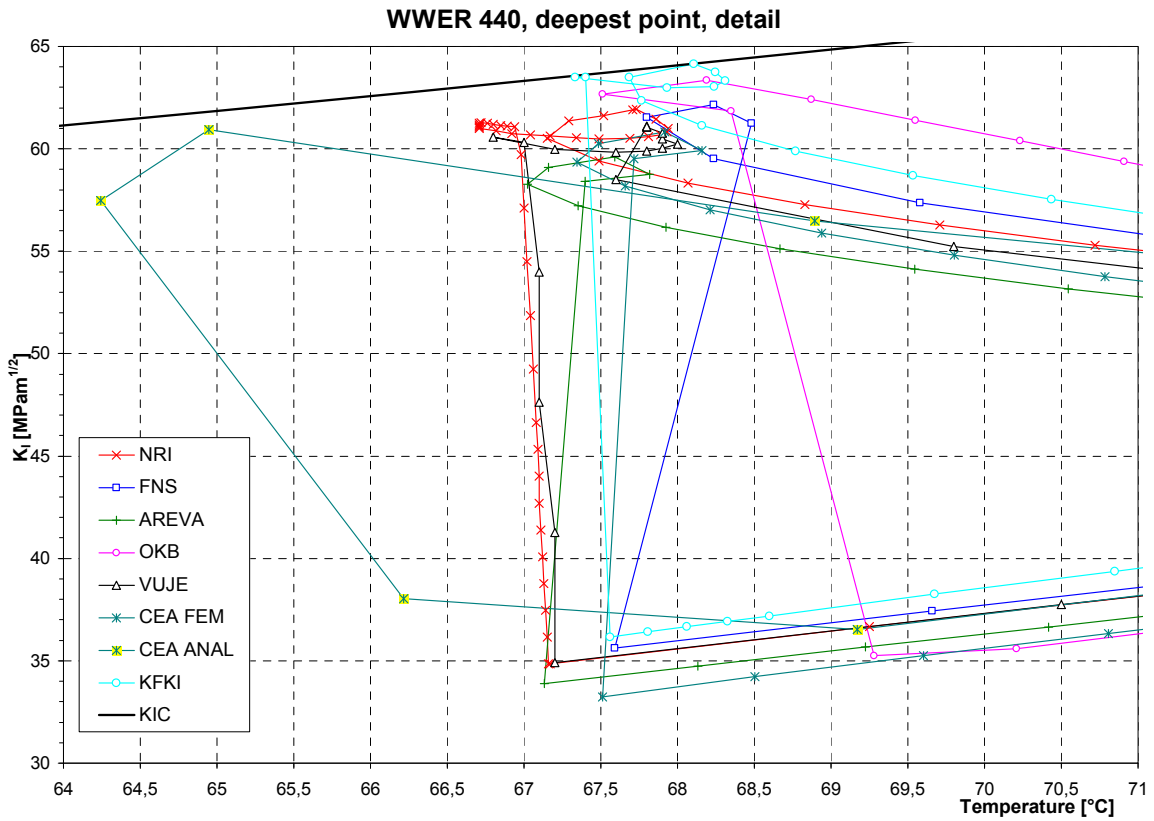


FIG. B22 – WWER case, K_b , K_{IC} vs. temperature, the deepest point, detail close to the critical time.

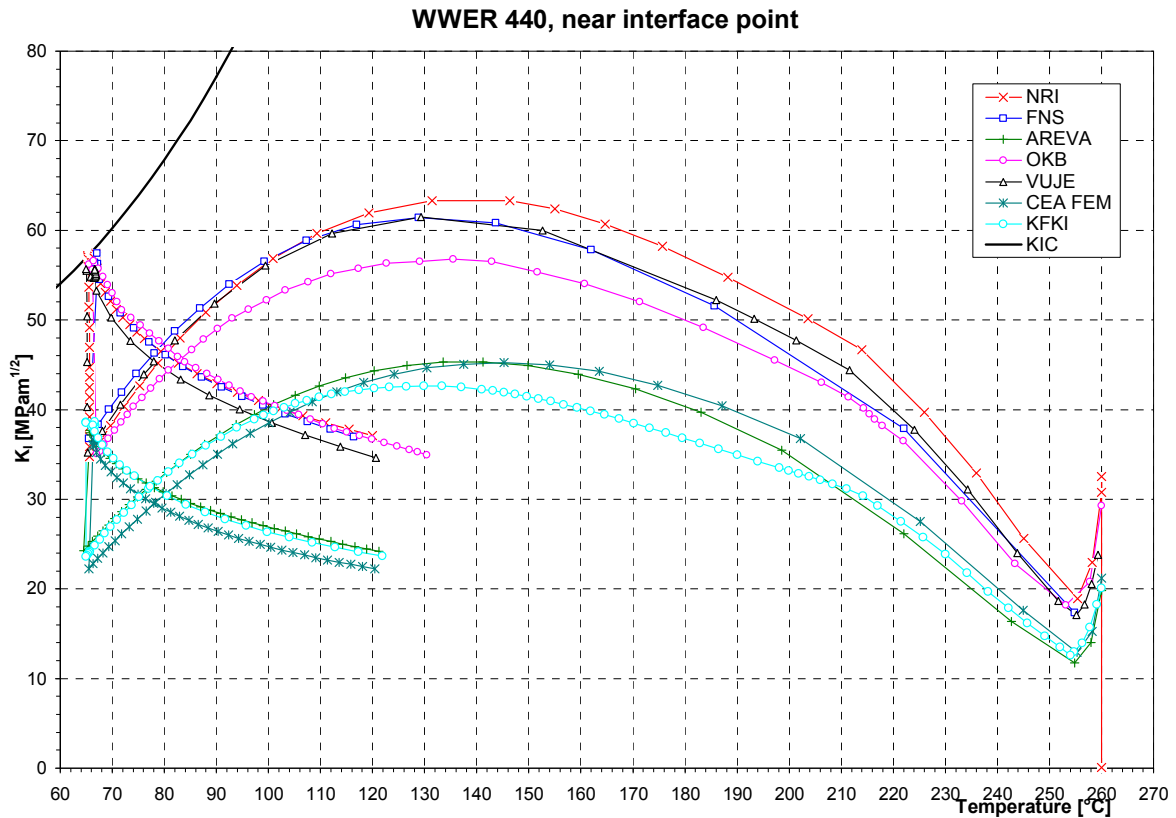


FIG. B23 – WWER case, K_I , K_{IC} vs. temperature, the near interface point, the whole transient.

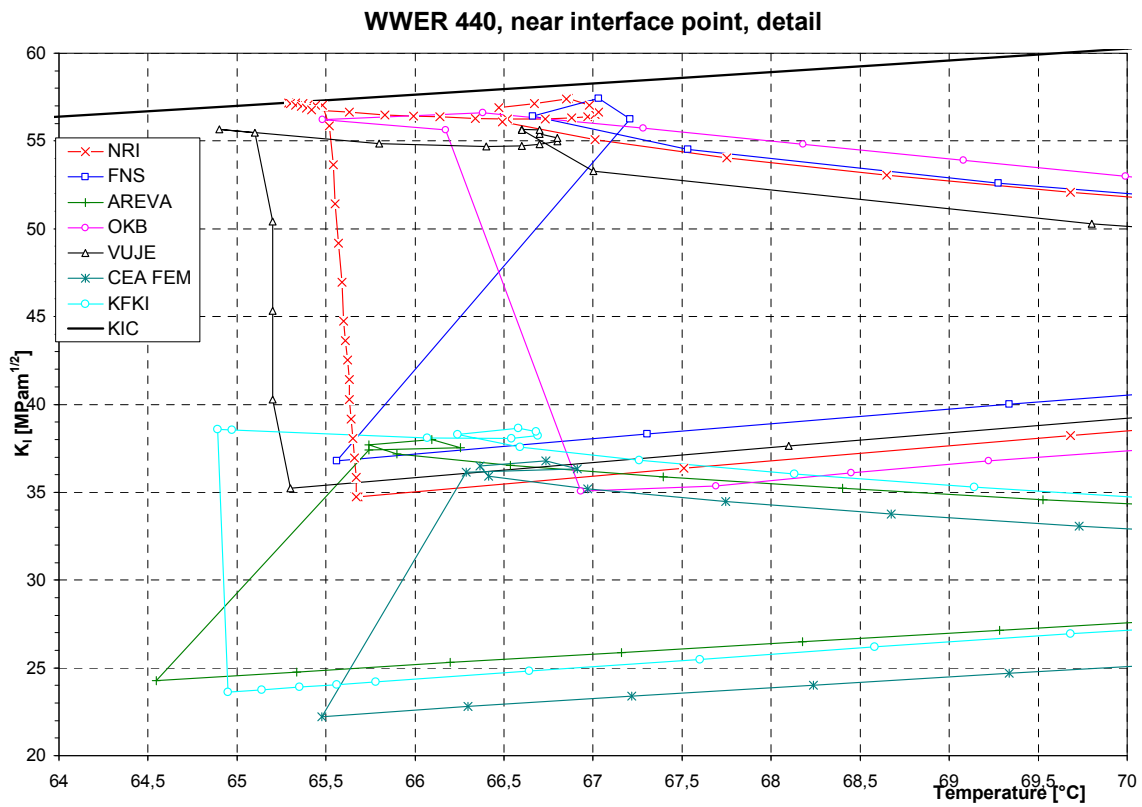


FIG. B24 – WWER case, K_I , K_{IC} vs. temperature, the near interface point, detail close to the critical time.

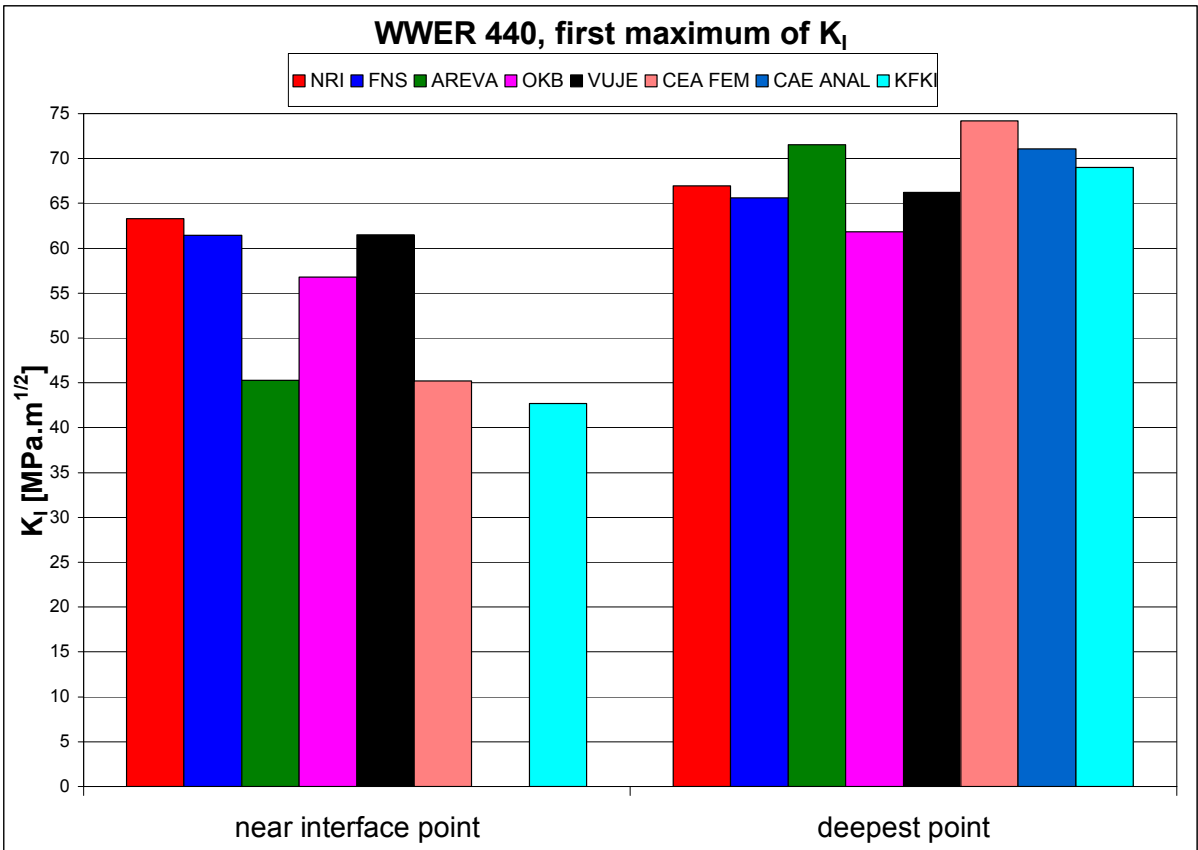


FIG. B25 – WWER case, first maximum of K_I

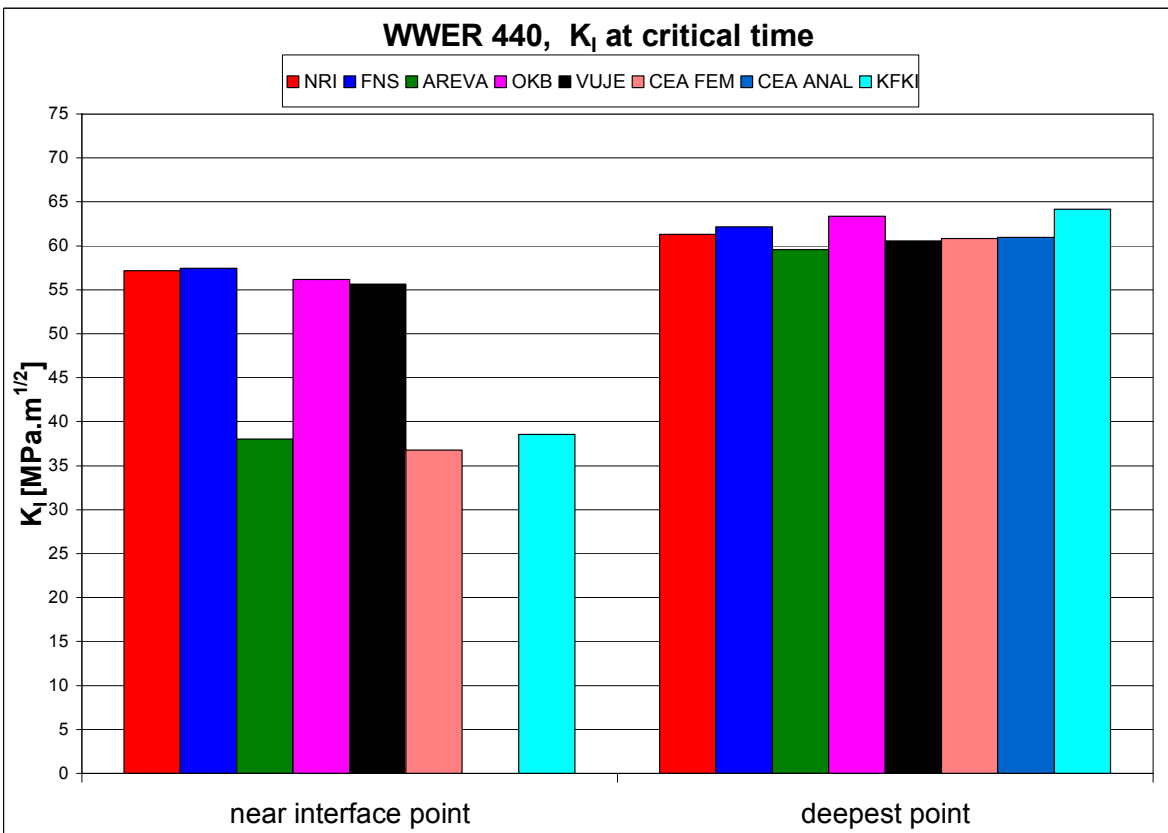


FIG. B26 – WWER case, K_I at critical time.

Comments to the results

We can see good accordance among all participants in calculated K_I values, better than in the older benchmarks [3, 5], with three exceptions – AREVA, KFKI and CEA solutions for the near interface point, discussed below.

For the first maximum of K_I and the deepest point of the crack the differences in K_I values are up to $12 \text{ MPa}\cdot\text{m}^{1/2}$. The highest deviation is observed for CEA and AREVA solutions. Both used the 1D calculations for temperature and stress fields and then analytical formulae for K_I calculations. The approach does not take into account the effect of cold plume, which is not negligible for the time interval close to K_I maximum. The analytical solution (omitting the cold plume effect) for the deepest point is conservative for axial crack.

For the first maximum of K_I and the near interface point of the crack the differences in K_I values are up to $20 \text{ MPa}\cdot\text{m}^{1/2}$. The highest deviation is observed for CEA, KFKI and AREVA solutions. Here the source of the deviation is in the shape of the crack close to the cladding / base material interface. The basis for development of the applied formulae for K_I solution (influence functions) was 3D finite element modelling of surface “semi-elliptical” cracks with the main axis of the semi-ellipse at the cladding / base material interface with and straight crack front across the cladding thickness (denoted as “shape 1”), while the other participants modelled exactly surface semi-elliptical cracks with the main axis of the semi-ellipse at the RPV inner surface (“shape 2”). Both crack shapes are seen in Figure B27 (with dimensions relevant to PWR case). Influence of the exact crack shape on the K_I solution for the deepest point is negligible, but for the near interface point is significant due to quite different crack shape (curvature) close to this point. See also results of the appropriate sensitivity study in Chapter 5 below. When excluding these two solutions, the differences are about $6 \text{ MPa}\cdot\text{m}^{1/2}$, i.e. about 10%, which is acceptable result. Within the group using shape 1 the difference is $2 \text{ MPa}\cdot\text{m}^{1/2}$. The small difference between KFKI and CEA (or AREVA) in the middle part of the transient is caused by applying cold plume by KFKI but not by CEA and AREVA.

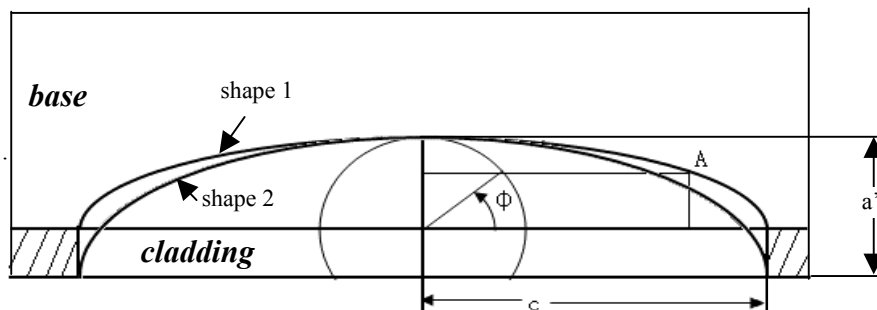


FIG. B27 – Two crack shapes for surface semi-elliptical crack (shape 1, shape 2).

For the critical time and the deepest point of the crack the differences in K_I values are less than $4 \text{ MPa}\cdot\text{m}^{1/2}$, i.e. about 7%, which is very good result. The accordance for this time is better than for the time of maximum K_I , because at the critical time the effect of cold plume is reduced and dominating loading is pressure. Therefore, the simplified solutions gave good results.

For the critical time and the near interface point of the crack the differences in K_I values are again up to $20 \text{ MPa}\cdot\text{m}^{1/2}$. The highest deviation is again observed for CEA, KFKI and AREVA solutions due to the same reason as discussed above – crack shape close to the material interface. When excluding these solutions, the differences are about $2 \text{ MPa}\cdot\text{m}^{1/2}$, i.e. about 3%, which is excellent result.

PWR case

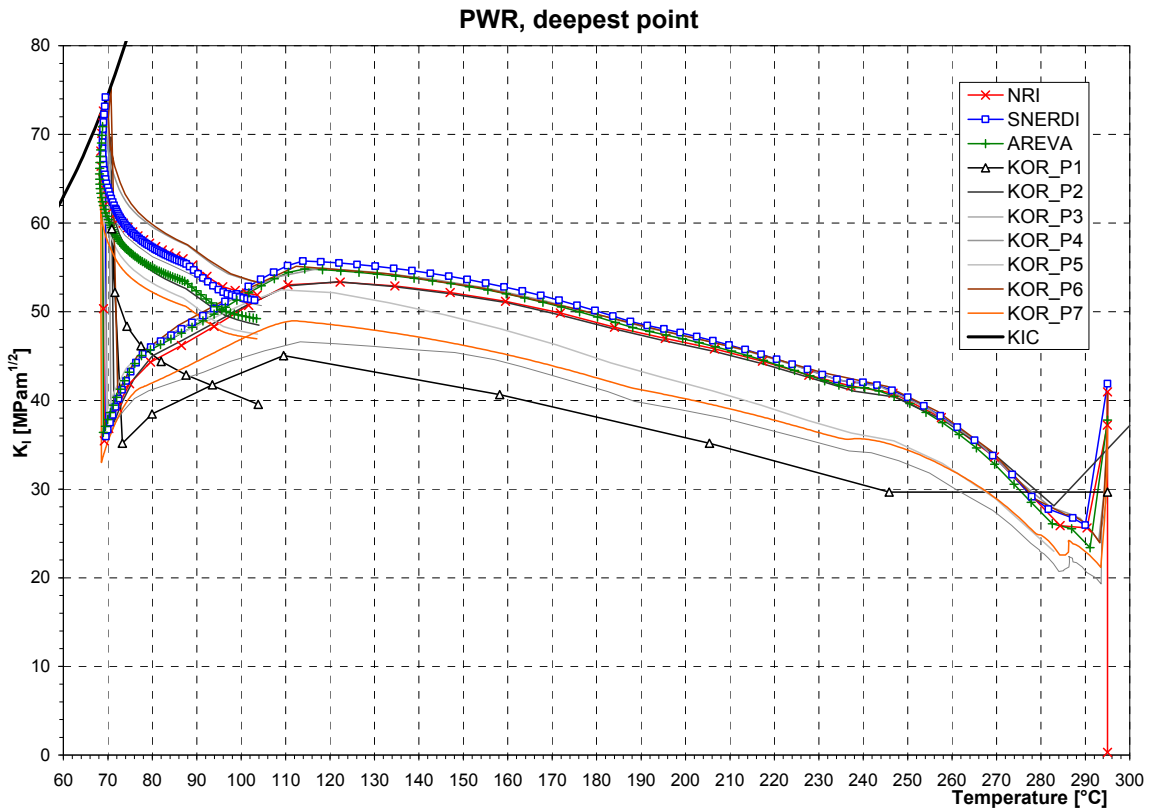


FIG. B28 – PWR case, K_I , K_{IC} vs. temperature, the deepest point, the whole transient.

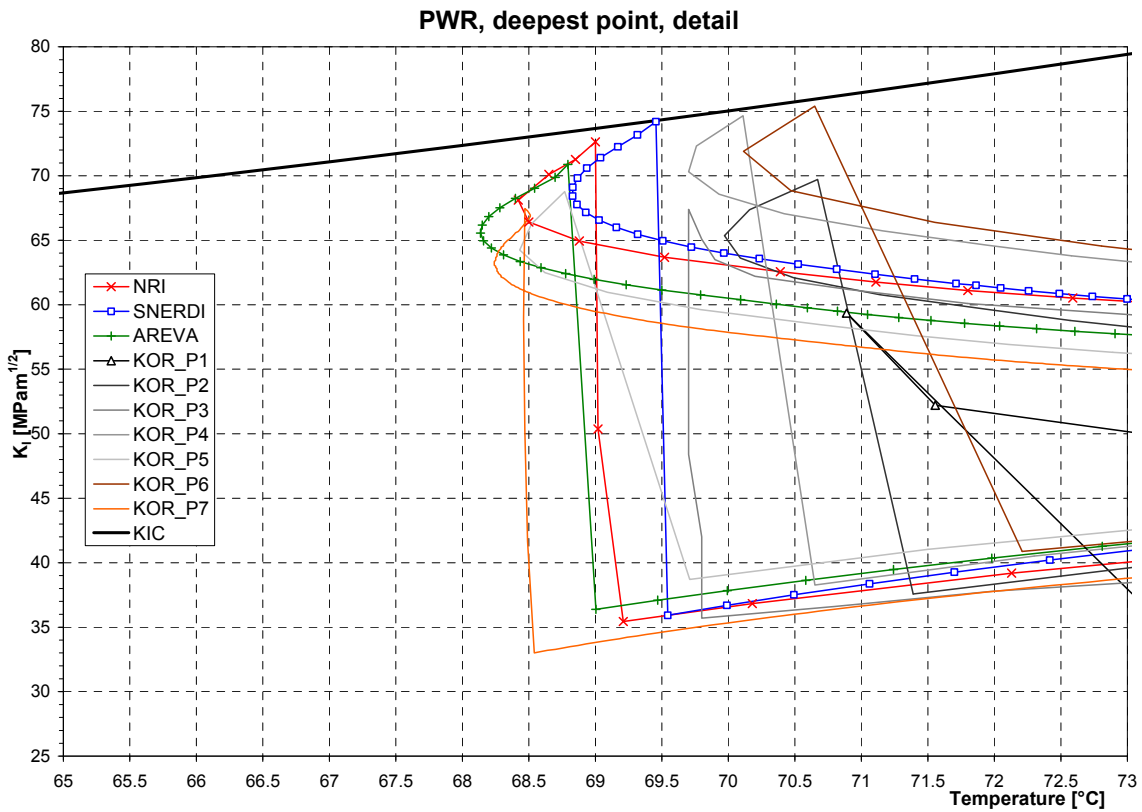


FIG. B29 – PWR case, K_I , K_{IC} vs. temperature, the deepest point, detail close to the critical time.

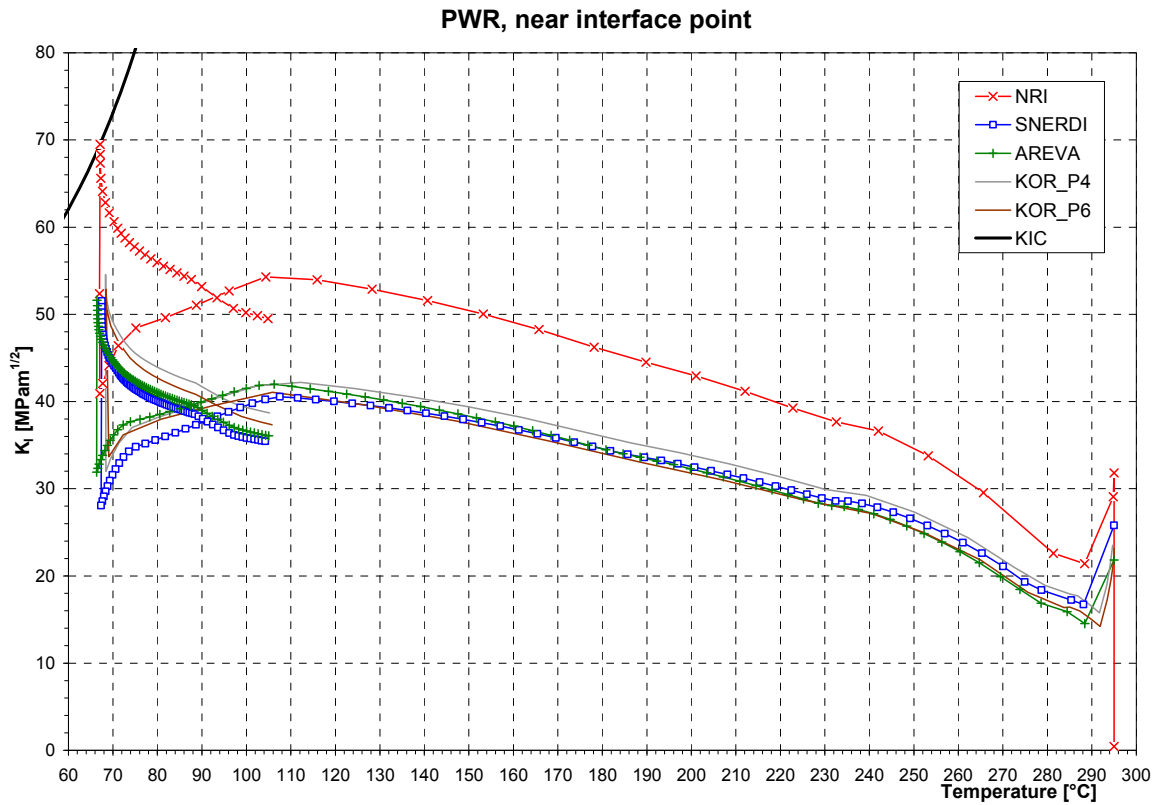


FIG. B30 – PWR case, K_I , K_{IC} vs. temperature, the near interface point, the whole transient.

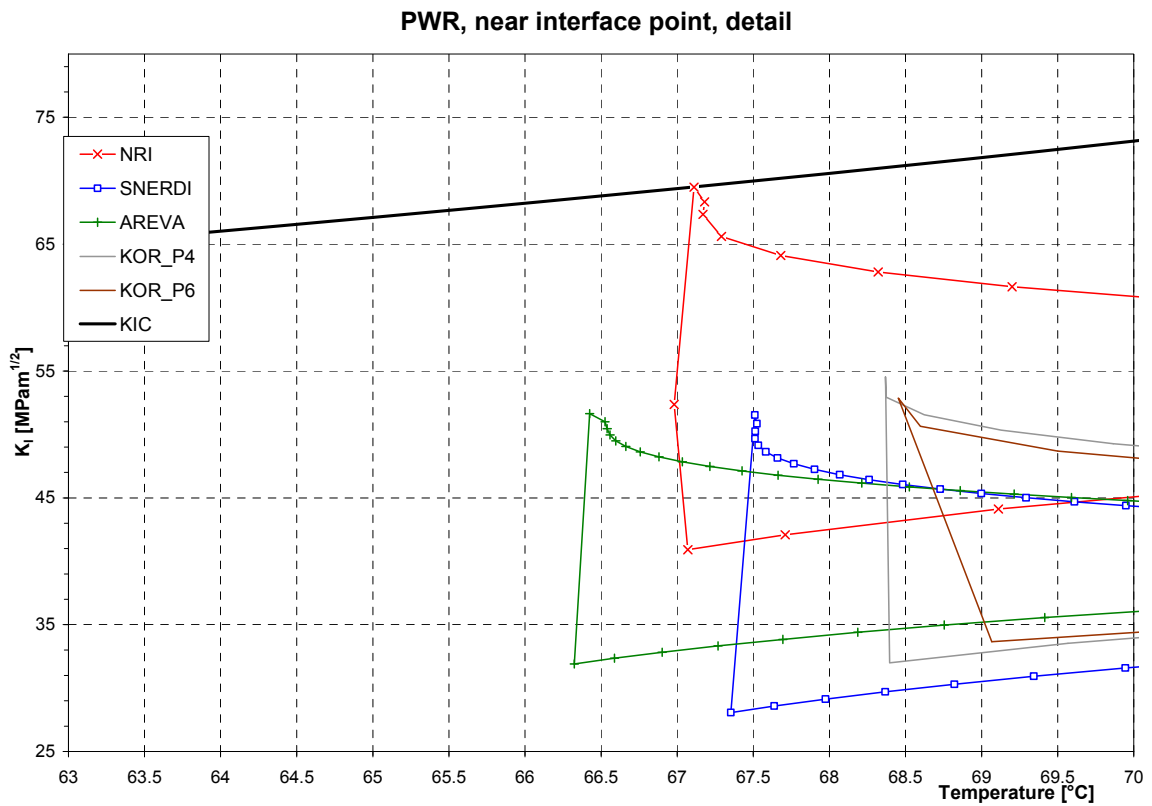


FIG. B31 – PWR case, K_I , K_{IC} vs. temperature, the near interface point, detail close to the critical time.

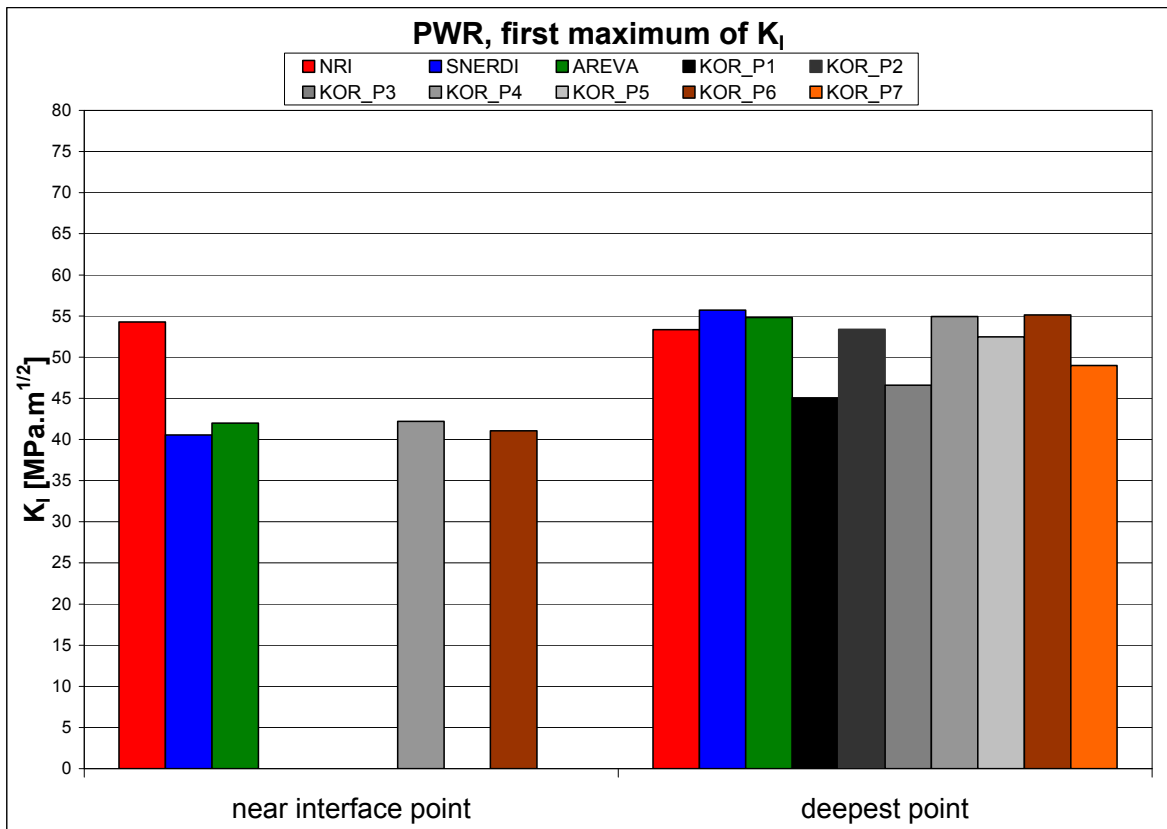


FIG. B32 – PWR case, first maximum of K_I .

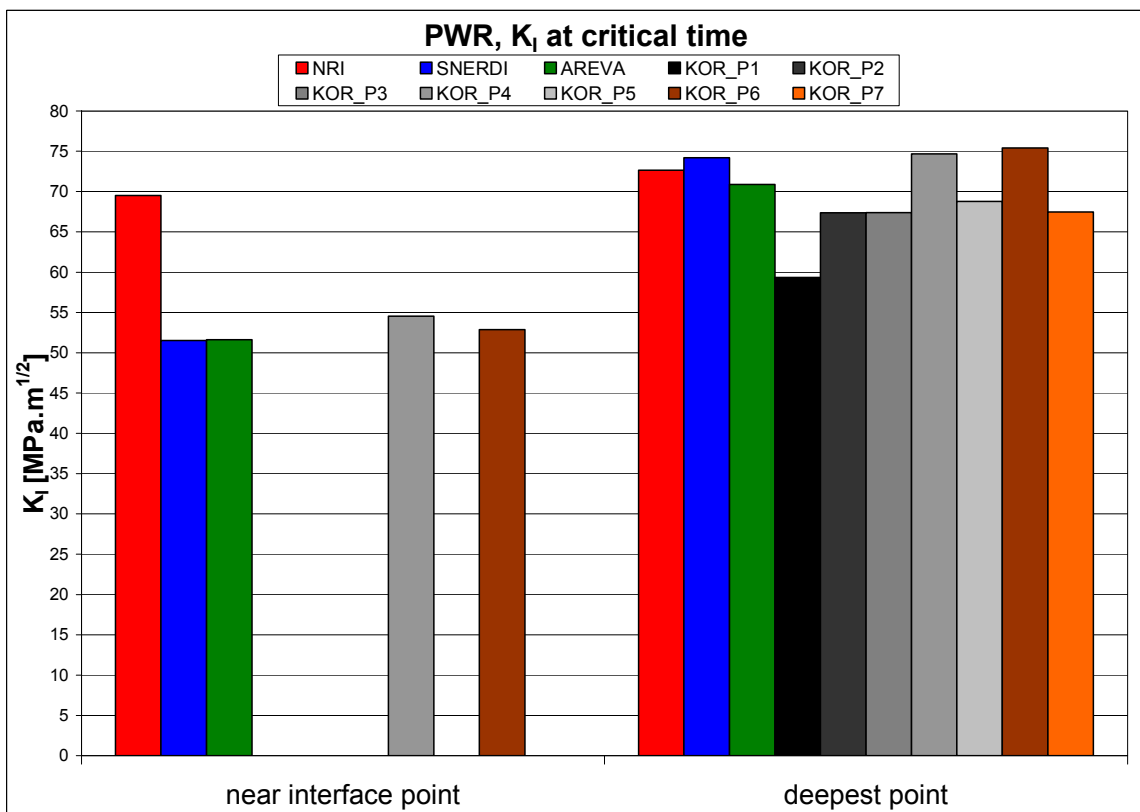


FIG. B33 – PWR case, K_I at critical time.

Comments to the results

We can see relatively good accordance for most participants in calculated K_I values. Only two Korean solutions (P4, P6) used direct FEM 3D calculations for determination of J-integral. The other used influence functions method for K_I calculations and did not produce any solution for the near interface point. OKB did not participated in fracture mechanics part of PWR benchmark. AREVA used also analytical solution, but they produced results also for near interface point. Only NRI used crack with shape 2, AREVA, SNERDI, P4, P6 used shape 1 (for definition of shapes see Figure B27), which is the reason why NRI has much higher K_I for the near interface point. The agreement for the near interface point of those four participants using shape 1 is quite good. For the deepest point the agreement is good, even for the analytical solution. Only P1 solution seems to be outlier, possibly due to too simplified solution (they had problems even with temperature fields calculations, as discussed above). The effect of cold plume (source of discrepancy for AREVA and CEA analytical solutions for WWER case) is not seen in this case, because according to the benchmark definition, symmetrical cooling or the RPV (i.e. no cold plumes) was supposed.

For the first maximum of K_I and the deepest point of the crack the differences in K_I values are up to $11 \text{ MPa}\cdot\text{m}^{1/2}$, i.e. about 20%. The analytical solution P1 and P3 are the main source of the differences.

For the first maximum of K_I and the near interface point of the crack the differences in K_I values for those who used shape 1 are only $2 \text{ MPa}\cdot\text{m}^{1/2}$. Shape 2 (NRI) gives on about $15 \text{ MPa}\cdot\text{m}^{1/2}$ higher results.

For the critical time and the deepest point of the crack the differences in K_I values are about $16 \text{ MPa}\cdot\text{m}^{1/2}$, but when excluding the questionable P1 solution, the differences (including several analytical solutions) are only $7 \text{ MPa}\cdot\text{m}^{1/2}$, i.e. about 10%, which is good result.

For the critical time and the near interface point of the crack the differences in K_I values for those who used shape 1 are only $3 \text{ MPa}\cdot\text{m}^{1/2}$. Shape 2 (NRI) gives on about $15 \text{ MPa}\cdot\text{m}^{1/2}$ higher results.

Additionally, a request was put to the participants to provide variation of K_I along crack front in dependency on the elliptical angle of individual points for prescribed time steps (the critical times) 3895 s for WWER case and 7200 s for PWR case. The definition of the elliptical angle Φ of point A on the semi-ellipse – shape 1 is drawn in Figure B27. Only limited number of participant responded to this request (moreover, some participants using analytical formulae usually do not have results for all crack front). In Figure B34 and B35 we see the comparison from WWER and PWR cases, respectively.

For WWER case, the accordance is quite good with exception of CEA, which can be explained by different shape of surface crack (see Figure B27 and the corresponding text). For PWR case we see some differences mainly in cladding and close to the interface, caused again by different shape of the crack. For corresponding shape of the crack, the accordance of the results in the base material is good. SNERDI performed also sensitivity study to clarify the influence of the crack shape; the result is seen in Figure B35.

WWER, K_I variation along crack front at 3895 s

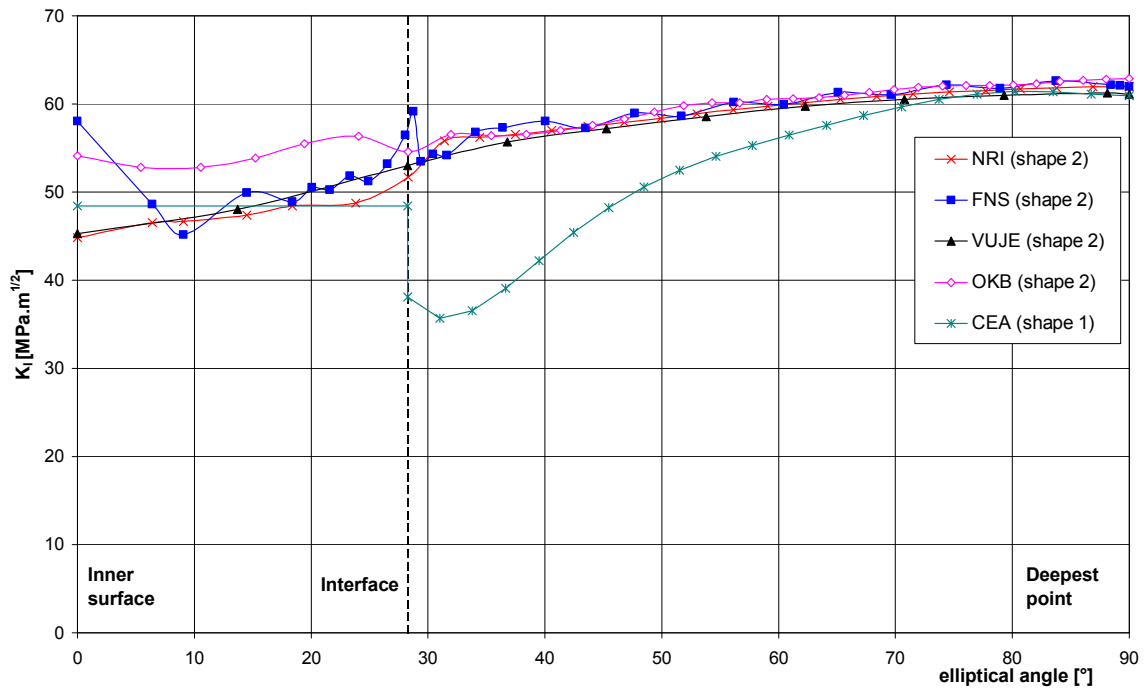


FIG. B34 – WWER case, variation of K_I along crack front at critical time.

PWR, K_I variation along crack front at 7200 s

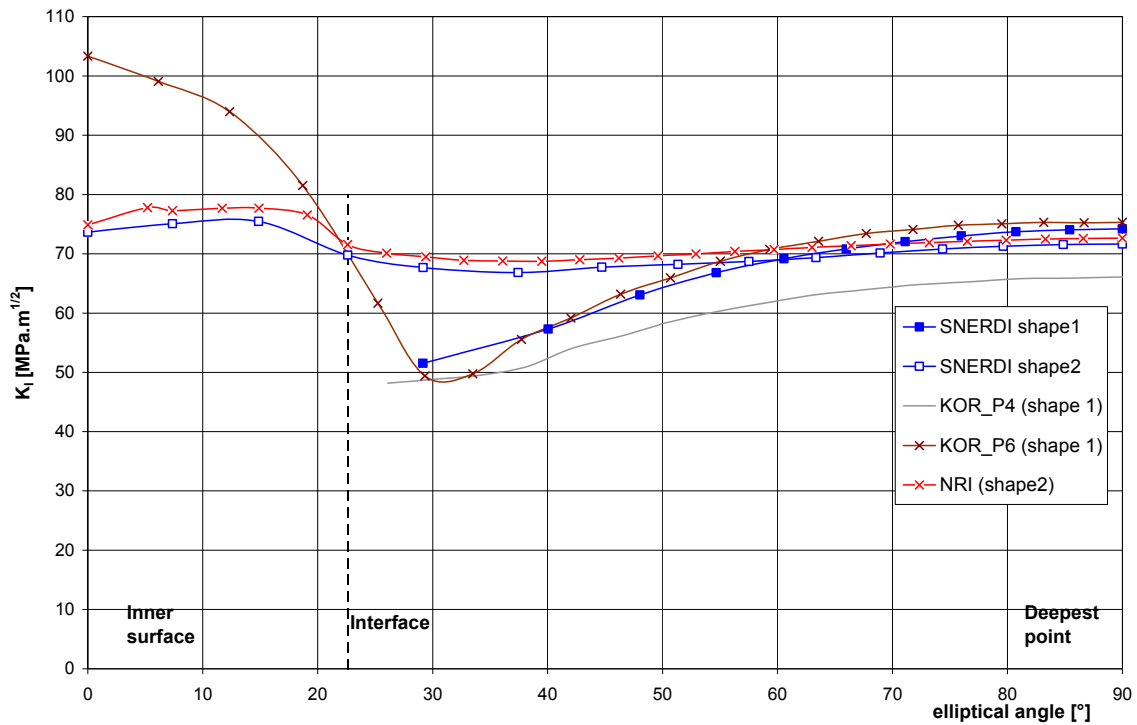


FIG. B35 – PWR case, variation of K_I along crack front at critical time.

4.4. Maximum allowable transition temperature

The comparison of resulting values of maximum allowable critical temperature of brittleness T_k^a for the WWER case is plotted in Figure B36 for both the deepest and the near interface points. Similar plot for maximum allowable reference temperature for nil ductility transition RT_{NDT}^a for the PWR case is plotted in Figure B37. These main results of the benchmark are also presented in tables B11 and B12. In both the tables and the figures, the shape of crack (Figure B27) is indicated. The critical times of the transients are compared in figures B38 and B39.

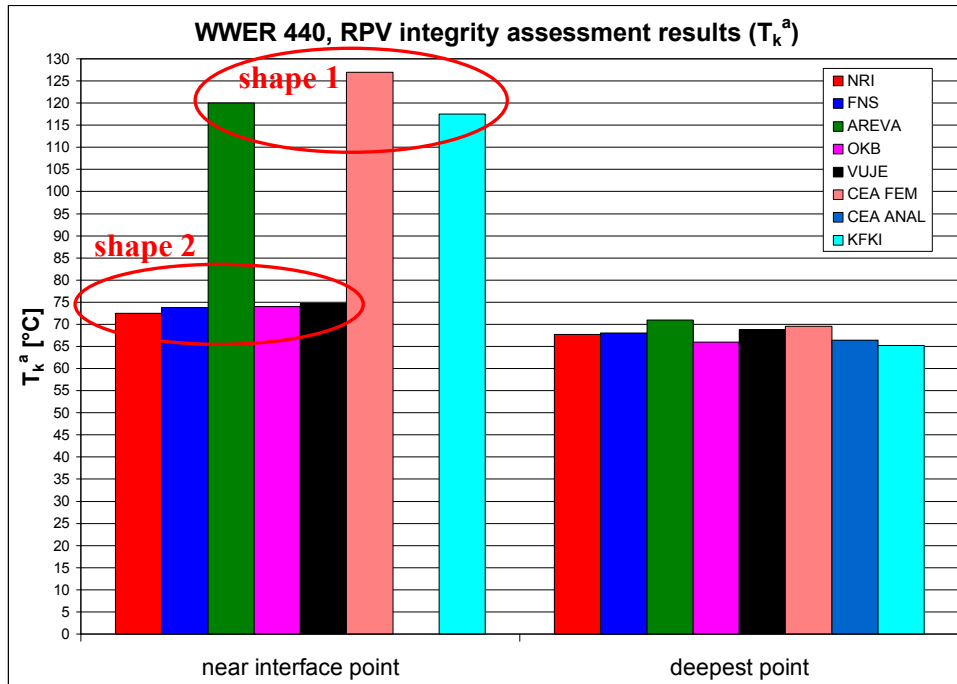


FIG. B36 – WWER case, maximum allowable critical temperature of brittleness T_k^a .

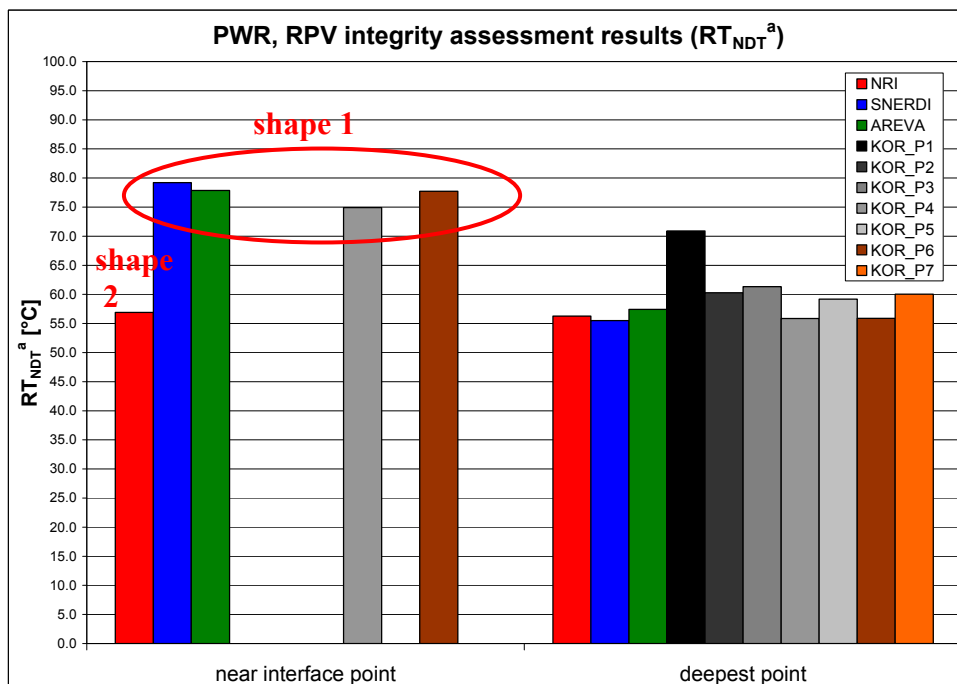


FIG. B37 – PWR case, maximum allowable reference temperature for nil ductility transition RT_{NDT}^a .

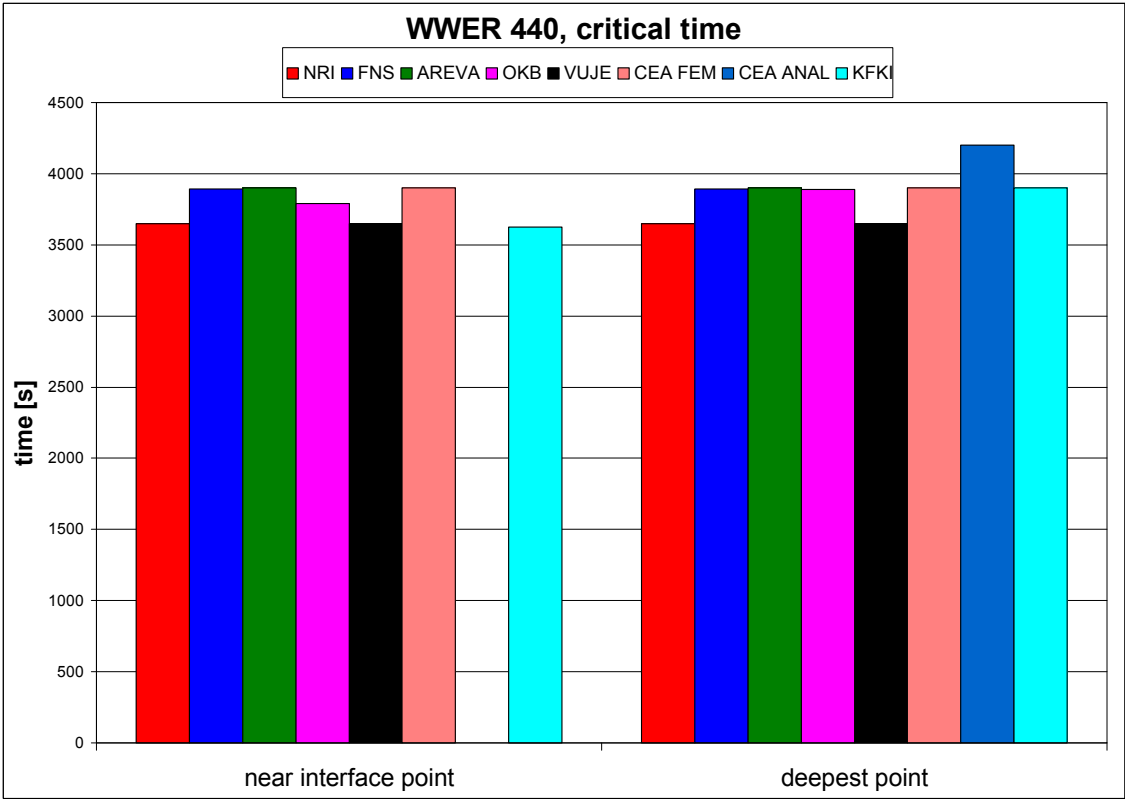


FIG. B38 – WWER case, critical time.

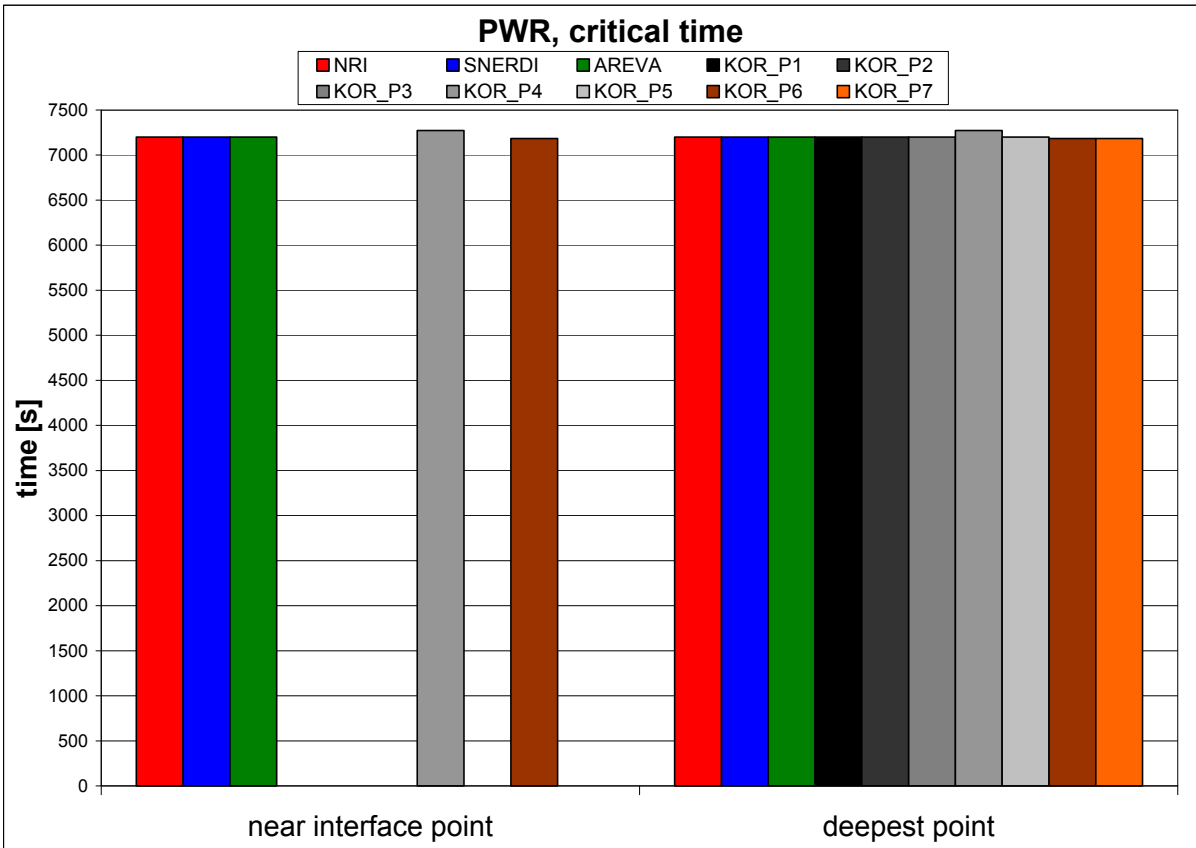


FIG. B39 – PWR case, critical time.

Table B11 – WWER case, maximum allowable critical temperature of brittleness T_k^a

Participant	shape of crack	T_k^a near interface point [°C]	T_k^a deepest point [°C]
NRI	2	72.5	67.7
FNS	2	73.8	68.0
AREVA	1	120.0	71.0
OKB	2	74.0	66.0
VUJE	2	74.6	68.8
CEA FEM	1	126.9	69.6
CEA ANAL	1	–	66.4
KFKI	1	117.5	65.2

Table B12 – PWR case, maximum allowable reference temperature for nil ductility transition RT_{NDT}^a

Participant	shape of crack	RT_{NDT}^a near interface point [°C]	RT_{NDT}^a deepest point [°C]
NRI	2	56.9	56.3
SNERDI	1	79.2	55.5
AREVA	1	77.9	57.5
KOR_P1	2		70.9
KOR_P2	2		60.3
KOR_P3	2		61.3
KOR_P4	1	74.9	55.9
KOR_P5	2		59.2
KOR_P6	1	77.8	55.9
KOR_P7	2		60.1

Comments to the results

For the WWER case, the differences in resulting T_k^a values for the deepest point (which is the worst one along the crack front) are 6°C, which is very good result, having in mind the complexity of the problem and different FEM codes and tools used for J (or G) calculations. The critical time was found in range 3650 s to 4200 s. The differences are caused mainly by differently fine time stepping close to critical point (Figure B22). Some participants skipped, due to coarse time stepping, the critical time at about 3650 s (just after sudden repressurization), but without significant influence on resulting T_k^a . 3895 s is the time of reaching the maximum pressure. For the near interface point, there are two groups of solutions based on crack shape close to the material interface (discussed above). One group (the majority) has the differences only 2°C, while the other solutions differ on about 50°C (with mutual difference 7°C). The critical time was found in range 3650 s to 3900 s.

For the PWR case, the differences in resulting RT_{NDT}^a values for the deepest point after excluding too simplified P1 solution are 5°C, which is very good result. The critical time was found in range 7185 s to 7273 s. The time 7185 s is the time just after sudden repressurization. For the near interface point, there are again two groups of solutions based on crack shape close to the material interface (discussed above). One group (only NRI) with main axis of the semi-ellipse lying on the inner surface (shape 2) has the solution on about 20°C lower than the other group putting main axis of the semi-ellipse on the interface (shape 1). The second group has the differences about 4 °C. The critical time was found again in range 7185 s to 7273 s.

Concerning the comparison of assessment according to the national codes, it has to be said that direct comparison of different solutions is practically impossible, because of different approach, i.e. the postulated crack (depth, shape, position, orientation), safety margins, transition temperature, size

correction and other features of the assessment according to individual codes. Which means, that the results of the national codes benchmark can be quite different by their nature, but it was found within the basic case, that the benchmark participants are able to obtain very comparable results for uniquely defined task.

The comparison of national codes approaches was outside of scope of the current project.

5. SENSITIVITY STUDIES

A comprehensive set of sensitivity studies was defined at the beginning of the project and divided among the participants. The list of originally proposed sensitivity studies is given in Appendix B4. During the solution of the project, the set of sensitivity studies changed a little.

The following participants performed the sensitivity studies: KINS, FORTUM, SNERDI, NRI, OKB and VUJE. Some information was also included from results obtained during past ICAS project [5] and also from experience of the participants from their older projects. The results obtained within CRP9 project are denoted by coloured text.

Results of the sensitivity studies are presented in Table B17 in a condensed manner, with identified the more conservative case, the significance of the individual tested parameters and with difference between basic case and sensitivity study expressed in terms of T_k^a or RT_{NDT} a (for the studies performed within CRP-9 project only). The significance of a parameter is denoted as “very significant” if its effect on resulting T_k^a or RT_{NDT} a in the sensitivity study performed is higher than approximately 20 °C, when it is between approx. 2 and 20 °C it is denoted as “significant” and below 2 °C it is denoted as “negligible”. Below the table follow figures taken from reports of individual participants, which depict the individual sensitivity studies. The references to the figures and to the reports are also included in Table B17.

It has to be noted, that the sensitivity studies were performed for the transients defined within this benchmark (some of them for WWER case, some for PWR case). Some sensitivity studies results can be dependent on the transient course (e.g. on level of pressure, temperature gradient, heat transfer coefficient).

Table B13 – Results of sensitivity studies

Sensitivity study	Organization performed	Comment	Results – more conservative case is indicated	Case for which performed	Significance of parameter	$\Delta T_k, \Delta RT_{NDR}$ a sensitivity study- basic case [°C]	Figure	Ref.
THERMAL HYDRAULIC INPUTS								
heat transfer coefficients in symmetrical case (by factor 2 to basic case)	AREVA	ID	higher HTC	surface	significant	3 WWER 8 PWR	B40, B41	[13]
plumes								
cold plumes vs. symmetrical case	AREVA, NRI		axial crack – axisymmetric is conservative circ. crack – plume is conservative	surface	significant		B42 B43	[13]
width and shape of the plumes	NRI	old results	narrow plume		significant			
OKB GP MIX vs. (local mixing)	OKB		local mixing		very significant	37	B44	[11]
PHYSICAL PROPERTIES								
thermal conductivity coefficient	NRI	old results	lower thermal conductivity		significant		B45	
thermal expansion coefficient		old results ICAS	higher thermal expansion coefficient		significant			[5]
Young module of cladding	FNS		higher E of cladding	surface elastic	significant	3.5	B46	[8]
			higher E of cladding	surface plastic	significant	3.4	B47	[8]
			lower E of cladding	underclad elastic	significant	8.4	B48	[8]

Sensitivity study	Organization performed	Comment	Results – more conservative case is indicated	Case for which performed	Significance of parameter	$\Delta T_r, \Delta RT_{NDR}$ a sensitivity study- basic case [$^{\circ}C$]	Figure	Ref.
			higher E of cladding	underclad plastic	significant	10.6	B49	[8]
STRESS FIELD								
linear elastic vs. elastic-plastic	FNS OKB SNERDI		elastic	surface deepest pt.	negligible	0.3 - 2	B46 vs. B47 B50 B51	[8] [10]
	FNS SNERDI		plastic	surface near interf.	negligible significant	0.8 8.7	B46 vs. B47 B52	[8] [10]
	FNS OKB SNERDI		plastic	underclad all points.	significant	7.4 4.4	B48 vs. B49 B50 B53,B54	[8] [10]
initial vs. irradiated stress strain curves of BM only	OKB SNERDI	old results new sensitivity study	initial	underclad surf., und.	negligible	2 < 0.5	B55 B56	[10]
initial vs. irradiated stress strain curves of both BM and cladding	VUJE		irradiated	surface	significant	10	B57	[14]
initial vs. irradiated stress strain curves of both BM and cladding	VUJE		initial	underclad	significant	19	B58	[14]
Treatment of cladding all props. as BM mech. props. as BM	KINS		less conservative the least conservative	surface, deepest pt.	significant	15 16	B59	[9]

Sensitivity study	Organization performed	Comment	Results – more conservative case is indicated	Case for which performed	Significance of parameter	$\Delta T_k, \Delta RT_{NDR}$ a sensitivity study- basic case [°C]	Figure	Ref.
RESIDUAL STRESSES IN WELDS								
YES vs. NO	FNS ICAS	old results	residual stress applied	surface all points	significant	~12	B60, Tab B14 B61	[8], [5]
cos shape vs. constant	FNS		constant	surface all points	negligible	~1	B60, Tab.B14	[8]
RESIDUAL STRESSES IN CLADDING								
YES vs. NO	ICAS	old results	residual stress applied	surface, deepest pt.	significant		B61	[5]

Sensitivity study	Organization performed	Comment	Results – more conservative case is indicated	Case for which performed	Significance of parameter	$\Delta T_k^a, \Delta RT_{NDR}^a$ sensitivity study- basic case [$^{\circ}C$]	Figure	Ref.
POSTULATED DEFECT								
underclad vs. surface	KINS OKB FNS	comparison of basic and national	surface	deepest pt.	very significant	~85	B62 B47-B49	[9], [8]
effect of defect depth	KINS OKB		can dependent on transient	surface, deepest pt.	significant		B63 B64	[9]
	KINS		deeper crack	surface, near interface pt.	very significant		B65 B66	[9]
effect of defect shape – aspect ratio	KINS ICAS SNERDI		smaller aspect ratio (longer crack)	surface, underclad, deepest pt.	significant very sign.	~130	B67 B68 B69	[9] [5]
	KINS SNERDI		can dependent on transient	surface, near interface pt.	significant	~10	B69 B70	[9]
elliptical vs. semi-elliptical underclad crack	KINS NRI (old results)		KINS – semi-elliptical NRI - elliptical	underclad, deepest pt.	negligible		B71 B72	[9], [13]
			NRI - elliptical	underclad, near interf.	very significant		B72	[13]
surface semi-elliptical crack – two shapes	SNERDI		main axis at interface (shape 1)	surface, deepest pt.	negligible	2	B73	[10]
			main axis at inner surface (shape 2)	surface, near interf.	significant	20	B74	[10]
effect of crack orientation	KINS AREVA, NRI		axial crack for CRP9 transients (dependent on transient!)	surface, deepest pt.	very significant	~25	B75 B76 B42	[9] [13]

Sensitivity study	Organization performed	Comment	Results – more conservative case is indicated	Case for which performed	Significance of parameter	$\Delta T_k^a, \Delta RT_{NDR}^a$ sensitivity study-basic case [$^{\circ}C$]	Figure	Ref.
FRACTURE MECHANICS								
comparison of K_I calculated by formulae with 3D modelling	SNERDI	formulae from ASME	3D FEM	surface, deepest pt.	negligible	2	B77	[10]
different ways for J/K calculations	NRI	old - different parameters	smaller theta field	surface, near interf.	significant			
			smaller theta field	surface, deepest pt.	negligible			
way of assessment (point-by-point vs. integral)	OKB		point-by-point	surface, underclad	significant	5	B78 B79	
effect of cladding thickness	ICAS	old results ICAS	thicker cladding ? (not clear effect)	surface, deepest pt	significant		B80	[5]
	ICAS	old results ICAS	thinner cladding	underclad, deepest pt.	significant		B80	[5]
stress discontinuity treatment	KINS		approximated by one polynomial both stress in cladding and in BM	surface, deepest	very significant		B81	[9]

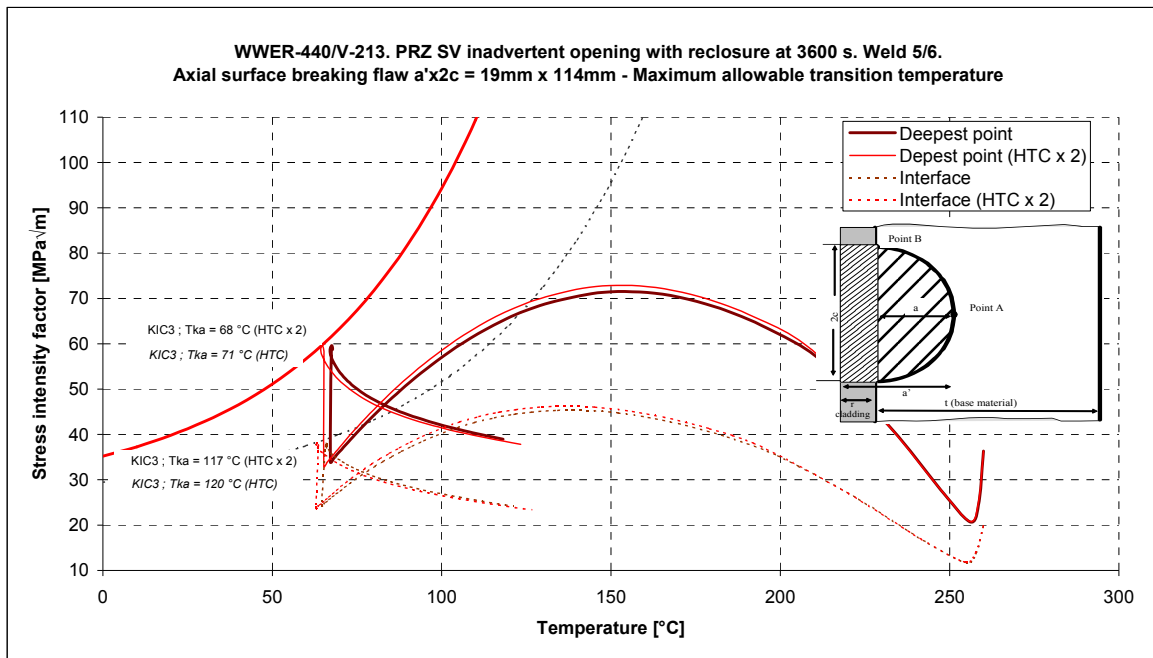


FIG. B40 – Sensitivity study, AREVA, influence of heat transfer coefficient, WWER case.

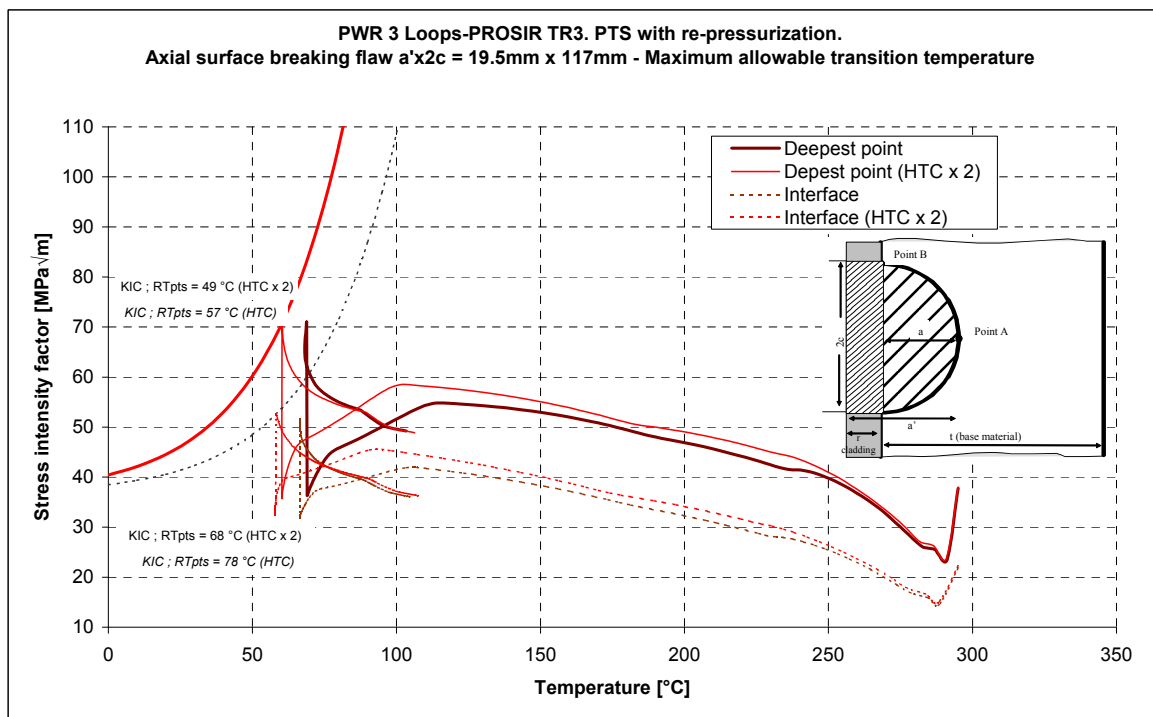


FIG. B41 – Sensitivity study, AREVA, influence of heat transfer coefficient, PWR case.

IAEA CRP9, effect of cold plume, axial crack, deepest point

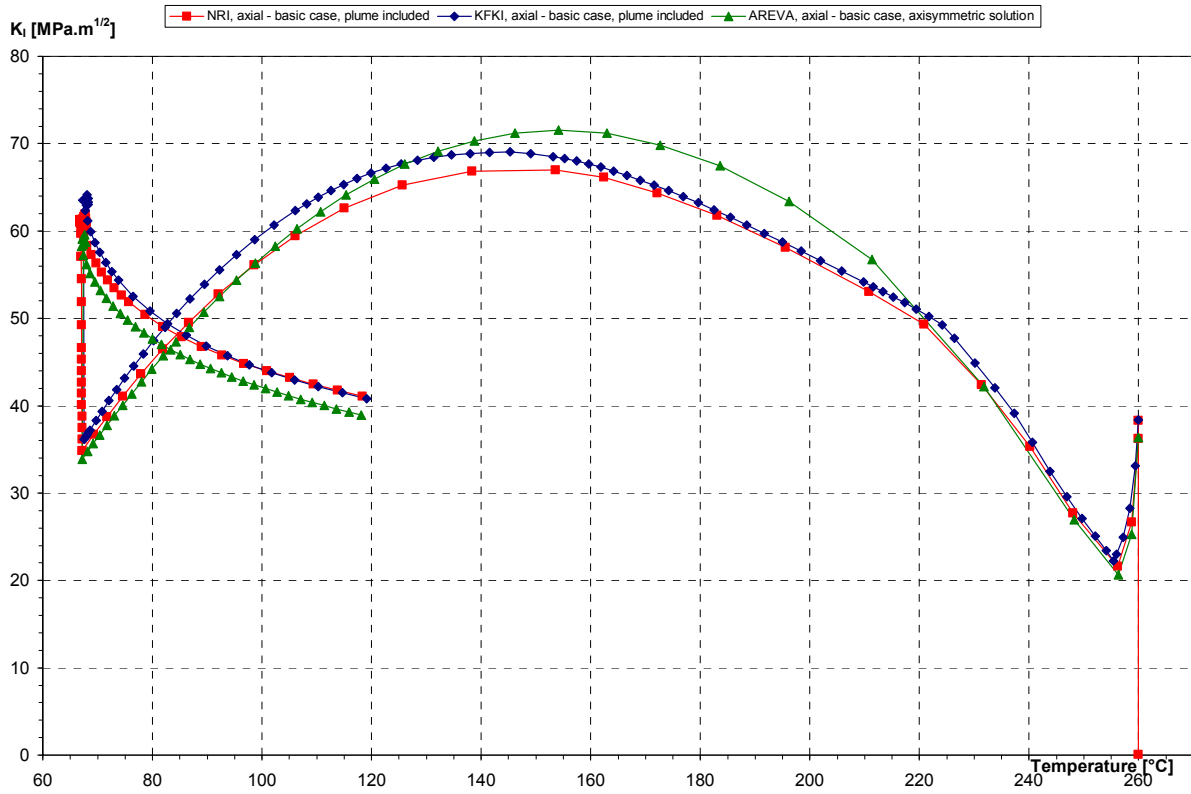


FIG. B42 – Sensitivity study WWER case, AREVA + NRI + KFKI, influence of cold plume on axial crack.

IAEA CRP9, effect of cold plume, circumferential crack, deepest point

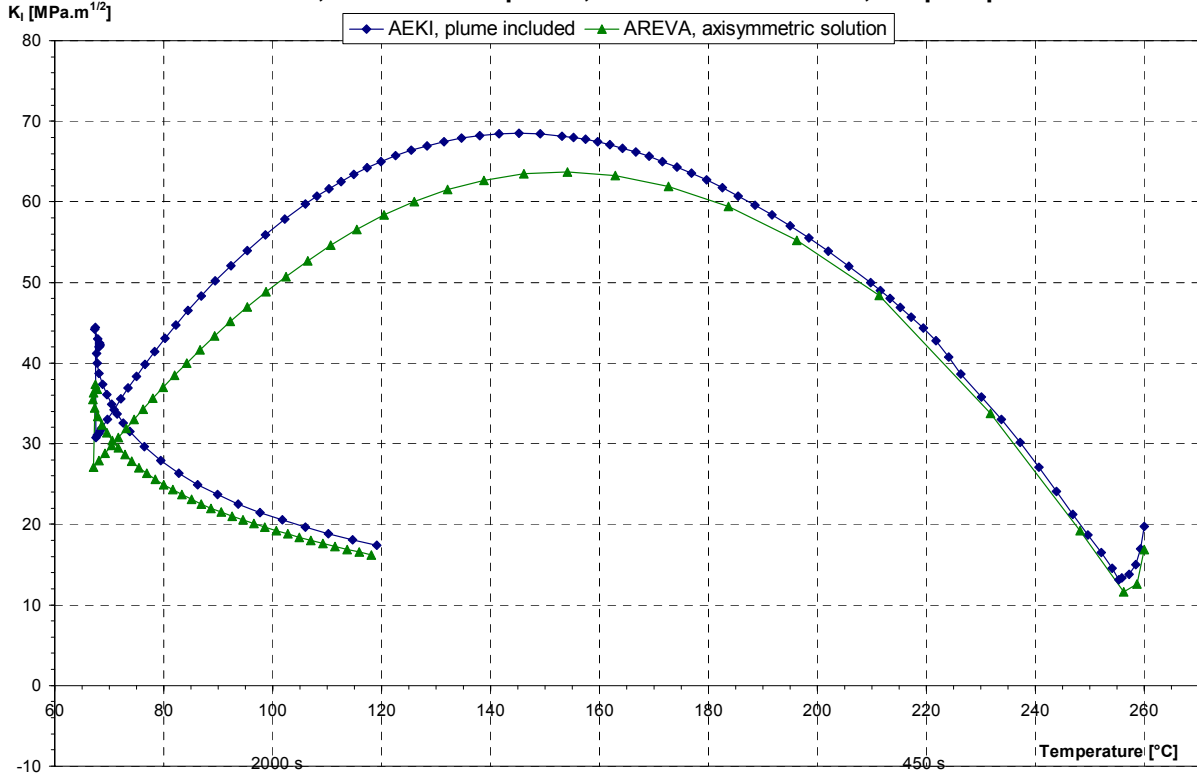


FIG. B43 – Sensitivity study WWER case, AREVA + KFKI, influence of cold plume on circumferential crack.

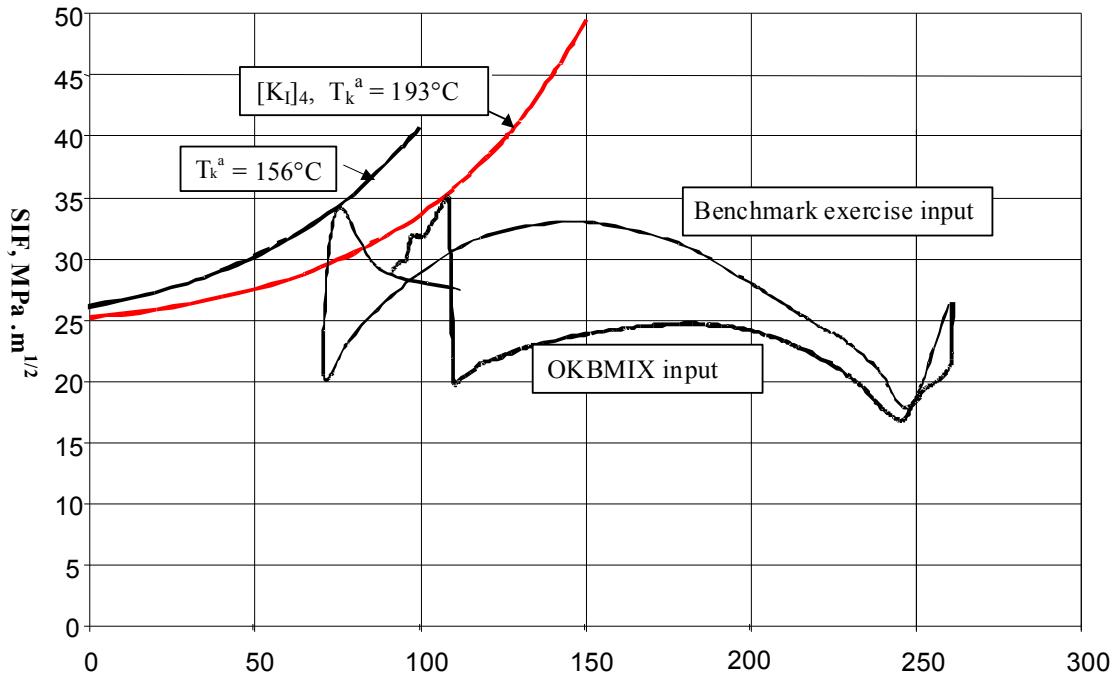


FIG. B44 – Sensitivity study WWER basic case, OKB, effect of thermal hydraulic mixing calculation.

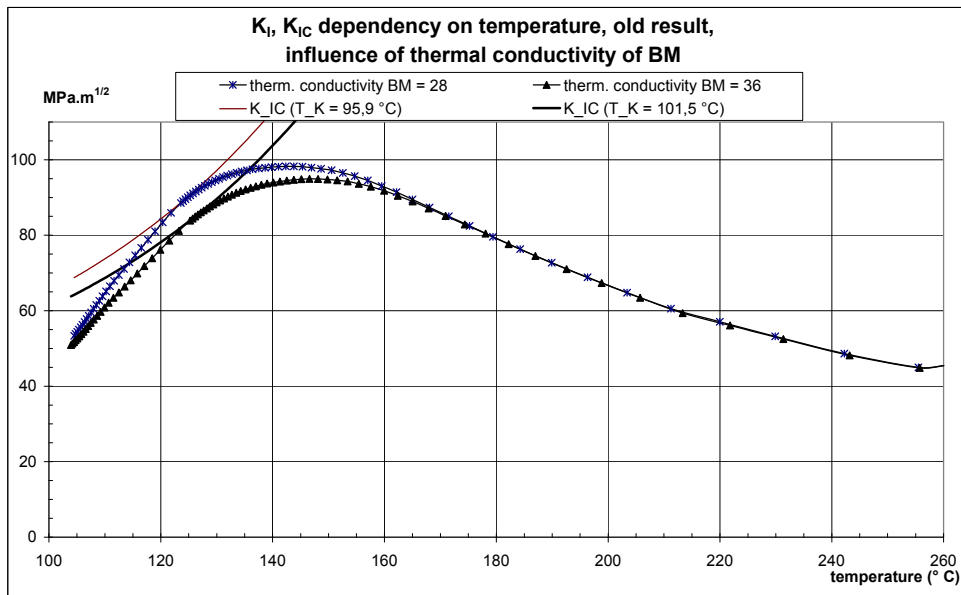


FIG. B45 – Sensitivity study, old result NRI, effect of thermal conductivity.

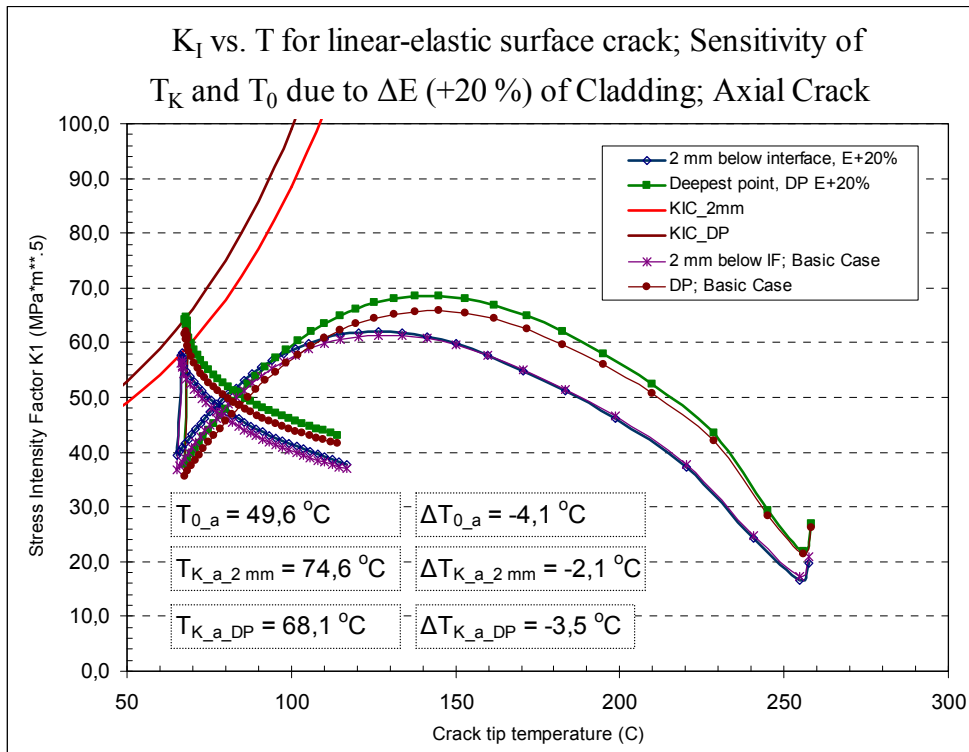


FIG. B46 – Sensitivity study, FNS, influence of E , surface crack with elastic material model.

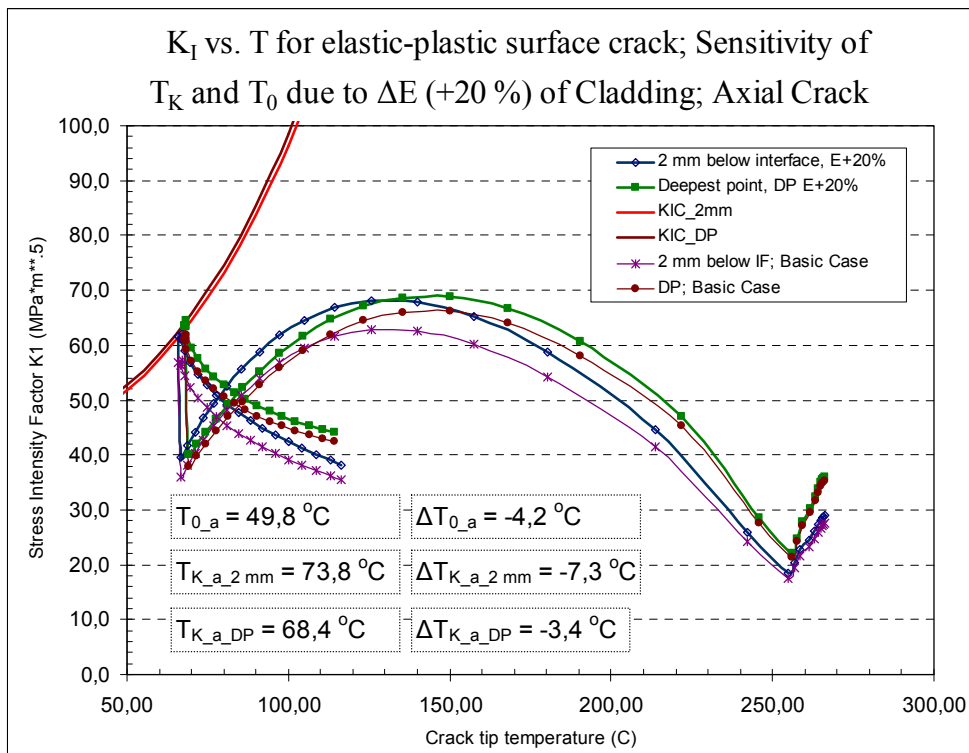


FIG. B47 – Sensitivity study, FNS, influence of E , surface crack with elastic-plastic material model.

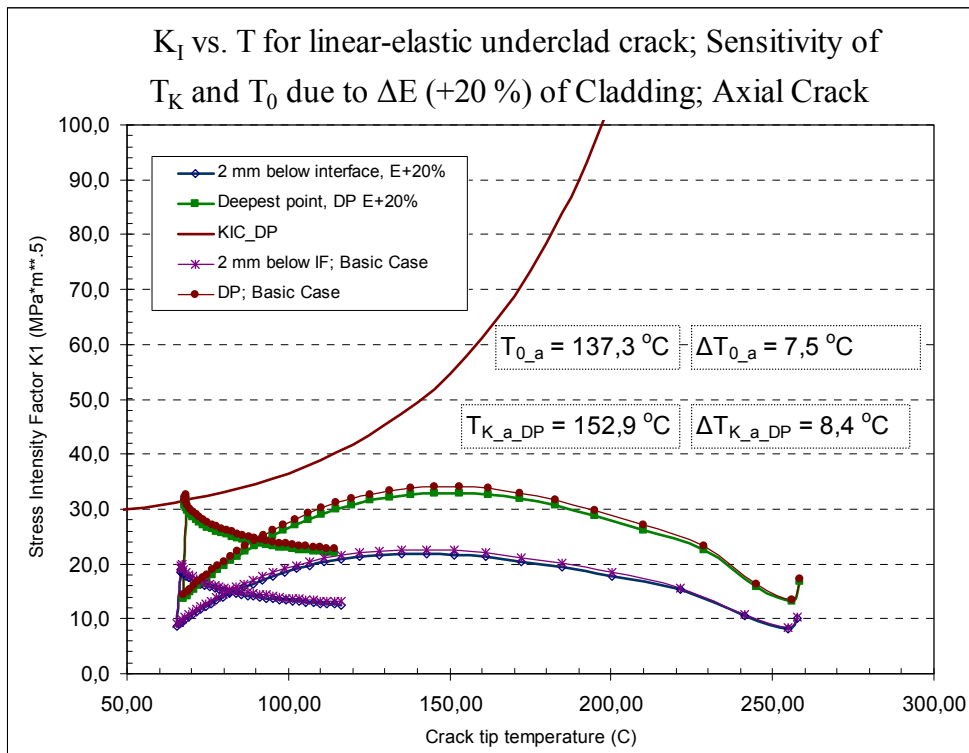


FIG. B48 – Sensitivity study, FNS, influence of E , underclad crack with elastic material model.

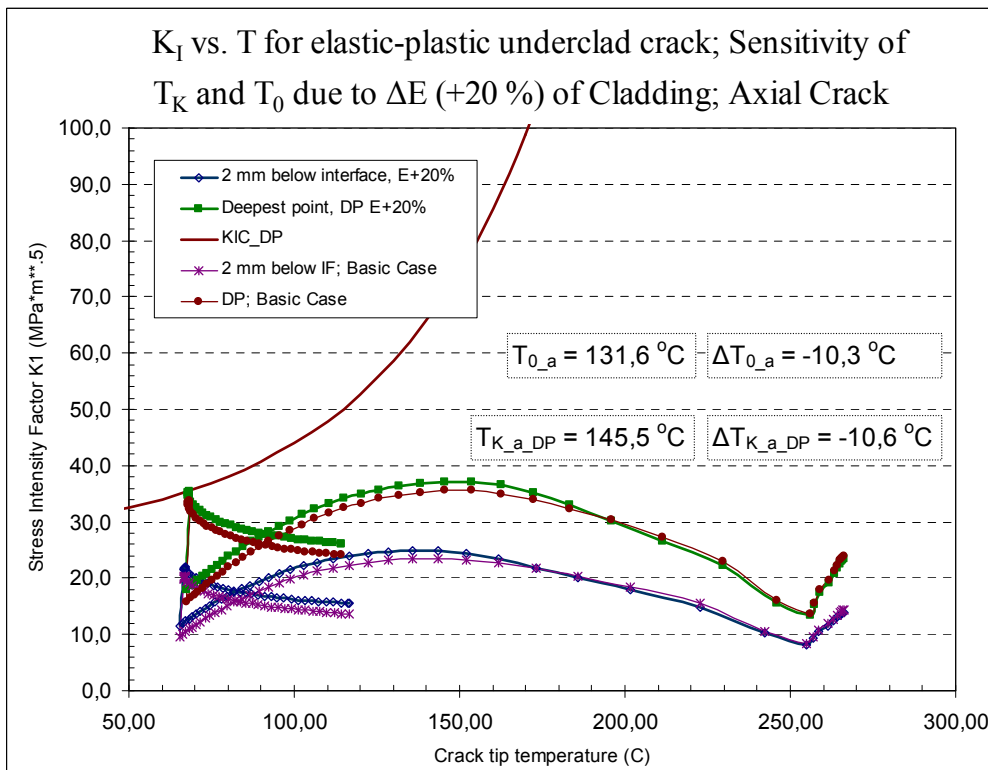


FIG. B49 – Sensitivity study, FNS, influence of E , underclad crack with elastic-plastic material model.

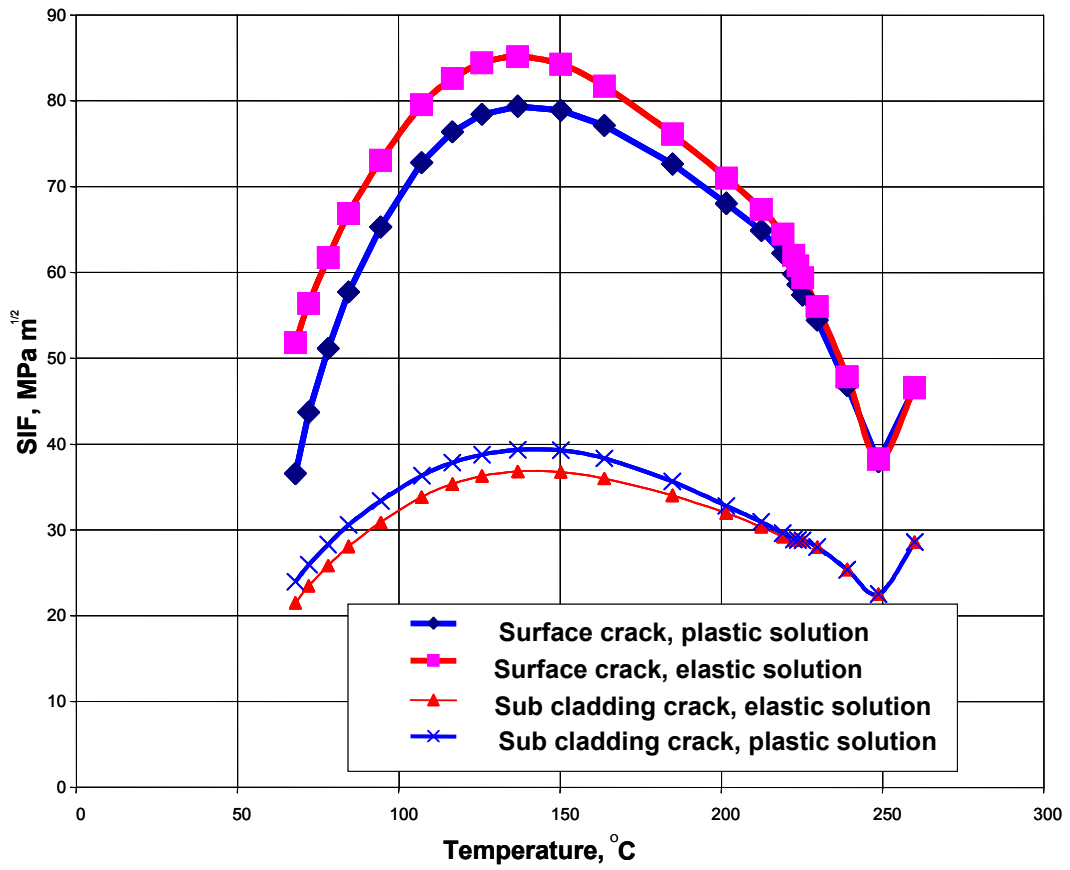


FIG. B50 – Sensitivity study, OKB, influence of elastic or elastic-plastic model.

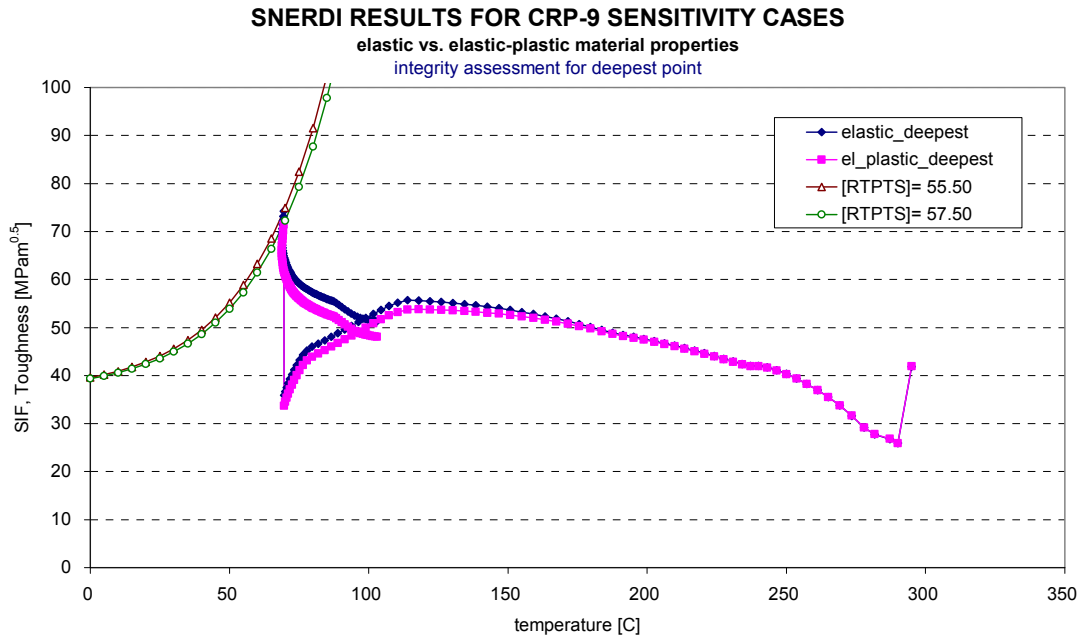


FIG. B51 – Sensitivity study, SNERDI, influence of elastic or elastic-plastic model, surface crack, deepest point.

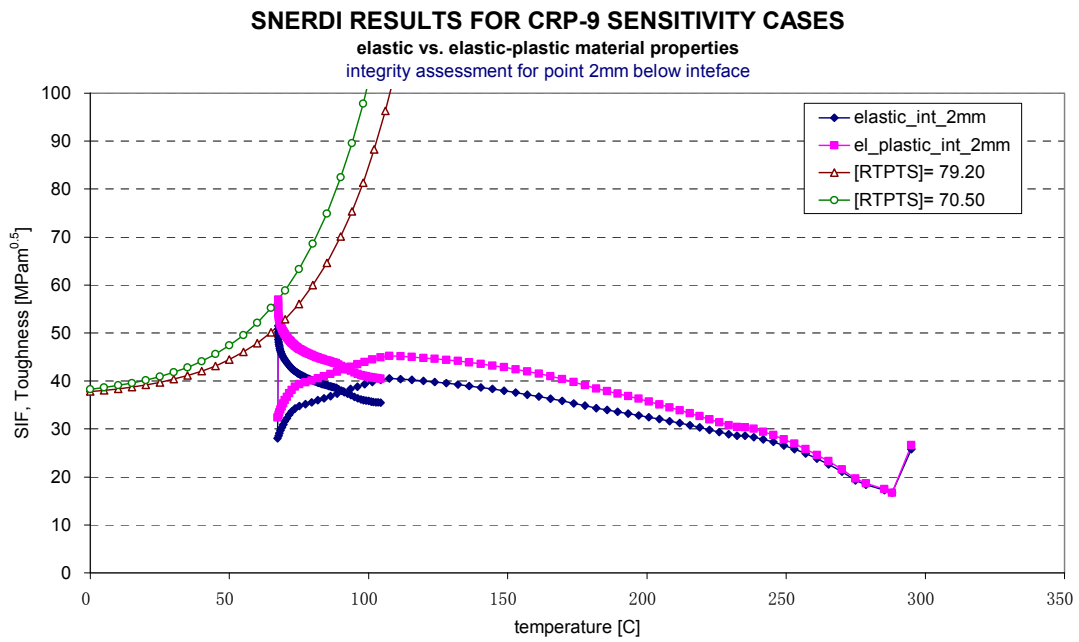


FIG. B52 – Sensitivity study, SNERDI, influence of elastic or elastic-plastic model, surface crack, near interface point.

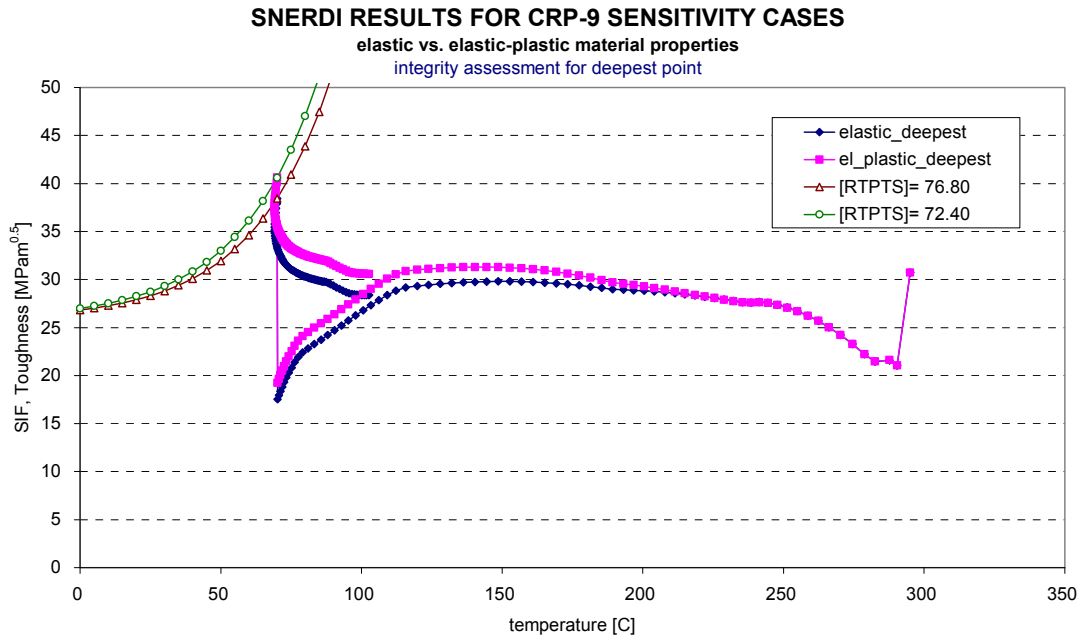


FIG. B53 – Sensitivity study, SNERDI, influence of elastic or elastic-plastic model, underclad crack, deepest point.

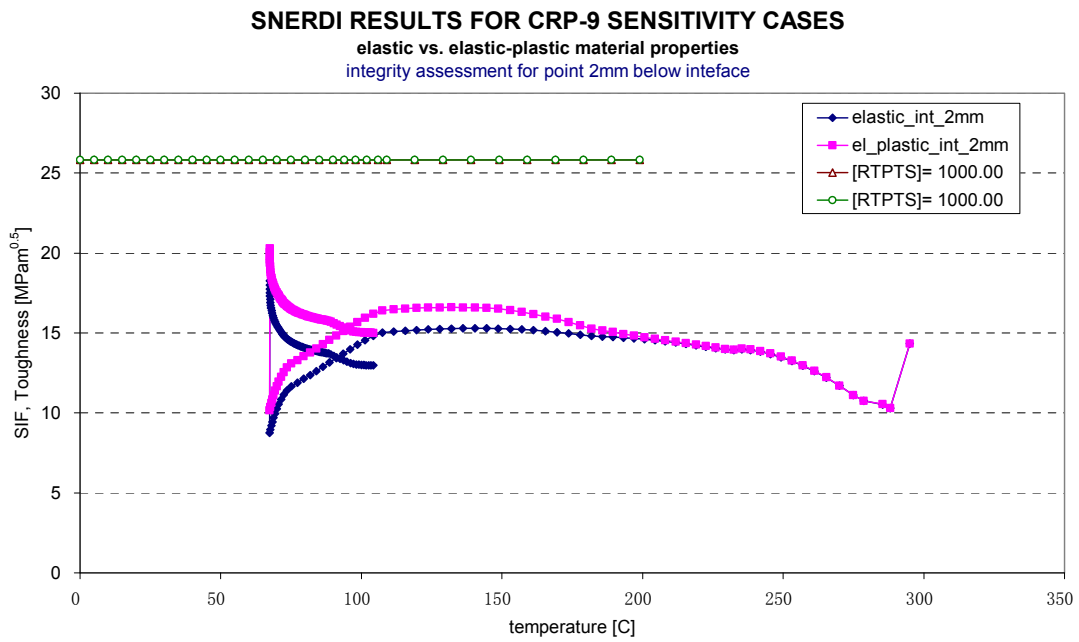


FIG. B54 – Sensitivity study, SNERDI, influence of elastic or elastic-plastic model underclad crack, near interface point.

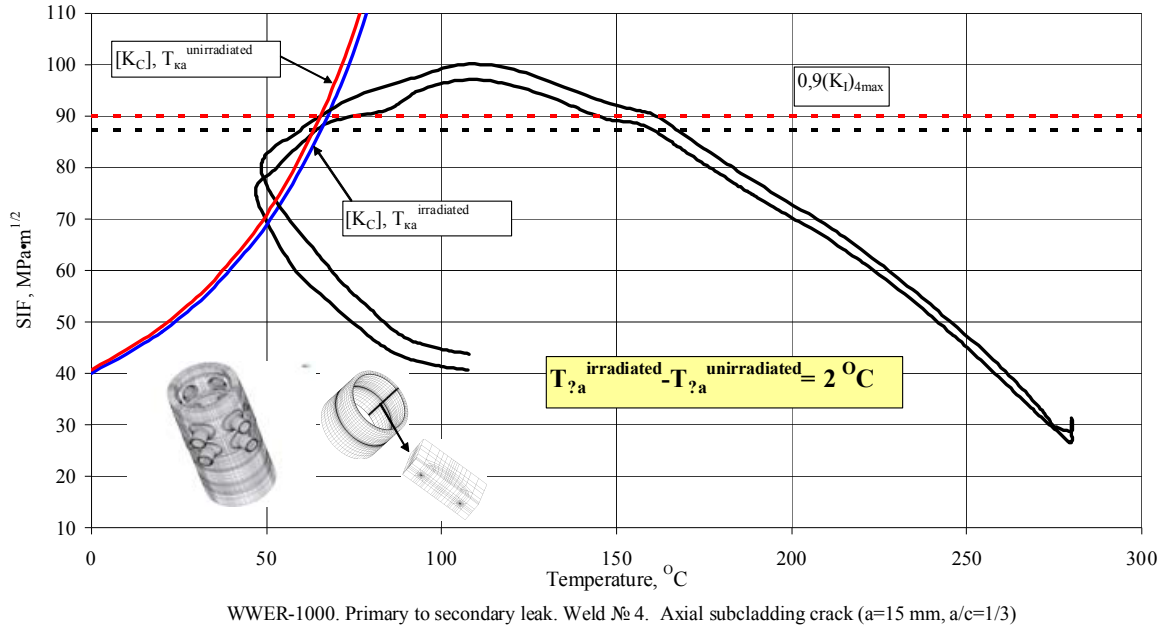


FIG. B55 – Sensitivity study, OKB, influence of initial or irradiated tensile properties, underclad crack.

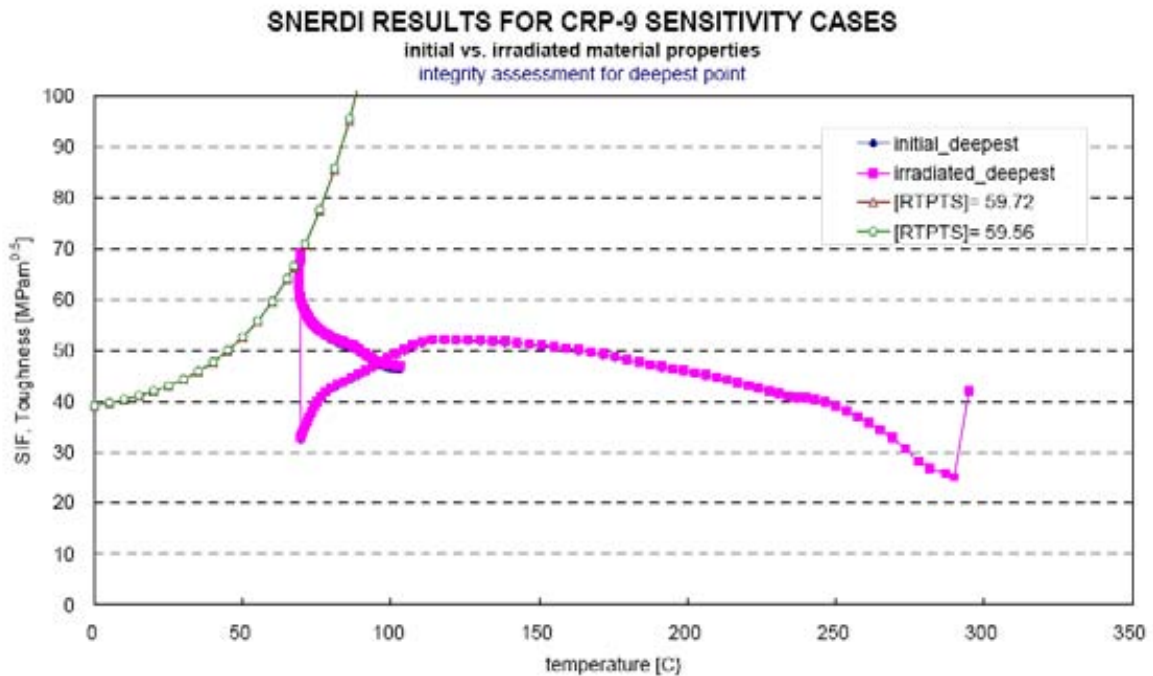


FIG. B56 – Sensitivity study, SNERDI, influence of initial or irradiated tensile properties, surface crack.

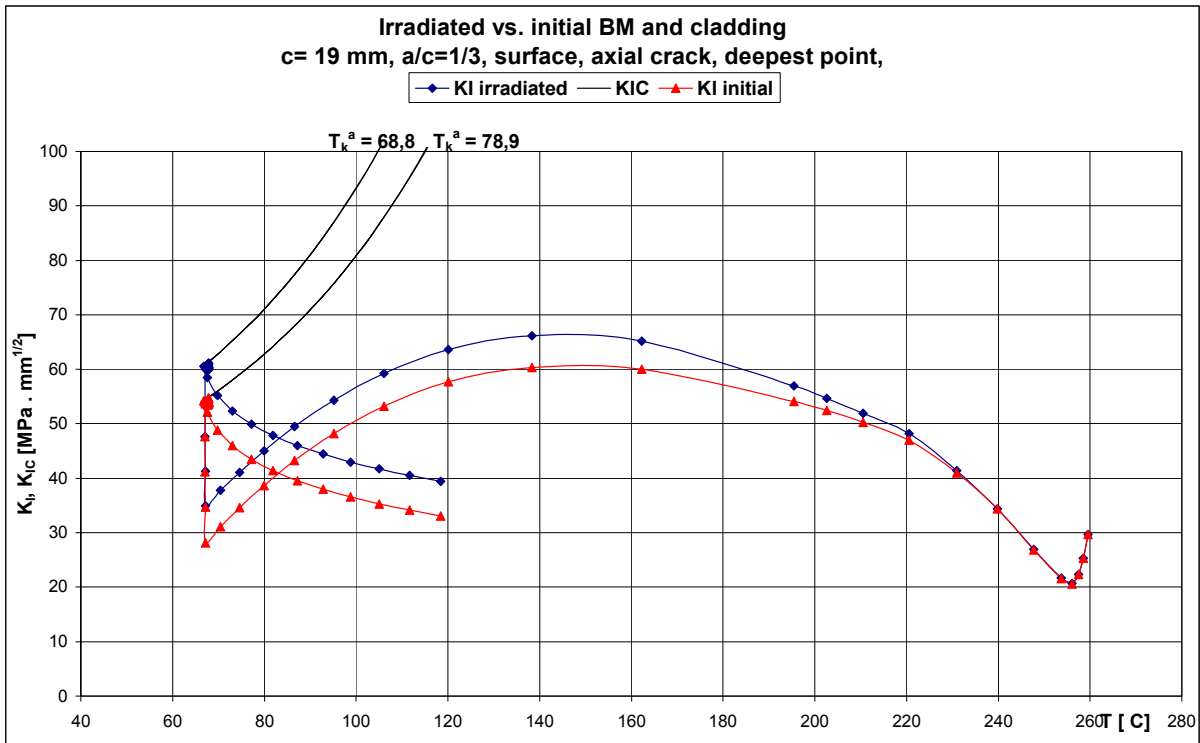


FIG. B57 – Sensitivity study, VUJE, influence of initial or irradiated tensile properties of BM and cladding, surface crack.

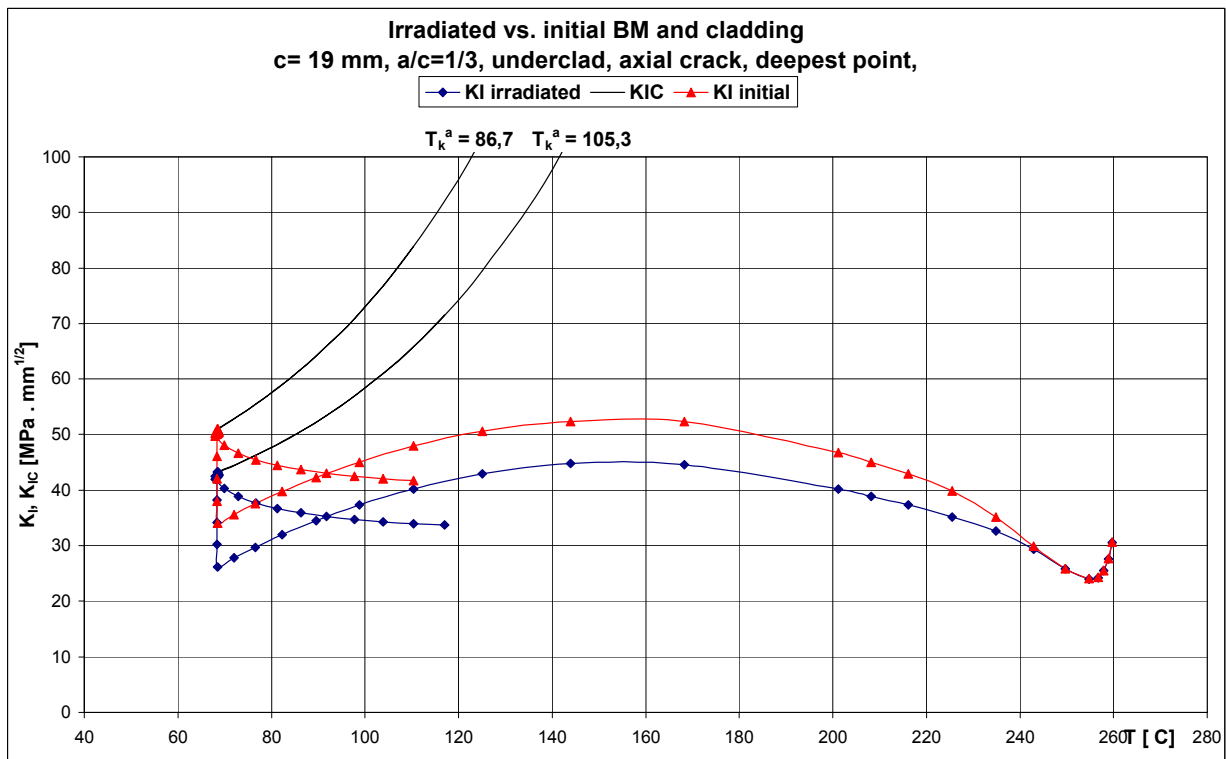


FIG. B58 – Sensitivity study, VUJE, influence of initial or irradiated tensile properties of BM and cladding, underclad crack.

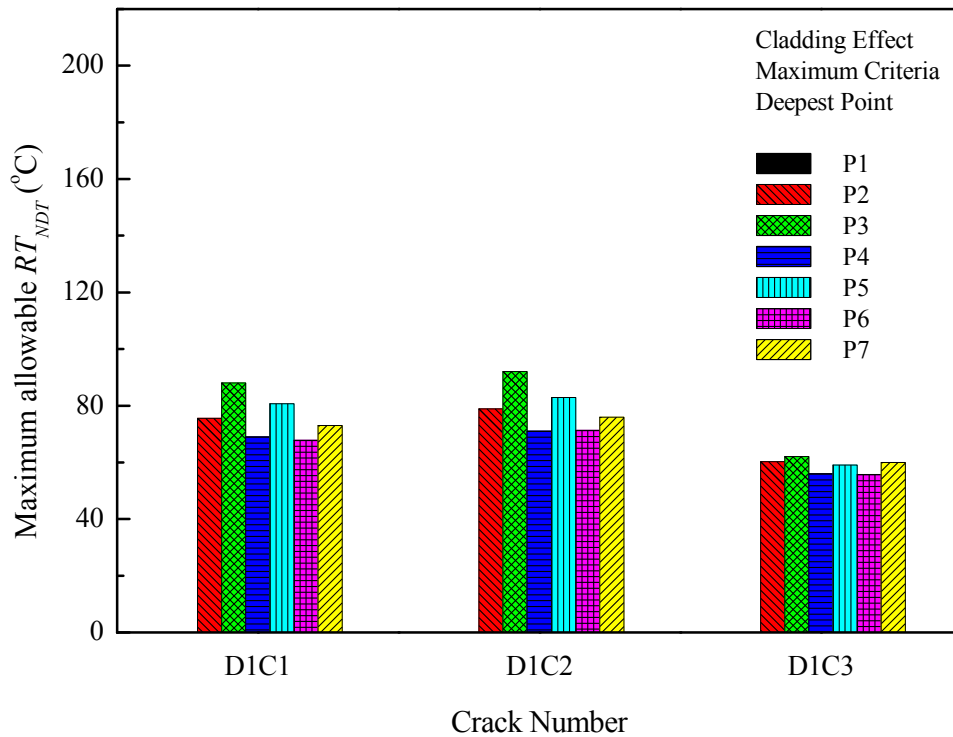


FIG. B59 – Sensitivity study, KINS, effect of material properties of cladding:

- C1: Cladding properties are assumed as identical to the base metal.
- C2: Cladding mechanical properties are assumed as identical to the base metal. Cladding thermal conductivity is considered. Additional stress from steep temperature gradient in cladding is evaluated.
- C3: Cladding is fully considered (basic case). Additional stresses from steep temperature gradient and differential thermal expansion are evaluated.

Table B14 – Effect of weld residual stress shape to the allowable T_k^a and T_0^a

Weld Residual Stress	T_k^a (deepest point)	T_0^a (deepest point, SC)	T_k^a (2 mm below IF)	T_0^a (2 mm, SC)	T_0^a (Integral Approach)
Not applied	68.1	44.0	74.6	50.3	49.6
Cosine shape	56.4	32.4	66.6	42.5	38.6
Constant 60 MPa	55.0	31.0	66.3	42.2	37.4
Δ °C	-1.4	-1.4	-0.3	-0.3	-1.2

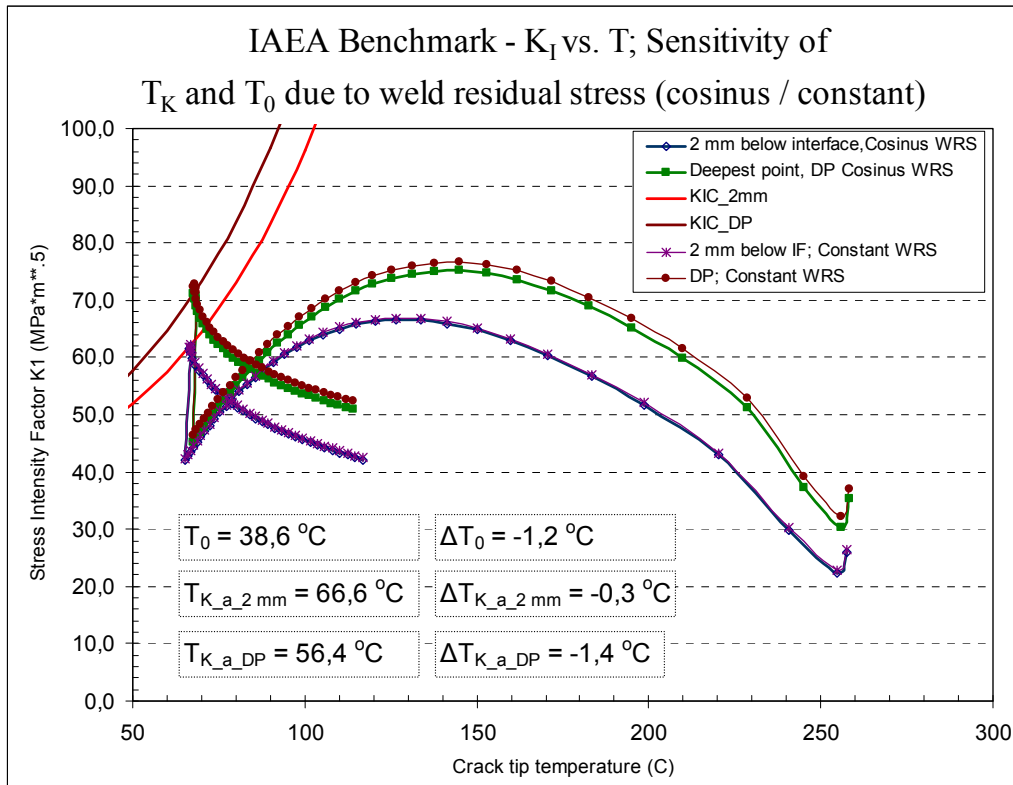


FIG. B60 – Sensitivity study, FNS, effect of weld residual stress shapes.

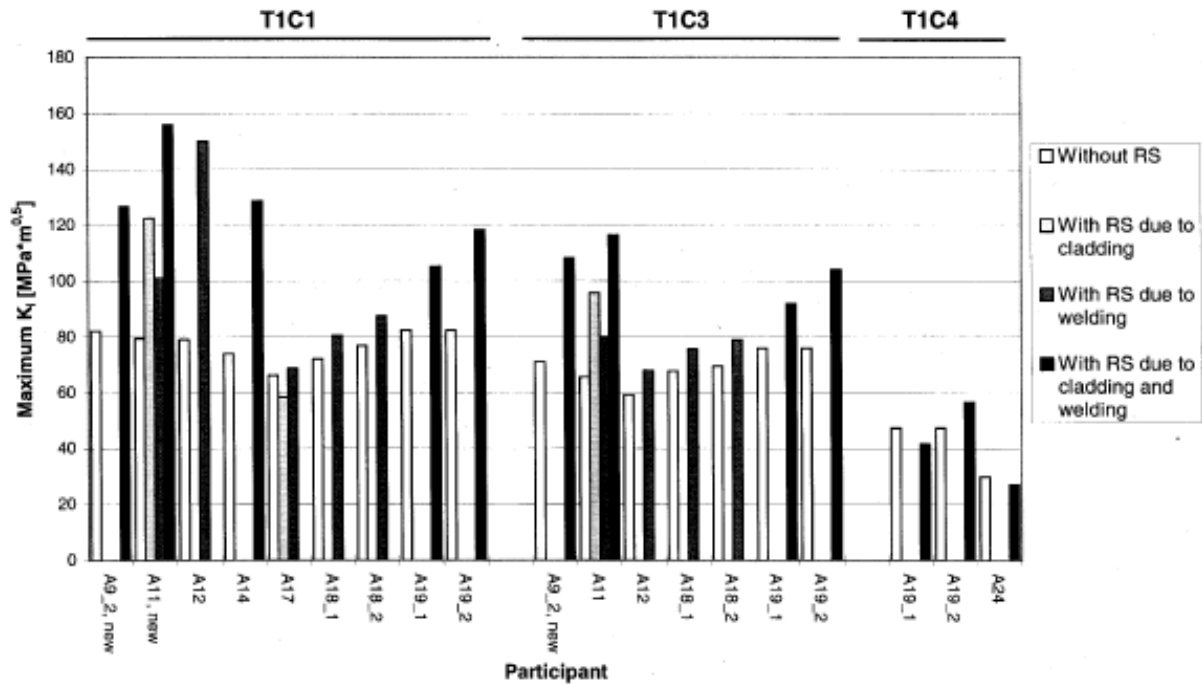


FIG. B61 – Sensitivity study, ICAS, effect of residual stress.

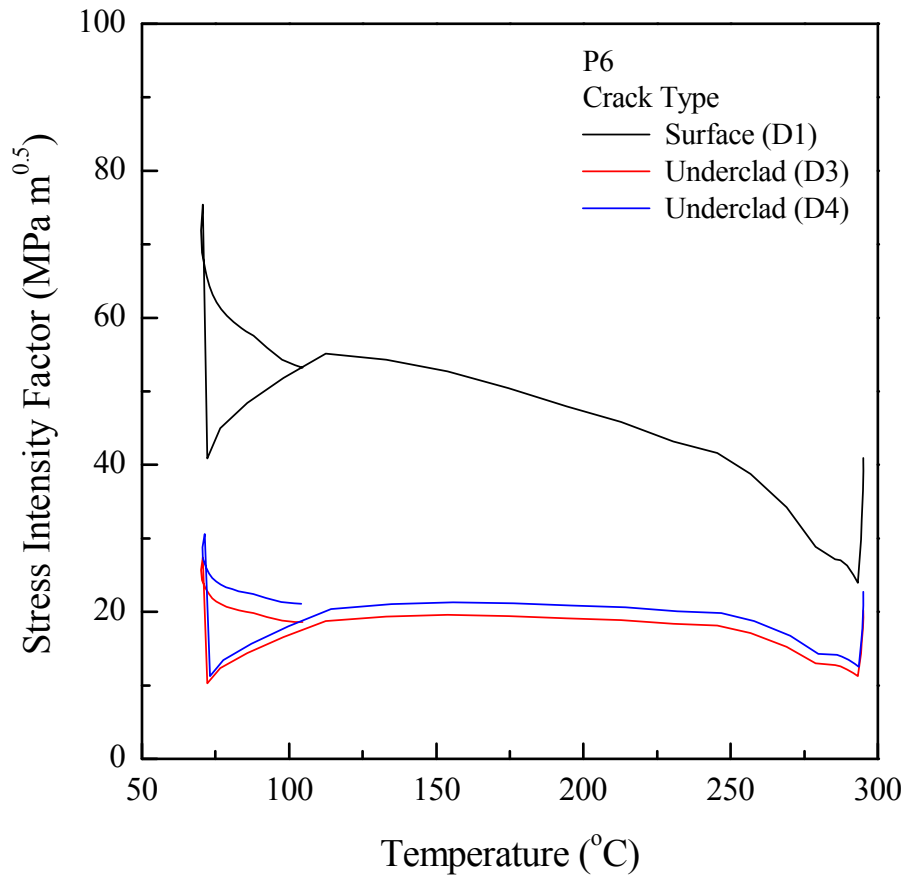


FIG. B62 – Sensitivity study, KINS, effect of crack type (D1, D3: $a = 12 \text{ mm}$, D4: $a = 15 \text{ mm}$).

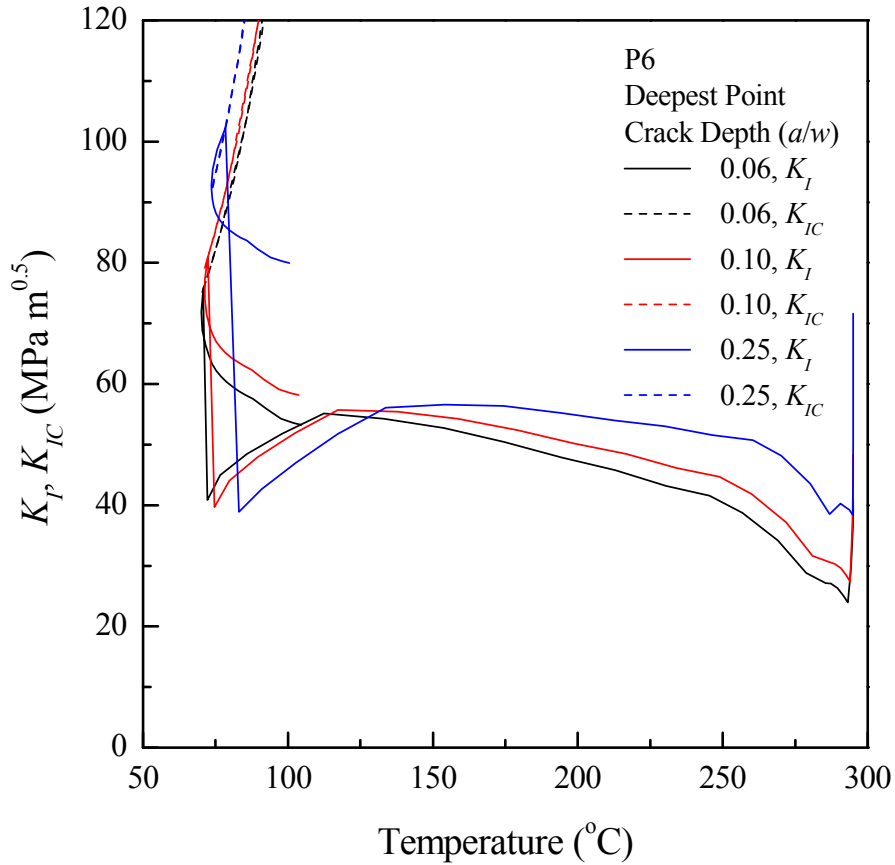


FIG. B63 – Sensitivity study, KINS, effect of crack depth (deepest point).

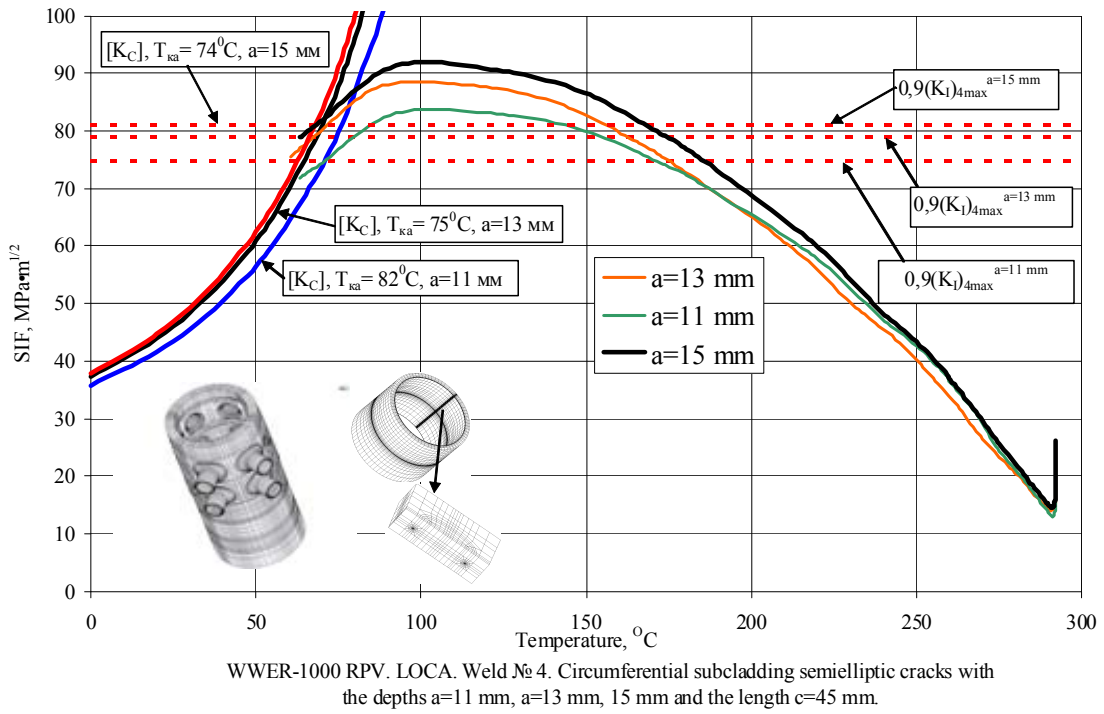


FIG. B64 – Sensitivity study, OKB, effect of crack depth (deepest point).

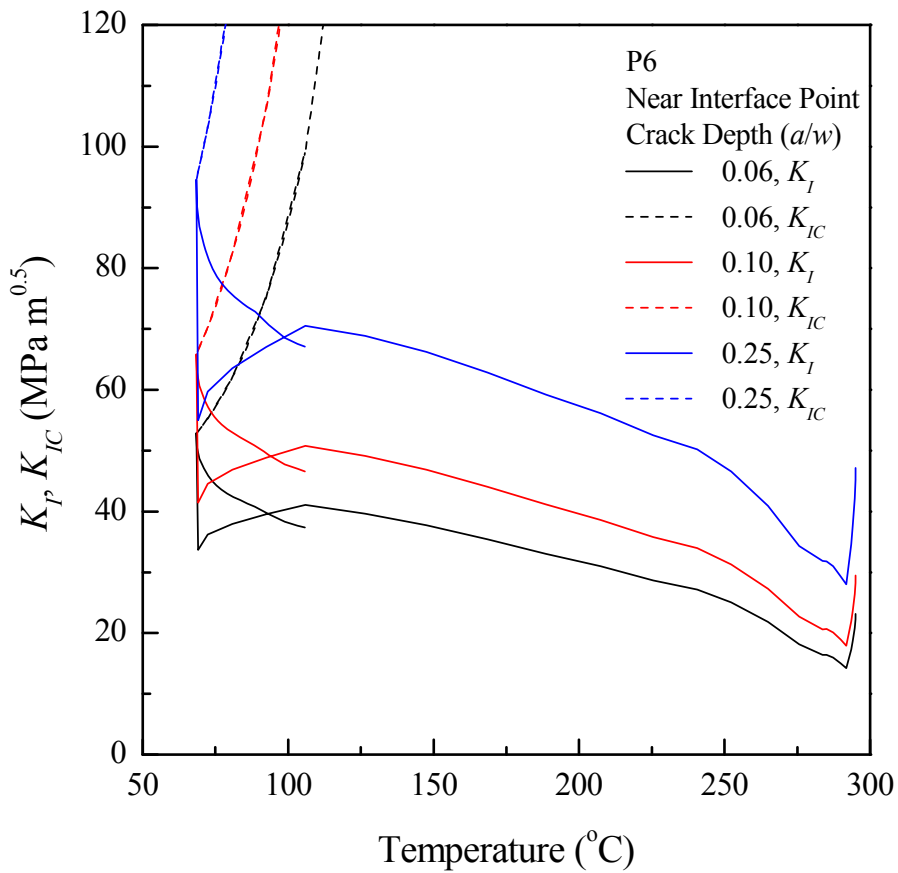


FIG. B65 – Sensitivity study, KINS, effect of crack depth (near interface point).

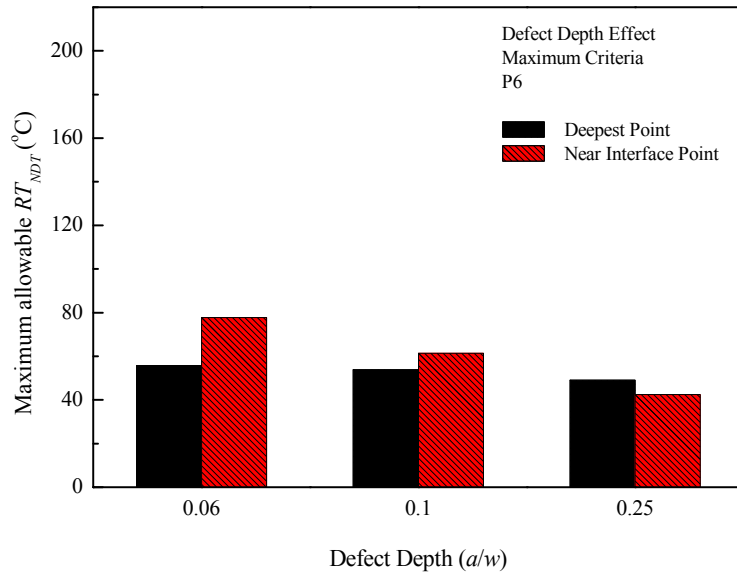


FIG. B66 – Sensitivity study, KINS, effect of crack depth.

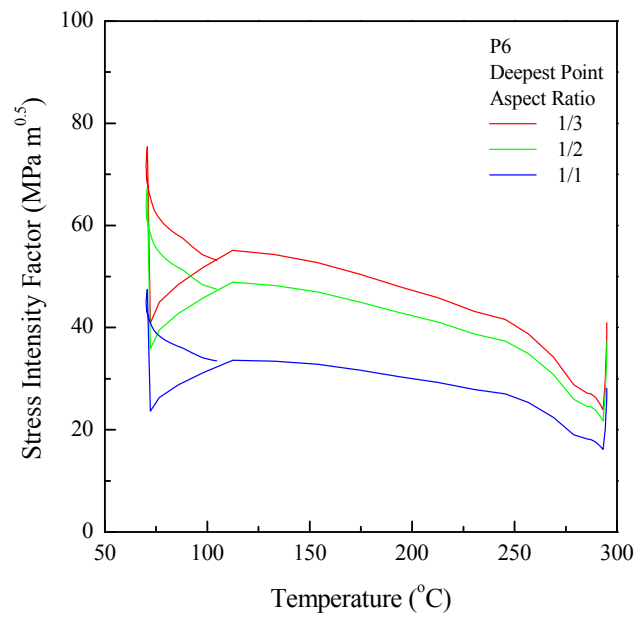


FIG. B67 – Sensitivity study, KINS, effect of crack aspect ratio (surface crack, deepest point).

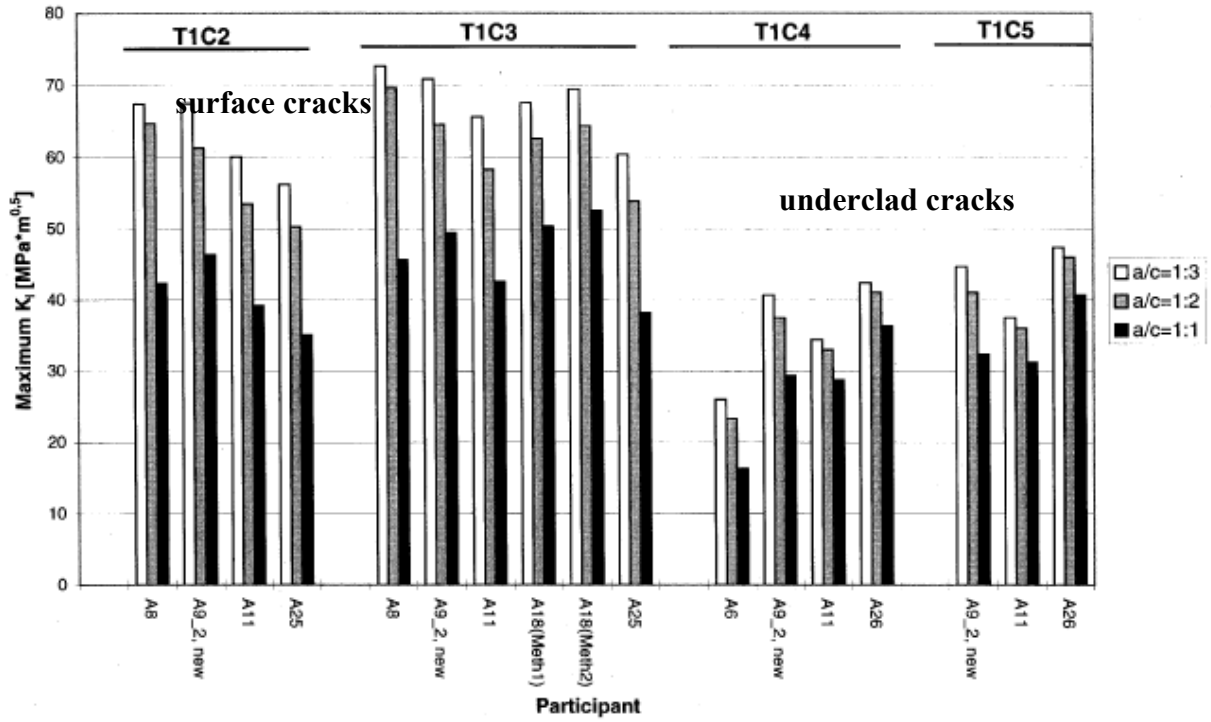


FIG. B68 – Sensitivity study, ICAS, effect of crack aspect ratio (deepest point).

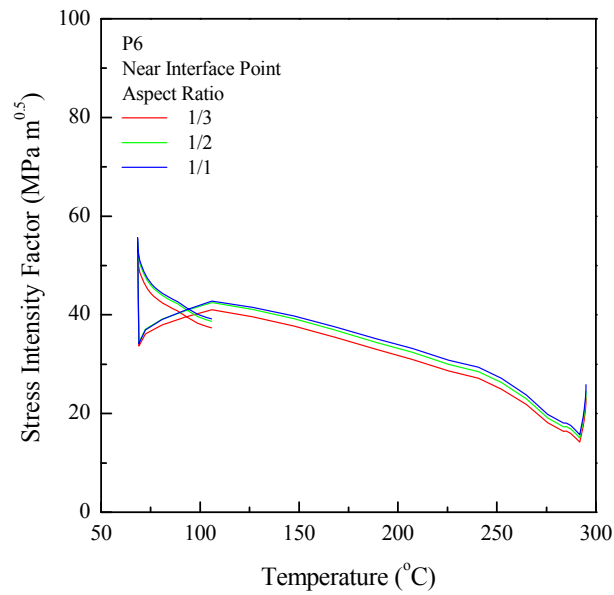


FIG. B69 – Sensitivity study, KINS, effect of crack aspect ratio (surface crack, near interface point).

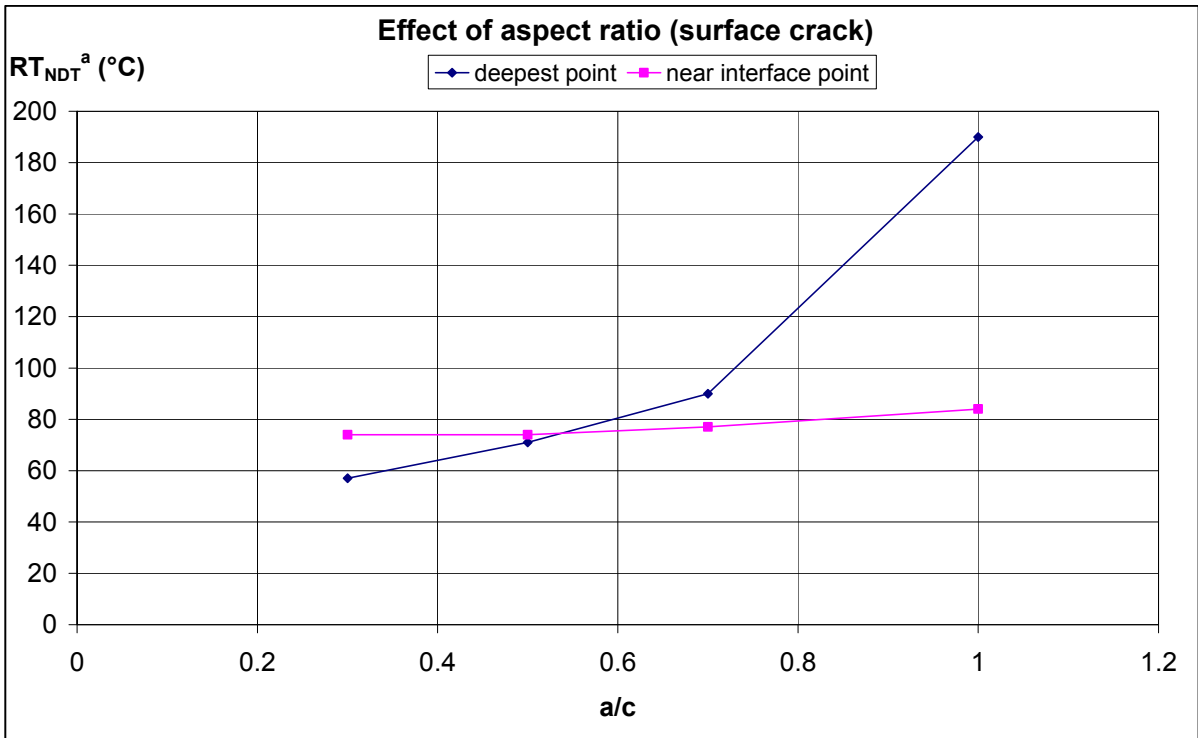


FIG. B70 – Sensitivity study, SNERDI, effect of crack aspect ratio (surface crack).

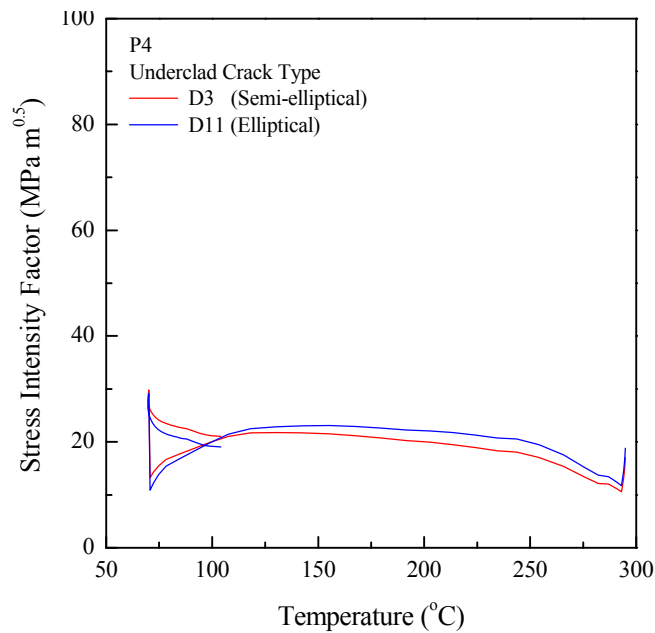


FIG. B71 – Sensitivity study, KINS, effect of crack shape – elliptical vs. semi-elliptical (deepest point).

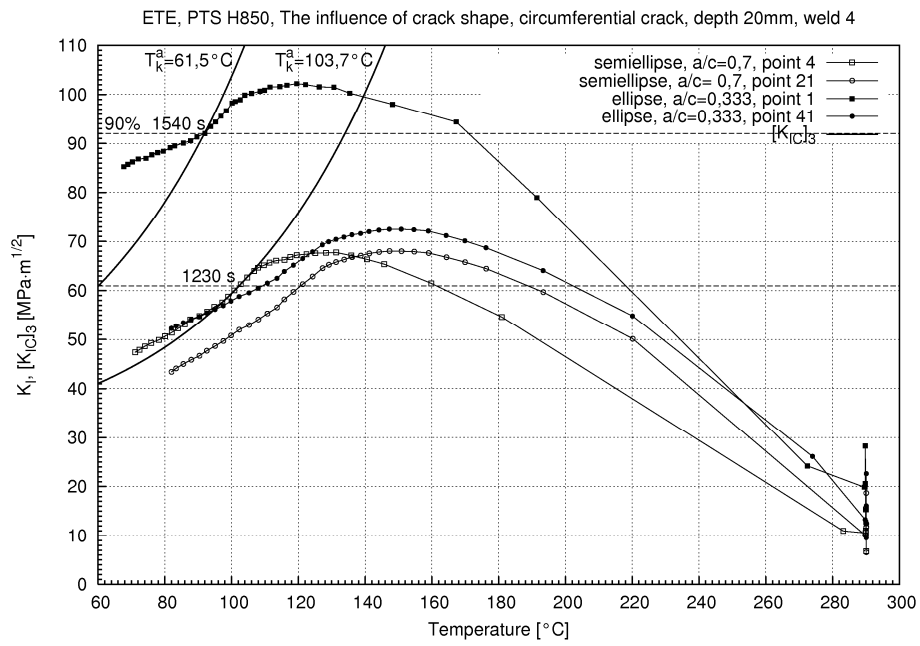


FIG. B72 – Sensitivity study, NRI old results, effect of crack shape – elliptical vs. semi-elliptical (points 1, 4 = near interface, point 21 = deepest).

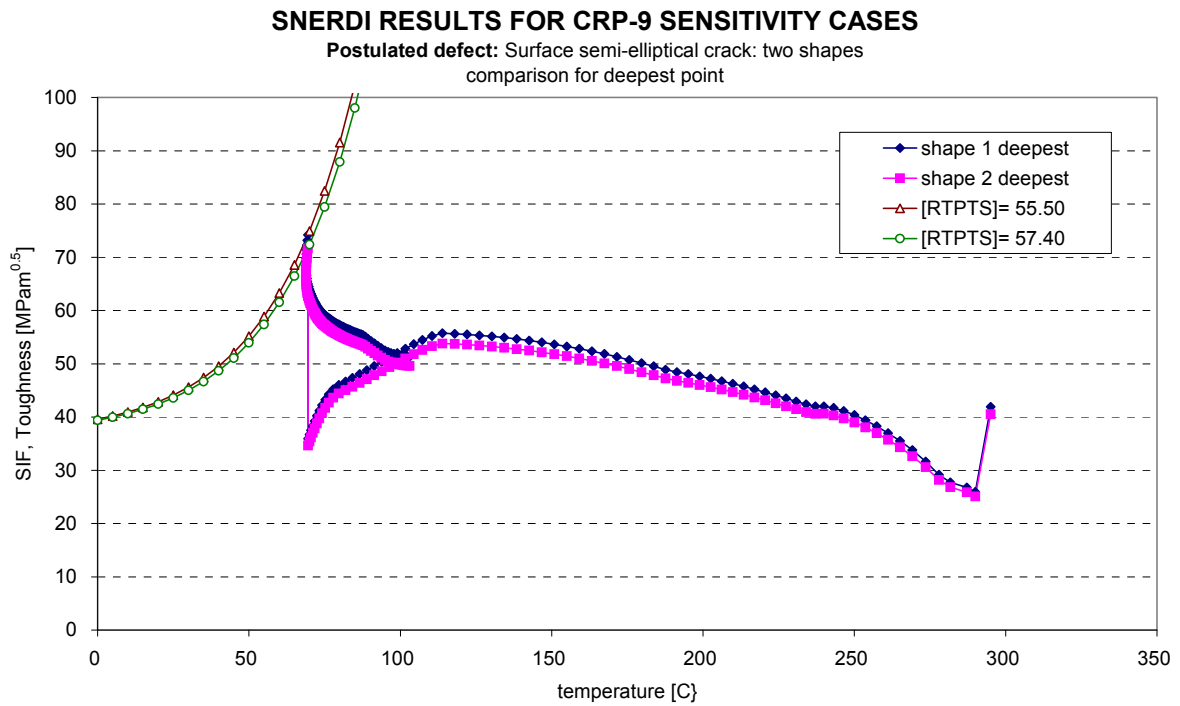


FIG. B73 – Sensitivity study, SNERDI, effect of crack shape (shape 1 vs. - shape 2), deepest point.

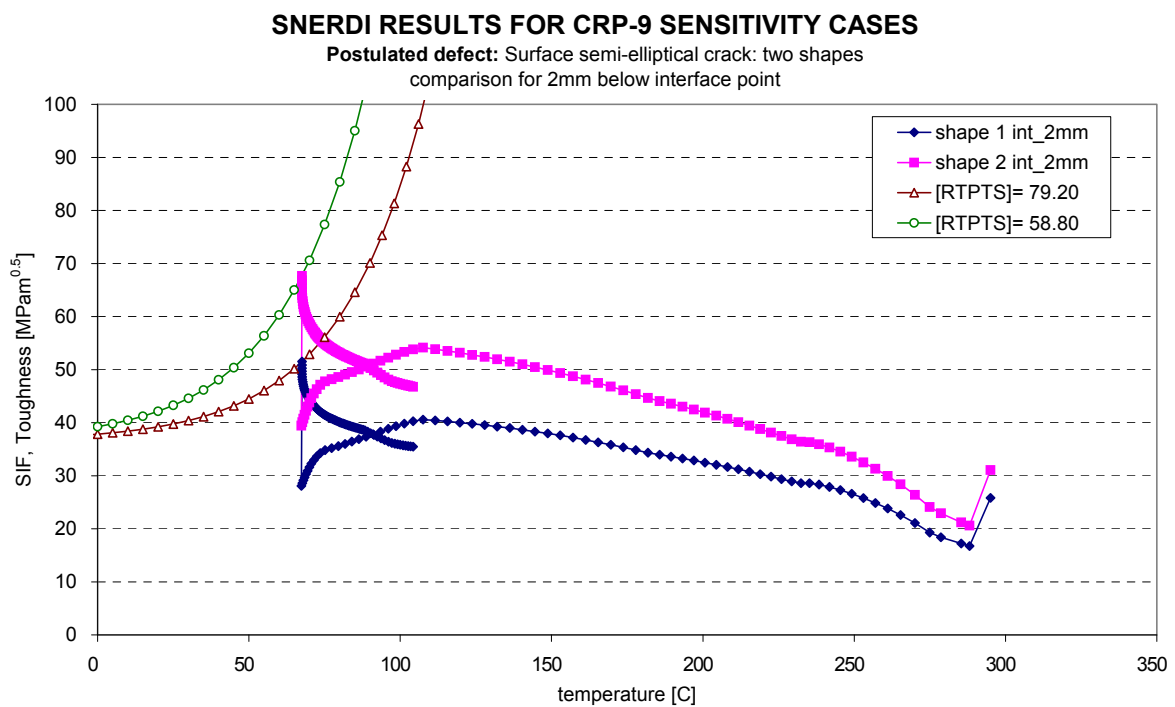


FIG. B74 – Sensitivity study, SNERDI, effect of crack shape (shape 1 vs. - shape 2), near interface point.

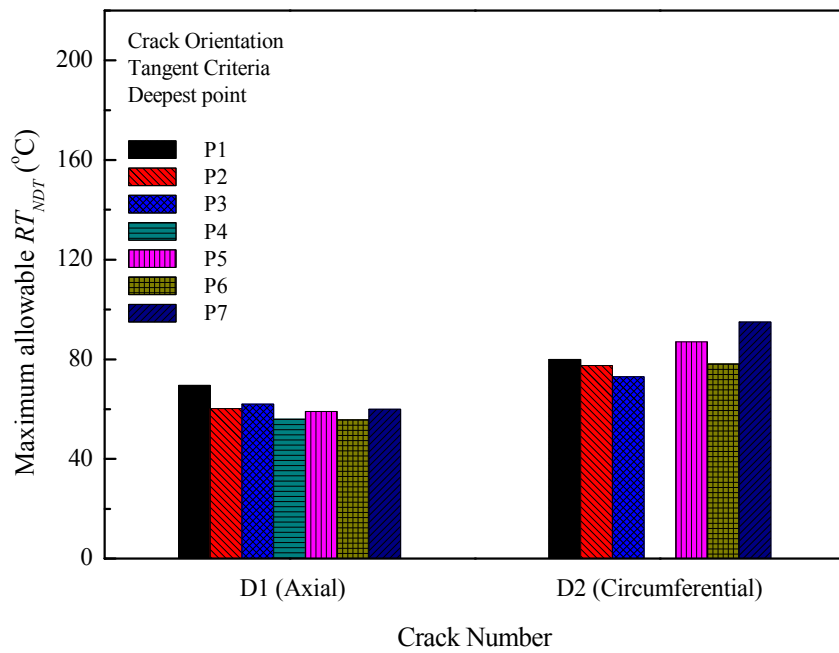


FIG. B75 – Sensitivity study, KINS, effect of crack orientation.

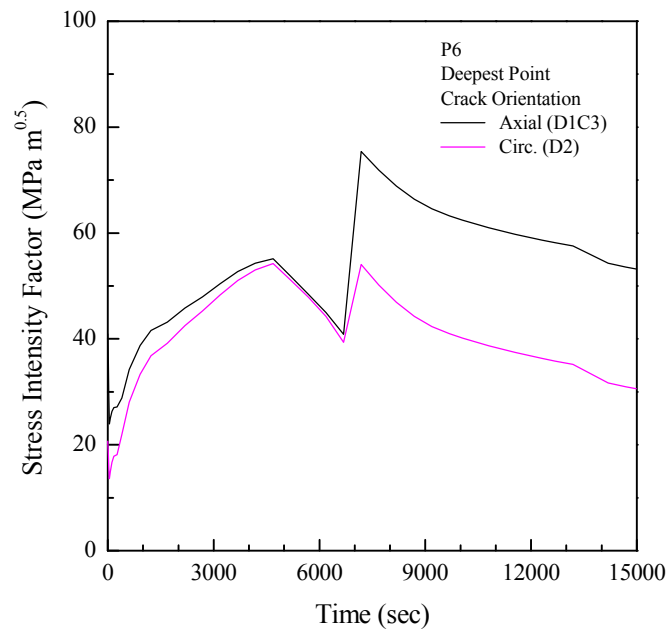


FIG. B76 – Sensitivity study, KINS, effect of crack orientation.

SNERDI RESULTS FOR CRP-9 SENSITIVITY CASES
FEM vs. ASME approach

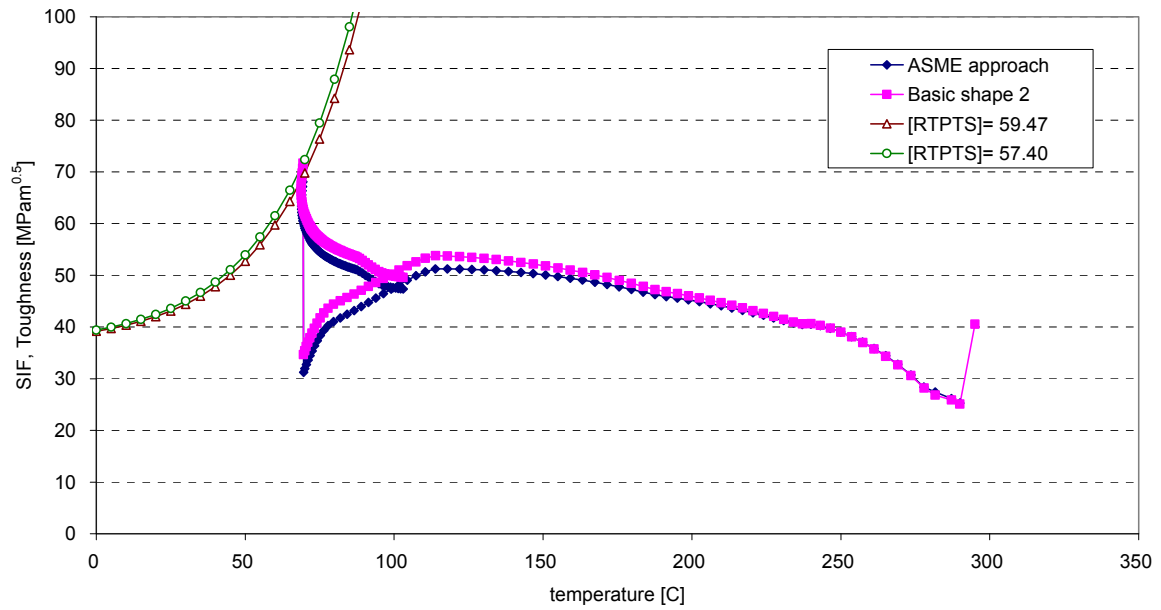
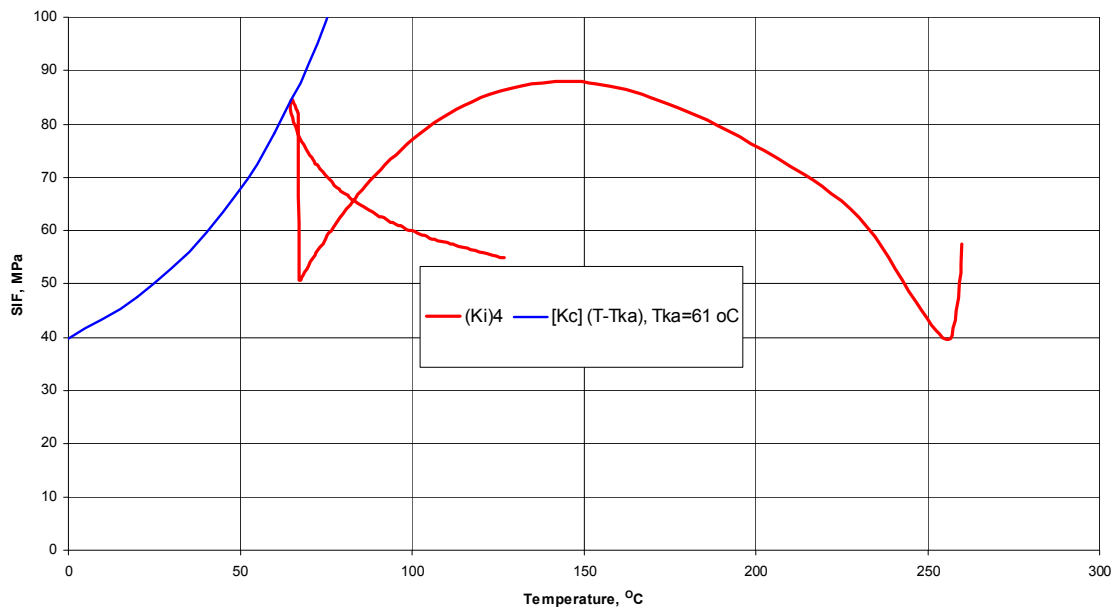
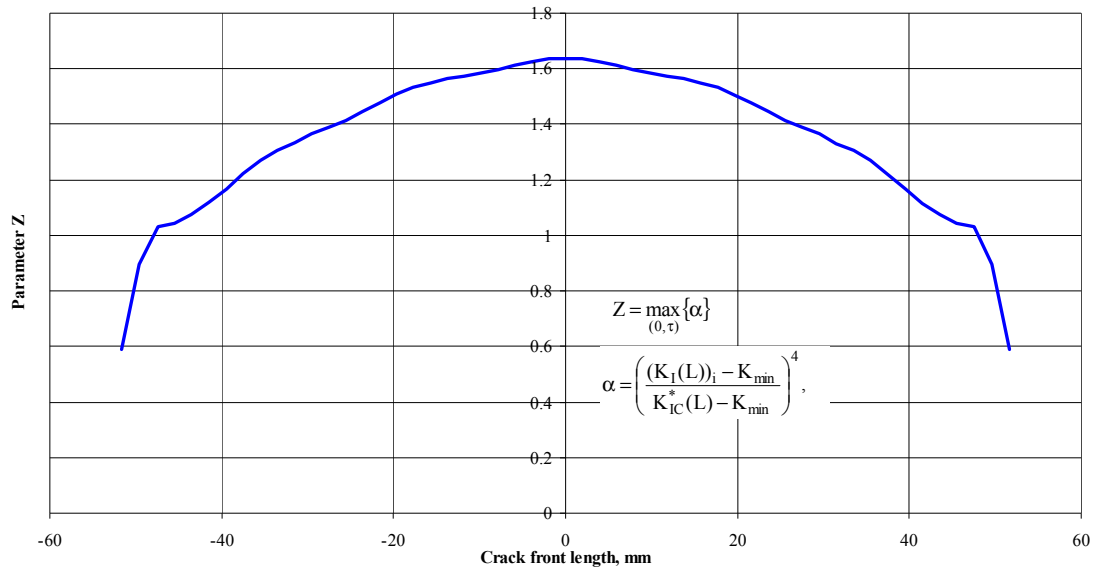


FIG. B77 – Sensitivity study, SNERDI, effect of K_I calculation (ASME formulae vs. FEM).



National code A. WWER-440/V-213. Point by point assessment

FIG. B78 – Sensitivity study, OKB, point-by-point vs. integral approach.



National code A. WWER-440/V-213. Integral approach evaluation. Tka=66 °C.

FIG. B79 – Sensitivity study, OKB, point-by-point vs. integral approach, cont.

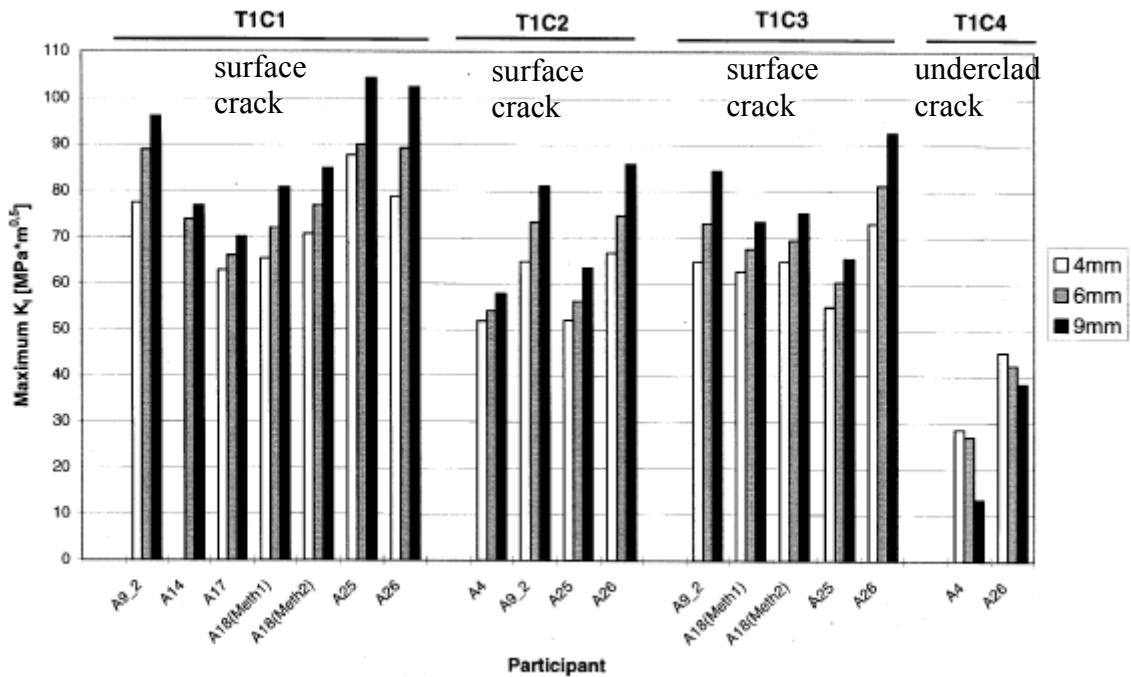


Fig. 5.1.26 Task PCT: Influence of the cladding thickness on the maximum stress intensity factor at the deepest point of the cracks.

FIG. B80 – Sensitivity study, ICAS, effect cladding thickness, C1, C2, C3 - crack depth increasing with cladding thickness, C4 – crack depth independent on cladding thickness.

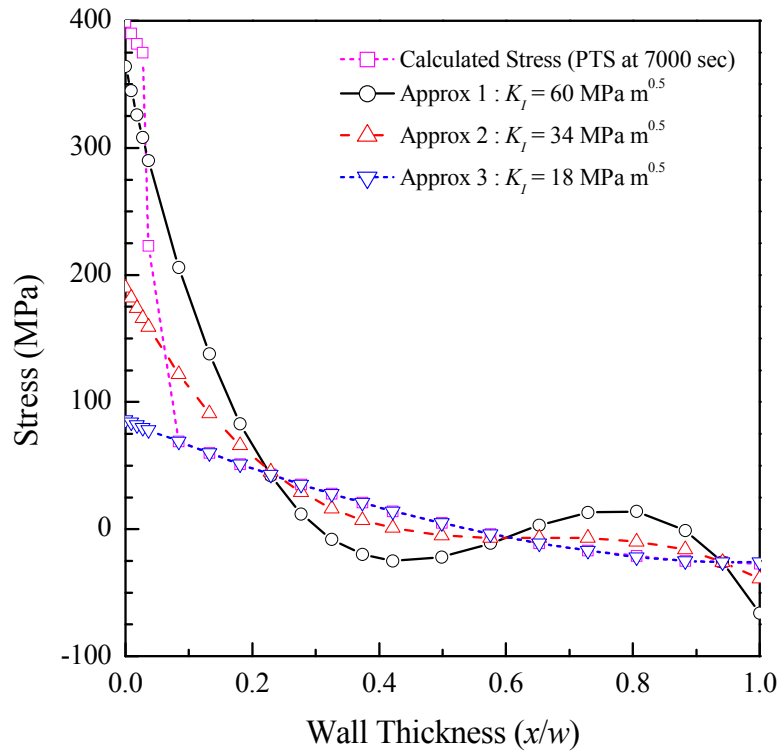


FIG. B81 – Sensitivity study, KINS, effect of stress approximation (surface crack, deepest point).

6. CONCLUSIONS

6.1. The transient analysed and national codes applied

WWER case

The PTS event “Pressurizer safety valve inadvertent opening with reclosure at 3600 s” was analysed within the benchmark. The scenario was taken from an older benchmark „WPB“ organized by IAEA in 1997–1998. Even if it is a realistic scenario for a reactor pressure vessel of the WWER 440/213 type, it is not specific for any individual NPP.

The course of the transient from the point of view of fracture mechanics assessment is as follows: K_I values slightly decrease at the beginning of the transient due to the pressure reduction, then they increase up to the maximum at about 1000 seconds due to increased temperature gradient. Then, a decrease again follows, as the temperature gradient through the vessel wall decreases. The repressurization at 3600 s is the critical phase for this scenario with sudden increase of K_I . The critical time is 3900 s, when the pressure reaches its maximum.

The resulting maximum allowable critical temperature of brittleness T_k^a for the basic case was within the range from 65 °C to 71 °C (results obtained by different participants). We have to repeat here that the scenario analysed was not specific for any WWER 440/213 NPP, but artificially (but realistically) defined for the purpose of the benchmark definition. It has to be noted, that the postulated defect (surface one with depth 19 mm) was relatively large one.

Finally, it can be concluded that the results of RPV integrity assessment strongly depend on the applied code.

PWR case

The course of the transient from the point of view of fracture mechanics assessment is very similar to the above described WWER case. The critical time was found in range 3650 s to 4200 s, i.e. after the repressurization.

Again we can conclude, that the results of RPV integrity assessment strongly depend on the applied code.

6.2. The benchmark results

Concerning the temperature analysis results, the solutions are generally in very good agreement. One minor deviation was found for P1 participant, who used too simplified analytical solution.

Concerning the stress analysis results, the solutions are generally in good agreement. Some differences were found mainly in cladding.

Concerning the stress intensity factor analysis results, the solutions are generally in good agreement. Some differences were again found mainly for some simplified solutions (P1). There were observed significant differences for the near interface point, which were explained by different shape of the crack (main axis of the ellipse lying in the inner surface or in the interface) used by different participants.

Concerning the main results of RPV integrity assessment (i.e. the maximum allowable transition temperature), the accordance is quite good with exception of the above-mentioned influence of crack shape (for the near interface point). Some minor differences were indicated in the determined critical time of the transient, as some participants used coarse time stepping close to expected critical time

(after repressurization). But this fact did not influence significantly the final results (maximum allowable transition temperature).

Finally it can be concluded that the differences among the results are reasonably low and that the methods and models used by the participants can be used for integrity assessment of real RPV.

6.3. The sensitivity studies

Large set of sensitivity studies was analysed and also supplemented by some older results. The significance of many parameters entering to the RPV integrity assessment was assessed with indicating the conservative “side” of each of them.

As very significant parameters were identified the following:

- Thermal hydraulic input data from the mixing code;
- Postulated crack, namely its:
 - position (surface vs. underclad),
 - depth,
 - shape (elliptical vs. semi-elliptical for assessment of the near interface point),
 - orientation (axial vs. circumferential);
- Treatment of cladding / BM stress discontinuity when applying formulae for K_I determination.

During the RPV integrity assessment the care has to be taken in preference to proper definition of these parameters (most of them are prescribed by the applied standards). Also other parameters not included into the sensitivity studies list (like K_{IC} curve) are of high importance.

On the other hand, as negligible parameters were found the following:

- Treatment of material behaviour (linear elastic vs. elastic-plastic) for assessment of surface crack;
- Exact stress-strain curve (initial or irradiated) of the base material for assessment of both surface and underclad crack;
- Shape of residual stress in weld profile (cosine vs. constant);
- Shape of the postulated crack (elliptical vs. semi-elliptical) for assessment of the deepest point;
- Shape of the postulated semi-elliptical crack (position of main axis, i.e. shape 1 vs. shape 2) for assessment of the deepest point.

These results are also useful, as no special care needs to be taken for these parameters during the RPV integrity assessment.

Other parameters included into sensitivity studies were found as significant and they have to be properly defined for the RPV integrity assessment.

Results of the sensitivity studies were found as very useful and many of them were incorporated to the main text of this handbook.

6.4. The benchmark

Essentially, the benchmark definition was clear and precise enough to exclude potential misunderstanding leading to large differences in the results, as was observed in some older benchmarks. Both the benchmark definition and the individual solutions were based on long-term experience of all participants with this type of calculations and with similar benchmarks. Despite of this, some minor misunderstandings appeared (mainly the question of crack shape influencing significantly the solution for the near interface point) due to not quite clear benchmark definition.

As a disadvantage of the benchmark can be mentioned its split to two subproblems (WWER and PWR cases). Even both benchmarks were very similar in their nature, even the transients were very similar, the group of participants split to two halves and the number of comparative results for individual

benchmarks was limited. Two participants (NRI, AREVA) solved both benchmarks (the basic cases), which can serve as interconnection between the two tasks.

Suggestions for future computational benchmarks:

- To limit the number of variants (geometries, material properties, transients, postulated cracks, etc.) to minimum, if possible to one variant, to obtain comparable results by all participants. If there is a need to analyse more cases, define them as “optional” or “sensitivity studies”. In the case of larger number of “basic” cases, most of participants select only some of them, unfortunately usually everybody selects something different;
- To define all input data as much precisely and uniquely as possible. Try to find all possible details of analysis and prescribe them in the benchmark definition;
- Even in case when the benchmark definition prescribes to follow a specified standard, it is recommendable to repeat at least the main data or requirements from the standard in the benchmark definition;
- If any participant recognises during the solution that some information or data are missing in the benchmark definition, he is highly recommended to ask the benchmark leader for supplying the necessary additional information or data, which then should be circulated among all participants.

Finally it can be stated, that participation in the IAEA CRP-9 PTS Benchmark was recognised as a very efficient way to improve the user qualification and to reduce user effect on results of analysis. The experience obtained within this benchmark provided a basis for creation of “Good Practice Handbook for Deterministic Evaluation of the Integrity of A Reactor Pressure Vessel During a Pressurized Thermal Shock”.

7. REFERENCES

- [1] INTERNATIONAL ATOMIC ENERGY AGENCY, WWER-440/213 RPV PTS Benchmark Exercise (WPB), Terms of Reference, IAEA-WWER-SC-205, IAEA, Vienna (1998).
- [2] INTERNATIONAL ATOMIC ENERGY AGENCY, WWER-440/213 RPV PTS Benchmark Exercise (WPB), Results of Phase 1. Thermal Hydraulic System and Mixing Analyses, IAEA-WWER-SC-211, IAEA, Vienna (1998).
- [3] INTERNATIONAL ATOMIC ENERGY AGENCY, WWER-440/213 RPV Pressurized Thermal Shock Analysis Benchmark Exercise (WPB), Results of Phase II. - Structural Analysis and Fracture Mechanics Analysis, IAEA, Vienna (1999).
- [4] PROBABILISTIC STRUCTURAL INTEGRITY OF A PWR REACTOR PRESSURE VESSEL, Round Robin Proposal, Rev. 4, OECD NEA, CSNI, PWG 3, IAGE, Metal group, Paris (2003).
- [5] Comparison Report of RPV Pressurised Thermal Shock International Comparative Assessment Study (PTS ICAS), OECD, NEA/CSNI/R(99)3, Paris (1999).
- [6] UNIFIED PROCEDURE FOR LIFETIME ASSESSMENT OF COMPONENTS AND PIPING IN WWER NPPS VERLIFE. Technical report, European Commission, 5th Euratom framework programme (2003).
- [7] PIŠTORA, V., Prostorový konečněprvkový model tlakové nádoby reaktoru VVER 440 v JE Dukovany pro hodnocení studených jazyků, UJV 10 821 T, Nuclear Research Institute Řež, Řež (1996).
- [8] NEUVONEN, A., IAEA CRP-9 Phase 1 Benchmark Calculations Final Results of Fortum Cases, Fortum Nuclear Services Ltd, Espoo (2007).
- [9] MYUNG, J. J, Benchmark calculations of structural integrity assessment for reactor pressure vessels during pressurized thermal shock, Korea Institute of Nuclear Safety, KINS/RR-453, Rev.1, Daejeon (2007).
- [10] HE, Y., IAEA CRP-9 calculation report for sensitivity cases, SNERDI, Shanghai (2007).
- [11] AKBASHEV, I., PIMINOV, V., Sensitivity study results, presentation on 2nd RCM of the IAEA CRP-9, IAEA, Vienna (2008).
- [12] PIŠTORA, V. et al., PTS Benchmark, final report, COVERS-WP4-D4.4 (2008).
- [13] CRP-9 Review and benchmark of calculation methods for structural integrity assessment of RPVs during PTS - Progress Report, AREVA NP GmbH report NTCM-G/2008/en/0271 (2008).
- [14] PIŠTORA, V., KAČOR, A., Comparison of “VERLIFE” and Russian Methodologies for Reactor Pressure Vessel Integrity Assessment, paper SMiRT18-F05_2, 18th International Conference on Structural Mechanics in Reactor Technology, Beijing (2005).

APPENDIX B1. PTS BENCHMARK DEFINITION

1.1. Basic benchmark case

1.1.1. WWER-440/V-213

- Linear- elastic calculations
- Cylindrical part of RPV (with correction to the bottom)
- VERLIFE material properties
- RPV Geometry – IAEA benchmark
 - (rin = 1,771 mm, cladding thickness = 9 mm, RPV base metal thickness = 140 mm)
- PTS regime – IAEA benchmark – PRZ SV inadvertent opening with closure at 3,600 s
- Thermal hydraulic file (CASE C)
- Two opposite plumes with defined width,
 - At level 0,785 m the width is 0.8m, and at level 3.485m the width is 1.8 m,
 - Plumes width above 0.785m and below 3.485m is constant. (see figure in appendix B2)
- Zero heat transfer from the outer surface
- Stress free temperature = 267°C
- Residual stresses in weld = 0
- Calculated position – weld 5/6
- Postulated defect – surface through clad breaking semi-elliptical crack
 - a = cladding + 10 mm = 19 mm, a/c = 1/3
 - axial orientation in weld metal
 - pressure load on crack surface
- Design fracture toughness curve
 - $[K_{IC}]^3 = 26 + 36 \cdot \exp [0,02 (T-T_k)]$, $[K_{IC}]^3 \max = 200 \text{ MPa.m}^{0.5}$
- Tangent approach
- No safety margins (coefficients)
- No fluence attenuation

Necessary data for calculations are given in Appendix B2

1.1.2. PWR- 3 LOOPS

- Linear- elastic calculations
- Cylindrical part of RPV (with correction to the bottom)
- ASME material properties – ASTM A 508 CL. 3
- RPV geometry – PROSIR
 - (rin=1,994 mm, cladding = 7,5 mm, RPV base metal thickness = 200 mm)
- PTS regime – TR 3 from PROSIR
- Thermal hydraulic file is included
- No cold plumes
- Zero heat transfer from the outer surface
- Stress free temperature = 300°C
- Residual stresses in weld = 0
- Calculated position – weld
- Postulated defect – surface through clad breaking semi-elliptical crack
 - a = cladding + 12 mm = 19,5 mm, a/c = 1/3
 - axial orientation in weld metal
 - pressure load on crack face
- design fracture toughness curve
 - ASME K_{IC} curve:
 - $K_{IC} = 36,5 + 3,1 \cdot \exp [0,036 (T-RT_{NDT}+55.5)]$, $K_{IC} \max = 220 \text{ MPa.m}^{0.5}$
- Tangent approach
- No safety margins (coefficients)
- No fluence attenuation

Necessary data for calculations are given in Appendix B3

APPENDIX B2. CRP-9 WWER BENCHMARK DATA

Material properties to be used for temperature and stress fields calculations within the assessment of reactor pressure vessel resistance against fast fracture.

1. List of symbols

T_{sf}	[°C]	stress-free temperature
T_{ref}	[°C]	reference temperature used for thermal expansion coefficient measurement
T	[°C]	temperature
E	[MPa]	Young modulus
ν	[1]	Poisson ratio
α_{ref}	[K ⁻¹]	thermal expansion coefficient established for T_{ref}
α_0	[K ⁻¹]	thermal expansion coefficient corrected to T_{sf}
λ	[Wm ⁻¹ K ⁻¹]	thermal conductivity
c_p	[Jkg ⁻¹ K ⁻¹]	specific heat
ρ	[kgm ⁻³]	density

2. Formula for thermal expansion coefficient correction:

The following formula for thermal expansion coefficient correction should be used in the case where the FEM code used for elastic-plastic calculations does not correct it automatically to stress-free-temperature T_{sf} (this is different from reference temperature T_{ref} used for thermal expansion coefficient measurement):

$$\alpha_0(T) = \frac{\alpha_{ref}(T) \cdot (T - T_{ref}) - \alpha_{ref}(T_{sf}) \cdot (T_{sf} - T_{ref})}{(T - T_{sf}) \cdot [1 + \alpha_{ref}(T_{sf}) \cdot (T_{sf} - T_{ref})]} \quad (B2.1)$$

3. Material properties for WWER 440 reactor pressure vessel

Base material: 15Kh2MFA (15Kh2MFAA in core region)

Weld metal: Sv-10KhMFT

Cladding 1st layer: Sv-07Kh25N13

Cladding 2nd layer (surface): Sv-08Kh19N10G2B

Stress-free temperature $T_{sf}=267$ °C.

$$T_{ref} = 20 \text{ °C}$$

Table B2.1 – Thermal-physical properties

Material	T	E	α_{ref}	α_0	ν	λ	c_p	ρ
	[°C]	[10 ³ MPa]	[10 ⁻⁶ K ⁻¹]	[10 ⁻⁶ K ⁻¹]	[1]	[Wm ⁻¹ K ⁻¹]	[Jkg ⁻¹ K ⁻¹]	[kgm ⁻³]
	20	210	-	12.9	0.3	35.9	445	7821
Base mat. or weld	100	205	11.9	13.3	0.3	37.3	477	7799
	200	200	12.5	13.9	0.3	38.1	520	7771
	300	195	13.1	14.5	0.3	37.3	562	7740
	20	165	-	15.9	0.3	15.1	461	7900
Cladding	100	160	14.6	16.5	0.3	16.3	494	7868
	200	153	15.7	16.5	0.3	17.6	515	7830
	300	146	16.0	16.8	0.3	18.8	536	7790

Material properties for part 1.2 – national codes

WWER-440:

Table B2.2 – Material properties of irradiated base and weld metal

<i>Property/Temperature</i>	<i>20°C</i>	<i>300°C</i>
Yield strength $R_{p0.2}$ (MPa)	625	555
Tangent modulus E_T (MPa)	8700	8700

Table B2.3 – Material properties of irradiated cladding

<i>Property/Temperature</i>	<i>20°C</i>	<i>300°C</i>
Yield strength $R_{p0.2}$ (MPa)	426	326
Tangent modulus E_T (MPa)	876	676

APPENDIX B3. CRP-9 PWR BENCHMARK DATA

Phases:

- Phase 1 : elastic basic case
- Phase 2 : national procedures
- Phase 3 : sensitivity studies

Basic data set

The next table B3.1 precise the major common data for the different cases.

Table B3.1a – General common data

RPV geometry	PWR 3-loop type	<ul style="list-style-type: none"> • inner surface radius: 1994mm • cladding thickness: 7.5mm • base metal thickness: 200mm • outer surface radius :2201.5mm
Properties of base metal, weld and cladding	Thermal - Mechanical	See Table B3.2 and B3.3
	Tensile- Stress-strain curves	See Table B3.4
	Toughness : <ul style="list-style-type: none"> • K_{IC} versus temperature • K_{Ia} versus temperature 	See Table B3.5
Transient load	<ul style="list-style-type: none"> • Tr3: PTS • (with repressurization) 	<ul style="list-style-type: none"> • pressure, temperature and heat exchange coefficient versus time • see Table B3.6

Table B3.1b – Specific data for phase 1 and 2

		Basic case: phase 1	National approaches: phase 2
Defect	Orientation: circumferential versus axial	Axial	Both directions
	Location: surface	<ul style="list-style-type: none"> • through cladding surface crack • see table 7 	<ul style="list-style-type: none"> • underclad cracks
	Size: depth and length Shape	<ul style="list-style-type: none"> • 19.5mm depth • a/c = 1/3 • semi-elliptical through clad crack (model 2) • see table 7 	<ul style="list-style-type: none"> • 15 mm maximum • a/c = 1/3 • semi-elliptical under clad crack (model 1) • see table 7
Other loads	<ul style="list-style-type: none"> • residual stresses 	<ul style="list-style-type: none"> • not considered in the weld • nevertheless, the free stress temperature of the vessel is: 300°C • no consideration of hydrotest • + pressure on the crack surface 	<ul style="list-style-type: none"> • can be considered in the weld • nevertheless, the free stress temperature of the vessel is: 300°C • no consideration of hydrotest
Fracture mechanic model	elastic K evaluation compare to K_{IC} (function of T); tangent criteria	<ul style="list-style-type: none"> • without plasticity correction 	<ul style="list-style-type: none"> • with plasticity correction
Safety factors		<ul style="list-style-type: none"> • all to 1 	<ul style="list-style-type: none"> • both results : • with safety factors of 1 and safety factors of the national code

Table B3.2 – Material thermal properties

	Temperature °C	Base metal and welds	Cladding
Thermal expansion in $10^{-6} \cdot ^\circ\text{C}^{-1}$ (mean value between 20°C and temperature)	20	10.9	16.4
	300	12.9	17.7
Conductivity λ in $\text{W}\cdot\text{m}^{-1}\cdot^\circ\text{C}^{-1}$	20	54.6	14.7
	300	45.8	18.6
Diffusivity $\mu=\lambda/\rho C$ in $10^{-6}\cdot\text{m}^2\cdot\text{s}^{-1}$	20	14.7	4.1
	300	10.6	4.3
Density ρ	20-300	7.6	7.6

Table B3.3 – Mechanical material properties (unirradiated state)

Unit : MPa	Temperature °C	Base metal	Welds	Cladding
Yield strength: $S_y (R_{p0.2})$	20	588	646	380
	300	517	563	270
Young modulus: E	20	204000	204000	197000
	300	185000	185000	176500
ν	20 - 300	0.3	0.3	0.3

Table B3.4 – Stress-strain curves (unirradiated state)

Total strain ϵ		0.01	0.02	0.03	0.04	0.05	0.06	0.07	0.08	0.09	0.10
σ/S_y for base met.	20°C	1.02	1.11	1.19	1.25	1.29	1.33	1.36	1.38	1.40	1.42
	300°C	1.11	1.21	1.28	1.33	1.37	1.41	1.43	1.45	1.47	
σ/S_y for weld	20°C	1.00	1.05	1.10	1.15	1.19	1.22	1.24	1.26	1.28	1.29
	300°C	1.07	1.15	1.21	1.26	1.30	1.34	1.36	1.39	1.41	1.43
σ/S_y for cladding	20°C	1.06	1.10	1.13	1.16	1.19	1.22	1.25	1.27	1.30	1.32
	300°C	1.07	1.11	1.14	1.17	1.20	1.23	1.26	1.29	1.31	1.34

Table B3.5 – Toughness curve for base metal

toughness : ASME-RCCM curve	Crack initiation	$K_{IC} = 36.5 + 3.1 \exp[0,036 (T-RT_{NDT} + 55.5)]$ $K_{IC \max} = 220 \text{ MPa}\cdot\text{m}^{0.5}$
	Crack arrest	$K_{Ia} = 29.4 + 1.4 \exp[0,026 (T-RT_{NDT} + 88.9)]$ $K_{Ia \max} = 220 \text{ MPa}\cdot\text{m}^{0.5}$

Table B3.6 – Tr3 transient description (typical PTS with repressurization)

Time in second	Pressure in MPa	Fluid temperature	Heat Exchange coefficient in $W/m^2 \cdot ^\circ C$
0	15,3	295	24125
45	7,8	287	24696
165	7,0	276	3453
255	7,3	279	1054
300	5,7	268	6232
375	5,5	261	1757
615	5,1	251	4834
1515	4,0	206	1581
2865	2,9	152	1838
4695	2,0	59	1147
6015	1,5	37	992
7125	2,5	48	877
7185	16,8	49	790
8970	17,1	69	602
13290	17,0	96	710
14025	17,1	106	1229
14985	17,1	115	1057

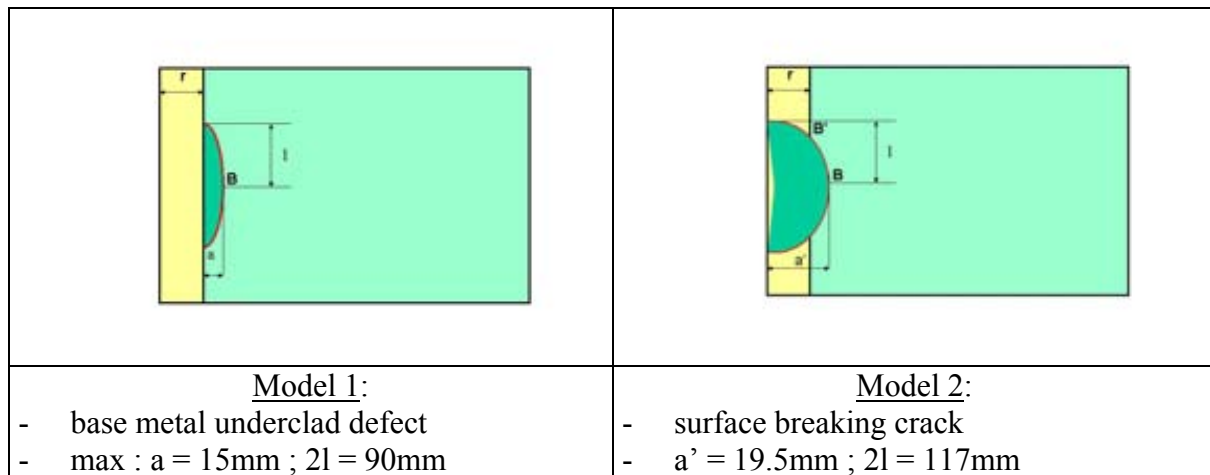


FIG. B3.1 – Locations and shapes of defects.

Sensitivity studies on underclad crack: Phase 3

The reference case for this sensitivity studies are the phase 2 limited case (to be confirmed before starting the sensitivity studies).

- S1 : effect of heat exchange coefficient on limited case of phase 2 : TR3 x 2
- S2 : plume or no plume on WWER hypotheses, using symmetric load at the top of the plume
- S3 : compare linear elastic and elasto-plastic on the limited case of phase 2
- S4 : with and without residual stress in the weld (0, cosin, constant, measured)
- S5 : effect of hydrotest (1.25 design pressure)
- S6 : effect of aspect ratio 1/3 to 1
- S7 : elliptical versus semi-elliptical crack shape
- S8 : Master curve 1% to 5% and ASME curve
- S9 : margins in crack depth, in toughness or in transition temperature

APPENDIX B4. SENSITIVITY STUDY DEFINITION

The following cases were agreed by the participants:

	Organization	Comment
1. THERMAL HYDRAULIC INPUTS		
heat transfer coefficients in symmetrical case (by factor 2)	AREVA	Semi-analytical
plumes		
• Cold plumes vs. symmetrical case	KFKI	
• Number of plumes (3 or 2 vs. 1)	NRI	
• Width and shape of the plumes	NRI	Old results, ICAS
• OKB GP mix	OKB GP	
2. PHYSICAL PROPERTIES		
• Thermal conductivity coefficient	(NRI) EdF	
• Thermal expansion coefficient	EdF	Old results, ICAS
• Young modulus of cladding	Fortum EdF	
3. STRESS FIELD		
• Linear elastic vs. elastic-plastic	VUJE	Comparison of basic and national
• Surface crack	SNERDI	
• Underclad crack	EdF	
▪ Initial vs. irradiated stress strain curves		
4. RESIDUAL STRESSES IN WELDS		
• YES vs. NO		Old results, ICAS
• cos shape vs. constant	Fortum	
5. RESIDUAL STRESSES IN CLADDING		
• Stress free temperature	EdF	Old results, ICAS
• Special shape (experimental)	AREVA(?)	
• After hydrotest – OKB GP	OKB GP	
6. POSTULATED DEFECT		
• Underclad vs. surface		Comparison of basic and national
• Effect of defect depth	KINS EdF	
• Effect of defect shape – aspect ratio	KINS EdF	
• Elliptical vs. semi-elliptical underclad crack	KINS EdF	NRI (old results)
• Surface semi-elliptical crack – two shapes	KINS SNERDI EdF	
7. FRACTURE MECHANICS		
• Comparison of formulae with 3D modelling	SNERDI	ASME
• Different ways for j/k calculations	NRI	Different parameters
• Effect of mesh density	KFKI	
• Interface problem including cladding toughness criteria	OKB GP	Semi-elliptical
• Effect of cladding thickness	KFKI EdF	Old results, ICAS

8. INTEGRITY ASSESSMENT		
• Design fracture toughness curves	NRI OKB GP EdF	
• Master Curve – 1%, 5%	NRI KFKI	
• Integral (IAEA/VERLIFE – Russian) vs. point by point	Fortum NRI OKB GP	
• Base Curve	OKB GP	
• Arrest vs. initiation		TBD on next meeting
• WPS (first part of PTS before reclosure vs. Russian approach)	NRI KFKI OKB GP	
• Constrain effect	OKB GP	
9. NOZZLE PROBLEMS	SNERDI OKB GP	AREVA – information on next meeting

Reported data:

- Similar to the basic case:
 - Variation of axial and hoop stresses through the RPV wall thickness in crack free region
- Variation of stress intensity values K_I as a function of temperature for:
 - WWER : deepest point and at point 2 mm below the interface
 - PWR : deepest point and at point 2 mm below the interface
- Maximum allowable transition temperature for:
 - Initiation
 - Arrest (if required)
- Description of the methodology used
- Description of the input data used

All results shall be supplied in Excel format

APPENDIX C

THERMOHYDRAULIC ANALYSIS OF PLUME EFFECTS

1. Introduction

If flow stagnation occurs in the primary system, the cooling process has to be investigated in a significantly smaller volume. In such cases it has to be taken into account that below the cold legs with cold water injection plumes will exist causing the temperature and heat transfer coefficient distribution to be non-uniform.

In case of flow stagnation, thermal mixing and plume cooling of the RPV wall occurs when the downcomer and the cold legs are totally filled with water. A cold stream, caused either by ECC water injection or by an increased heat removal from the primary to the secondary side in affected loops, flows in the cold loop towards the RPV inlet and falls into the downcomer forming a quasi-planar buoyant plume. In case of direct ECC water injection into the downcomer, as applied in WWER., the plume origin is at the lower edge of the injection nozzle.

Condensation and stripe cooling of the RPV wall takes place when the cold legs are partially filled with steam and the collapsed water level in downcomer is below lower edge of cold leg. A cold stream caused by ECC water injection flows at the bottom of the cold leg towards the RPV inlet and falls into the downcomer forming a stripe directly in contact with the RPV wall. The stripe detaches from the RPV wall when higher cold leg ECC injection rates are applied. In case of direct ECC water injection into the downcomer, the ECC water impinges on the core barrel forming a water film which flows along the core barrel. To account for these effects, sophisticated 3D computer codes or engineering calculation methods verified on experimental data are needed to account for the associated condensation processes.

Figure C1 shows schematics of simplified strip and plume cooling scenarios used for modelling purposes. It should however be remembered that these are intrinsically dynamic, time-dependent phenomena.

The analysis of non-uniform mixing conditions is a highly complex task requiring specialized knowledge of the phenomena based on experimental evidence, of thermal hydraulics and of the modelling tools. Several organizations have developed codes based on a combination of analytical models and empirical data. The following sections provide brief details of approaches developed in Germany and Russia.

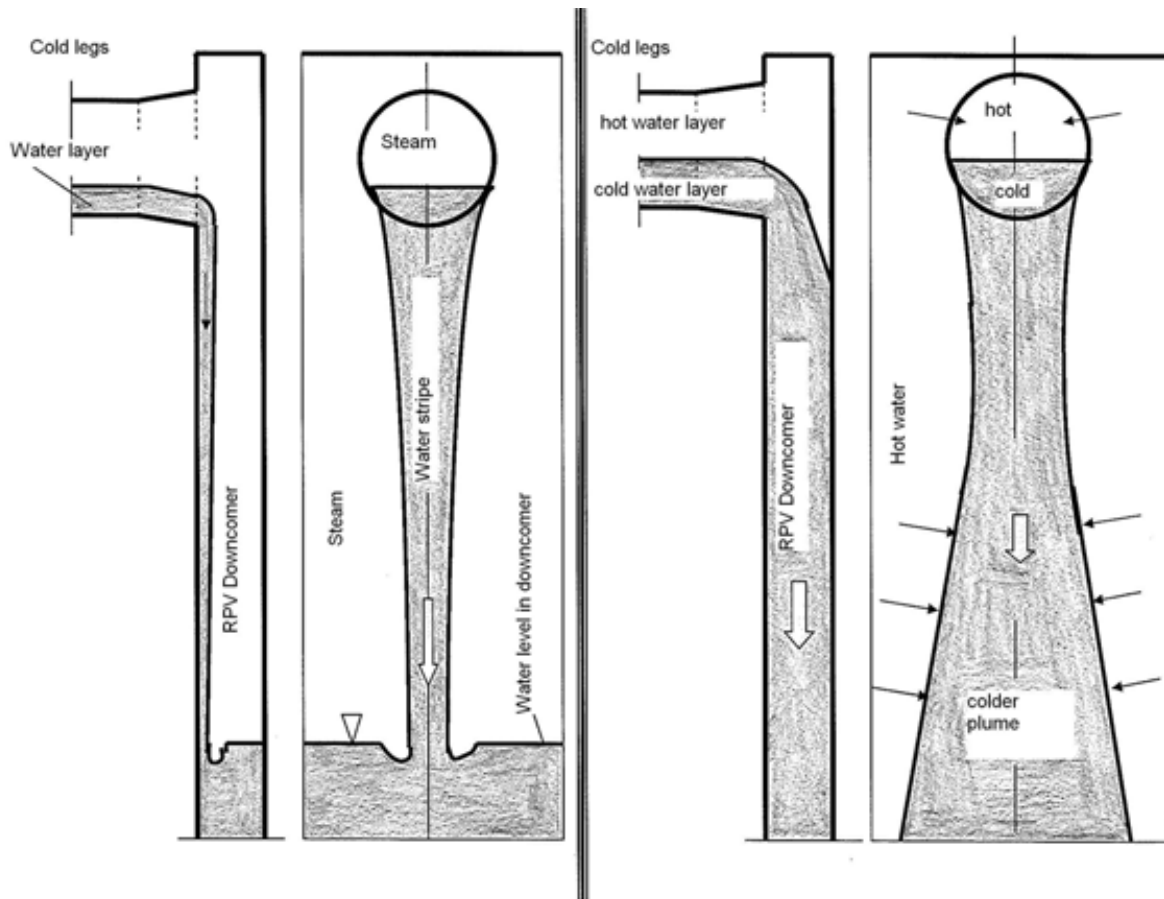


FIG. C1 – Stripe cooling (left part) and plume cooling (right part) of the RPV inside wall.

2. Number of plumes

The number of plumes depends on the break location and the configuration of the injection system. In case of a hot side break one plume establishes in downcomer below every cold leg with cold water injection. That is, four plumes exist in downcomer when best estimate ECC-injection is applied in a four loop plant. Two plumes exist in the downcomer if the number of cold side injections is reduced to two because of single failure and repair. To maximize the RPV load it is assumed that in a four loop plant the two plumes are below two neighbored cold legs. According to tests performed in the 1:1-scaled Upper Plenum Test Facility (UPTF) plumes below neighbouring cold legs interact with one another. Due to this interaction the neighbored plumes approach each other (Figure C2) and build one plume in the lower half of downcomer.

In newer German PWRs a single plume can establish in downcomer in case the hot side high pressure injection into the defect loop is switched from hot side to cold side injection.

The most asymmetric situation of only one plume around the RPV may be of importance for numerical fracture mechanic simulations.

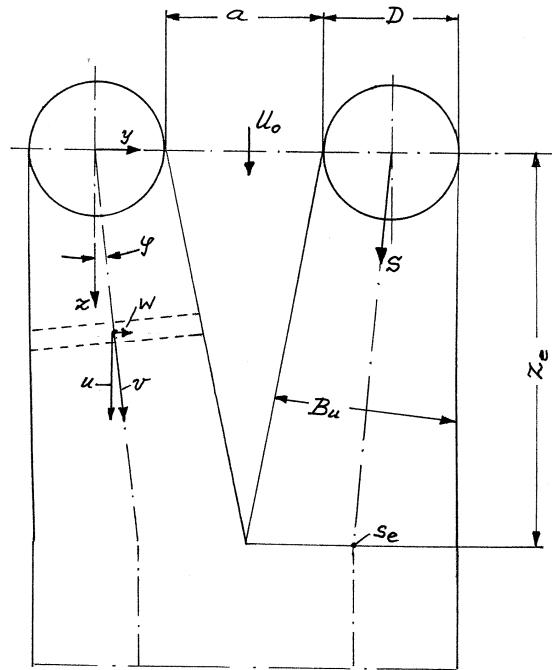


FIG.C2 – Plume interaction.

3. Width and shape of the plumes

Free planar plume data as well as downcomer plume data [1] indicate a Gaussian type azimuthal profile for the density difference between the plume density ρ and the ambient fluid density ρ_a or the corresponding fluid temperature difference $(T_a - T)$. The half plume width $H = B/2$ (B = plume width) in the plume region can be defined by

$$(\rho - \rho_a) = (\rho_{CL} - \rho_a) \exp\left[-\left(\frac{y}{H}\right)^2\right] \quad (C1)$$

Coordinate y is perpendicular to the plume symmetry- (centre-) line.

The plume width B , the centre line density ρ_{CL} and the centre line velocity U_{CL} are functions of the distance from lower edge of cold leg. These functions are determined by means of the system of differential equations in the engineering model applied or these plume parameters are output of the applied three-dimensional general-purpose computational fluid dynamic (CFD) code

The width of the Gaussian type azimuthal velocity profile is about 10% smaller than the width B of the density difference profile. The velocity profile determines the profile of the forced convection part of the mixed convection RPV-wall to water heat transfer coefficient

4. Mixing models

All mixing models used, three-dimensional general-purpose computational fluid dynamic (CFD) codes or engineering models need verification against experimental data, if possible data from 1:1 scaled test facilities. An example for mixing and condensation engineering models verified against UPTF-data is given in KWU-MIX below [2]

4.1. Fluid-fluid-mixing in cold leg

When ECC water is injected into the cold leg during a period of loop flow stagnation, the cold ECC water mixes with the hotter ambient water in the cold leg. Hot water is flowing from the downcomer into the cold leg and along the upper part of the cold leg flow area to the mixing location whereas mixed colder water flows counter to the hot water along the lower part of cold leg flow area to RPV inlet.

There are two possible flow patterns near the ECC injection locations in the stagnating cold legs: Stratified flow and flow circulation. The flow pattern change occurs at a densitometric Injection-Froude-Number of about 4. The densitometric Injection-Froude-Number is defined by

$$Fr_{ECC} = \frac{V_{no}}{\sqrt{g d (\rho_{ECC} - \rho_h) / \rho_{ECC}}} \quad (C2)$$

Stratified flow demands for a densitometric Froude Number Fr_{ECC} of less than about 4. Unstable flow circulation near the injection location, caused by the momentum of the injected ECC water, occurs at densitometric Froude Numbers higher than about 4. Unstable flow circulation falls back into stable stratified flow in a distance of about two times the inner cold leg diameter from the injection location. In stratified flow mixing takes place on the ECC water jet, while in case of circulating flow the mixing occurs at the location of flow pattern change from circulation to stratified flow between injection nozzle and RPV inlet.

In the cold leg significant thermal mixing is restricted to the injection location or to the location of flow pattern change. Mixing between the hot and cold water layer between injection location respectively location of flow pattern change and RPV inlet is relatively small, but taken into account in the correlation by using the cold layer fluid temperatures measured near RPV inlet.

Superposed loop flow always increases the degree of mixing as compared to loop stagnation. That is why in PTS-analyses often loop stagnation is assumed for conservative reasons. If the superposed loop flow is considered the criterion of Nourbakhsh [3] can be used to separate conditions which lead to complete mixing of ECC water with the loop water within the cold leg. In case the mixing is not complete the models for loop stagnation can be applied.

In the following chapters only the models assuming loop stagnation are outlined.

4.2. Mixing model for stratified flow near injection nozzles ($Fr_{ECC} < 4$)

The entrainment coefficient ε is defined by :

$$\varepsilon = \frac{m_e}{m_{ECC}} \approx \frac{T_{mix} - T_{ECC}}{T_h - T_{mix}} \quad (C3)$$

The entrainment coefficient ε decreases monotonously with increasing ECC water injection rate.

Different mixing correlations are known for side and top injection. For top injection the well known correlation of Sun and Oh [4], Häfner [5] derived from the CREARE test results can be applied.

The HDR- and UPTF-TRAM cold leg mixing results for side injection and stratified flow in cold leg are well represented by a correlation developed by Häfner [12]. This correlation for *sideways injection* (injection nozzle centre line in horizontal plane) reads

$$\varepsilon = 3.99 \eta - 1.17$$

$$\eta = \frac{\frac{L}{d} h_c}{Fr_{ECC}^{0.575}}$$

$$L = 0.5 D \left[1 + \frac{1 - \sin \Theta}{\sin \Theta} \left(1 - \exp \left(\frac{-Fr_{ECC}^2}{15} \right) \right) \right] \quad (C4)$$

The (critical) water depth h_c in a circular pipe is defined by the following two equations:

$$h_c = D \sin^2 \left(\frac{\Phi}{4} \right) \quad (C5)$$

$$\frac{(\Phi - \sin \Phi)^3}{\sin \left(\frac{\Phi}{2} \right)} = \frac{512 Q^2 \rho_c}{g D^5 (\rho_c - \rho_h)} \quad (C6)$$

In case of a decreased cold leg water level this mixing model is applied as long as the centre of the injection nozzle exit is below the cold leg water surface.

4.3. *Mixing model for circulating flow near injection nozzles ($Fr_{ECC} > 4$)*

Flow circulation near the injection nozzle leads to a uniform fluid temperature (close to the ECC injection temperature) in the vertical cold leg cross sections nearby the injection nozzle and, in UPTF with pump simulators closed, between injection nozzle and main coolant pump.

As the ECC water jet penetrates into a cold water volume of almost the same temperature, jet entrainment and jet orientation are of minor importance in this case. The mixing, which takes place at the locus of flow pattern transition from circulation to stratification, is forced by the pressure difference

$$\Delta p = g (\rho_{ECC} - \rho_h)(D - h_c) \quad (C7)$$

Both, the pressure losses mainly in the hot water flow path and the counter current flow limitation, act against the forcing pressure difference Δp and limit the mixing. Pressure losses and counter current flow limitation are the so called limitations by the far field, because they reflect flow characteristics outside the mixing region [6].

The pressure loss in the hot water flow path includes the losses due to flow from the downcomer into the cold leg, wall friction and hot/cold water layer interfacial friction on the way from RPV inlet to the mixing location. h_c is the critical water depth defined above.

According to the general equations describing stable stratified flow in horizontal circular tubes [7], the change of the cold water layer depths H_c can be expressed by

$$\frac{dH_c}{dx} = \frac{R}{\Delta \rho g (1 - Fr_h^2 - Fr_c^2)} \quad (C8)$$

Starting with $x = 0$ at the RPV inlet, H_c has to be smaller than the cold leg inner diameter D along the cold leg in the stratified region. $H_c = D$ indicates the locus of counter current flow limitation. That is the maximum hot water inflow from the downcomer is reached.

The Froude-Numbers Fr_i ($i = h, c$) are defined as follows:

$$Fr_i = \frac{\rho_i Q_i^2 W}{g \Delta \rho A_i^3} \quad (C9)$$

The term $R \cdot dx$ represents the pressure loss along dx . In the limiting case $H_c(x) = D$ the following equation holds:

$$g (D - H_c) \Delta \rho = \frac{\Delta p_{losses}}{(1 - Fr_h^2 - Fr_c^2)} \quad (C10)$$

The pressure losses are correlated using the volumetric flow rate of the hot stream.

$$\Delta p_{losses} = C_0 \frac{\zeta}{A_h^2} Q_h^2 \frac{\rho_h}{2} \quad (C11)$$

ζ pressure loss coefficient for hot water intake from the downcomer into the cold leg, assuming the cold leg is completely filled with hot water only

The constant correction factor C_0 is added to account for wall and interfacial friction and for the increase in hot water entrance pressure loss due to the cold water layer height. The correction factor C_0 is determined by comparing the model with the data.

The hot water volumetric flow rate Q_h is determined by iteratively solving the equations C9 to C11 for a given ECC water injection rate and given temperatures of ECC water and hot water. The cold water layer height H_c is calculated by means of equations C5 and C6.

The result of the iteration is the entrainment ratio $\epsilon_{circ} = Q_h \rho_h / m_{ECC}$ for flow circulation near the injection nozzle

In case of a *decreased cold leg water level* the inner cold leg diameter D is replaced by the cold leg water height in the formula. The pressure loss coefficient ζ for hot water intake is a function of the downcomer gap width and of the hydraulic diameter of the hot water flow path in the cold leg.

When the cold leg water surface is below injection nozzle exit elevation, steam condensation on the ECC water jet and on the water surface near injection location is quantified first. In the second step the cold leg water layer height is compared to the critical cold leg water height necessary for ECC water plus condensate flow into the downcomer according to equation C5. No fluid-fluid mixing is assumed in the cold leg in case the cold leg water height is lower than the critical water height.

Table C1 – UPTF-TRAM C1: Mixing in water-filled cold leg

UPTF C1 RUN No.	Time	ECC-Rate	T _{ECC}	T _{hot}	T _{cold}	Entrainment coefficient	
	[min]	[kg/s/leg]	[°C]	[°C]	[°C]	Experiment	Calculation
1a01	33.3	7.32	32.84	189.2	126.4	1.444	1.281
1a01	116.7	7.2	30.31	178.6	109.77	1.125	1.233
1a01	150.	11.38	30.04	171.2	95.42	0.845	0.902
1a01	216.7	11.59	29.88	152.4	83.34	0.763	0.833
2a1	33.33	19.62	31.21	188.1	96.31	0.691	0.68
2a1	100.	41.5	30.99	147.1	68.54	0.472	0.59
3b1	20.	66.06	31.96	180.3	74.39	0.392	0.457
4a1	13.33	157.82	32.27	176.2	46.24	0.106	0.094
5a1	13.33	39.3	30.11	183.7	92.07	0.66	0.534
5a1	30.	40.79	31.61	144.1	68.04	0.474	0.596

Table C1 compares the cold leg entrainment coefficients drawn from the measured temperatures and calculated with the models described. The inner diameter of UPTF cold leg was 0.75m, the inner diameter of the UPTF injection nozzle was 0.222 m. The angle between cold leg and ECC nozzle centre line was 60°, the ECC injection nozzle centre line was in the horizontal plane. No loop flow, pressure > 16.4 bar.

The table includes the Run number., the time after start of ECC injection, the ECC injection rate and temperature (T_{ECC}), the hot water temperature T_{hot} in the upper part of cold leg cross section outside the mixing region and the temperature T_{cold} of mixed water in lower part of cold leg cross section outside the mixing region.

4.4. Fluid-fluid mixing in downcomer

The water layer exiting the cold leg with mean temperature

$$T_{mix} = \frac{\varepsilon T_h + T_{ECC}}{1 + \varepsilon} \quad (C12)$$

is falling into the downcomer forming a quasi planar plume. To determine the distributions of the fluid temperature and the wall-to-fluid heat transfer coefficient on the inner RPV surface, the temperature or density and the velocity along the plume centre line are needed together with the widths of the density and velocity profiles perpendicular to the plume flow direction. Typical plume centre line velocities are of the order of 1 m/s. For that reason the mixed convection wall-to-water heat transfer coefficient inside plume is mainly forced convection and thus depending on the plume velocity.

Also the wall-to-fluid heat transfer coefficient outside plume is an important thermal hydraulic boundary condition for the fracture mechanic analysis. The forced convection part of this mixed convection heat transfer coefficient is caused by the up flow velocity between the plumes. This up flow replaces the water entrained by the ECC water in the cold legs and entrained by the cold water plumes in the downcomer. The quantification of plume entrainment is therefore necessary for the determination of the heat transfer distribution on the inner RPV wall surface.

According to Fox [8] the system of non-linear ordinary differential-equations describing a free planar plume with Gaussian type distributions of density and velocity perpendicular to the plume centre line reads (after integration along the coordinate y perpendicular to the plume centre line coordinate x) :

$$\frac{d(UB)}{dx} = \frac{2V_e}{I_1} \quad (C13)$$

$$\frac{d(U^2B)}{dx} = \frac{g I_3 P B}{\rho_{a0} I_2} \quad (C14)$$

$$\frac{d(UBP)}{dx} = \frac{I_1 U B}{I_4} \left(\frac{d\rho_a}{dx} \right) \quad (C15)$$

$$\frac{d(U^3B)}{dx} = \frac{2 g I_4 P U B}{\rho_{a0} I_5} + \frac{2 / I_6 / U^3}{I_5} \quad (C16)$$

U,B,P and ρ_a are functions of x.

$$P(x) = \rho(x, y=0) - \rho_a(x) \quad (C17)$$

The velocity u(x,y) inside the plume is expressed by:

$$u(x, y) = U(x) \exp(-\eta^2) \quad \text{with} \quad \eta = \frac{y}{B(x)} \quad (C18)$$

The fluid density $\rho(x,y)$ inside plume reads:

$$\rho(x, y) = \rho_a(x) + P(x) \exp\left(-\frac{\eta^2}{\lambda^2}\right) \quad (C19)$$

with $\lambda = \frac{\text{width of density profile}}{\text{width of velocity profile}}$

The values of the constants are:

$$I_1 = \int_{-\infty}^{+\infty} \exp(-\eta^2) d\eta = \sqrt{\pi}$$

$$I_2 = \int_{-\infty}^{+\infty} \exp(-2\eta^2) d\eta = \sqrt{\frac{\pi}{2}}$$

$$I_3 = \int_{-\infty}^{+\infty} \exp\left(-\frac{\eta^2}{\lambda^2}\right) d\eta = \lambda \sqrt{\pi}$$

$$I_4 = \int_{-\infty}^{+\infty} \exp\left[-\left(1 + \frac{1}{\lambda^2}\right) \eta^2\right] d\eta = \frac{\lambda \sqrt{\pi}}{\sqrt{1 + \lambda^2}}$$

$$I_5 = \int_{-\infty}^{+\infty} \exp(-3\eta^2) d\eta = \sqrt{\frac{\pi}{3}}$$

I_6 and λ are parameters which have to be fixed by comparing the model with experimental data.

The measured Gaussian type velocity and density (temperature) profile data [9] indicate

$$\lambda = (50/41)^{1/2} = 1.1045.$$

A comparison of the model to the UPTF TRAM C1 fluid-fluid mixing data reveals $/ I_6 / = 0.005$.

It is interesting to note that the turbulent shear stress $/I_6/$ is the only free parameter in the model to be adjusted by means of the UPTF Data.

Combination of equation C14 and equation C16 leads to

$$\frac{d(U B)}{dx} = \frac{2 g}{\rho_{a0}} \left(\frac{I_3}{I_2} - \frac{I_4}{I_5} \right) \frac{P B}{U} + \frac{2 / I_6 / U}{I_5} \quad (C20)$$

Comparing equation C20 with equation C13 results in an expression for the entrainment velocity V_e :

$$V_e = \frac{g I_1}{\rho_{a0}} \left(\frac{I_3}{I_2} - \frac{I_4}{I_5} \right) \frac{P B}{U} + \frac{I_1 / I_6 / U}{I_5} \quad (C21)$$

I_6 is negative, the minus sign of $-I_6/$ is considered in the equation for V_e .

To take wall friction into account, the momentum balance equation (Equation C14) has to be extended.

The friction force reads (factor 2 because the plume touches both downcomer walls):

$$\frac{dF_{fric}}{dx} = 2 \int_{-\infty}^{+\infty} \tau_w(x, y) dy = \int_{-\infty}^{+\infty} C_f \rho(x, y) u(x, y)^2 dy \approx C_f(\text{Re}(U)) \int_{-\infty}^{+\infty} \rho(x, y) u(x, y)^2 dy$$

$$\frac{dF_{fric}}{dx} \approx C_f(\text{Re}(U(x))) B(x) U^2(x) \left[\rho_a(x) \int_{-\infty}^{+\infty} \exp(-2\eta^2) d\eta + P(x) \int_{-\infty}^{+\infty} \exp\left(-\eta^2 \left\{ \frac{1+2\lambda^2}{\lambda^2} \right\}\right) d\eta \right]$$

$$\frac{dF_{fric}}{dx} \approx C_f(\text{Re}) B(x) U^2(x) \left[I_2 \rho_a(x) + I_7 P(x) \right] ; \quad I_7 = \frac{\lambda \sqrt{\pi}}{\sqrt{1+2\lambda^2}} \quad (C22)$$

The dependence of C_f on Reynolds Number Re is expressed by the following well known correlation :

$$\begin{aligned} \text{Re} < 2320. & \quad C_f = \frac{16}{\text{Re}} \\ 2320. \leq \text{Re} \leq 10^5 & \quad C_f = 0.079 \text{Re}^{-0.25} \\ \text{Re} \geq 10^5 & \quad C_f = 0.0008 + 0.05525 \text{Re}^{-0.237} \end{aligned} \quad (C23)$$

The force balance on plume mass element $\rho B S dx$ (S = downcomer gap width) reads:

$$\begin{aligned} \text{momentum change} & = \text{buoyancy force} - \text{friction force} \\ d(\rho_{a0} I_2 S B(x) U^2(x)) & = g I_3 S P(x) B(x) dx - C_f B(x) U^2(x) [I_2 \rho_a(x) + I_7 P(x)] dx \end{aligned} \quad (C24)$$

Finally we get the new momentum equation :

$$\frac{d(U^2(x) B(x))}{dx} = \frac{g I_3 P(x) B(x)}{\rho_{a0} I_2} - \frac{C_f(\text{Re}) B(x) U^2(x) [I_2 \rho_a(x) + I_7 P(x)]}{S I_2 \rho_{a0}} \quad (C25)$$

The change of the momentum equation causes a modified expression for the entrainment velocity V_e :

Combination of the equality

$$\frac{d(U B)}{dx} = \frac{2}{U} \frac{d(U^2 B)}{dx} - \frac{1}{U^2} \frac{d(U^3 B)}{dx} \quad (C26)$$

with equations C13, C16 and C25 leads to:

$$V_e = \frac{g I_1 P B}{\rho_{a0} U} \left(\frac{I_3}{I_2} - \frac{I_4}{I_5} \right) - \frac{I_1 C_f B U (I_2 \rho_a + I_7 P)}{\rho_{a0} S I_2} + \frac{I_1 / I_6 / U}{I_5} \quad (C27)$$

The system of non-linear equations C13, C15, C16 and C25 can be transferred into the following system of linear differential equations:

$$\frac{dP}{dx} = \frac{I_1}{I_4} \left(\frac{d\rho_a}{dx} \right) - \frac{2 V_e P}{I_1 U B} \quad (C28)$$

$$\frac{dU}{dx} = \frac{g I_3 P}{\rho_{a0} I_2 U} - \frac{C_f U (I_2 \rho_a + I_7 P)}{S I_2 \rho_{a0}} - \frac{2 V_e}{I_1 B} \quad (C29)$$

$$\frac{dB}{dx} = \frac{4 V_e}{I_1 U} - \frac{g I_3 B P}{\rho_{a0} I_2 U^2} + \frac{C_f B (I_2 \rho_a + I_7 P)}{S I_2 \rho_{a0}} \quad (C30)$$

Equations C27–C30 are used to determine U, P, B and thus the fluid density (temperature) along plume centre line.

There is no possibility to quantify the three-dimensional mixing close to the cold leg by means of a planar plume model. Therefore the following correction is applied to the calculated temperature T_{calc} in the region close to the cold leg to get agreement with the data :

$$T_{cor} = T_{calc} - f_{cor} (T_a - T_{ECC}) \quad (C31)$$

Table C2 – Parameter f_{cor} as a function of the ECC water rate per cold leg

ECC injection rate per cold leg (kg/s)	7.	11.	20.	40.	> 70.
f_{cor}	0.22	0.165	0.14	0.07	0

5. Stripe cooling

Stripe cooling of the RPV wall can occur when the downcomer water level is decreased and ECC water is injected into the cold legs. The ECC water is heated up by steam condensation before it reaches the downcomer water level. Depending on the ECC injection rate per cold leg the water stripe can flow down the core barrel (higher injection rates) or the RPV wall (lower injection rates).

UPTF test results revealed the following threshold ECC injection rates per cold leg (independent of nitrogen effects) :

Table C3 – UPTF-TRAM C2 data (D = inner diameter, L = length of diffusor, TV = test vessel)

UPTF-TRAM C2	Cold Leg 2	Cold Leg 3
Radius at TV-inlet	66 mm	115 mm
Diffusor at TV inlet	D = 0.75m → 0.927m, L = 0.4105 m	None
Threshold ECC rate per CL	~ 20 kg/s	~ 50 kg/s

The UPTF-TRAM C2 data are the only 1:1 scaled stripe cooling data. These full scale data also indicate that sub-scale data and existing condensation models based on sub-scale data have to be used with care, when applying them to the reactor.

5.1. Direct contact steam condensation on ECC water inside the cold leg

A special test series was performed in the 1:1 scaled UPTF (Test Phase UPTF-TRAM C2) to quantify the steam condensation on the ECC water injected into the cold leg in case of a decreased downcomer water level. The steam condensation inside the cold leg and on the falling water stripe in the downcomer were quantified separately. The effect of nitrogen out of the accumulators on the steam condensation in cold leg and downcomer was investigated as well.

Steam condensation on the ECC water jet in the cold leg without nitrogen effect could be well represented by means of the model of Shklover and Rodivilin [10].

In this model the water temperature T_2 at the jet end, which is defined as the locus of jet impingement on the water level in the cold leg, is calculated according to :

$$T_2 = \frac{(2 - A) T_{no} + 2 A T_{sat}}{2 + A}$$

$$A = \frac{0.08 L^{0.25} V_{no}^{0.2} r^{0.1}}{d^{0.05} Pr^{0.57} c_w^{0.1} \nu^{0.2} (T_{sat} - T_{no})^{0.1}} \quad (C32)$$

The jet diameter d is equal to the ECC nozzle inner diameter as long as the ECC nozzle flow area is completely water-filled. In case of *sideways injection* the nozzle is water-filled as long as the water height H_c corresponding to exit Froude Number 1 (Equation C9) is greater or equal to d . When small ECC rates are applied, H_c can be smaller than d . If $H_c < d$ the nozzle inner diameter is replaced by

$$d_{eff} = \sqrt{\frac{4 A_c}{\pi}} \quad (C33)$$

with the flow area A_c in ECC nozzle outlet corresponding to water height H_c .

The steam condensation on the cold water layer in the cold leg near the ECC injection location is determined by means of the surface renewal theory. Following this theory the heat transfer coefficient responsible for the steam condensation on the free surface of the mixing volume takes the final form

$$\alpha = 2 \sqrt{\frac{\rho_w c_w \lambda_w V_e}{\pi}} \sqrt{\frac{Q}{2 Vol_{mix} \nu}} \quad (C34)$$

The corresponding fluid temperature difference is: saturation temperature minus T_2 .

The kinetic energy of the impinging ECC water jet is transferred into vortices inside the liquid mixing volume Vol_{mix} below the cold leg water surface adjacent to the ECC port and thus dissipated.

The ECC water jet impinges on the cold leg water surface with the velocity

$$V_e = \sqrt{V_0^2 + 2 g \Delta h} \quad (C35)$$

The UPTF data were correlated using a mixing volume Vol_{mix} defined as the actual liquid volume below the cold leg liquid surface adjacent to the ECC port with length equal to the inner diameter of cold leg. The width of the surface of the mixing volume corresponds to the actual liquid height in cold leg. The liquid height itself depends on the volumetric flow rate at cold leg outlet.

A comparison with the UPTF-TRAM-C2 data revealed the following fitting constants for nitrogen free condensation:

- the parameter A is multiplied by 0.6
- α is multiplied by 0.15

The 1:1 scaled UPTF tests showed that steam condensation on the cold leg liquid layer surface outside the injection region is surprisingly small. This is because there is no ECC water impingement in this region and the counter-current steam / liquid flow between end of injection region and RPV inlet leads to an isolating saturated liquid layer close to the liquid surface.

5.2. Direct contact steam condensation on the falling water stripe in downcomer

The UPTF water stripe temperatures measured adjacent to the test vessel wall were used to model the steam condensation on the falling water stripes in downcomer. The nitrogen-free condensation data were represented by a constant Stanton Number St :

$$St = \frac{\alpha(z)}{V(z) c_w(z) \rho(z)} = 0.018 \quad (C36)$$

To represent the data, the following stripe width B_0 in stripe origin “0” (cold leg brink) has to be used

$$B_0 = a W$$

$$W = 2 \sqrt{0,725 H_c (D - 0,725 H_c)} \quad (C37)$$

H_c water depth in cold leg corresponding to Froude Number 1
water depth at the cold leg outlet (at the brink) = $0.725 H_c$

Table C4 – Parameter a as a function of the ECC water rate per cold leg

ECC rate per cold leg	0 kg/s to 15 kg/s	15 kg/s to 30 kg/s	> 30 kg/s
Parameter a	0.75	0.75 to 0.85	0.85

The stripe thickness S_0 in the stripe origin is defined by :

$$S_0 = \frac{Q_0}{V_0 B_0} \quad (C38)$$

The stripe water velocity to be used in the correlation in elevation z relative to lower edge of cold leg is

$$V(z) = \sqrt{V_0^2 + 2 g z} \quad (C39)$$

$z > 0$ means elevations below lower edge of cold leg.

The local water volumetric flow rate $Q(z)$ is the flow rate in the stripe origin (cold leg outlet) plus the flow rate increase due to steam condensation between origin ($z = 0$) and locus z .

The local stripe width $B(z)$, defining the local steam/water contact area increment $B(z)*dz$, is approximated by

$$B(z) = \frac{Q(z)}{S(z) V(z)} = \frac{\sqrt{Q(z) B_0}}{\sqrt{S_0} \sqrt{V_0^2 + 2 g z}} \text{ using the assumption } \frac{S_0}{B_0} = \frac{S(z)}{B(z)} \quad (C40)$$

Steam condensation on the smaller side $S(z)$ of the rectangle $S(z)*B(z)$ is neglected in the model.

The heat transfer coefficient $\alpha(z)$ is defined by:

$$\alpha(z) = \frac{Q(z) \rho(z) c_w(z) \frac{dT_w}{dz}}{B(z) (T_{sat} - T_w(z))} \quad (C41)$$

The condensate is immediately mixed with the stripe water in the model. The local stripe water volumetric flow $Q(z)$ is therefore expressed by the local water stripe temperature $T_w(z)$

$$Q(z) = Q_0 \frac{(h_s - T_{w,0} c_{w,0})}{(h_s - T_w(z) c_w(z))} \quad (C42)$$

Combination of equations C36, C40, C41 and C42 leads to an equation for the water stripe temperature $T_w(z)$, which after integration along the stripe path between the source and elevation z results in the following equation for the stripe temperature

$$\frac{(P(z) + P_s)(P_0 - P_s)}{(P(z) - P_s)(P_0 + P_s)} = \exp \left\{ \frac{2 P_s St}{5 g P_0 S_0 \sqrt{V_0}} \left((V_0^2 + 2 g z)^{\frac{5}{4}} - V_0^{\frac{5}{2}} \right) \right\} \quad (C43)$$

with the abbreviations

$$P(z) = \sqrt{h_s - c_{p,w} T_w(z)} \quad \text{and} \quad P_x = \sqrt{h_s - c_{p,w} T_x} \quad ; \quad X = 0, S$$

In equation C43 the specific heat c_w of the stripe water is corresponding to temperature $(T_{w,0} + T_w(z))/2$.

The water temperature in stripe origin is the water temperature adjacent to bottom of cold leg outlet. The cold leg condensation model is based on mean water layer temperatures neglecting the thermal stratification in the water layer. To correctly represent the data a stripe origin temperature equal to $T_{CL} - 8K$ has to be used were T_{CL} is the mean temperature of the cold water layer in the cold leg near RPV inlet.

6. OKBMIX Code

OKBMIX code is based on the engineering technique and it was developed in OKB Gidropress on the basis of experimental and analytical data. OKBMIX code is used for local mixing modelling in RPV under PTS (ECCS water mixing in pipelines and RPV chambers). The basic approaches for thermal-hydraulic parameters definition in the main circulating pipeline and in a gap between core barrel and RPV wall at cold water injection during accidents with PTS are stated in paper reference [13].

Results of this ECCS water mixing process engineering calculations are necessary input data for definition thermal-hydraulic boundary conditions for subsequent fracture-mechanics analysis. The general approach is similar to those in the KWU-MIX code reference [2], but for the reactor

downcomer mixing process description own experimental dependences obtained with the models and by natural measurements at 4 unit Kola NPP (WWER-440) are used. For the main circulating pipeline mixing process description the experimental dependences obtained with the transparent models are used. Such transparent models mixing process investigations have been carried out as by OKB Gidropress, as by Finnish IVO firm [14, 15]. The references used for development of an engineering technique and algorithm of calculation, are presented in [13].

Comparison of the published techniques known at the present moment [2, 13, 16] with results of experiments has shown, that criteria dependences for definition of temperature in a mixing zone obtained in OKB Gidropress have universal character and can be used for calculations of mixing processes as in the main circulating pipeline and as in the gap between core barrel and reactor vessel wall at ECCS water injection during accidents both in the liquid coolant, and in saturated pairs.

7. References

- [1] DOLAN, F. X., VALENZULA, J. A., Thermal and Fluid Mixing in a 1/2-Scale Test Facility, Vol. 1&2, EPRI NP-3802 (1985).
- [2] HERTLEIN, R., Mixing and Condensation Models Based on UPTF TRAM Test Results, Annual Meeting on Nuclear Technology, Fachsitzung experimentelle und theoretische Untersuchungen zu Borverdünnungstransienten in DWR, Inforum Verlags- und Verwaltungsgesellschaft, Bonn (2003).
- [3] NOURBAKHS, H. P., THEOFANOUS, T. G., A Criterion for Predicting Thermal Stratification Due to High-Pressure Injection in a Circulating Reactor Loop, p. 77–79 in Nuclear Science and Engineering, No. 94 (1986).
- [4] SUN, K. M., OH, S., A Correlation for Entrainment of Water in a Reactor Cold Leg by Coolant Injection under Stagnant Loop Flow ASME: Paper No. 83-WA/HT-39 (1983).
- [5] HÄFNER, W., Contribution of Battelle Ingenieurtechnik GmbH Germany presented at the Reactor Pressure Vessel International Comparative Assessment Study (RPV ICAS) Task Thermal Hydraulics, February 25–27, Orlando (1998).
- [6] JIRKA, G. H., HARLEMAN, F., Stability and Mixing of Vertical Plane Buoyant Jet in Confined Depth, p. 275–304 in Journal of Fluid Mechanics, 94, (1979).
- [7] BRAUNER, N., MARON, D. M., Stability Analysis of Stratified Liquid-Liquid Flows, p. 103–121 in International Journal of Multiphase Flow, Vol. 18, No. 1 (1992).
- [8] FOX, D. G., Forced Plume in a Stratified Fluid, p. 5818–5835 in Journal of Geophysical Research 75 (1970).
- [9] CHEN, C. J., RODI, W., Vertical Turbulent Buoyant Jets - A Review of Experimental Data, Pergamon Press, New York (1980).
- [10] SHKLOVER, G. G., RODIVILIN, M. D., Generalisation of Experimental Data on Steam Condensation under Vacuum on a Vertical Water Jet, p.27–29 in Teploenergetica, No. 17 (1970).
- [11] HUGHES, E. D., DUFFEY, R. B., Direct Contact Condensation and Momentum Transfer in Turbulent Separated Flows, p. 599–619 in International Journal of Multiphase Flow, Vol. 17, No. 5 (1991).

- [12] HÄFNER, W., WOLF, L., Derivation of Mixing Parameters from the HDR-Thermal Mixing Experiments, p. 41–57 in *International Journal of Pressure Vessel and Piping*, No. 33 (1988).
- [13] BEZRUKOV, Y. A., LOGVINOV, S. A., ULYANOVSKY, V. N., STREBNEV, N. A., A Study of Boron and Temperature Mixing in the Downcomer and the Lower Part of a WWER Reactor Vessel. p. 122–130 in *Nuclear Technology*, Vol. 146, No. 2 (2004).
- [14] MUSTONEN, P., Fluid and mixing tests on the LOVIISA pressure vessel downcomer, Helsinki, (1984).
- [15] TUOMISTO, H., Thermal-hydraulics of the LOVIISA reactor pressure vessel overcooling transients, Helsinki (1987).
- [16] TEOFANOUS, T. G., YAN, H., A Unified Interpretation of One-Fifth to Full Scale Thermal Mixing Experiments Related to Pressurized Thermal Shock, NUREG/CR-5677, Washington (1991).

APPENDIX D

K ESTIMATION METHODS

1. Introduction

The parameter used to characterise the loading condition at the postulated flaw is the crack driving force (CDF) or stress intensity factor (SIF), typically denoted by K_I . In many cases K_I can be determined from analytic formulae based on linear-elastic fracture mechanics or tabulated collections of stress intensity values for given defect and vessel geometries. This appendix provides a summary K_I estimation methods used in PTS analyses.

These are divided in three sections:

- Methods valid for K_I calculation in a vessel without consideration of cladding;
- Influence function methods with consideration of the vessel cladding;
- Solutions for the nozzle corner problem.

In complement to these solutions, one should notice that the first approach (without consideration of the cladding) is not appropriate for the cladded structures since the stress discontinuity at the interface cannot be accurately fitted by polynomial fits.

2. K_I estimation without consideration of vessel cladding

2.1. ASME Section XI Formulae

Using the representative stresses at crack location determined by stress analysis the K_I can be calculated by polynomial equation for both surface crack and subsurface crack.

Surface crack

The stress normal to the crack face at the crack location is represented by polynomial fit over the crack depth:

$$\sigma = A_0 + A_1\left(\frac{x}{a}\right) + A_2\left(\frac{x}{a}\right)^2 + A_3\left(\frac{x}{a}\right)^3 \quad (D1)$$

and:

$$K_I = \left[(A_0 + A_p)G_0 + A_1G_1 + A_2G_2 + A_3G_3 \right] \sqrt{\frac{\pi a}{Q}} \quad (D2)$$

where:

x = distance through the wall from inner surface

a = crack depth

A_0, A_1, A_2, A_3 = constants which are obtained by stress distribution over the crack depth

A_p = the internal pressure

G_0, G_1, G_2, G_3 = tabulated influence functions

Q = crack shape parameter expressed as follows:

$$Q = 1 + 4.593 \left(\frac{a}{l} \right)^{1.65} - q_y$$

q_y is the plastic zone correction factor calculated as follows:

$$q_y = \frac{1}{6} \left(\frac{A_0G_0 + A_pG_0 + A_1G_1 + A_2G_2 + A_3G_3}{\sigma_{ys}} \right)^2$$

l = crack length

Subsurface crack:

K_I can be calculated using membrane and bending stresses at crack location:

$$K_I = [\sigma_m \cdot M_m + \sigma_b \cdot M_b] \sqrt{\frac{\pi a}{Q}} \quad (D3)$$

where:

σ_m, σ_b = membrane and bending stresses determined according to Equation D1

a = one-half of the axis of elliptical crack

M_m = tabulated correction factor for membrane stresses

M_b = tabulated correction factor for membrane stresses.

Q = crack shape parameter expressed as follows:

$$Q = 1 + 4.593 \cdot \left(\frac{a}{l}\right)^{1.65} - q_y$$

q_y = the plastic zone correction factor calculated using the following equation:

$$q_y = \frac{1}{6} \left[\frac{\sigma_m M_m + \sigma_b M_b}{\sigma_{ys}} \right]^2$$

2.2. Russian approach

Surface semi-elliptic crack

Analytical formulae for stress intensity factor for surface semi-elliptic crack [1, 2]

$$K_I = \sigma_i \cdot Y_i \cdot \sqrt{a} \quad (i = C \text{ or } D) \quad (D4)$$

with: σ_i = normalized stresses (MPa)

a = depth of crack (m)

$$Y_i = \frac{(2 - 0.82 \cdot a/c) \cdot \gamma_i}{\left[1 - (0.89 - 0.57 \sqrt{a/c})^3 \cdot [a/(S + S_H)]^{1.5} \right]^{3.25}}$$

with (Figure D1):

$\gamma_C = 1$ for point C

$$\gamma_D = \left[1.1 + 0.35 \cdot \left(\frac{a}{S + S_H}\right)^2 \right] \cdot \sqrt{\frac{a}{c}} \quad \text{for point D.}$$

S is the RPV wall thickness (m)

S_H is the cladding thickness (m) (for RPV without cladding $S_H = 0$).

For arbitrary distribution of stresses (Figure D1) the coordinate $x_j = a \cdot j/20$ ($j=0, 1, 2, \dots, 20$) is calculated. In each point x_j the stress $\sigma_j = \sigma_z(x=x_j)$ ($\sigma_z(x)$ -distribution of the tensile stresses in the crack-free body) is determined.

Normalized stresses σ_C for point C and σ_D for point D are calculated by the following formula:

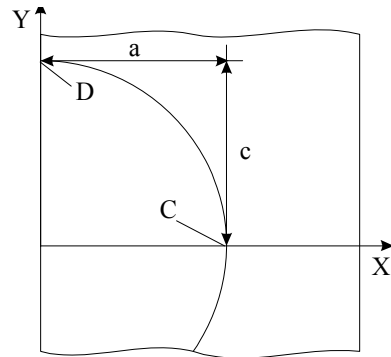
$$\sigma_C = \sum_{j=0}^{20} (C_j + (a/c) \cdot D_j + \lambda \cdot E_j) \cdot \sigma_j \quad (D5)$$

$$\sigma_D = \sum_{j=0}^{20} F_j \sigma_j \quad (D6)$$

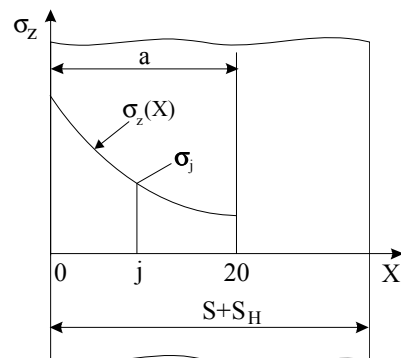
where: Coefficients C_j , D_j , E_j , F_j are tabulated values given in Table D1,

$$\lambda = \frac{a}{S \cdot (1 - 1.9 \cdot (a/c)^{0.75} + 0.9 \cdot (a/c)^{1.5})}$$

The formulae are correct at $a \leq c$ and $a \leq 0,7(S+S_H)$.



a)



b)

FIG. D1 a) Surface semi-elliptic crack in RPV wall and D , C - considered points, a , c - semi-axes;
b) Stress distribution in RPV wall without crack.

Table D1 – Values of A_j and B_j factors – surface crack

	C_j	D_j	E_j	F_j
0	0.0189	-0.0085	0.0278	0.270
1	0.0373	-0.0165	0.0548	0.198
2	0.037	-0.0160	0.0510	0.112
3	0.0368	-0.0155	0.0472	0.080
4	0.0367	-0.0149	0.0431	0.062
5	0.0366	-0.0142	0.0390	0.050
6	0.0367	-0.0134	0.0347	0.041
7	0.0368	-0.0125	0.0303	0.035
8	0.0371	-0.0115	0.0257	0.029
9	0.0376	-0.0105	0.0207	0.025
10	0.0382	-0.0093	0.0155	0.021
11	0.0391	-0.0080	0.0100	0.018
12	0.0402	-0.0063	0.0042	0.015
13	0.0418	-0.0045	-0.0023	0.012
14	0.0438	-0.0020	-0.0094	0.010
15	0.0466	0.0010	-0.0175	0.008
16	0.0507	0.0051	-0.0273	0.006
17	0.0571	0.0108	-0.0405	0.004
18	0.0685	0.0209	-0.0595	0.003
19	0.1022	0.0477	-0.0948	0.001
20	0.1203	0.0781	-0.1527	0.000

Subsurface elliptic crack

Analytical formula for stress intensity factor for subsurface elliptic crack [2]:

$$K_I = Y_i \cdot \sigma_i \cdot \sqrt{a} \quad (i = A, C \text{ or } D) \quad (D7)$$

with: σ_i = normalized stresses (MPa)

a = depth of crack (m).

$$Y_i = \left[1 - \left(\frac{a}{h+a} \right)^{1.8} \cdot \left(1 - 0.4 \cdot \frac{a}{c} - \gamma_i \right) \right]^{-0.54} \cdot \left[\frac{\pi}{1 + 1.464 \cdot (a/c)^{1.65}} \right]^{-0.5}$$

with:

$$\gamma_A = \left(0.5 - \frac{h+a}{S} \right)^2 \quad \text{for point A}$$

$$\gamma_C = 0.8 \cdot \left(0.5 - \frac{h+a}{S} \right)^{0.4} \quad \text{for point C.}$$

S is RPV wall thickness (including cladding – in m).

Location of point A and C on the crack front is shown in Figure D2.

For arbitrary distribution of stresses (Figure D2) the coordinate $x_j = a \cdot j/20$ ($j=0, 1, 2, \dots, 20$) is calculated. In each point x_j the stress $\sigma_j = \sigma_z(x=x_j)$ ($\sigma_z(x)$ - distribution of the tensile stresses in the crack-free body) is determined.

Values of σ_A and σ_C are calculated by the formulae:

$$\sigma_A = \sum_{j=0}^{20} \left(A_j + \frac{a}{c} \cdot B_j \right) \cdot \sigma_j \quad (D8)$$

$$\sigma_C = \sum_{j=0}^{20} \left(A_{20-j} + \frac{a}{c} \cdot B_{20-j} \right) \cdot \sigma_j \quad (D9)$$

where A_j and B_j are tabulated in the Table D2.

The shape factor and normalized stress for point D of the crack contour is allowed to be calculated by the following formulae:

$$Y_D = \sqrt{\frac{a}{c} \cdot Y_A \cdot Y_B} \quad (D10)$$

$$\sigma_D = \frac{\sigma_A + \sigma_C}{2} \quad (D11)$$

The formulae are correct at $a \leq c$, $a \leq 9 \cdot h$ and $h+a \leq S/2$ (Figure D2)

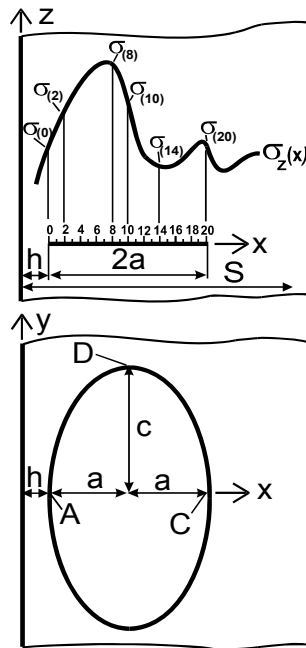


FIG. D2 – Stress and geometry description of embedded elliptical crack.

Table D2 – Values of A_j and B_j factors

j	A_j	B_j
0	0.1888	0.0843
1	0.1538	0.0433
2	0.0972	0.0136
3	0.0764	0.0036
4	0.0640	-0.0018
5	0.0533	-0.0050
6	0.04487	-0.0073
7	0.0434	-0.0088
8	0.0390	-0.0099
9	0.0352	-0.0106
10	0.0319	-0.0111
11	0.0288	-0.0113
12	0.0260	-0.0114
13	0.0234	-0.0114
14	0.0208	-0.0110
15	0.0184	-0.0106
16	0.0159	-0.0100
17	0.0134	-0.0092
18	0.0134	-0.0079
19	0.0106	-0.0058
20	0.0019	-0.0017

2.3. K_I estimation according to Chinese Code GB/T 19624-2004

The normal stress applied at the position where the flaw is located is taken as the stress used in K_I estimation. The normal stress is obtained from the flaw free component using linear elastic method. For the nonlinear stress distribution through wall thickness the linearization disposal for the flaw region should be performed. It should be assure that the linearized stress is not lower than the original stress within flaw region. The linearization illustration examples for surface flaw and embedded flaw are shown in figures D3 and D4.

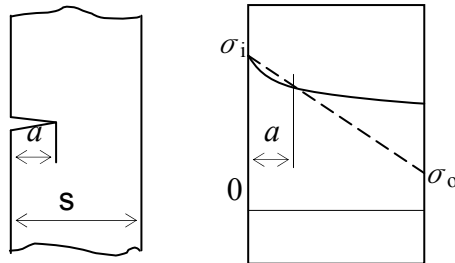


FIG. D3 – linearization illustration example for surface flaw.

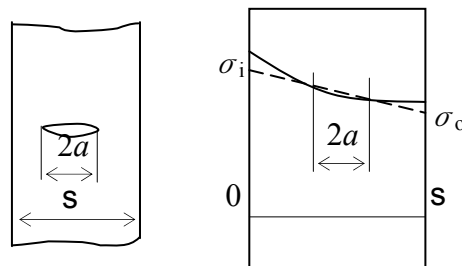


FIG. D4 – linearization illustration example for embedded flaw.

The linearized stress can resolve into membrane stress σ_m and bending stress σ_b as follows:

$$\sigma_m = \frac{\sigma_i + \sigma_o}{2}, \quad \sigma_b = \frac{\sigma_i - \sigma_o}{2} \quad (D12)$$

The original stress can be obtained by means of simplified 1-D axisymmetrical FEM or other approaches.

K_I estimation method for surface flaw

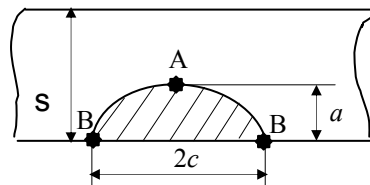


FIG. D5 – Semi-elliptical surface flaw.

For the vessel with semi-elliptical surface flaw (Figure D5), K_I is defined by:

$$K_I = [(\sigma_m + p) \cdot f_m + \sigma_b \cdot f_b] \cdot \sqrt{\pi a} \quad (D13)$$

where:

$$f_m^A = \frac{1}{\left[1 + 1.464 \cdot (a/c)^{1.65}\right]^{0.5}} \left\{ 1.13 - 0.09 \frac{a}{c} + \left(-0.54 + \frac{0.89}{0.2 + a/c}\right) \cdot \left(\frac{a}{S}\right)^2 \right. \\ \left. + \left[0.5 - \frac{1}{0.65 + a/c} + 14 \cdot (1 - a/c)^{24}\right] \cdot \left(\frac{a}{S}\right)^4 \right\}$$

$$f_b^A = \left\{ 1 + \left(-1.22 - 0.12 \cdot \frac{a}{c}\right) \cdot \frac{a}{S} + \left[0.55 - 1.05 \cdot \left(\frac{a}{c}\right)^{0.75} + 0.47 \cdot \left(\frac{a}{c}\right)^{1.5}\right] \cdot \left(\frac{a}{S}\right)^2 \right\} \cdot f_m^A$$

$$f_m^B = \left\{ \left[1.1 + 0.35 \cdot \left(\frac{a}{S}\right)^2\right] \cdot \left(\frac{a}{c}\right)^{0.5} \right\} \cdot f_m^A$$

$$f_b^B = \left\{ 1 - 0.34 \cdot \frac{a}{s} - \frac{0.11 \cdot a^2}{c \cdot S} \right\} \cdot f_m^B$$

p = applied pressure, MPa

K_I estimation method for embedded flaw

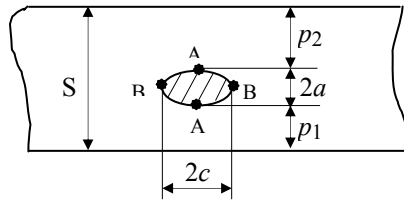


FIG. D6 – Embedded elliptical flaw.

For the vessel with embedded elliptical flaw (Figure D6), K_I is calculated by:

$$K_I = [\sigma_m \cdot f_m + \sigma_b \cdot f_b] \sqrt{\pi a} \quad (D14)$$

where:

$$f_m^A = \frac{1.01 - 0.37 \cdot \frac{a}{c}}{\left\{ 1 - \left(\frac{2a/S}{1 - 2e/S}\right)^{1.8} \left(1 - 0.4 \frac{a}{c} - \left(\frac{e}{S}\right)^2\right) \right\}^{0.54}}$$

$$f_b^A = \frac{\left(1.01 - 0.37 \cdot \frac{a}{c}\right) \left[2 \cdot \frac{e}{S} + \frac{a}{S} + 0.34 \cdot \frac{a^2}{c \cdot S}\right]}{\left\{1 - \left(\frac{2a/S}{1 - 2e/S}\right)^{1.8} \left[1 - 0.4 \frac{a}{c} - \left(\frac{e}{S}\right)^2\right]\right\}^{0.54}}$$

$$f_m^B = \frac{1.01 - 0.37 \cdot \frac{a}{c}}{\left\{1 - \left(\frac{2a/S}{1 - 2e/S}\right)^{1.8} \left[1 - 0.4 \frac{a}{c} - 0.8 \cdot \left(\frac{e}{S}\right)^{0.4}\right]\right\}^{0.54}}$$

$$f_b^B = \frac{\left(1.01 - 0.37 \cdot \frac{a}{c}\right) \left[2 \cdot \frac{e}{S} - \frac{a}{S} - \frac{0.34 \cdot a^2}{c \cdot S}\right]}{\left\{1 - \left[\frac{2a/S}{1 - 2e/S}\right]^{1.8} \left[1 - 0.4 \frac{a}{c} - 0.8 \cdot \left(\frac{e}{S}\right)^{0.4}\right]\right\}^{0.54}}$$

where e is the deviation of embedded flaw from the centre of wall thickness (in mm): $e = S/2 - a - p_1$ (Figure D6).

3. K_I calculation methods with consideration of cladding

3.1. Codified RSE-M approach

K_I estimation scheme for underclad cracks at each instant t of the PTS is derived for the following formula (Figure D7):

$$K_I^A(t) = \frac{F_b^A}{\sqrt{1 + 1.464 \left(\frac{a}{l}\right)^{1.65}}} \int_{-a}^a \frac{\sigma(u, t)}{\sqrt{\pi a}} \sqrt{\frac{a+u}{a-u}} du \quad (D15)$$

$$K_I^B(t) = \frac{F_b^B}{\sqrt{1 + 1.464 \left(\frac{a}{l}\right)^{1.65}}} \int_{-a}^a \frac{\sigma(u, t)}{\sqrt{\pi a}} \sqrt{\frac{a+u}{a-u}} du \quad (D16)$$

The edge factors at points A and B are defined by:

$$F_b^A = 0.998742 + 0.14801 \cdot z - 1.133379 \cdot z^2 + 5.491256 \cdot z^3 - 8.981896 \cdot z^4 + 5.765252 \cdot z^5$$

$$F_b^B = 1 - 0.012328 \cdot z + 0.396205 \cdot z^2 - 0.527964 \cdot z^3 + 0.432714 \cdot z^4 \text{ (if } 0 \leq z \leq 0.92)$$

$$F_b^B = -414.20286 + 1336.75998 \cdot z - 1436.11970 \cdot z^2 + 515.14949 \cdot z^3 \text{ (if } 0.92 \leq z \leq 1)$$

$$z = \frac{a}{r + d + a}$$

The stress field $\sigma(x, t)$ normal to the crack surface is determined by either finite element analysis or validated analytical approaches.

A plasticity correction must be taken into account by the β correction:

$$K_J(t) = K_I(t) + [\beta(u) - 1]K_I(u) \quad (D17)$$

With: $u = \min(t, t_{\max})$, t_{\max} corresponding to the time at maximum K_I ,

$$\beta^A = 1 + 0.3 \cdot \tanh\left(\frac{36 \cdot r_y^A}{r + d}\right), \quad \beta^B = 1 + 0.5 \cdot \tanh\left(\frac{36 \cdot r_y^A}{r + d}\right) \quad \text{and} \quad r_y^A = \frac{1}{6 \cdot \pi} \left(\frac{K_I^A}{\sigma_y^A}\right)^2$$

s_y^A is the yield stress (depending on temperature) of the material at point A (i.e. the cladding if $d = 0$).

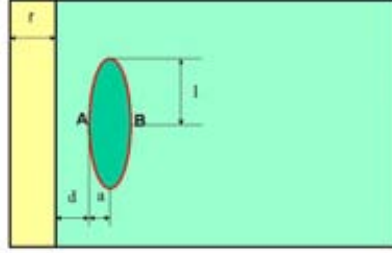


FIG. D7 – Embedded flaw definition.

3.2. Complementary compendium to be included in RSE-M

Recent work performed by CEA [6] gives a detailed approach for K_I estimation of surface and sub-clad cracks.

First calculation step is the nominal stress field representation: the stress field normal to the crack surface and calculated without considering defect. This stress fields can be determined by finite element calculation.

Main difficulty at this step is the representation of the stress discontinuity at the interface between the cladding and the ferritic steel (discontinuity due to the difference of mechanical properties). The propose procedure to describe the stress field is the following:

- The origin of the axis is taken on the inner surface (and not at the interface between the two materials). This choice gives consistent description between through and under clad defects. This axis is normalised by the entire thickness (cladding + ferritic: $r + t$ – see fig. D-9);
- The stress field in the ferritic material is fitted alone by a 4th degree polynomial form to have a good description of the stress though the thickness.

$$\sigma = \sigma_0 + \sigma_1 \cdot \frac{x}{t+r} + \sigma_2 \cdot \left(\frac{x}{t+r}\right)^2 + \sigma_3 \cdot \left(\frac{x}{t+r}\right)^3 + \sigma_4 \cdot \left(\frac{x}{t+r}\right)^4 \quad (D18)$$

- Then, the supplement of stress in the cladding is fitted by a linear fit.

$$\sigma = \sigma_{0r} + \sigma_{r1} \cdot \frac{x}{t+r} \quad (D19)$$

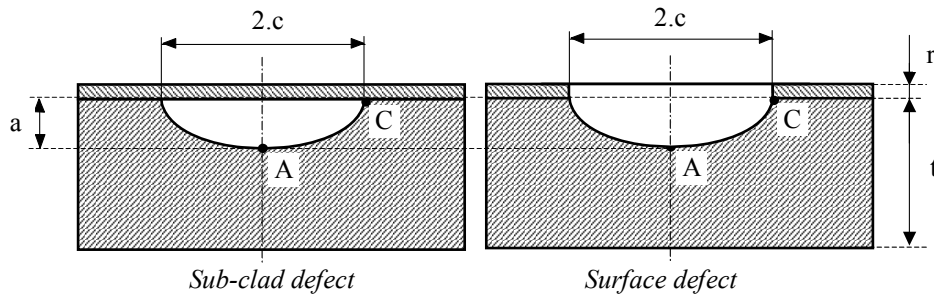


FIG. D8 – Description of considered defects.

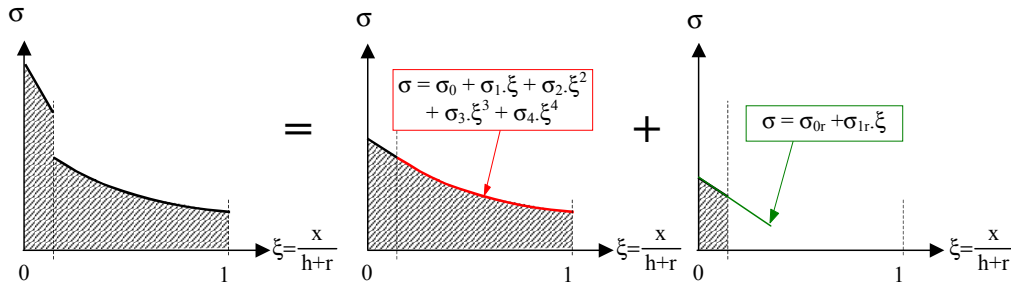


FIG. D9 – Stress description.

From this fitting, 7 stress coefficients: σ_0 to σ_4 , σ_{0r} and σ_{1r} are obtained.

Knowing the stress coefficients, the K_I value is calculated using the influence function methodology. In this case, the influence function used in the calculations are determined by precise finite element calculation then tabulated in compendium.

The compendium for cladded structures (given in tables D3 to D10) is expressed function of the non dimensional parameters a/r , a/c and E_1/E_2 where:

- a is the crack depth in the ferritic material;
- r is the cladding thickness;
- E_1 and E_2 are the cladding and ferritic Young modulus.

This compendium gives the possibility to calculate K_I at the deepest point of the crack (point A in Figure D8) or the point at the interface of the two materials (point C).

K_I parameter is then determined by the following formulae:

For a surface crack:

$$K_I = \left\{ (\sigma_0 + p) i_0 + \sigma_1 i_1 \xi_a + \sigma_2 i_2 \xi_a^2 + \sigma_3 i_3 \xi_a^3 + \sigma_4 i_4 \xi_a^4 + \sigma_{0r} i_{0r} + \sigma_{1r} i_{1r} \xi_a \right\} \sqrt{\pi(a+r)}$$

with: p = internal pressure)

(D20)

$$\xi_a = \frac{a+r}{h+r}$$

For the sub-clad crack:

$$K_I = \left(\sigma_0 i_0 + \sigma_1 i_1 \xi_a + \sigma_2 i_2 \xi_a^2 + \sigma_3 i_3 \xi_a^3 + \sigma_4 i_4 \xi_a^4 \right) \sqrt{\pi a}$$

(D21)

For values of a/r , a/c and E_1/E_2 not given in the compendium, a linear interpolation on the a/r , a/c and E_1/E_2 dimensions is recommended.

For sub-clad defects, the calculated K_I value must be corrected by the β correction described in previous chapter. This correction is only applicable for point A on Figure D8 (not yet available for point C).

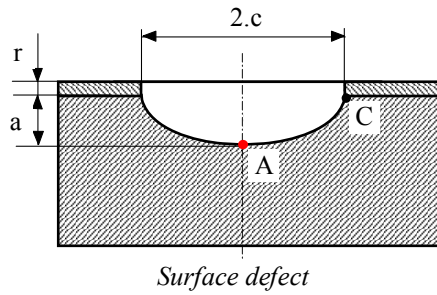


Table D3 – Influence functions for a through clad defect ($E_1/E_2 = 1$ – point A)

a / c	a / r	E1 / E2	i0	i1	i2	i3	i4	i0r	i1r
1	0.125	1	0.229	0.215	0.205	0.196	0.189	3.51E-2	2.72E-2
1	0.25	1	0.308	0.277	0.256	0.239	0.226	4.80E-2	2.99E-2
1	0.5	1	0.399	0.337	0.3	0.275	0.255	6.17E-2	2.73E-2
1	1	1	0.488	0.385	0.333	0.299	0.274	6.95E-2	1.99E-2
1	1.5	1	0.532	0.407	0.347	0.309	0.282	6.76E-2	1.47E-2
1	2	1	0.558	0.419	0.355	0.314	0.286	6.30E-2	1.11E-2
1	3	1	0.588	0.432	0.363	0.320	0.290	5.36E-2	6.95E-3
1	4	1	0.604	0.439	0.367	0.323	0.292	4.59E-2	4.71E-3
0.5	0.125	1	0.339	0.302	0.278	0.260	0.245	0.100	7.15E-2
0.5	0.25	1	0.464	0.382	0.336	0.305	0.281	0.141	7.81E-2
0.5	0.5	1	0.602	0.451	0.381	0.337	0.306	0.179	7.01E-2
0.5	1	1	0.721	0.502	0.411	0.357	0.320	0.185	4.92E-2
0.5	1.5	1	0.771	0.522	0.422	0.364	0.325	0.168	3.48E-2
0.5	2	1	0.798	0.533	0.428	0.368	0.328	0.150	2.56E-2
0.5	3	1	0.827	0.544	0.434	0.372	0.331	0.121	1.53E-2
0.5	4	1	0.843	0.550	0.437	0.374	0.332	0.101	1.02E-2
0.25	0.125	1	0.466	0.381	0.337	0.307	0.284	0.203	0.127
0.25	0.25	1	0.649	0.477	0.400	0.353	0.320	0.289	0.140
0.25	0.5	1	0.819	0.550	0.443	0.382	0.340	0.338	0.122
0.25	1	1	0.927	0.592	0.466	0.396	0.350	0.307	7.85E-2
0.25	1.5	1	0.962	0.606	0.474	0.401	0.353	0.261	5.27E-2
0.25	2	1	0.979	0.612	0.477	0.403	0.355	0.224	3.76E-2
0.25	3	1	0.998	0.619	0.481	0.405	0.356	0.174	2.18E-2
0.25	4	1	1.010	0.624	0.483	0.407	0.357	0.143	1.43E-2
0.125	0.125	1	0.634	0.460	0.388	0.344	0.313	0.358	0.194
0.125	0.25	1	0.845	0.563	0.452	0.389	0.347	0.462	0.204
0.125	0.5	1	0.984	0.621	0.485	0.411	0.363	0.465	0.161
0.125	1	1	1.047	0.645	0.499	0.419	0.368	0.377	9.53E-2
0.125	1.5	1	1.064	0.651	0.502	0.421	0.369	0.309	6.20E-2
0.125	2	1	1.073	0.655	0.504	0.422	0.370	0.261	4.35E-2
0.125	3	1	1.085	0.659	0.506	0.423	0.370	0.200	2.50E-2
0.125	4	1	1.098	0.664	0.508	0.425	0.371	0.164	1.64E-2
0.0625	0.125	1	0.829	0.544	0.437	0.378	0.338	0.543	0.269
0.0625	0.25	1	0.983	0.620	0.486	0.413	0.364	0.584	0.248
0.0625	0.5	1	1.061	0.654	0.506	0.426	0.374	0.523	0.179
0.0625	1	1	1.095	0.667	0.513	0.430	0.376	0.404	0.102
0.0625	1.5	1	1.104	0.671	0.515	0.431	0.377	0.326	6.54E-2
0.0625	2	1	1.110	0.673	0.515	0.431	0.377	0.274	4.57E-2
0.0625	3	1	1.124	0.677	0.518	0.432	0.377	0.211	2.63E-2
0.0625	4	1	1.142	0.684	0.521	0.434	0.378	0.174	1.74E-2

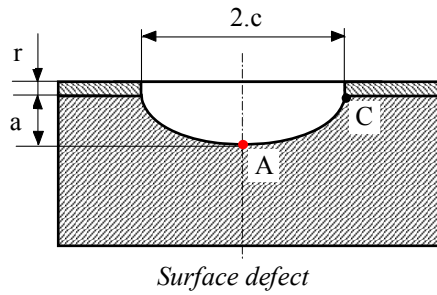


Table D4 – Influence functions for a through clad defect ($E_1/E_2 = 0.7$ – point A)

a / c	a / r	E1 / E2	i0	i1	i2	i3	i4	i0r	i1r
1	0.125	0.7	0.238	0.223	0.211	0.202	0.193	4.09E-02	3.15E-02
1	0.25	0.7	0.321	0.286	0.262	0.244	0.230	5.62E-02	3.46E-02
1	0.5	0.7	0.416	0.345	0.306	0.278	0.258	7.24E-02	3.15E-02
1	1	0.7	0.506	0.393	0.337	0.302	0.276	8.06E-02	2.28E-02
1	1.5	0.7	0.549	0.413	0.350	0.311	0.283	7.71E-02	1.66E-02
1	2	0.7	0.574	0.424	0.357	0.316	0.287	7.09E-02	1.24E-02
1	3	0.7	0.600	0.436	0.365	0.321	0.291	5.88E-02	7.58E-03
1	4	0.7	0.615	0.443	0.369	0.324	0.293	4.95E-02	5.07E-03
0.5	0.125	0.7	0.362	0.320	0.293	0.272	0.255	0.117	8.30E-02
0.5	0.25	0.7	0.497	0.402	0.351	0.316	0.290	0.166	9.05E-02
0.5	0.5	0.7	0.644	0.471	0.393	0.345	0.312	0.209	8.08E-02
0.5	1	0.7	0.761	0.518	0.420	0.363	0.324	0.211	5.55E-02
0.5	1.5	0.7	0.805	0.535	0.429	0.369	0.328	0.188	3.85E-02
0.5	2	0.7	0.827	0.543	0.433	0.372	0.330	0.165	2.79E-02
0.5	3	0.7	0.849	0.552	0.438	0.375	0.332	0.130	1.64E-02
0.5	4	0.7	0.860	0.556	0.441	0.376	0.333	0.107	1.07E-02
0.25	0.125	0.7	0.506	0.408	0.358	0.324	0.299	0.235	0.147
0.25	0.25	0.7	0.706	0.508	0.421	0.368	0.331	0.334	0.161
0.25	0.5	0.7	0.881	0.578	0.460	0.393	0.348	0.385	0.137
0.25	1	0.7	0.977	0.612	0.477	0.403	0.355	0.339	8.63E-02
0.25	1.5	0.7	1.002	0.621	0.482	0.406	0.357	0.283	5.70E-02
0.25	2	0.7	1.012	0.624	0.484	0.407	0.358	0.240	4.01E-2
0.25	3	0.7	1.021	0.628	0.485	0.408	0.358	0.183	2.29E-2
0.25	4	0.7	1.029	0.631	0.487	0.409	0.359	0.149	1.49E-2
0.125	0.125	0.7	0.690	0.494	0.412	0.363	0.329	0.406	0.219
0.125	0.25	0.7	0.914	0.597	0.475	0.405	0.360	0.518	0.228
0.125	0.5	0.7	1.047	0.649	0.502	0.423	0.371	0.512	0.177
0.125	1	0.7	1.093	0.664	0.509	0.426	0.373	0.407	0.103
0.125	1.5	0.7	1.100	0.666	0.510	0.426	0.373	0.329	6.59E-02
0.125	2	0.7	1.103	0.666	0.510	0.426	0.373	0.275	4.59E-02
0.125	3	0.7	1.107	0.668	0.511	0.426	0.372	0.208	2.60E-02
0.125	4	0.7	1.115	0.670	0.512	0.427	0.373	0.169	1.69E-02
0.0625	0.125	0.7	0.888	0.577	0.461	0.396	0.353	0.594	0.294
0.0625	0.25	0.7	1.044	0.652	0.507	0.428	0.376	0.634	0.270
0.0625	0.5	0.7	1.117	0.680	0.522	0.436	0.382	0.564	0.193
0.0625	1	0.7	1.138	0.685	0.523	0.436	0.381	0.431	0.108
0.0625	1.5	0.7	1.138	0.684	0.522	0.435	0.380	0.345	6.91E-02
0.0625	2	0.7	1.138	0.683	0.521	0.435	0.379	0.288	4.79E-02
0.0625	3	0.7	1.144	0.685	0.522	0.435	0.379	0.219	2.73E-02
0.0625	4	0.7	1.158	0.690	0.524	0.436	0.380	0.180	1.79E-02

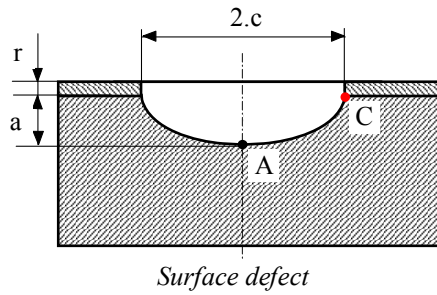


Table D5 – Influence functions for a through clad defect ($E_1/E_2 = 1$ – point C)

a / c	a / r	E1 / E2	i0	i1	i2	i3	i4	i0r	i1r
1	0.125	1	0.262	0.226	0.197	0.173	0.153	0.139	0.115
1	0.25	1	0.353	0.268	0.209	0.166	0.133	0.179	0.123
1	0.5	1	0.458	0.282	0.186	0.127	8.85E-2	0.224	0.113
1	1	1	0.565	0.263	0.139	7.89E-2	4.74E-2	0.262	8.73E-2
1	1.5	1	0.619	0.241	0.112	5.80E-2	3.31E-2	0.272	6.80E-2
1	2	1	0.652	0.225	9.61E-2	4.77E-2	2.69E-2	0.270	5.43E-2
1	3	1	0.689	0.202	7.92E-2	3.84E-2	2.20E-2	0.257	3.72E-2
1	4	1	0.709	0.188	7.07E-2	3.45E-2	2.01E-2	0.241	2.72E-2
0.5	0.125	1	0.292	0.242	0.207	0.179	0.156	0.175	0.136
0.5	0.25	1	0.397	0.284	0.216	0.168	0.133	0.230	0.145
0.5	0.5	1	0.515	0.297	0.190	0.128	8.79E-2	0.286	0.133
0.5	1	1	0.617	0.274	0.142	7.97E-2	4.73E-2	0.315	9.94E-2
0.5	1.5	1	0.661	0.249	0.114	5.84E-2	3.30E-2	0.312	7.54E-2
0.5	2	1	0.685	0.230	9.70E-2	4.76E-2	2.66E-2	0.301	5.91E-2
0.5	3	1	0.709	0.203	7.84E-2	3.75E-2	2.12E-2	0.277	3.95E-2
0.5	4	1	0.722	0.187	6.91E-2	3.31E-2	1.90E-2	0.256	2.86E-2
0.25	0.125	1	0.304	0.238	0.198	0.169	0.146	0.203	0.147
0.25	0.25	1	0.409	0.275	0.203	0.156	0.122	0.264	0.155
0.25	0.5	1	0.509	0.280	0.175	0.115	7.76E-2	0.308	0.137
0.25	1	1	0.581	0.249	0.125	6.75E-2	3.85E-2	0.317	9.88E-2
0.25	1.5	1	0.608	0.220	9.57E-2	4.64E-2	2.47E-2	0.305	7.36E-2
0.25	2	1	0.620	0.198	7.82E-2	3.57E-2	1.85E-2	0.290	5.72E-2
0.25	3	1	0.632	0.169	5.94E-2	2.57E-2	1.34E-2	0.264	3.79E-2
0.25	4	1	0.637	0.151	5.01E-2	2.15E-2	1.14E-2	0.243	2.74E-2
0.125	0.125	1	0.311	0.228	0.186	0.156	0.133	0.225	0.151
0.125	0.25	1	0.391	0.253	0.184	0.139	0.108	0.268	0.152
0.125	0.5	1	0.458	0.247	0.152	9.76E-2	6.46E-2	0.289	0.129
0.125	1	1	0.505	0.210	0.101	5.23E-2	2.82E-2	0.287	9.08E-2
0.125	1.5	1	0.520	0.180	7.36E-2	3.28E-2	1.58E-2	0.274	6.73E-2
0.125	2	1	0.526	0.158	5.72E-2	2.33E-2	1.06E-2	0.261	5.22E-2
0.125	3	1	0.530	0.129	4.00E-2	1.48E-2	6.57E-3	0.238	3.47E-2
0.125	4	1	0.532	0.113	3.18E-2	1.15E-2	5.26E-3	0.220	2.51E-2
0.0625	0.125	1	0.295	0.211	0.170	0.142	0.120	0.230	0.152
0.0625	0.25	1	0.349	0.224	0.162	0.121	9.31E-2	0.255	0.148
0.0625	0.5	1	0.396	0.211	0.128	8.12E-2	5.26E-2	0.269	0.124
0.0625	1	1	0.429	0.174	8.12E-2	4.00E-2	2.04E-2	0.266	8.77E-2
0.0625	1.5	1	0.439	0.146	5.61E-2	2.31E-2	1.01E-2	0.255	6.55E-2
0.0625	2	1	0.442	0.125	4.17E-2	1.52E-2	6.02E-3	0.243	5.12E-2
0.0625	3	1	0.442	9.88E-2	2.69E-2	8.52E-3	3.20E-3	0.224	3.44E-2
0.0625	4	1	0.441	8.33E-2	2.01E-2	6.11E-3	2.42E-3	0.209	2.51E-2

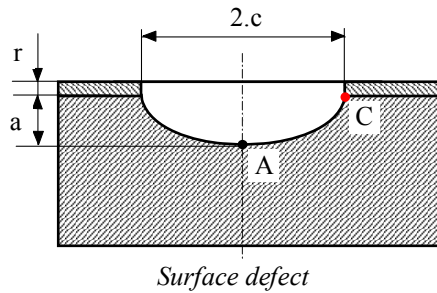


Table D6 – Influence functions for a through clad defect ($E_1/E_2 = 0.7$ – point C)

a / c	a / r	E1 / E2	i0	i1	i2	i3	i4	i0r	i1r
1	0.125	0.7	0.308	0.265	0.231	0.202	0.178	0.173	0.142
1	0.25	0.7	0.412	0.310	0.241	0.191	0.152	0.220	0.150
1	0.5	0.7	0.532	0.323	0.212	0.144	0.100	0.275	0.138
1	1	0.7	0.651	0.298	0.156	8.82E-2	5.28E-2	0.320	0.105
1	1.5	0.7	0.707	0.271	0.125	6.43E-2	3.65E-2	0.328	8.13E-2
1	2	0.7	0.738	0.250	0.106	5.24E-2	2.94E-2	0.323	6.44E-2
1	3	0.7	0.770	0.222	8.60E-2	4.15E-2	2.37E-2	0.303	4.35E-2
1	4	0.7	0.784	0.204	7.60E-2	3.67E-2	2.14E-2	0.282	3.16E-2
0.5	0.125	0.7	0.344	0.284	0.242	0.209	0.182	0.215	0.167
0.5	0.25	0.7	0.466	0.329	0.249	0.193	0.153	0.282	0.177
0.5	0.5	0.7	0.599	0.340	0.216	0.144	9.91E-2	0.349	0.160
0.5	1	0.7	0.706	0.309	0.159	8.85E-2	5.24E-2	0.377	0.118
0.5	1.5	0.7	0.747	0.277	0.126	6.39E-2	3.59E-2	0.369	8.87E-2
0.5	2	0.7	0.767	0.253	0.106	5.15E-2	2.86E-2	0.353	6.91E-2
0.5	3	0.7	0.784	0.220	8.40E-2	3.97E-2	2.23E-2	0.321	4.57E-2
0.5	4	0.7	0.790	0.200	7.30E-2	3.46E-2	1.98E-2	0.294	3.28E-2
0.25	0.125	0.7	0.356	0.277	0.230	0.196	0.168	0.246	0.178
0.25	0.25	0.7	0.476	0.316	0.233	0.178	0.138	0.318	0.186
0.25	0.5	0.7	0.584	0.317	0.197	0.129	8.66E-2	0.366	0.163
0.25	1	0.7	0.656	0.277	0.138	7.38E-2	4.19E-2	0.371	0.116
0.25	1.5	0.7	0.679	0.241	0.104	4.99E-2	2.62E-2	0.355	8.54E-2
0.25	2	0.7	0.688	0.215	8.40E-2	3.78E-2	1.93E-2	0.336	6.61E-2
0.25	3	0.7	0.693	0.181	6.26E-2	2.67E-2	1.36E-2	0.304	4.35E-2
0.25	4	0.7	0.693	0.161	5.21E-2	2.20E-2	1.15E-2	0.278	3.12E-2
0.125	0.125	0.7	0.358	0.262	0.213	0.179	0.153	0.266	0.180
0.125	0.25	0.7	0.445	0.287	0.208	0.157	0.121	0.313	0.179
0.125	0.5	0.7	0.516	0.276	0.169	0.108	7.12E-2	0.337	0.151
0.125	1	0.7	0.562	0.231	0.111	5.65E-2	3.02E-2	0.332	0.105
0.125	1.5	0.7	0.575	0.196	7.92E-2	3.49E-2	1.66E-2	0.316	7.75E-2
0.125	2	0.7	0.579	0.171	6.09E-2	2.43E-2	1.09E-2	0.300	6.00E-2
0.125	3	0.7	0.579	0.138	4.19E-2	1.51E-2	6.55E-3	0.272	3.96E-2
0.125	4	0.7	0.576	0.119	3.29E-2	1.16E-2	5.15E-3	0.251	2.86E-2
0.0625	0.125	0.7	0.337	0.242	0.195	0.163	0.139	0.267	0.179
0.0625	0.25	0.7	0.396	0.254	0.183	0.138	0.106	0.296	0.173
0.0625	0.5	0.7	0.447	0.238	0.144	9.06E-2	5.86E-2	0.312	0.145
0.0625	1	0.7	0.480	0.193	8.95E-2	4.37E-2	2.21E-2	0.307	0.102
0.0625	1.5	0.7	0.488	0.160	6.10E-2	2.49E-2	1.07E-2	0.294	7.58E-2
0.0625	2	0.7	0.489	0.136	4.49E-2	1.61E-2	6.24E-3	0.281	5.91E-2
0.0625	3	0.7	0.486	0.107	2.85E-2	8.76E-3	3.18E-3	0.258	3.96E-2
0.0625	4	0.7	0.482	8.90E-2	2.09E-2	6.13E-3	2.34E-3	0.240	2.88E-2

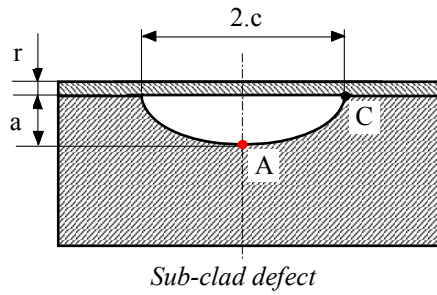


Table D7 – Influence functions for an under clad defect ($E_1/E_2 = 1$ – point A)

a / c	a / r	E1 / E2	i0	i1	i2	i3	i4
1	0.125	1	0.550	0.550	0.550	0.550	0.550
1	0.25	1	0.550	0.537	0.524	0.512	0.500
1	0.5	1	0.551	0.526	0.504	0.484	0.466
1	1	1	0.551	0.511	0.477	0.448	0.423
1	1.5	1	0.554	0.493	0.445	0.409	0.379
1	2	1	0.557	0.482	0.429	0.389	0.357
1	3	1	0.560	0.476	0.418	0.376	0.345
1	4	1	0.565	0.468	0.406	0.363	0.331
0.5	0.125	1	0.570	0.464	0.399	0.355	0.323
0.5	0.25	1	0.642	0.642	0.642	0.642	0.642
0.5	0.5	1	0.643	0.626	0.610	0.594	0.579
0.5	1	1	0.645	0.613	0.585	0.559	0.536
0.5	1.5	1	0.647	0.594	0.550	0.513	0.481
0.5	2	1	0.653	0.572	0.511	0.464	0.426
0.5	3	1	0.660	0.560	0.490	0.439	0.400
0.5	4	1	0.666	0.553	0.478	0.425	0.385
0.25	0.125	1	0.677	0.545	0.463	0.408	0.368
0.25	0.25	1	0.686	0.541	0.456	0.399	0.359
0.25	0.5	1	0.677	0.677	0.677	0.677	0.677
0.25	1	1	0.680	0.661	0.643	0.626	0.610
0.25	1.5	1	0.682	0.648	0.617	0.590	0.564
0.25	2	1	0.687	0.629	0.581	0.540	0.505
0.25	3	1	0.696	0.607	0.540	0.488	0.448
0.25	4	1	0.706	0.595	0.518	0.462	0.420
0.125	0.125	1	0.714	0.588	0.505	0.447	0.404
0.125	0.25	1	0.729	0.581	0.491	0.430	0.386
0.125	0.5	1	0.741	0.578	0.483	0.421	0.377
0.125	1	1	0.689	0.689	0.689	0.689	0.689
0.125	1.5	1	0.692	0.673	0.654	0.637	0.621
0.125	2	1	0.696	0.660	0.629	0.600	0.574
0.125	3	1	0.701	0.642	0.592	0.550	0.515
0.125	4	1	0.713	0.620	0.551	0.498	0.456
0.0625	0.125	1	0.723	0.609	0.529	0.471	0.427
0.0625	0.25	1	0.732	0.602	0.516	0.456	0.411
0.0625	0.5	1	0.749	0.596	0.502	0.439	0.393
0.0625	1	1	0.764	0.594	0.495	0.430	0.384
0.0625	1.5	1	0.693	0.693	0.693	0.693	0.693
0.0625	2	1	0.696	0.677	0.658	0.641	0.624
0.0625	3	1	0.700	0.665	0.633	0.604	0.578
0.0625	4	1	0.706	0.646	0.596	0.554	0.518

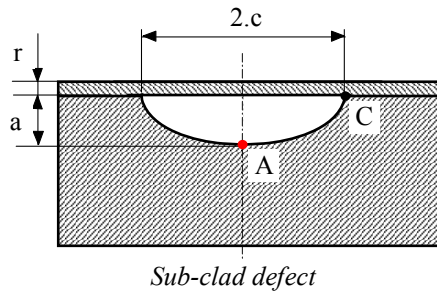


Table D8 – Influence functions for an under clad defect ($E_1/E_2 = 0.7$ – point A)

a / c	a / r	E1 / E2	i0	i1	i2	i3	i4
1	0.125	0.7	0.558	0.558	0.558	0.558	0.558
1	0.25	0.7	0.558	0.544	0.531	0.518	0.506
1	0.5	0.7	0.559	0.533	0.511	0.490	0.471
1	1	0.7	0.560	0.517	0.482	0.452	0.426
1	1.5	0.7	0.562	0.498	0.449	0.411	0.381
1	2	0.7	0.565	0.487	0.432	0.391	0.359
1	3	0.7	0.568	0.480	0.421	0.378	0.346
1	4	0.7	0.573	0.472	0.408	0.364	0.332
0.5	0.125	0.7	0.578	0.468	0.401	0.357	0.324
0.5	0.25	0.7	0.657	0.657	0.657	0.657	0.657
0.5	0.5	0.7	0.658	0.640	0.622	0.606	0.590
0.5	1	0.7	0.660	0.626	0.596	0.569	0.545
0.5	1.5	0.7	0.662	0.606	0.560	0.521	0.487
0.5	2	0.7	0.669	0.583	0.519	0.470	0.431
0.5	3	0.7	0.675	0.570	0.497	0.444	0.403
0.5	4	0.7	0.681	0.562	0.484	0.428	0.388
0.25	0.125	0.7	0.692	0.553	0.468	0.411	0.370
0.25	0.25	0.7	0.701	0.549	0.460	0.402	0.361
0.25	0.5	0.7	0.695	0.695	0.695	0.695	0.695
0.25	1	0.7	0.698	0.678	0.659	0.642	0.625
0.25	1.5	0.7	0.701	0.665	0.632	0.603	0.576
0.25	2	0.7	0.706	0.645	0.593	0.550	0.514
0.25	3	0.7	0.716	0.621	0.550	0.496	0.453
0.25	4	0.7	0.726	0.608	0.527	0.469	0.424
0.125	0.125	0.7	0.734	0.601	0.513	0.452	0.408
0.125	0.25	0.7	0.749	0.592	0.497	0.434	0.389
0.125	0.5	0.7	0.761	0.589	0.489	0.425	0.380
0.125	1	0.7	0.709	0.709	0.709	0.709	0.709
0.125	1.5	0.7	0.712	0.691	0.672	0.654	0.636
0.125	2	0.7	0.716	0.679	0.645	0.615	0.587
0.125	3	0.7	0.723	0.659	0.606	0.562	0.524
0.125	4	0.7	0.734	0.636	0.562	0.506	0.462
0.0625	0.125	0.7	0.745	0.623	0.539	0.478	0.433
0.0625	0.25	0.7	0.755	0.616	0.525	0.462	0.416
0.0625	0.5	0.7	0.772	0.608	0.510	0.444	0.397
0.0625	1	0.7	0.786	0.605	0.502	0.435	0.388
0.0625	1.5	0.7	0.713	0.713	0.713	0.713	0.713
0.0625	2	0.7	0.717	0.696	0.676	0.658	0.640
0.0625	3	0.7	0.721	0.684	0.650	0.619	0.591
0.0625	4	0.7	0.728	0.664	0.611	0.566	0.528

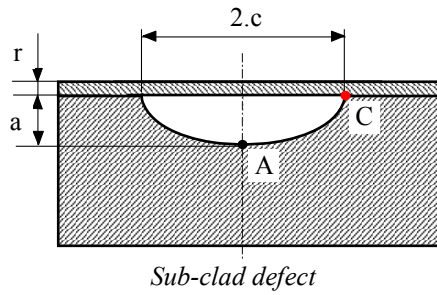


Table D9 – Influence functions for an under clad defect ($E_1/E_2 = 1$ – point C)

a / c	a / r	E1 / E2	i0	i1	i2	i3	i4
1	0.125	1	0.263	0.263	0.263	0.263	0.263
1	0.25	1	0.264	0.238	0.214	0.193	0.174
1	0.5	1	0.264	0.217	0.178	0.147	0.121
1	1	1	0.265	0.186	0.131	9.27E-2	6.61E-2
1	1.5	1	0.267	0.148	8.32E-2	4.80E-2	2.85E-2
1	2	1	0.270	0.125	6.05E-2	3.08E-2	1.67E-2
1	3	1	0.272	0.111	4.79E-2	2.26E-2	1.19E-2
1	4	1	0.277	0.093	3.51E-2	1.56E-2	8.21E-3
0.5	0.125	1	0.281	0.083	2.90E-2	1.27E-2	6.91E-3
0.5	0.25	1	0.244	0.244	0.244	0.244	0.244
0.5	0.5	1	0.245	0.220	0.197	0.177	0.160
0.5	1	1	0.245	0.200	0.164	0.134	0.110
0.5	1.5	1	0.246	0.171	0.119	8.36E-2	5.89E-2
0.5	2	1	0.248	0.135	7.47E-2	4.20E-2	2.42E-2
0.5	3	1	0.251	0.114	5.34E-2	2.61E-2	1.35E-2
0.5	4	1	0.253	0.100	4.16E-2	1.86E-2	9.16E-3
0.25	0.125	1	0.257	0.083	2.95E-2	1.21E-2	5.91E-3
0.25	0.25	1	0.261	0.073	2.38E-2	9.58E-3	4.80E-3
0.25	0.5	1	0.215	0.215	0.215	0.215	0.215
0.25	1	1	0.216	0.193	0.173	0.155	0.139
0.25	1.5	1	0.216	0.176	0.143	0.116	9.45E-2
0.25	2	1	0.217	0.149	0.103	7.11E-2	4.92E-2
0.25	3	1	0.219	0.117	6.26E-2	3.40E-2	1.87E-2
0.25	4	1	0.220	9.70E-2	4.34E-2	2.00E-2	9.50E-3
0.125	0.125	1	0.222	8.40E-2	3.28E-2	1.34E-2	5.87E-3
0.125	0.25	1	0.224	6.80E-2	2.20E-2	7.86E-3	3.24E-3
0.125	0.5	1	0.227	5.87E-2	1.69E-2	5.71E-3	2.40E-3
0.125	1	1	0.185	0.185	0.185	0.185	0.185
0.125	1.5	1	0.185	0.165	0.147	0.132	0.118
0.125	2	1	0.185	0.150	0.121	9.79E-2	7.92E-2
0.125	3	1	0.185	0.126	8.61E-2	5.88E-2	4.02E-2
0.125	4	1	0.186	9.74E-2	5.11E-2	2.70E-2	1.43E-2
0.0625	0.125	1	0.187	8.01E-2	3.46E-2	1.51E-2	6.70E-3
0.0625	0.25	1	0.188	6.86E-2	2.54E-2	9.63E-3	3.78E-3
0.0625	0.5	1	0.190	5.44E-2	1.61E-2	5.08E-3	1.76E-3
0.0625	1	1	0.191	4.61E-2	1.18E-2	3.37E-3	1.16E-3
0.0625	1.5	1	0.156	0.156	0.156	0.156	0.156
0.0625	2	1	0.156	0.139	0.124	0.111	9.91E-2
0.0625	3	1	0.156	0.126	0.102	8.20E-2	6.62E-2
0.0625	4	1	0.156	0.106	7.19E-2	4.87E-2	3.31E-2

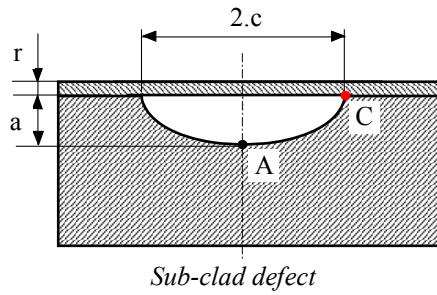


Table D10 – Influence functions for an under clad defect ($E_1/E_2 = 0.7$ – point C)

a / c	a / r	E1 / E2	i0	i1	i2	i3	i4
1	0.125	0.7	0.284	0.284	0.284	0.284	0.284
1	0.25	0.7	0.284	0.256	0.231	0.208	0.187
1	0.5	0.7	0.284	0.233	0.192	0.158	0.131
1	1	0.7	0.285	0.200	0.141	0.101	7.20E-2
1	1.5	0.7	0.287	0.160	9.04E-2	5.25E-2	3.14E-2
1	2	0.7	0.290	0.136	6.61E-2	3.39E-2	1.86E-2
1	3	0.7	0.293	0.120	5.25E-2	2.51E-2	1.33E-2
1	4	0.7	0.298	0.101	3.87E-2	1.74E-2	9.26E-3
0.5	0.125	0.7	0.302	8.99E-2	3.20E-2	1.43E-2	7.79E-3
0.5	0.25	0.7	0.262	0.262	0.262	0.262	0.262
0.5	0.5	0.7	0.262	0.236	0.212	0.191	0.171
0.5	1	0.7	0.263	0.215	0.176	0.144	0.118
0.5	1.5	0.7	0.264	0.184	0.129	9.04E-2	6.39E-2
0.5	2	0.7	0.266	0.146	8.09E-2	4.58E-2	2.66E-2
0.5	3	0.7	0.269	0.123	5.82E-2	2.87E-2	1.50E-2
0.5	4	0.7	0.271	0.108	4.55E-2	2.06E-2	1.03E-2
0.25	0.125	0.7	0.276	0.090	3.26E-2	1.36E-2	6.73E-3
0.25	0.25	0.7	0.280	0.079	2.64E-2	1.08E-2	5.48E-3
0.25	0.5	0.7	0.229	0.229	0.229	0.229	0.229
0.25	1	0.7	0.230	0.206	0.184	0.165	0.148
0.25	1.5	0.7	0.230	0.187	0.152	0.124	0.101
0.25	2	0.7	0.231	0.159	0.110	7.61E-2	5.28E-2
0.25	3	0.7	0.233	0.125	6.72E-2	3.66E-2	2.03E-2
0.25	4	0.7	0.235	1.04E-1	4.68E-2	2.17E-2	1.04E-2
0.125	0.125	0.7	0.236	9.00E-2	3.55E-2	1.47E-2	6.51E-3
0.125	0.25	0.7	0.239	7.32E-2	2.40E-2	8.71E-3	3.66E-3
0.125	0.5	0.7	0.242	6.33E-2	1.85E-2	6.39E-3	2.74E-3
0.125	1	0.7	0.195	0.195	0.195	0.195	0.195
0.125	1.5	0.7	0.195	0.174	0.155	0.139	0.124
0.125	2	0.7	0.195	0.158	0.128	0.103	8.37E-2
0.125	3	0.7	0.195	0.133	9.10E-2	6.22E-2	4.26E-2
0.125	4	0.7	0.196	0.103	5.41E-2	2.86E-2	1.52E-2
0.0625	0.125	0.7	0.197	8.47E-2	3.67E-2	1.61E-2	7.19E-3
0.0625	0.25	0.7	0.198	7.26E-2	2.70E-2	1.03E-2	4.09E-3
0.0625	0.5	0.7	0.200	5.77E-2	1.73E-2	5.50E-3	1.94E-3
0.0625	1	0.7	0.202	4.90E-2	1.27E-2	3.69E-3	1.30E-3
0.0625	1.5	0.7	0.163	0.163	0.163	0.163	0.163
0.0625	2	0.7	0.163	0.146	0.130	0.116	0.104
0.0625	3	0.7	0.163	0.132	0.106	8.57E-2	6.92E-2
0.0625	4	0.7	0.163	0.111	7.51E-2	5.10E-2	3.46E-2

4. K_I estimation method for nozzle problems

4.1. ASME approach

The nozzle region is the several regions in RPV which are subjected to high stresses due to the discontinuity of intersection of vessel and nozzle during in-service and hydrotest. A quite high stress concentration factor and peak stresses occur at the inner corner of nozzle and the possibility of the fatigue failure exists for the cyclic operating loading. The nozzle region is often a part of most concerning positions for designer. Under the cyclic loading the initial flaw is likely to origin from this region.

The definition of a circular flaw for the nozzle region of RPV refers to WRCB 175 [2] and illustrated in Figure D10. The K_I expression for the pressure load is given as follows:

$$K_I = \sigma_h \cdot F\left(\frac{a}{r_n}\right) \cdot \sqrt{\pi \cdot a} \quad (D22)$$

Where:

σ_h = shell hoop stress (MPa)

a = depth of flaw (mm)

$F(a/r_n)$ = coefficient shown in Figure D11 for only pressure load

r_n = apparent radius of nozzle, mm and the relationship is as follows:

$$r_n = r_i + 0.29 \cdot r_c$$

with:

r_i = actual inner radius of nozzle, mm

r_c = inner corner radius, mm

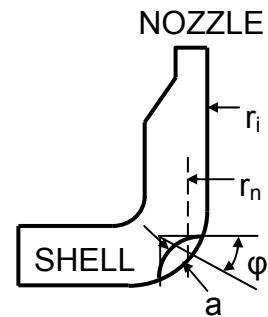


FIG. D10 – Flaw definition for nozzle region of RPV.

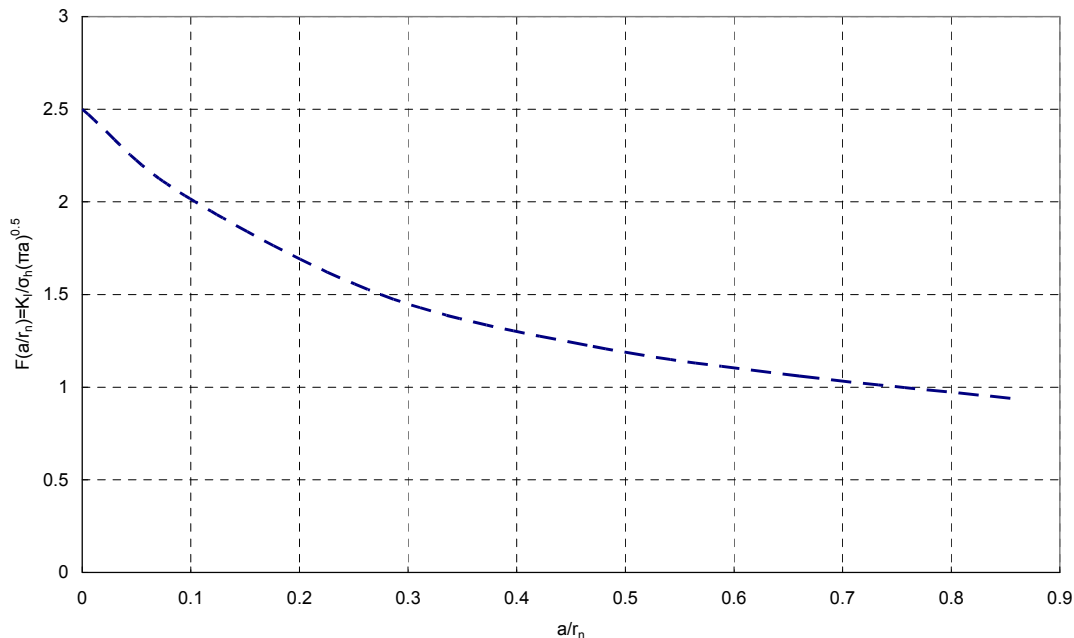


FIG. D11 – Estimated value of $F(a/r_n)$ for only pressure load.

4.2. Chinese code method

The analytical formula for the inner corner of nozzle region with a circular crack is given below as per reference [4]:

$$K_I = P_m \cdot \left(1 + \sqrt{\frac{R_{in} \cdot B_n}{R_i \cdot B}} \right) \cdot f_{cc} \cdot \sqrt{\pi a} \quad (D23)$$

where, f_{cc} can be obtained from following Table D3:

a/B	0.0	0.1	0.2	0.3	0.4	0.5	0.6	0.7	0.8
f_{cc}	1.88	1.74	1.60	1.49	1.38	1.30	1.22	1.18	1.13

P_m is membrane stress of vessel and the applicable conditions: $a/B \leq 0.8$ and $R_{in}/R_i \leq 0.4$

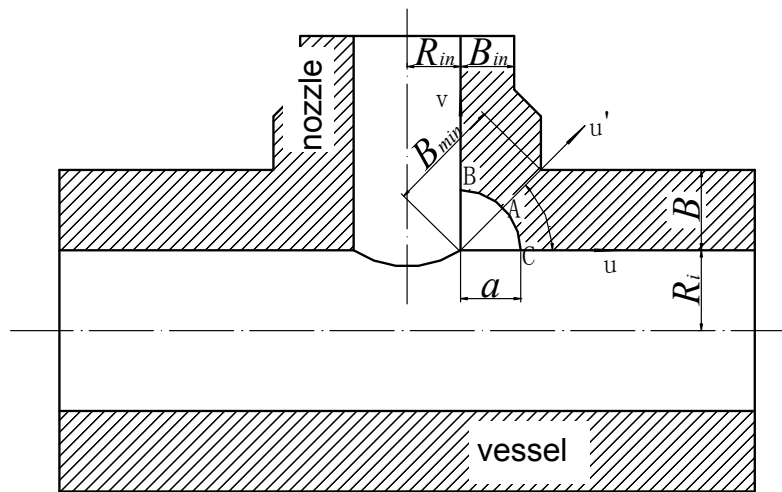


FIG. D12 – Inner corner of nozzle region with a circular crack.

For the PTS event the time dependent pressure and thermal loads will be applied to RPV simultaneously. In that case the FEM approach is recommended. The finite element mesh of nozzle region with flaw of $a/t = 0.1$ should be built.

5. References

- [1] CALCULATION PROCEDURE FOR EVALUATION OF BRITTLE STRENGTH OF VVER RPV DURING OPERATION, MRKR-SKhR-2004, RD EO 0606-2005, St. Petersburg, Moscow (2004).
- [2] RULES FOR MAKING UP THE CALCULATION MODELS AND DETERMINATION OF THE LOADING PARAMETERS OF THE STRUCTURE COMPONENTS WITH DETECTED FLAWS, Methodological recommendations, MP 125-02-95NPO TsNIITMASH, Moscow (1995).
- [3] PVRC Recommendation on toughness requirements for ferritic materials, Welding Research Council Bulletin Series 175

- [4] Safety assessment for in-service pressure vessels containing defects, GB/T 19624 (2004).
- [5] AMERICAN SOCIETY OF MECHANICAL ENGINEERS, ASME Boiling and Pressure Vessel code section XI, Rules for in-service inspection of nuclear power plant components, New York (2004).
- [6] MARIE, S., MENAGER, Y., CHAPULIOT, S., Stress intensity factors for underclad and through clad defects in a reactor pressure vessel submitted to a pressurized thermal shock, p. 746–760 in International Journal of Pressure Vessels and Piping, No. 82 (2005).

APPENDIX E

RUSSIAN STANDARD FOR DETERMINATION OF K_{IC}

1. Introduction

Fracture toughness temperature dependence $K_{IC}(T)$ for base and weld metals of RPV is determined according to the procedures given in Russian Standard MKc-KR-2000 [1]. Russian Standard [1] consisting of two Parts foresees determination of $K_{IC}(T)$ curve for case when the lateral shift condition is valid (Part I) and for case when the lateral shift condition is invalid, i.e. a shape of $K_{IC}(T)$ curve varies due to the irradiation effect. Part I is the Basic Curve approach. Part II is based on the Prometyy local approach to brittle fracture. Hereafter some main considerations used for the procedures in [1] are represented.

2. Part I: Basic Curve Concept

The main considerations of the concept are the following:

1. A scatter in K_{IC} results is described by the Weibull distribution function with three parameters taken as

$$P_f = 1 - \exp \left[- \left(\frac{K_{IC} - K_{min}}{K_0 - K_{min}} \right)^b \right] \quad (E1)$$

where $b=4$ independent of material, test temperature and specimen thickness; P_f - the probability of finding of fracture toughness value being less than K_{IC} , K_0 - scale parameter dependent of temperature and specimen thickness, K_{min} - the minimum value of fracture toughness.

2. The effect of specimen thickness on fracture toughness is described by equation

$$\frac{K_{IC}^X - K_{min}}{K_{IC}^Y - K_{min}} = \left(\frac{B_Y}{B_X} \right)^{1/4} \quad (E2)$$

where K_{IC}^X , K_{IC}^Y - fracture toughness values for specimens of thickness $B=B_X$ and $B=B_Y$ for the same probability P_f .

3. The Basic Curve, $\bar{K}_{IC}(T-T_k)$, is defined as the dependence $K_{IC}(T-T_k)$ for specimens with thickness $B=150$ mm and the brittle fracture probability $P_f=0.05$. Here parameter T_k is the critical temperature of brittle fracture. The Basic Curve is given by equation

$$\bar{K}_{IC} = \alpha + \beta \exp[\gamma(T - T_k)] \quad (E3)$$

where parameters α , β and γ are taken as $\alpha = 23$ MPa \sqrt{m} , $\beta = 48$ MPa \sqrt{m} and $\gamma=0.019^\circ\text{C}^{-1}$. Value of K_{min} may be taken to be equal to 20 MPa \sqrt{m} as well as in [2].

It should be noted that the curve described by equation in item 3 is the lower envelopes of test results on fracture toughness for reactor pressure vessel materials of WWER accumulated during more than 20 years.

4. It is assumed that for the embrittled materials (in particular, for irradiated) only one parameter, T_k , varies, the rest of parameters in the Basic Curve (Equation E3) does not vary. This last consideration is, as a matter of fact, the lateral shift condition.

The Basic Curve concept is a very similar to that of the Master Curve [2]. Both approaches use the temperature lateral shift and the parameter T_k for the Basic Curve as well as the parameter T_0 for the Master Curve is the adjusted parameter actually. It should be also noted that procedures for determination of T_k and T_0 are similar. Using the parameter T_k for the Basic Curve for RPV materials of WWER is connected with the presentation of available experimental data on fracture toughness for these materials as a function of the relative temperature $T-T_k$.

Value of T_k may be determined both on the basis of Charpy specimen tests as $T_k = T_{k0} + \Delta T_k$ (here T_{k0} is the critical temperature for material in the initial state) and on the basis of small-sized fracture toughness specimen tests.

3. Part 2: Probabilistic model for predicting the $K_{JC}(T)$ curve

In the present Section, the formulation of the local cleavage fracture criterion in a probabilistic manner, the probabilistic model (now known as the Prometey model) for predicting the $K_{JC}(T)$ curve and methods for experimental determination of the necessary parameters are represented.

The local criterion for cleavage fracture

The formulation of the local cleavage fracture criterion in a probabilistic manner includes the following steps [3, 4, 5].

1. The polycrystalline material is viewed as an aggregate of cubic unit cells. The mechanical properties for each unit cell are taken as the average properties obtained by standard specimen testing. The size of the unit cell ρ_{uc} is never less than the average grain size. The stress and strain fields in the unit cell are assumed to be homogeneous.

2. The local criterion for cleavage fracture of a unit cell is taken as [3, 4, 6]

$$\sigma_{nuc} \equiv \sigma_1 + m_{T\epsilon} \sigma_{eff} \geq \sigma_d \quad (E4a)$$

$$\sigma_1 \geq S_C(\epsilon) \quad (E4b)$$

where the critical brittle fracture stress, $S_C(\epsilon)$, is calculated by

$$S_C(\epsilon) = [C_1^* + C_2^* \exp(-A_d \epsilon)]^{-1/2} \quad (E5)$$

Here, σ_1 is the maximum principal stress, the effective stress is $\sigma_{eff} = \sigma_{eq} - \sigma_Y$, σ_{eq} is the equivalent stress, σ_Y is the yield stress, $\epsilon = \int d\epsilon_{eq}^p$ is the accumulated plastic strain (Odqvist's parameter), $d\epsilon_{eq}^p$ is the equivalent plastic strain increment, C_1^* , C_2^* , A_d are material constants, σ_d is the strength of carbides or "carbide-matrix" interfaces or other particles on which cleavage microcracks are nucleated, $m_{T\epsilon}$ is a parameter that depends on temperature T and plastic strain and may be written [4, 5] as

$$m_{T\epsilon} = m_T(T) m_\epsilon(\epsilon), \quad (E6)$$

$$m_\epsilon(\epsilon) = S_0 / S_C(\epsilon), \quad (E7)$$

$$m_T(T) = m_0 \sigma_{Ys}(T) \quad (E8)$$

where $S_0 = S_C(\epsilon=0)$, m_0 is a constant which may be experimentally determined and σ_{Ys} is the temperature-dependent component of the yield stress.

3. To formulate criteria (Equation E1) in a probabilistic way, it is assumed that the parameter σ_d is stochastic and the remainder of the parameters controlling brittle fracture are deterministic.

4. To describe the distribution function for the parameter σ_d , the Weibull law is used: the minimum strength of carbides in the unit cell on which cleavage microcracks are nucleated, is assumed to obey

$$p(\sigma_d) = 1 - \exp \left[- \left(\frac{\sigma_d - \sigma_{d0}}{\tilde{\sigma}_d} \right)^\eta \right] \quad (E9)$$

where $p(\sigma_d)$ is the probability of finding in the considered unit cell a carbide with minimum strength less than σ_d ; $\tilde{\sigma}_d$, σ_{d0} and η are Weibull parameters.

The weakest link model is used to describe the brittle fracture of the polycrystalline material.

Prometey probabilistic model for the $K_{JC}(T)$ curve prediction

A probabilistic model for predicting the $K_{JC}(T)$ curve [5] (now known as the Prometey model) is based on the brittle fracture criterion described above. The stress and strain fields near the crack tip are calculated by FEM or on the crack extension line with an approximate analytical solution [5].

The brittle fracture probability of a specimen, P_f , is presented in the form used in [7].

$$P_f = 1 - \exp \left[- \left(\frac{\sigma_w}{\tilde{\sigma}_d} \right)^\eta \right] \quad (E10)$$

where the Weibull stress σ_w is calculated as [8].

$$\sigma_w = \left[\sum_{i=1}^k \left(\max(S_{nuc}^i) - \sigma_{d0} \right)^\eta \right]^{1/\eta} \quad (E11)$$

$$S_{nuc}^i \equiv \begin{cases} \sigma_{nuc}^i, & \text{when } \sigma_1^i \geq S_C(\mathfrak{a}_i) \text{ and } \sigma_{nuc}^i > \sigma_{d0} \\ \sigma_{d0}, & \text{when } \sigma_1^i < S_C(\mathfrak{a}_i) \text{ or } \sigma_{nuc}^i \leq \sigma_{d0} \end{cases}$$

Here σ_{d0} is minimum value of σ_d ; k is the number of unit cells. For each unit cell, the parameter $\max(S_{nuc}^i)$ is the maximum value of S_{nuc}^i from the beginning of deformation up to the current moment. Equations E10 and E11 provide the calculation of the dependence $P_f(K_I)$ as the parameter σ_w is a function of K_I .

To predict the $K_{JC}(T)$ curve on the basis of the Prometey model, it is necessary to know the parameters $S_C(\mathfrak{a})$, $m_T(T)$, $\tilde{\sigma}_d$, σ_{d0} and η and also parameters describing plastic deformation to enable the stress and strain fields to be calculated. These parameters are taken as follows.

The stress-strain curve is approximated by

$$\sigma_{eq}(T, \mathfrak{a}) = \sigma_Y(T) + A_0(T) \cdot \mathfrak{a}^{n(T)} \quad (E12)$$

where A_0 and n are the strain hardening coefficients dependent on temperature. The temperature dependence of the yield stress is taken in the form

$$\sigma_Y(T) = \sigma_{YG} + \sigma_{Ys}(T) \quad (E13)$$

where σ_{YG} is the temperature-independent component of the yield stress and the temperature-dependent component σ_{Ys} is approximated by

$$\sigma_{Ys}(T) = b \cdot \exp(-hT_a) \quad (E14)$$

where b and h are the material constants independent of temperature, T_a is taken in Kelvin degrees.

Calibration of the model parameters

The parameters $S_C(\epsilon)$, $m_T(T)$, σ_{d0} and parameters describing plastic deformation are determined from uniaxial tension tests of standard cylindrical specimens [5, 9].

The dependence of the critical brittle fracture stress S_C on plastic strain is given by Equation E5. For each specimen tested over the brittle fracture temperature range, the average fracture stress, σ_f , and the plastic strain at fracture, ϵ_f , have to be determined. When using Bridgman's equations, the maximum value of σ_1 at fracture is calculated and it is taken, as is common practice, that $S_C = \max \sigma_1$.

The parameter $m_T(T)$ is calculated from Equation E8. The dependence $\sigma_Y(T)$ is approximated by equations E13 and E14.

The parameter σ_{d0} is defined as the minimum possible value of the carbide strength, and may be taken as $\sigma_{d0} = S_0$ [6].

The parameters $\tilde{\sigma}_d$ and η may be determined from test results of small-sized fracture toughness specimens at one temperature [9, 10].

The procedure for determination of $\tilde{\sigma}_d$ and η assuming that the parameter m_0 is known is as follows. The parameter m_0 may be found from cracked specimens tested at two different temperatures and an iterative process [5].

1. Small-sized fracture toughness specimens are tested at temperature T and values of K_{JC} are determined.
2. Stress and strain fields for each cracked specimen are calculated according to an analytical solution in [5] or by FEM.
3. Some initial value of $\eta = \eta_0$ is taken.
4. Values of σ_w for each cracked specimen are calculated by Equation E11 using the stress and strain fields obtained from step 2.
5. The parameters $\tilde{\sigma}_d$ and η in Equation E10 are determined by the maximum likelihood method.
6. The values of η and η_0 are compared:
 - a. if $\eta \cong \eta_0$ then the iterative process is interrupted;
 - b. if $\eta \neq \eta_0$ then the value of parameter η_0 is taken to be equal to η and the process is repeated according to steps 4 – 6.

The local criterion parameters $\tilde{\sigma}_d$ and η may be also calibrated from test results of tensile notched cylindrical specimens [5].

4. Concluding remarks

Applications of the Prometey model are completely represented in [5, 9, 10, 11].

The Prometey model predicts a variation in the shape of the $K_{JC}(T)$ curve when increasing the radiation embrittlement degree [10]. In this connection it should be noted that currently the Master Curve approach [2] is a widely used method for predicting the temperature dependence of fracture toughness for RPV steels. However, the applicability of the Master Curve approach may be restricted for highly embrittled steels as this approach uses the lateral temperature shift to describe the $K_{JC}(T)$ curves [9, 10].

The Prometey model does not include any assumptions concerning the shape of the $K_{JC}(T)$ curve and the temperature lateral shift condition, and provides a prediction of the $K_{JC}(T)$ curve allowing for the possibility of both a shift and a variation in shape.

At the present time the Prometey model is used in Russian Standard [1] (Russian utility Standard approved by Russian regulatory) as one of the recommended procedure for determination of the $K_{JC}(T)$ curve for RPV materials of WWER-440 and WWER-1000.

Now engineering method named the Unified Curve concept [12] and based on the results calculated by the Prometey model is being elaborated as a new normative method for the $K_{JC}(T)$ curve prediction.

5. References

- [1] PROCEDURE FOR DETERMINATION OF FRACTURE TOUGHNESS TEMPERATURE DEPENDENCE FOR RPV MATERIALS OF VVER-440 AND VVER-1000, MKc-KR-2000, RD EO 0350-02, Saint-Petersburg, Moscow (2001).
- [2] AMERICAN SOCIETY FOR TESTING AND MATERIALS, ASTM E 1921-02, Standard Test Method for Determination of Reference Temperature, T_0 , for Ferritic Steels in the Transition Range, Annual Book of ASTM Standards, West Conshohocken (2002).
- [3] MARGOLIN, B. Z., SHVETSOVA, V.A., Brittle fracture criterion: physical and mechanical approach, p. 3–16, Problemy Prochnosti, No. 2 (1992).
- [4] MARGOLIN, B. Z., SHVETSOVA, V. A., KARZOV, G. P., Brittle fracture of nuclear pressure vessel steels Part I, Local criterion for cleavage fracture, p. 73–87 in International Journal of Pressure Vessels & Piping, No. 72 (1997).
- [5] MARGOLIN, B. Z., GULENKO, A. G., SHVETSOVA, V. A., Improved probabilistic model for fracture toughness prediction based for nuclear pressure vessel steels, p. 843–855 in International Journal of Pressure Vessels & Piping, No. 75 (1998).
- [6] MARGOLIN, B. Z., SHVETSOVA, V. A., GULENKO, A. G., KOSTYLEV, V. I., Application of a new cleavage fracture criterion for fracture toughness prediction for RPV steels, p. 697–713 in Fatigue Fracture Engineering Material Structure, No. 29 (2006).
- [7] BEREMIN, F. M., A local criterion for cleavage fracture of a nuclear pressure vessel steel, p. 2277–2287 in Met. Trans., No. 14A (1983).
- [8] MARGOLIN, B. Z., KOSTYLEV, V. I., MINKIN, A. I., The effect of ductile crack growth on the temperature dependence of cleavage fracture toughness for a RPV steel with various degrees of embrittlement, p. 285–296 in International Journal of Pressure Vessels & Piping, No. 80 (2003).
- [9] MARGOLIN, B. Z., SHVETSOVA, V. A., GULENKO, A. G., ILYIN A. V., NIKOLAEV V. A., SMIRNOV V. I., Fracture toughness predictions for a reactor pressure vessel steel in the initial and highly embrittled states with the Master Curve approach and a probabilistic model, p. 219–231 in International Journal of Pressure Vessels & Piping, No. 79 (2002).

- [10] MARGOLIN, B. Z., KARZOV G. P., SHVETSOVA, V. A., KEIM E., CHAOUADI R., Application of local approach concept of cleavage fracture to VVER materials. in: Service experience and failure assessment applications, p. 113–120 in the proceedings from the 2002 ASME Pressure Vessels and Piping Conference, August 5–9, 2002, Vancouver, ASME, New York (2002).
- [11] MARGOLIN, B. Z., SHVETSOVA, V. A., GULENKO, A. G., Radiation embrittlement modelling for reactor pressure vessel steels: I. Brittle fracture toughness prediction, p. 715–729 in International Journal of Pressure Vessels & Piping, No. 76 (1999).
- [12] MARGOLIN B. Z., GULENKO A. G., NIKOLAEV V. A., RYADKOV L. N., A new engineering method for prediction of the fracture toughness temperature dependence for RPV steels, p. 817–829 in International Journal of Pressure Vessels & Piping, No. 80 (2003).

APPENDIX F

CALCULATION OF CYCLIC CRACK GROWTH

Fatigue crack growth assessment is usually performed for real defects revealed by NDE. But in some cases fatigue crack growth assessment should be performed under PTS analysis with postulated defect. The necessity of performance of such assessment is regulated by the national codes. For example maximum technological defect possible to exist is considered as the postulated defect according to Russian Code [1] and fatigue crack growth assessment should be performed for this postulated defect.

The following is a summary of an analytical procedure for fatigue crack growth assessment:

- Determine the initial sizes of the crack (crack depth a_0 and crack length c_0) according to the used code. For the real defects revealed by NDE these sizes and the crack location should be determined according to the used code requirements;
- Determine the number of conditions (cyclic loads) for considered operational lifetime;
- Calculate K_I values for each condition. Some codes prescribes to use elastic fracture mechanic in this case;
- Calculate fatigue crack growth Δa with the following formula

$$\Delta a = \sum_{j=1}^{j=m} n_j \left(\frac{da}{dN} \right)_j \quad (F1)$$

where m is the number of conditions (cyclic loads) for considered operational lifetime;

n_j is the number of cycles for each condition;

$\frac{da}{dN}$ is the crack growth rate defined by Paris law. It depends on stress intensity factor

range ΔK , stress intensity ratio factor R ($R=K_{\min}/K_{\max}$) and environment effect:

$$\frac{da}{dN} = C(\Delta K)^m$$

- finally the crack with the depth $a_p=a_0+\Delta a$ and the length $c_p=c_0+\Delta c$ is considered.

This is a common way for fatigue crack growth assessment prescribed by all national codes. The following parameters are important for fatigue crack growth calculations:

- Crack size. Fatigue growth is insignificant for cracks with the depth less than 10% of RPV wall thickness (especially for sub-cladding cracks) in the cylindrical part of RPV. But it should be essentially higher for deeper cracks and surface cracks;
- Crack location. Stresses under normal operation are significantly higher in RPV nozzle area than in RPV cylindrical part and fatigue growth of the crack at the nozzle area is essentially higher in comparison with the fatigue crack growth in RPV cylindrical part;
- Paris law coefficients. Environment effect is important for surface cracks and it leads to increasing of the crack growth. A higher values of coefficient R also leads to increasing of the crack growth. Russian Standard MRKR-SKhR-2004 and VERLIFE procedure prescribes to use the same Paris law coefficients for WWER RPV materials:

for the cladding:

on the air:

$$\frac{da}{dN} = 5.2 \cdot 10^{-12} \left(\frac{\Delta K}{(1-R)^{0.25}} \right)^{3.3} \quad (F2)$$

taking into account environment effect:

$$\frac{da}{dN} = 1.04 \cdot 10^{-11} \left(\frac{\Delta K}{(1-R)^{0.25}} \right)^{3.3} \quad (F3)$$

for the base and weld metals:

on the air:

$$\frac{da}{dN} = 2.8 \cdot 10^{-11} \left(\frac{\Delta K}{(1-R)^{0.25}} \right)^{2.7} \quad (F4)$$

taking into account environment effect:

$$\frac{da}{dN} = 2.1 \cdot 10^{-17} \left(\frac{\Delta K}{(1-R)^{0.5}} \right)^{7.2} \quad \text{at } \Delta K/(1-R)^{0.5} < 31.8 \quad (F5)$$

$$\frac{da}{dN} = 1.08 \cdot 10^{-8} \left(\frac{\Delta K}{(1-R)^{0.5}} \right)^{1.4} \quad \text{at } \Delta K/(1-R)^{0.5} \geq 31.8 \quad (F6)$$

where ΔK - stress intensity factor range,

R - stress intensity ratio factor ($R=K_{\min}/K_{\max}$), $\frac{da}{dN}$ in $\frac{m}{\text{cycle}}$, ΔK in $\text{MPa}\sqrt{m}$.

Fatigue crack growth laws for PWR environment are presented in the Table F1.

— K_I estimation. Analytical formulas or FEM calculations can be applied for K_I estimation by the appropriate way.

Table F1 – Fatigue crack growth laws for PWR environment

Material	$\frac{da}{dN} = C \Delta K_{eff}^n$ $\left(\frac{da}{dN} \text{ in m/cycle}, \Delta K_{eff}, \Delta K_{cp} \text{ in MPa}\sqrt{m} \right)$		
	R	Level of ΔK ($\text{MPa}\sqrt{m}$)	Safe laws
Low-alloy steel type 16 MND 5, SA 508 cl 3 or SA 533 gr B, 20 MN5 M.	≤ 0.3	$\Delta K_{cp} < 16.5$	Select the less favourable of the following 2 laws: $da/dN = 1.64 \cdot 10^{-16} (\Delta K_{eff})^8$ calculation of ΔK_{eff} according to II.1 with: $f(R) = 1$ $da/dN = 7.95 \cdot 10^{-12} (\Delta K_{eff})^{2.93}$ calculation of ΔK_{eff} according to II.1 with: $f(R) = \frac{1}{(1-R)^{0.25}}$
		$16.5 \leq \Delta K_{cp} < 100$	$da/dN = 1.98 \cdot 10^{-8} (\Delta K_{eff})^{1.4}$ calculation of ΔK_{eff} according to II.1 with: $f(R) = 1$
		$\Delta K_{cp} \geq 100$	$da/dN = 4.75 \cdot 10^{-13} (\Delta K_{eff})^{3.73}$ calculation of ΔK_{eff} according to II.1 with: $f(R) = 1$

Table F1 – Fatigue crack growth laws for PWR environment (continued)

Material	$da/dN = C \Delta K_{eff}^n$ $\left(da/dN \text{ in m/cycle}, \Delta K_{eff}, \Delta K_{cp} \text{ in MPa}\sqrt{m} \right)$		
	R	Level of ΔK (MPa \sqrt{m})	Safe laws
Low-alloy steel type 16 MND 5, SA 508 cl 3 or SA 533 gr B, 20 MN5 M.	≥ 0.6	$\Delta K_{cp} < 12$	Select the less favourable of the following 2 laws: $da/dN = 5.21 \cdot 10^{-15} (\Delta K_{eff})^8$ calculation of ΔK_{eff} according to II.1 with: $f(R) = 1$ $da/dN = 7.95 \cdot 10^{-12} (\Delta K_{eff})^{2.93}$ calculation of ΔK_{eff} according to II.1 with: $f(R) = \begin{cases} \text{for } R \leq 0.9 : \\ \frac{1}{(1-R)^{0.25}} \\ \text{for } R > 0.9 : \\ \frac{1}{(1-R/2)} \end{cases}$
		$\Delta K_{cp} \geq 12$	$da/dN = 7.03 \cdot 10^{-8} (\Delta K_{eff})^{1.4}$ calculation of ΔK_{eff} according to II.1 with: $f(R) = 1$
	$0.3 < R < 0.6$	Linear interpolation on coefficient C	

Table F1 – Fatigue crack growth laws for PWR environment (continued)

MATERIAL	$\frac{da}{dN} = C \Delta K_{eff}^n$ $\left(\frac{da}{dN} \text{ in m/cycle}, \Delta K_{eff}, \Delta K_{cp} \text{ in MPa}\sqrt{\text{m}} \right)$
Low-alloy steel type 16 MND 5 (SA 533 grade B cl. 1 or SA 508 cl.3) and related welded joints with a low sulphur content $S < 0.007\%$	$n = 3.13$ 2-standard deviations law: $C = 2.57 \times 10^{-11}$ average law: $C = 1.47 \times 10^{-11}$ calculation of ΔK_{eff} according to II.1 with: - for $\Delta K_{cp} \leq 20$: $f(R) = \frac{1}{(1-R)^{0.25}}$ for $R \leq 0.9$ $f(R) = \frac{1}{1 - \frac{R}{2}}$ for $R > 0.9$ - for $\Delta K_{cp} \geq 40$: $f(R) = 1$ - for $20 < \Delta K_{cp} < 40$: $f(R)$ is interpolated between the value for $\Delta K_{cp} < 20$ and the value for $\Delta K_{cp} \geq 40$
Forged or rolled austenitic stainless steel and related welded joints	$n = 4$ 2-standard deviations law: $C = 1.8 \times 10^{-12}$ mean law: $C = 6.5 \times 10^{-13}$ calculation of ΔK_{eff} according to II.1 with: $f(R) = \frac{1}{\left(1 - \frac{R}{2}\right)}$

Table F1 – Fatigue crack growth laws for PWR environment (continued)

Material	Level of ΔK (MPa \sqrt{m})	$\frac{da}{dN} = C \Delta K_{eff}^n$ $\left(\frac{da}{dN} \text{ in m/cycle}, \Delta K_{eff}, \Delta K_{cp} \text{ in MPa}\sqrt{m} \right)$
Low-alloy steel type 16 MND 5 (SA 508 cl. 3 or SA 533 gr. B)	$\Delta K \leq 20$	$\frac{da}{dN} = 3.975 \cdot 10^{-12} (\Delta K_{eff})^{2.93}$ calculation of ΔK_{eff} according to II.1 with: for $R \leq 0.9$: $f(R) = \frac{\Delta k}{(1-R)^{0.25}}$ for $R > 0.9$: $f(R) = \frac{\Delta k}{\left(1 - \frac{R}{2}\right)}$
	$20 < \Delta K < 60$	$\frac{da}{dN} = 1.3 \cdot 10^{-11} (\Delta K_{eff})^{2.67}$ calculation of ΔK_{eff} according to II.1 with: $f(R) = 1$
	$60 \leq \Delta K$	$\frac{da}{dN} = 2.375 \cdot 10^{-13} (\Delta K_{eff})^{3.73}$ calculation of ΔK_{eff} according to II.1 with: $f(R) = 1$
Stainless steel	All ΔK	$\frac{da}{dN} = 1.875 \cdot 10^{-13} (\Delta K_{eff})^4$ calculation of ΔK_{eff} according to II.1 with: $\Delta K_{eff} = \frac{\Delta K}{1 - \frac{R}{2}}$

References

- [1] CALCULATION PROCEDURE FOR EVALUATION OF BRITTLE STRENGTH OF VVER RPV DURING OPERATION, MRKR-SKhr-2004, RD EO 0606-2005, St. Petersburg, Moscow (2004).
- [2] UNIFIED PROCEDURE FOR LIFETIME ASSESSMENT OF COMPONENTS AND PIPING IN VVER NPPS "VERLIFE", Version 5, Řež (2003).

APPENDIX G

EXAMPLES OF NOZZLE ANALYSIS

1. Introduction

Within the PTS analysis it is necessary to show that the integrity criteria are satisfied for postulated defects located at the RPV locations with the worst properties, highest neutron fluence and also for the maximum tensile stresses. Under PTS transient the latter act at the nozzle area and this location should be considered in the PTS analysis. Examples of PTS analysis for the nozzles are presented below (WWER and PWR). Analytical formula for stress intensity factor for crack at the nozzle corner under pressure loading is available in Appendix D (accepted solution according to [1]).

2. WWER example

PTS analysis was performed for the WWER-1000 RPV. Analysis was performed for the list of transients. These transients were selected according to [2]. Global parameters were computed with the Russian Code TRAP. Thermal input (fluid temperature distribution and RPV wall-to-fluid heat transfer coefficient distribution) were computed with the code OKBMIX (see Appendix C). Figure G1 presents the fluid temperature distribution and RPV wall-to-fluid heat transfer coefficient distribution at the RPV inner surface.

On the first step, the elastic calculations were performed for all considered transients. RPV 3D FE mesh used in elastic analysis is presented on Figure G2. Calculations were performed with the use of MSC.Marc code. Stress intensity factor was calculated with the use of analytical formulae. All inlet and outlet nozzles (with cold ECCS water injection) were considered. Different crack positions (cross sections) at the nozzle corner were considered (Figure G3). Minimum allowable critical temperature T_k^a was obtained for all crack locations and positions under each considered transient. Governing transient and postulated crack location and position for the nozzle area were obtained on the basis of these calculations results.

On the second step, the elastic-plastic calculation of J-integral was performed for the governing postulated crack location and position for the governing transient. "Primary to secondary LOCA" was considered as the governing transient. Postulated crack at the lower corner of inlet nozzle D_{nom} 850 (cold leg # 3) was considered.

According to [3] the axial under-cladding semi-elliptical crack with initial depth $a_0 = 0,07S = 20$ mm and length $2c_0 = 6a_0 = 120$ mm was assumed as the calculated crack. Cyclic crack growth calculation for service lifetime was performed and the crack with the depth of 26 mm and the length of 156 mm was considered in the further analysis.

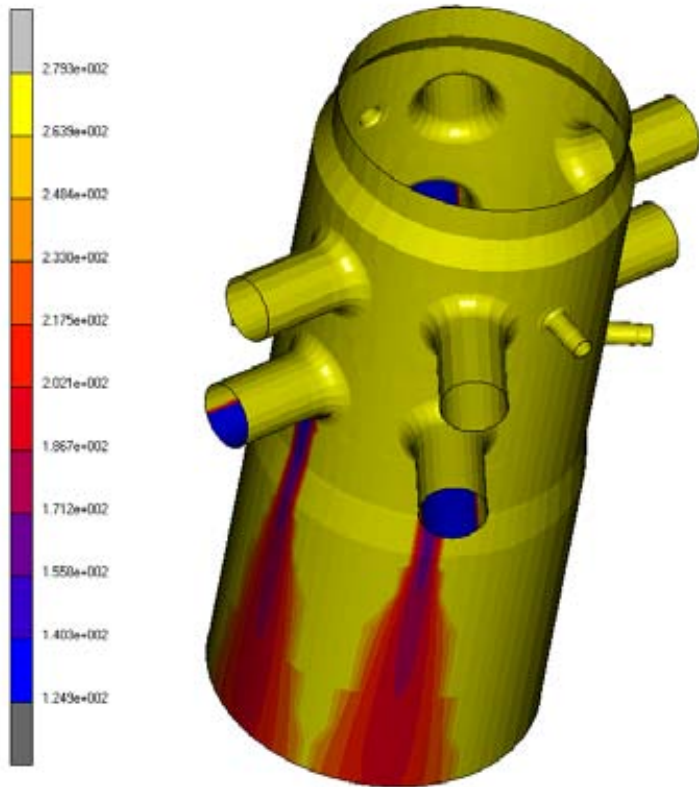


FIG. G1 – Temperature distribution at the RPV inner surface.

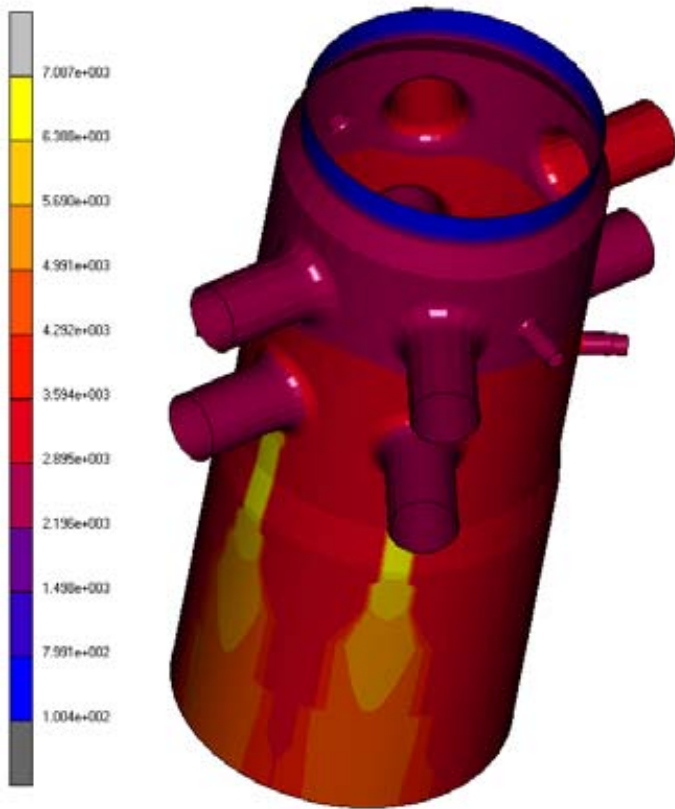


FIG. G2 – Heat transfer coefficients distribution at the RPV inner surface.

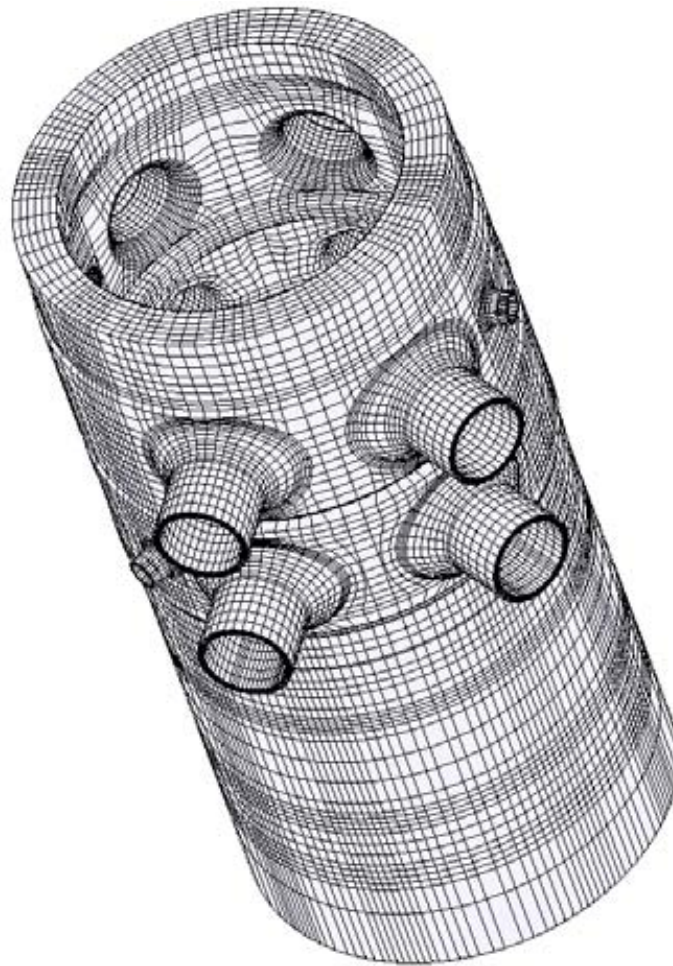


FIG. G3 – RPV 3D FE mesh.

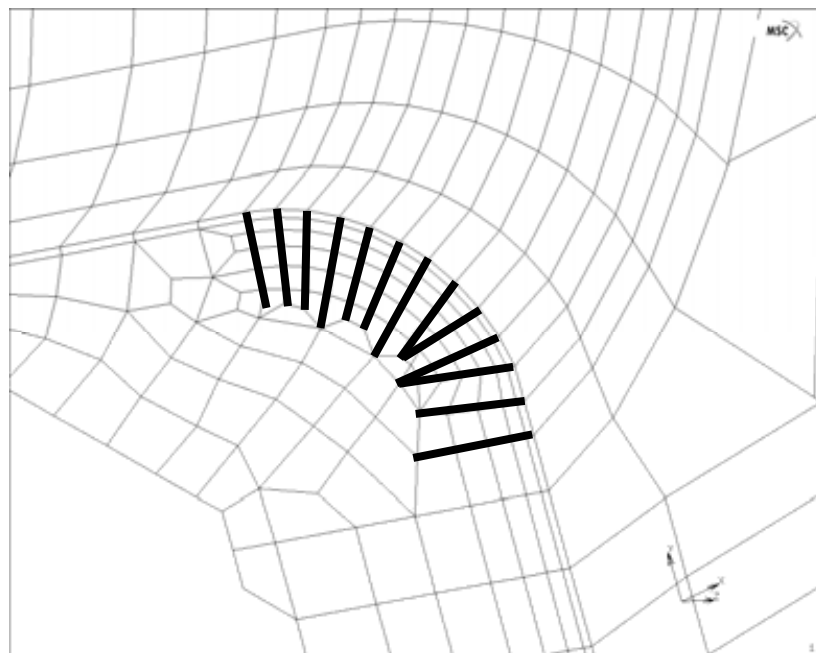


FIG G4 – Considered cross sections (crack positions).

Residual stresses and plastic strains in the cladding and in the RPV nozzle area base metal (due to the cladding manufacturing) were taken into account according to [3]. These stresses and strains were simulated by specially selected thermal loading. Hydrotest effect was simulated by pressure loading under the appropriate temperature.

FE models of inlet nozzle D_{nom} 850 with crack simulation are presented on figures G4 and G5. Figure G5 presents finite element model of inlet nozzle D_{nom} 850 with simulation of the crack front in the base metal. Figure G6 presents finite element model of inlet nozzle D_{nom} 850 with simulation of the crack front in the cladding. "Global-local" option provided by MSC.Marc code. Finite element mesh presented at the Figure G3 was used as the global model.

Results of $(K_I)_4$ calculation for the crack front points in the base metal are presented on figures G7 and G8. $(K_I)_4$ values were obtained from KJ with application of appropriate margin factor 1,1 ($(K_I)_4=1,1K_I$). Results of $(K_I)_4$ calculation were used in the integral approach calculations. Minimum allowable critical temperature value T_k^a was obtained from the integral approach calculation results (See Table G1, formulae for α and Z parameters are presented in Appendix H). The integral approach calculation was performed. Base curve approach was used and WPS effect was taken into account in calculations.

The integrity assessment of the cladding was performed with the use of K_I calculation results for the crack front points in the cladding (Figure G9). Evaluation of ductile tearing risk was performed for the cladding according to [3].

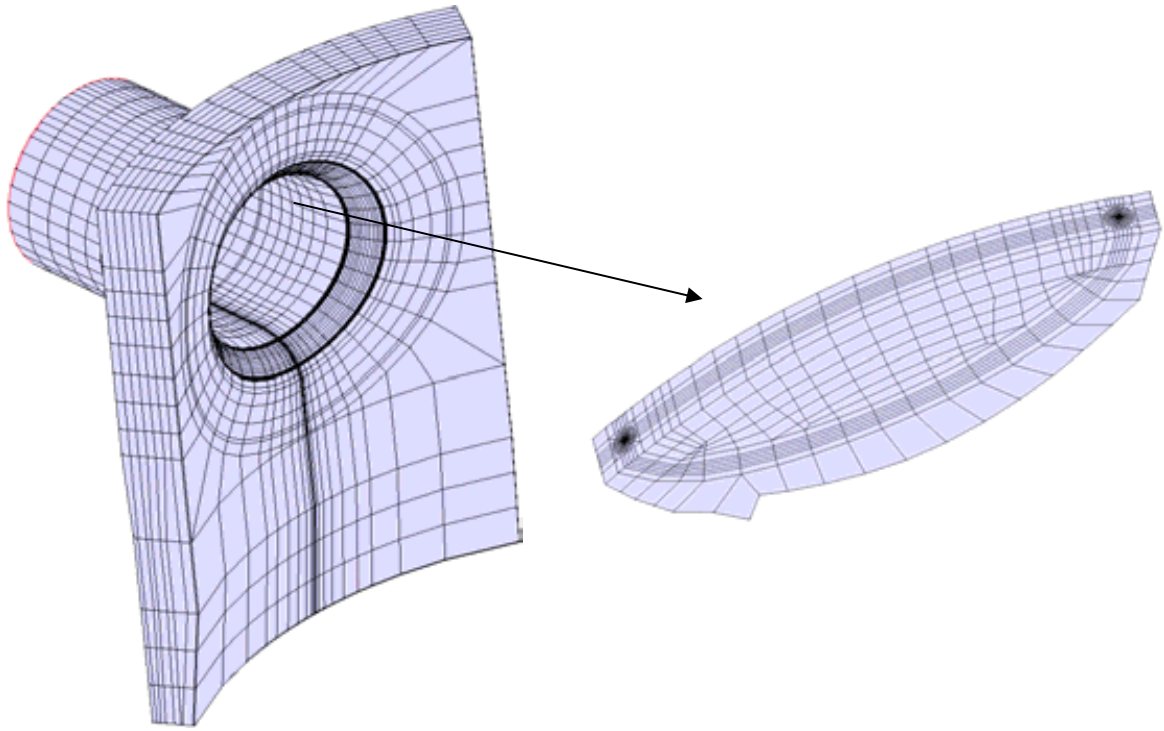


FIG. G5 – FE model of inlet nozzle Dnom 850 with simulation of the crack front in the base metal.

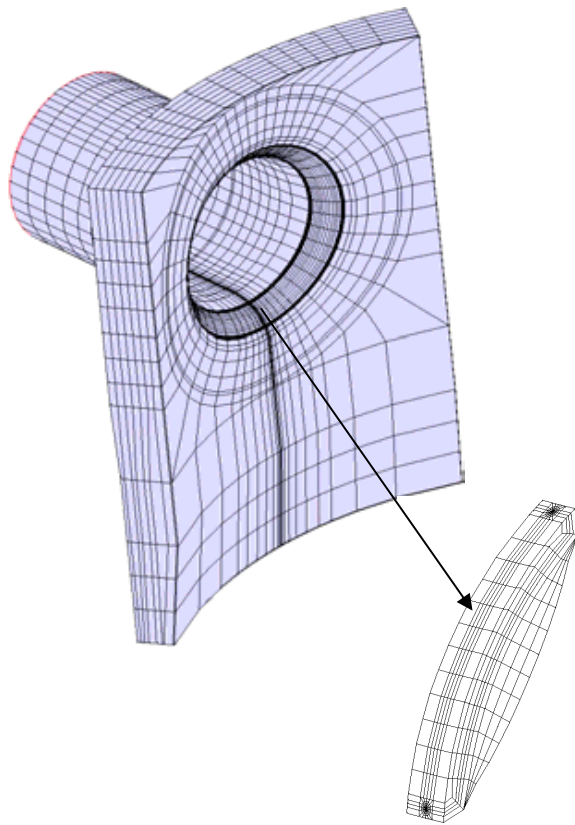


FIG. G6 – FE model of inlet nozzle Dnom 850 with simulation of the crack front in the cladding.

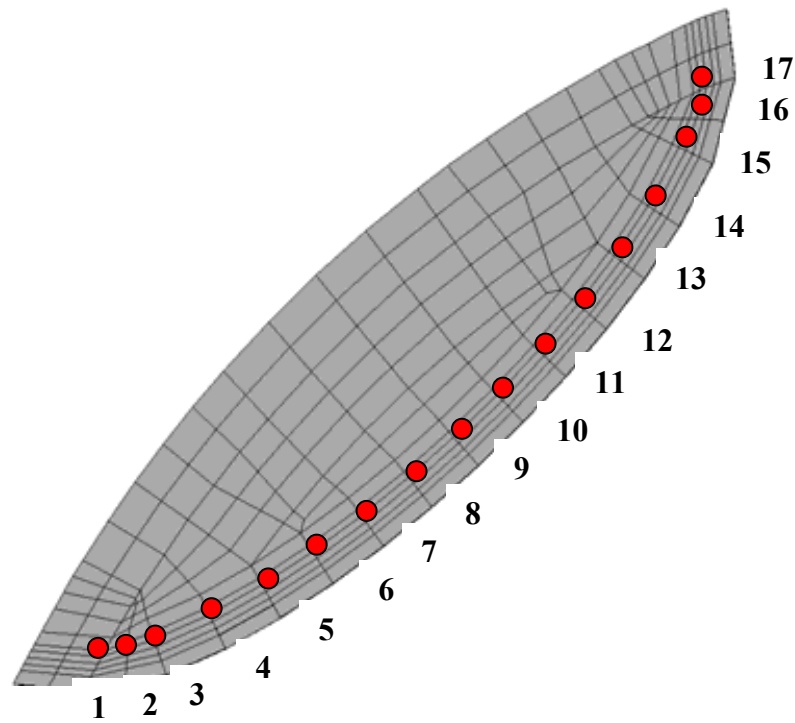
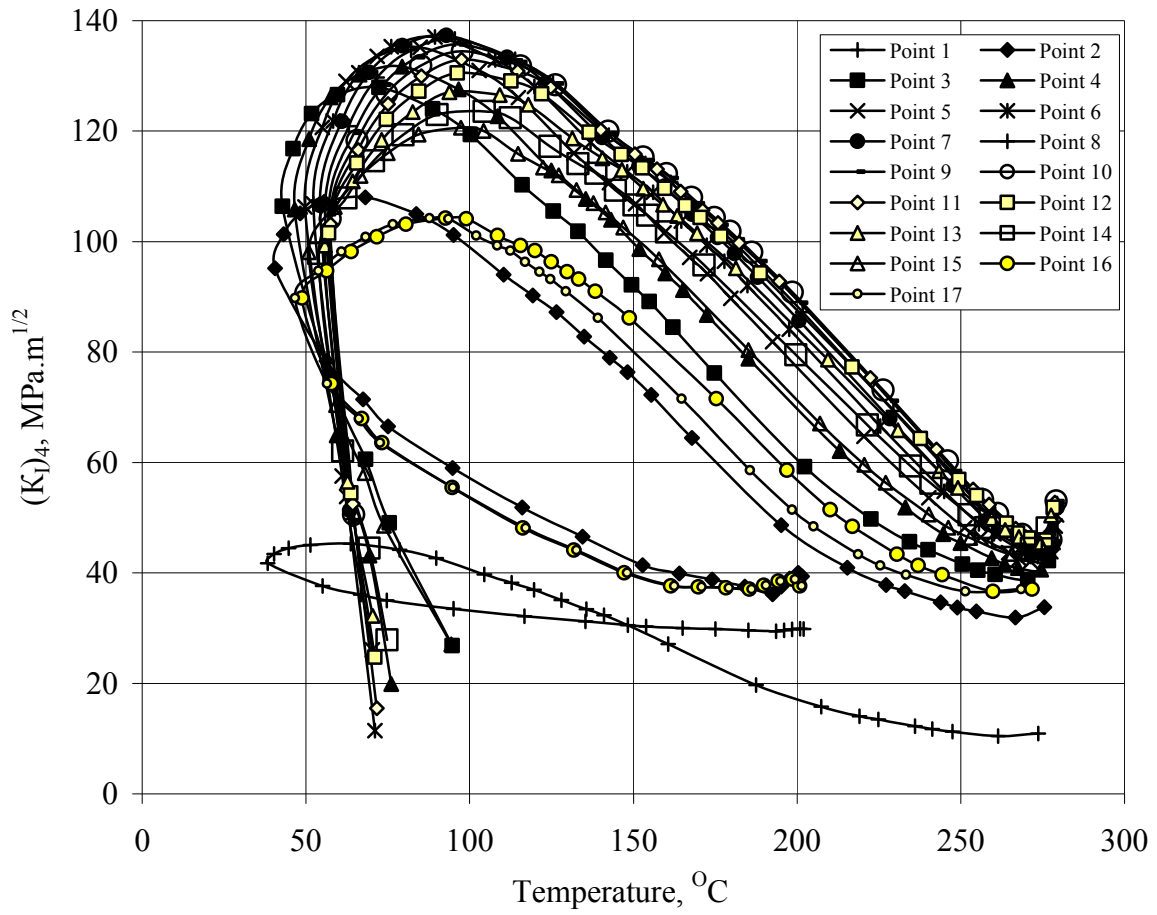


FIG. G7 – Primary to secondary LOCA. Results of $(K_I)_4$ calculation for the crack front point in the base metal. $(K_I)_4$ -temperature curves.

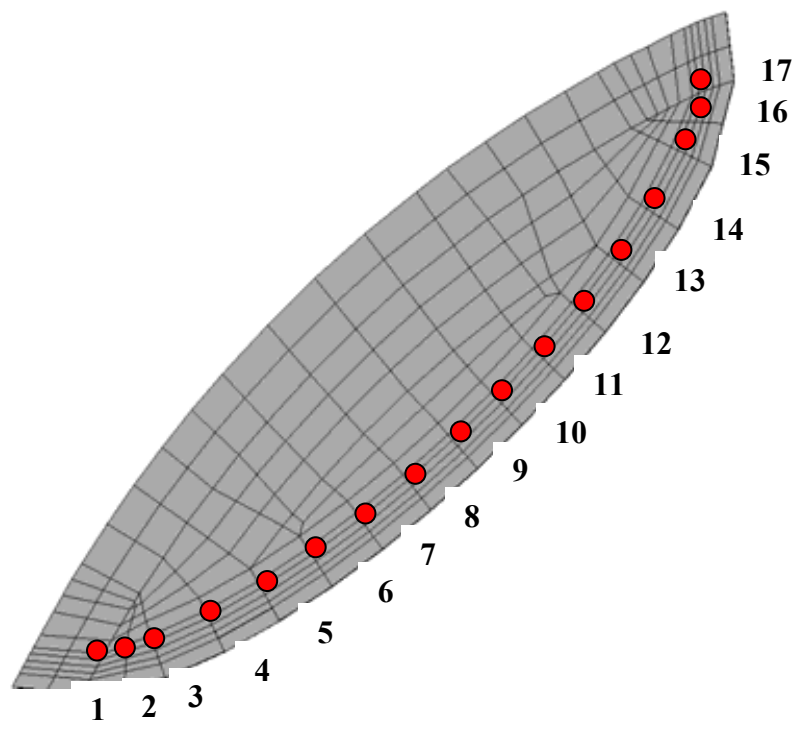
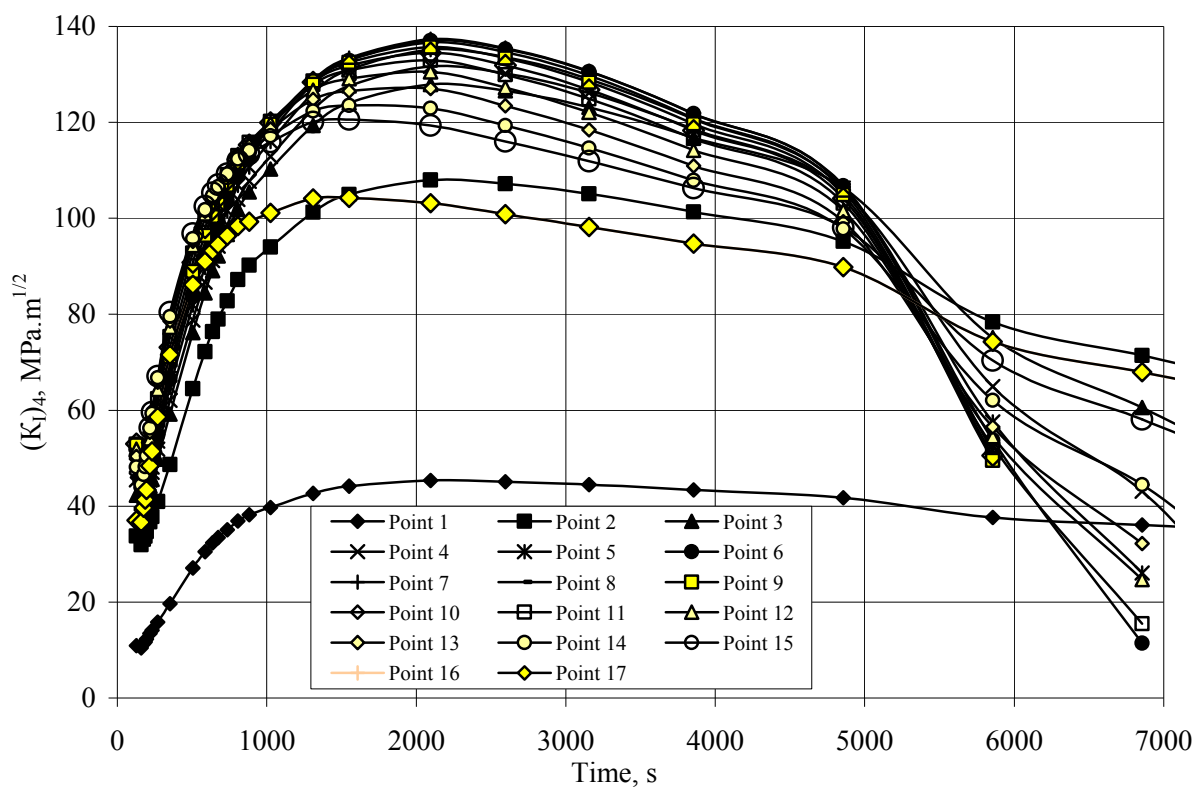


FIG. G8 – Primary to secondary LOCA. Results of $(K_I)_4$ calculation for the crack front point in the base metal. $(K_I)_4$ -transient time curves.

Table G1 – Primary to secondary LOCA. Inlet nozzle Dnom 850. Integral approach calculation

Point	Crack front length coordinate, mm	Time moment corresponding to the α parameter maximum, s	Temperature, °C	K_{IC} , MPa·m ^{1/2}	$(K_I)_4$, MPa·m ^{1/2}	Z parameter
1	0,00	3856,07	40,29	88,16	43,99	0,02
2	5,11	3856,07	43,23	91,91	101,46	1,65
3	10,17	3856,07	46,16	95,85	116,84	2,66
4	20,46	3856,07	51,01	102,89	118,58	2,00
5	30,69	3856,07	55,00	109,18	120,65	1,62
6	40,91	3856,07	58,32	114,78	121,85	1,33
7	51,15	3856,07	61,01	119,60	121,78	1,09
8	61,37	3856,07	63,14	123,58	120,87	0,90
9	71,60	3856,07	64,69	126,60	119,67	0,76
10	81,83	3856,07	65,64	128,49	118,28	0,67
11	92,06	4856,07	57,49	113,36	103,13	0,63
12	102,29	4856,07	56,95	112,43	101,56	0,61
13	112,52	4856,07	55,75	110,42	99,27	0,59
14	122,74	4856,07	53,86	107,33	97,83	0,63
15	133,99	4856,07	50,86	102,66	98,01	0,79
16	139,56	4856,07	48,78	99,57	89,80	0,59
17	145,13	4856,07	46,63	96,51	89,80	0,69

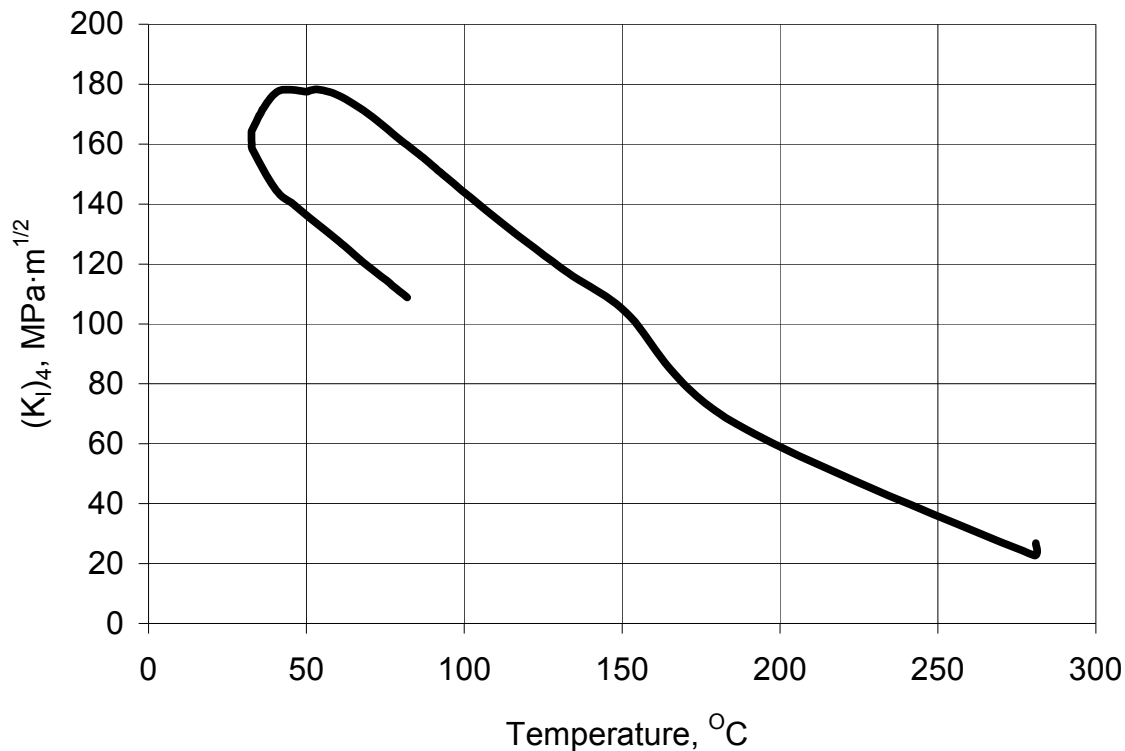


FIG. G9 – Primary to secondary LOCA. Results of $(K_I)_4$ calculation for the crack front point in the cladding (maximum $(K_I)_4$ values).

3. Example of nozzle integrity assessment for PWR

The following presents the German experience of PTS analysis on nozzle for PWR. Global parameters (e.g. primary system absolute pressure, natural circulation mass flow rates, safety injection (ECCS) rates) were computed with the Code RELAP5/MOD3.2 and the fluid temperature distribution and RPV wall-to-fluid heat transfer coefficient distribution in downcomer and inside the RPV-nozzles were computed with the code KWU-MIX (based on results of full scale experiments, see Appendix C). Both codes are validated by German authority.

KWU-Mix code take into account mechanisms like stratification and stripe / plume effect:

For stratification, when Emergency Core Cooling ECC water is injected, the cold ECC water mixes with the hotter ambient water in the leg. Hot water is flowing from the downcomer into the cold leg respectively from the upper plenum into hot leg and along the upper part of the leg flow area to the mixing location whereas mixed colder water counter-flows to the hot water along the lower part of the leg flow area to RPV inlet respectively into the upper plenum.

There are two possible flow patterns near the ECC injection locations in the cold legs and in hot leg: Stratified flow and flow circulation (Figure G10).

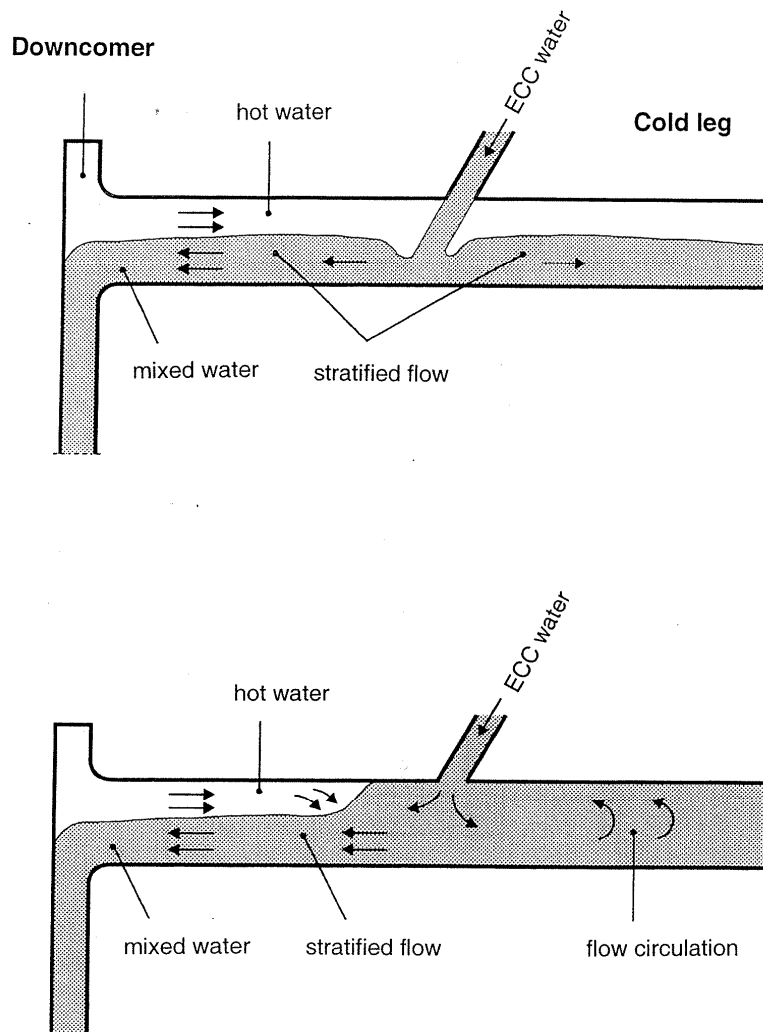


FIG. G10 – Flow pattern during ECC injection.

Thermal hydraulic code delivers the boundary data of the 3D finite element model like water level in nozzle, heat transfer coefficient, fluid temperature as well as inner pressure during the transient. The most severe loading concerning the nozzle area were small LOCA transient (small leak leading to no natural circulation and no significant pressure decrease in the RPV during the transient).

Thermal and mechanical analyses are treated as an uncoupled problem with the commercial software ABAQUS and 3D model is considered due to the complexity of the thermal hydraulic boundary. Typical temperature distribution during LOCA from [4] in German RPVs is represented in Figure G11. Corresponding tangential stresses are in Figure G12. Residual stresses in the cladding due to cladding manufacturing are simulated with the use of free-stress temperature.

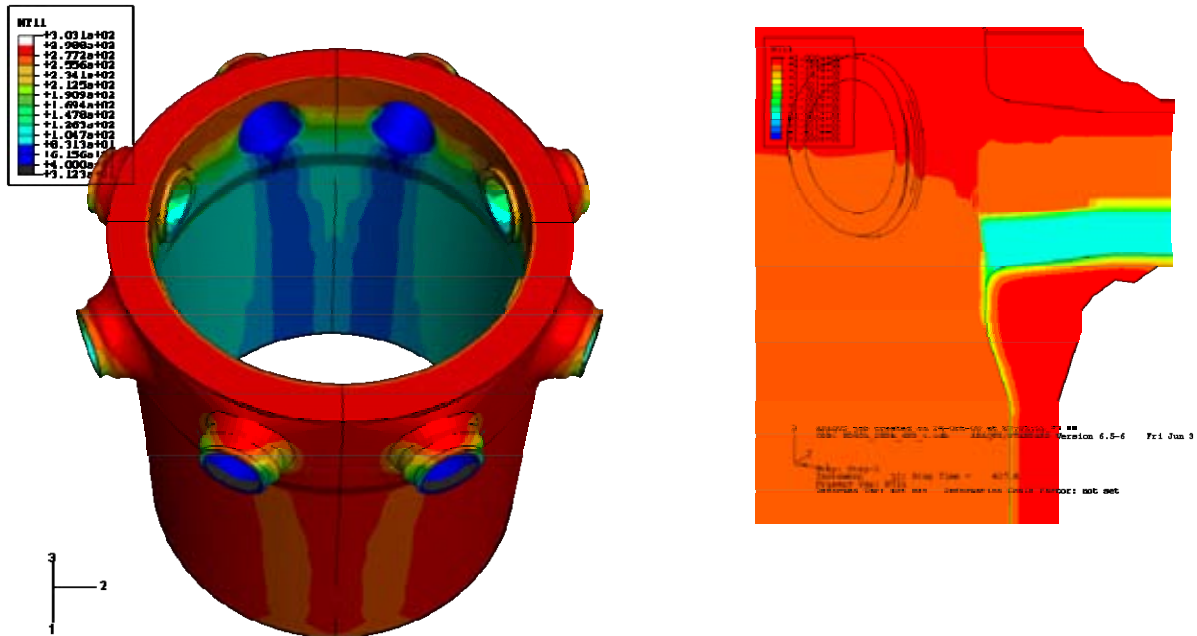


FIG. G11 – Temperature calculation under small LOCA hot legs 40cm^2 break (global model and inlet nozzle region) for KONVOI model.

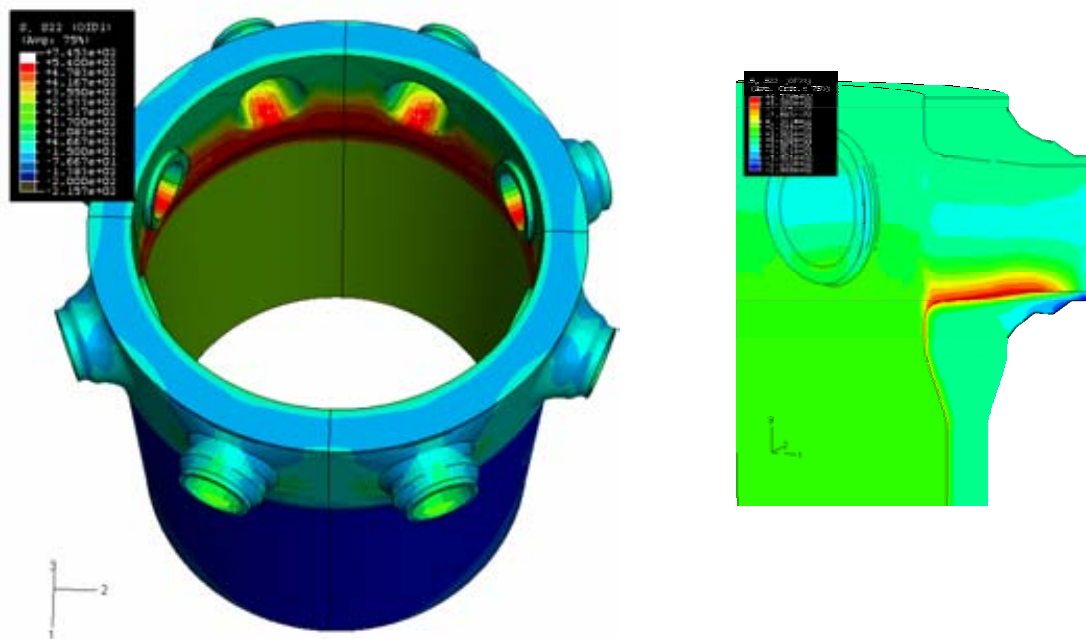


FIG. G12 – Tangential stress calculation under small LOCA at the inlet nozzle region.

In the case of the study published in [4] for German NPPs, under-clad crack were postulated (because the RPVs were crack free after the fabrication) at the inlet and outlet nozzle. The NDE sensibility is 5 mm, application of a safety margin of 2 yields to consideration of a crack with a depth of 10 mm in the base material. The crack shape $a/2c=1/6$ was considered.

Analytical solution of K_I could be considered for postulated crack depth selection (parameter study) only if results are validated by comparison 3D FE model with crack.

Once the crack has been defined, an additional finite element sub-model analysis with postulated crack is performed. This is a part of the global model, temperature and stresses are used as input boundary for the local analysis.

A sub-model of the nozzle corner is shown in Figure G13. The 6 o'clock position is seen in the centre of the model. Around the crack front typical fracture mechanics elements with independent crack tip nodes are used. Details of postulated crack in outlet nozzle are in Figure G14.

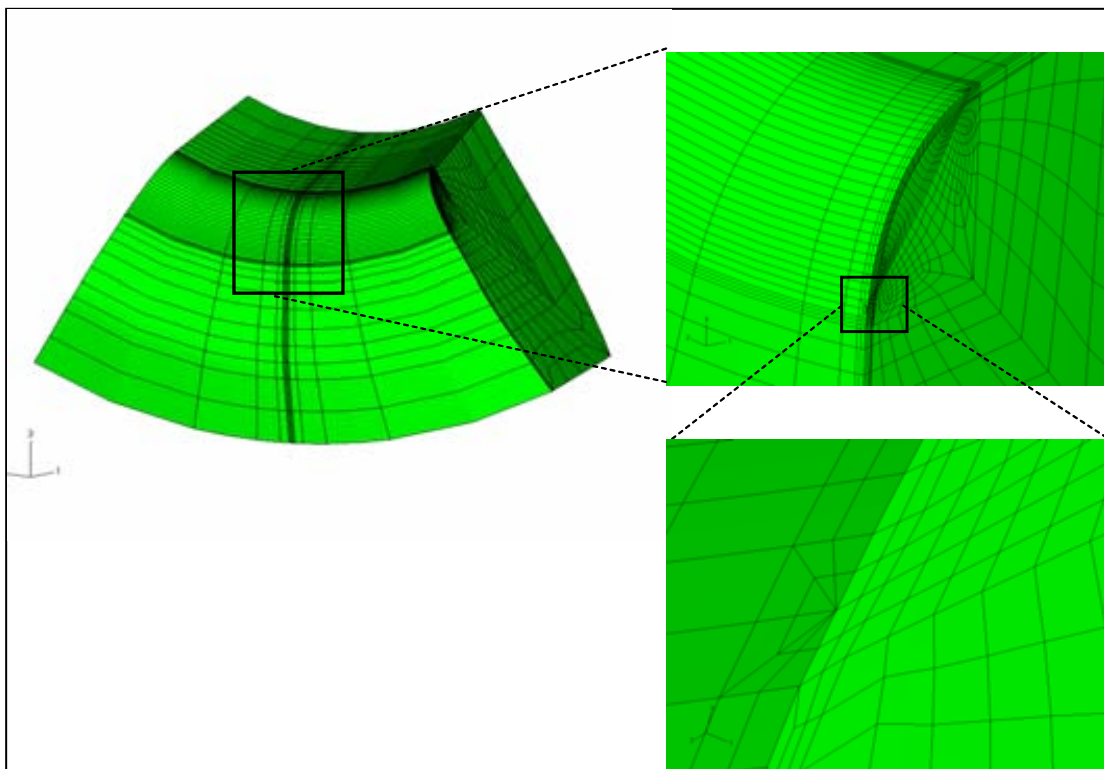


FIG. G13 – Detail of the inlet nozzle corner crack with straight crack front in base material.

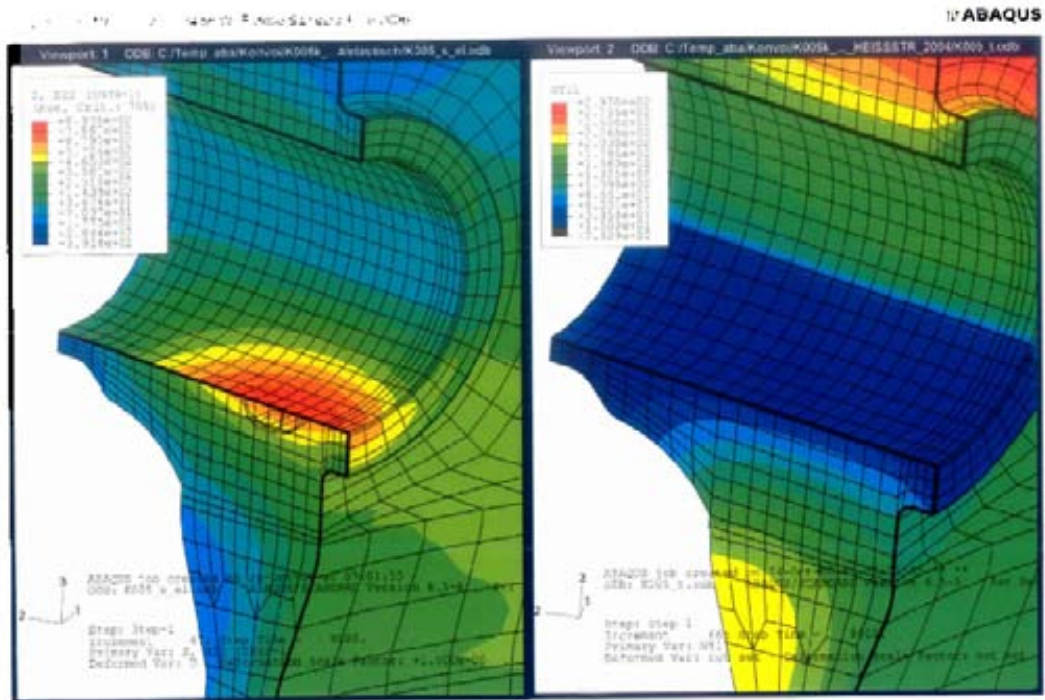


FIG. G14 – Detail of the outlet nozzle corner crack with half elliptical shape in base material.

The J integral is evaluated on both crack front (in base metal and cladding). Stress intensity factors along the crack front in base are calculated from the J-integral and are compared with K_{IC} curve.

The maximum J-integral along the crack front for each time of the transient is considered for further calculation of the stress intensity factor K_I according the following equation, where E is the Young modulus and ν the Poisson number.

$$K_I = \sqrt{\frac{E \cdot J}{1 - \nu^2}} \quad (G1)$$

The stress intensity factors K_I and the temperature for the corresponding position are reported in Figure G15 as well as the material toughness curve (RT_{NDT} concept), with and without taking credit of the WPS effect as described in the KTA 3201.2 § 7.9.3.3.

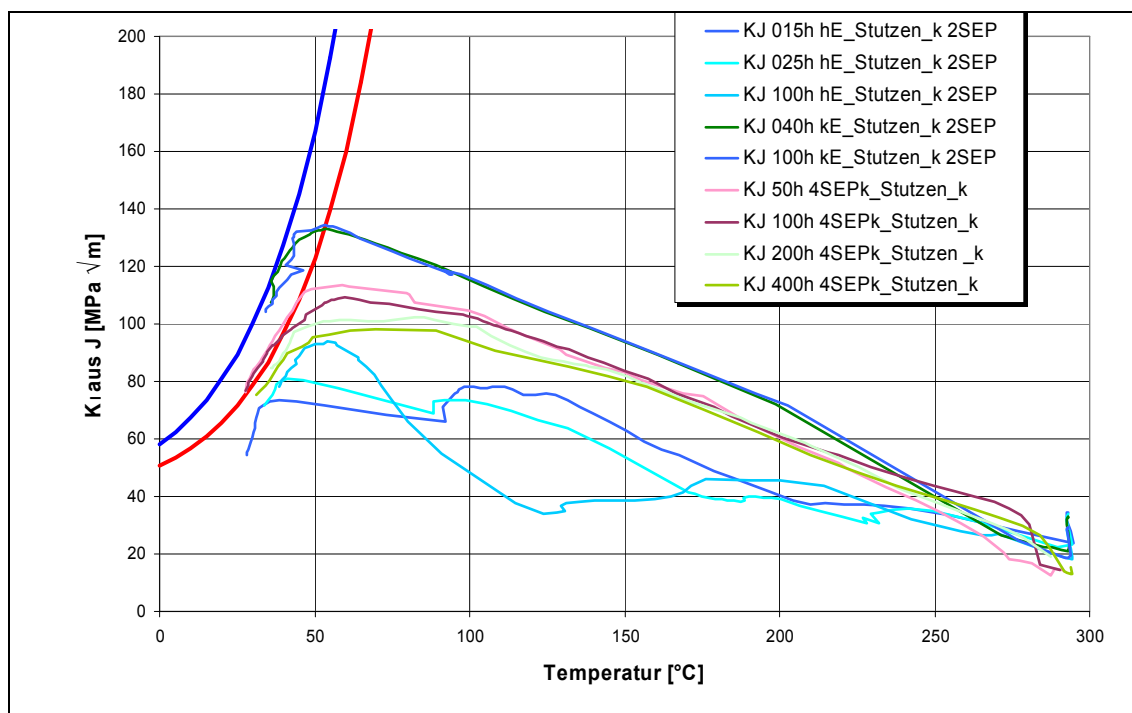


FIG. G15 – Comparison of results of inlet nozzle (ECC: cold/hot leg) during different LOCA for KONVOI plants.

The evaluation of tearing risk is performed by comparison of the K_I with the ductile tearing toughness K_{JC} .

$$K_{JC}^2 = \frac{E \cdot J_{0.2}}{1 - \nu^2} \text{ at crack tip or } K_{JC}^2 = E \cdot J_{0.2} \text{ at surface point} \quad (G2)$$

4. References

- [1] PVRC Recommendation on toughness requirements for ferritic materials, Welding Research Council Bulletin Series 175
- [2] INTERNATIONAL ATOMIC ENERGY AGENCY, Guidelines on Pressurized Thermal Shock Analysis for WWER Nuclear Power Plants, IAEA-EBP-WWER-08 Rev.1, IAEA, Vienna (2006).
- [3] CALCULATION PROCEDURE FOR EVALUATION OF BRITTLE STRENGTH OF VVER RPV DURING OPERATION, MRKR-SKhR-2004, RD EO 0606-2005, St. Petersburg, Moscow (2004).
- [4] KEIM, E., HERTLEIN, R., ILG, U., KÖNIG, G., SCHLÜTER, N., WIDERA, M., Brittle fracture safety analysis of RPV based on progressive thermo hydraulic analysis, Seminar “Werkstoff- & Bauteilverhalten in der Energie- & Anlagentechnik“, 11–12 October 2007, Stuttgart (2007).

NOMENCLATURE, ABBREVIATIONS AND SYMBOLS

a, c	Minor resp. major semi-axes of a postulated defect
a/c, 2a/c	Aspect ratio of a postulated semi-elliptical or elliptical defect
A_0	Water layer cross sectional area corresponding to D and water height 0,725 H_c
A_5	Total elongation
ABB-CE	Combustion Engineering
AEKI	Atomic Energy Research Institute
A_F^T	Irradiation embrittlement factor at irradiation temperature T
AMES	Ageing Management European Strategy
ASME	American Society of Mechanical Engineers
ASTM	American Society for Testing and Materials
B_i	Crack front length
BM	Base metal
BWR	Boiling water reactor
CEA	Commissariat à l'Energie Atomique (Atomic Energy Committee)
CDF	Crack driving force
C_f	Wall friction factor
CFD	Computational fluid dynamics
CFR	Code of Federal Regulations
c_p	Specific heat
CRISM	Central Research Institute of Structural Materials
CRP	Coordinated research programme
c_w	Specific heat of water at constant pressure
DBA	Design basis accident
DFM	Deterministic fracture mechanics
E	Young's modulus
EC	European Commission
ECC	Emergency core coolant
ECCS	Emergency core cooling system
EdF	Electricité de France
EPFM	Elastic plastic fracture mechanics
FE	Finite element
FEM	Finite element method
FF	Fluence factor
F_n	Neutron fluence
Δh	Elevation difference between nozzle outlet and cold leg water surface
HAZ	Heat affected zone
HPI	High pressure injection
HTC	Heat transfer coefficient
IAEA	International Atomic Energy Agency
IASCC	Irradiation assisted stress corrosion cracking
ISI	In-service inspection
ISO	International Organization for Standardization
JEAC/JEA	Japanese Electric Association

J-R	J-integral-resistance
JRC	Joint Research Centre
JRQ	Japan Reference Quality
KCV	Impact strength (measured value in CVN impact test)
KFKI	Atomic Energy Research Institute
K_I	Stress intensity factor
$K_{IC}; K_{JC}$	Fracture toughness
KINS	Korean Institute of Nuclear Safety
KTA	Nuclear Technical Commission
KWU	Kraftwerk Union AG
LEFM	Linear elastic fracture mechanics
LOCA	Loss of coolant accident
LOFA	Loss of flow accident
LTOP	Low-temperature overpressure protection
LWR	Light water reactor
MS	Member States
NDE	Non-destructive examination
NDT	Non-destructive testing / Nil-ductility temperature
NPP	Nuclear power plant
NRC	Nuclear Regulatory Commission
NRI	Nuclear Research Institute Řež plc
NUSS	IAEA Nuclear Safety Standards
OKB	Experimental Design Bureau
ORNL	Oak Ridge National Laboratories
PFM	Probabilistic fracture mechanics
PSA	Probabilistic safety assessment
P-T	Pressure-temperature
PTS	Pressurized thermal shock
PWR	Pressurized water reactor
R_m	Ultimate tensile strength
$R_{p0.2}$	Yield strength
RPV	Reactor pressure vessel
RT_{NDT}	Reference temperature
SAR	Safety analysis report
SI	Structural integrity
SIF	Stress intensity factor
SNERDI	Shanghai Nuclear Engineering Research and Design Institute, China
SSC	System, structure and component
T_0	Transition temperature
T_0^{ini}	Initial value of transition temperature
TEM	Transmission electron microscopy
ΔT_F	Shift in T_k due to irradiation
$\Delta T_{F, res}$	Residual shift in T_k after annealing
THM	Thermal-hydraulic mixing
T_{irr}	Irradiation temperature

T_k	Ductile-brittle transition temperature; critical temperature of brittleness
T_{k0}	Initial ductile-brittle transition temperature
T_k^a	Maximum allowable critical brittle fracture temperature
T_{k0}	Initial value of critical brittle fracture temperature
ΔT_n	Shift in T_k due to fatigue damage
T_R	Reference temperature
TRS	Technical Report Series
TT	Transition temperature
ΔT_T	Shift in T_k due to thermal ageing
TWCF	Through-wall cracking frequency
UK	United Kingdom
US	United States
USA	United States of America
USE	Upper shelf energy
V_0	Mean water velocity at cold leg outlet corresponding to water height 0,725 H_c
Vol_{mix}	Mixing volume
VERLIFE	Unified procedure for lifetime assessment of components and piping in WWER NPPs
VUJE	Nuclear Power Plant Research Institute
VVER	(see WWER)
WM	Weld metal
WPS	Warm prestress
WWER	Water cooled water moderated power reactor
α	Coefficient of linear thermal expansion / Heat transfer coefficient
β	Coefficient of thermal expansion of water
ε	Dissipation; power loss per unit liquid mass in the mixing volume V_{mix}
ν	Poisson's ratio
λ	Thermal conductivity
ρ	Density
$\Delta\rho$	Density difference cold fluid - hot fluid
σ	Standard deviation
ν	Cinematic viscosity
τ_w	Wall sheer stress
Φ	Top angle in a vertical triangle with top edge at the cold leg centre line and with base line formed by the hot layer/cold layer interface
Θ	Angle formed by the centre line of the injection nozzle and the cold leg centre line

CONTRIBUTORS TO DRAFTING AND REVIEW

Akbashev, I.	Experimental Design Bureau (OKB) Hidropress Russian Federation
Blasset, S.	AREVA NP GmbH Germany
Brumovský, M.	Nuclear Research Institute Řež plc Czech Republic
Chapuliot, S	Commissariat à l'Energie Atomique (CEA) France
Costzlev, V.	Central Research Institute of Structural Materials, Prometey Russian Federation
Ézsöl, G.	Atomic Energy Research Institute (AEKI KFKI) Budapest Hungary
Faidy, C.	Electricité de France France
Fekete, T.	Atomic Energy Research Institute Budapest Hungary
He, Y.	Shanghai Nuclear Engineering Research and Design Institute China
Hermanský, P.	Nuclear Power Plant Research Institute (VUJE) Slovakia
Hertlein, R.	AREVA NP GmbH Germany
Hrázsky, M.	Nuclear Power Plant Research Institute (VUJE) Slovakia
Jo Jhung, M.	Korean Institute of Nuclear Safety Republic of Korea
Kang, K.S.	International Atomic Energy Agency
Keim, E.	AREVA NP GmbH Germany
Kupca, L.	International Atomic Energy Agency
Margolin, B.	Central Research Institute of Structural Materials, Prometey Russian Federation
Neuvonen, A.	Fortum Nuclear Services Finland
Piminov, V.	Experimental Design Bureau (OKB) Hidropress Russian Federation
Pišťora, V.	Nuclear Research Institute Řež plc Czech Republic
Taylor, N.	Institute for Energy EC-Joint Research Centre Netherlands



Where to order IAEA publications

In the following countries IAEA publications may be purchased from the sources listed below, or from major local booksellers. Payment may be made in local currency or with UNESCO coupons.

Australia

DA Information Services, 648 Whitehorse Road, Mitcham Victoria 3132
Telephone: +61 3 9210 7777 • Fax: +61 3 9210 7788
Email: service@dadirect.com.au • Web site: <http://www.dadirect.com.au>

Belgium

Jean de Lannoy, avenue du Roi 202, B-1190 Brussels
Telephone: +32 2 538 43 08 • Fax: +32 2 538 08 41
Email: jean.de.lannoy@infoboard.be • Web site: <http://www.jean-de-lannoy.be>

Canada

Bernan Associates, 4611-F Assembly Drive, Lanham, MD 20706-4391, USA
Telephone: 1-800-865-3457 • Fax: 1-800-865-3450
Email: order@bernan.com • Web site: <http://www.bernan.com>

Renouf Publishing Company Ltd., 1-5369 Canotek Rd., Ottawa, Ontario, K1J 9J3
Telephone: +613 745 2665 • Fax: +613 745 7660
Email: order.dept@renoufbooks.com • Web site: <http://www.renoufbooks.com>

China

IAEA Publications in Chinese: China Nuclear Energy Industry Corporation, Translation Section, P.O. Box 2103, Beijing

Czech Republic

Suweco CZ, S.R.O. Klecakova 347, 180 21 Praha 9
Telephone: +420 26603 5364 • Fax: +420 28482 1646
Email: nakup@suweco.cz • Web site: <http://www.suweco.cz>

Finland

Akateeminen Kirjakauppa, PL 128 (Keskuskatu 1), FIN-00101 Helsinki
Telephone: +358 9 121 41 • Fax: +358 9 121 4450
Email: akatilaus@akateeminen.com • Web site: <http://www.akateeminen.com>

France

Form-Edit, 5, rue Janssen, P.O. Box 25, F-75921 Paris Cedex 19
Telephone: +33 1 42 01 49 49 • Fax: +33 1 42 01 90 90 • Email: formedit@formedit.fr

Lavoisier SAS, 14 rue de Provigny, 94236 Cachan Cedex
Telephone: + 33 1 47 40 67 00 • Fax +33 1 47 40 67 02
Email: livres@lavoisier.fr • Web site: <http://www.lavoisier.fr>

Germany

UNO-Verlag, Vertriebs- und Verlags GmbH, August-Bebel-Allee 6, D-53175 Bonn
Telephone: +49 02 28 949 02-0 • Fax: +49 02 28 949 02-22
Email: info@uno-verlag.de • Web site: <http://www.uno-verlag.de>

Hungary

Librotrade Ltd., Book Import, P.O. Box 126, H-1656 Budapest
Telephone: +36 1 257 7777 • Fax: +36 1 257 7472 • Email: books@librotrade.hu

India

Allied Publishers Group, 1st Floor, Dubash House, 15, J. N. Heredia Marg, Ballard Estate, Mumbai 400 001,
Telephone: +91 22 22617926/27 • Fax: +91 22 22617928
Email: alliedpl@vsnl.com • Web site: <http://www.alliedpublishers.com>

Bookwell, 24/4800, Ansari Road, Darya Ganj, New Delhi 110002
Telephone: +91 11 23268786, +91 11 23257264 • Fax: +91 11 23281315
Email: bookwell@vsnl.net • Web site: <http://www.bookwellindia.com>

Italy

Libreria Scientifica Dott. Lucio di Biasio "AEIOU", Via Coronelli 6, I-20146 Milan
Telephone: +39 02 48 95 45 52 or 48 95 45 62 • Fax: +39 02 48 95 45 48

Japan

Maruzen Company, Ltd., 13-6 Nihonbashi, 3 chome, Chuo-ku, Tokyo 103-0027
Telephone: +81 3 3275 8582 • Fax: +81 3 3275 9072
Email: journal@maruzen.co.jp • Web site: <http://www.maruzen.co.jp>

Korea, Republic of

KINS Inc., Information Business Dept. Samho Bldg. 2nd Floor, 275-1 Yang Jae-dong SeoCho-G, Seoul 137-130
Telephone: +02 589 1740 • Fax: +02 589 1746
Email: sj8142@kins.co.kr • Web site: <http://www.kins.co.kr>

Netherlands

Martinus Nijhoff International, Koraalrood 50, P.O. Box 1853, 2700 CZ Zoetermeer
Telephone: +31 793 684 400 • Fax: +31 793 615 698 • Email: info@nijhoff.nl • Web site: <http://www.nijhoff.nl>

Swets and Zeitlinger b.v., P.O. Box 830, 2160 SZ Lisse
Telephone: +31 252 435 111 • Fax: +31 252 415 888 • Email: infoho@swets.nl • Web site: <http://www.swets.nl>

New Zealand

DA Information Services, 648 Whitehorse Road, MITCHAM 3132, Australia
Telephone: +61 3 9210 7777 • Fax: +61 3 9210 7788
Email: service@dadirect.com.au • Web site: <http://www.dadirect.com.au>

Slovenia

Cankarjeva Založba d.d., Kopitarjeva 2, SI-1512 Ljubljana
Telephone: +386 1 432 31 44 • Fax: +386 1 230 14 35
Email: import.books@cankarjeva-z.si • Web site: <http://www.cankarjeva-z.si/uvoz>

Spain

Díaz de Santos, S.A., c/ Juan Bravo, 3A, E-28006 Madrid
Telephone: +34 91 781 94 80 • Fax: +34 91 575 55 63 • Email: compras@diazdesantos.es
carmela@diazdesantos.es • barcelona@diazdesantos.es • julio@diazdesantos.es
Web site: <http://www.diazdesantos.es>

United Kingdom

The Stationery Office Ltd, International Sales Agency, PO Box 29, Norwich, NR3 1 GN
Telephone (orders): +44 870 600 5552 • (enquiries): +44 207 873 8372 • Fax: +44 207 873 8203
Email (orders): book.orders@tso.co.uk • (enquiries): book.enquiries@tso.co.uk • Web site: <http://www.tso.co.uk>

On-line orders:

DELTA Int. Book Wholesalers Ltd., 39 Alexandra Road, Addlestone, Surrey, KT15 2PQ
Email: info@profbooks.com • Web site: <http://www.profbooks.com>

Books on the Environment:

Earthprint Ltd., P.O. Box 119, Stevenage SG1 4TP
Telephone: +44 1438748111 • Fax: +44 1438748844
Email: orders@earthprint.com • Web site: <http://www.earthprint.com>

United Nations (UN)

Dept. 1004, Room DC2-0853, First Avenue at 46th Street, New York, N.Y. 10017, USA
Telephone: +800 253-9646 or +212 963-8302 • Fax: +212 963-3489
Email: publications@un.org • Web site: <http://www.un.org>

United States of America

Bernan Associates, 4611-F Assembly Drive, Lanham, MD 20706-4391
Telephone: 1-800-865-3457 • Fax: 1-800-865-3450
Email: order@bernan.com • Web site: <http://www.bernan.com>

Renouf Publishing Company Ltd., 812 Proctor Ave., Ogdensburg, NY, 13669
Telephone: +888 551 7470 (toll-free) • Fax: +888 568 8546 (toll-free)
Email: order.dept@renoufbooks.com • Web site: <http://www.renoufbooks.com>

Orders and requests for information may also be addressed directly to:

Sales and Promotion Unit, International Atomic Energy Agency

Vienna International Centre, PO Box 100, 1400 Vienna, Austria
Telephone: +43 1 2600 22529 (or 22530) • Fax: +43 1 2600 29302
Email: sales.publications@iaea.org • Web site: <http://www.iaea.org/books>